Exploring the Therapeutic Potential of Fucoidans and Sodium Alginates from South African Brown Seaweeds: Insights into their Anti-diabetic and Anti-cancer Properties and Mechanisms

A thesis submitted in fulfilment of the requirements for the degree of

DOCTOR OF PHILOSOPHY

in

Biochemistry

at

RHODES UNIVERSITY

by

CHANTAL DÉSIRÉE DAUB

ORCID: 0000-0001-7914-6229

Supervisor: Prof Brett I. Pletschke

Co-supervisor: Prof. Adrienne L. Edkins

February 2025

Abstract

The increasing prevalence of type 2 diabetes and cancer poses significant global health challenges, prompting the need for novel treatment strategies due to the shortcomings of current approaches. Exploring natural bioproducts, particularly those sourced from marine environments, has emerged as a promising route. Among these compounds, polysaccharides such as fucoidan and sodium alginate, found abundantly in brown seaweeds, have demonstrated intriguing anti-diabetic and anti-cancer properties. However, despite previous studies highlighting their bioactivities, the underlying mechanisms remain poorly understood. In addition, South African brown seaweeds, have not been thoroughly explored for their potential. Therefore, the aim of this study was to screen fucoidans and sodium alginates from South African seaweeds to investigate their bioactivity against enzymatic targets relevant to type 2 diabetes mellitus (T2DM) and assess their effects on various cellular processes pertinent to anti-cancer activity, whilst also attempting to gain further insights into the mechanism of their bioactivities.

Fucoidans and sodium alginates used in this study were successfully extracted from four brown seaweed species, namely *Ecklonia maxima*, *Ecklonia radiata*, *Sargassum elegans*, and *Sargassum cymosum*, sourced from the South African shoreline. Chemical composition and structural features were comprehensively assessed using HPLC, FTIR, NMR, TGA, and XRD spectroscopy. The results showed that fucoidans from *Ecklonia* species were predominantly composed of monosaccharides, with glucose as the primary component, while those from *Sargassum* species contained higher sulphate levels and lower carbohydrate contents, consisting mainly of L-fucose. Sodium alginates were characterised by a higher content of mannuronic acid than guluronic acid. Structural elucidation provided further information on the presence of key structural features in both fucoidans and sodium alginates.

Analysis of the anti-diabetic potential of fucoidan and sodium alginate extracts was done by evaluating their inhibitory effects on the key carbohydrate-degrading enzymes relevant to Type 2 diabetes treatment: α-amylase, α-glucosidase, sucrase, and maltase. The results showed significant enzyme inhibition by fucoidans extracted from *E. maxima*, *E. radiata*, and *S. elegans*. Importantly, fucoidans from *E. radiata* and *S. elegans* demonstrated potent inhibition of α-glucosidase, maltase, and sucrase, surpassing the efficacy of the commercial anti-diabetic drug acarbose. In contrast, *E.*

maxima fucoidan could only compete with acarbose's efficacy when inhibiting α-glucosidase. A very significant finding of the study was that none of the fucoidans exhibited inhibitory effects on α-amylase. Furthermore, insights into the inhibition mechanism of α-glucosidase, maltase, and sucrase by the fucoidans were gained using linear and nonlinear regression methods. EnzymeML, a modern approach to enzyme kinetics analysis, identified the fucoidans from *E. radiata* and *S. elegans* as mixed-type inhibitors of α-glucosidase, exhibiting characteristics of both competitive and uncompetitive substrate inhibition along with evidence of enzyme inactivation. Traditional kinetic analysis revealed a mixed inhibition pattern of fucoidans from *E. radiata* and *S. elegans* for sucrase and maltase inhibition.

The anti-cancer effects of the fucoidans and sodium alginates were also assessed in the HCT116 colon cancer cell line, using standard techniques such as cell viability, proliferation, adhesion, migration, spheroid formation, and colony formation assays. Human colon cancer cells were the most sensitive to the treatment with *E. maxima* and *S. cymosum* fucoidan, which inhibited crucial metastasis-related processes such as cell adhesion, cell migration, spheroid formation, and anchorage-independent colony growth. Although a single underlying mechanism could not be pinpointed, these effects appear to be driven by changes in key interconnected signalling pathways, such as Wnt/β-catenin, AKT, FAK, and the Hippo pathway. Together, these changes in cellular functions and signalling pathways indicate a multifaceted impact on processes critical for metastatic progression. In summary, this study demonstrates promising anti-diabetic and anti-cancer activities for fucoidan extracts from South African seaweeds. Furthermore, this study also contributes to a deeper understanding of these activities by offering insights into their possible mechanisms of action.

Plagiarism declaration

I, Chantal Désirée Daub, declare that this thesis submitted for a Doctor of Philosophy in Science at Rhodes University is my own work. It has not been submitted before for a degree at this University or any other university. All sources in this thesis and significant contributions have been accurately reported and acknowledged.

Signature: 

Date: 24.02.2025

Acknowledgements

I would like to give a special thanks to my supervisor, Prof. B.I. Pletschke, and co-supervisor, Prof. A.L. Edkins, for their unwavering support and guidance throughout my postgraduate studies. Thank you for giving me the opportunity to work on this research project. Your constant encouragement and support have meant so much to me, and it has been an absolute honour to work under your guidance.

To Dr. B. Mabate, thank you for your significant contributions to my research. Your insights and support have been invaluable, and I cannot thank you enough.

To the Enzyme Science Programme (ESP)-Bioproducts research group, with special thanks to Dr. L. Mkabayi, your kindness and constant support have been a great source of motivation. I would also like to thank the Biomedical Biotechnology Research Unit (BIOBRU). Special thanks within this group go to Dr. K. Schwarz, Dr. A. Chakraborty, and J. Watson for their patience and mentorship in teaching me various cell culture techniques.

To Max Häußler and Prof. J. Pleiss, I appreciate your collaboration and contributions to the enzyme work in this thesis. Your insights have provided me with a deeper understanding of biotechnological enzyme research and have taught me valuable skills. To Dr. C. Davison in the Female Cancers Research Unit at Rhodes University (FemCR2U), thank you for mentoring me in specialised techniques and for your experimental contributions to this work.

To my family and friends, your endless love and support have been a constant motivator. A special mention to my mother, Mrs. N. Daub, and my father, Mr. U. Daub, for always believing in me and encouraging me every step of the way. To my partner, Mr. T. Hussey, thank you for your encouragement and for taking the time to proofread my work.

Finally, I wish to acknowledge the Pearson Young Memorial scholarship for providing the funding that made it possible for me to complete this study.

Table of Contents

List of figures

List of tables

List of research outputs

a. Publications in peer reviewed journals:

1. **Daub, C.D**., Mabate, B., Malgas, S., & Pletschke, B.I. (2020). Fucoidan from *Ecklonia maxima* is a Powerful Inhibitor of the Diabetes-related Enzyme, α-Glucosidase. *International Journal of Biological Macromolecules*, 151: 412–420. https://doi.org/10.1016/j.ijbiomac.2020.02.161
2. Mabate, B., **Daub, C.D**., Malgas, S., Edkins, A.L., & Pletschke, B.I. (2021). Fucoidan Structure and its Impact on Glucose Metabolism: Implications for Diabetes and Cancer Therapy. *Marine Drugs*, *19* (1):30. https://doi.org/10.3390/md19010030
3. Mabate, B., **Daub, C.D.**, Malgas, S., Edkins, A.L., & Pletschke, B.I. (2021). A Combination Approach in Inhibiting Type 2 Diabetes-related Enzymes using *Ecklonia radiata* Fucoidan and Acarbose. *Pharmaceutics (Special Issue)*, 13(11):1979. https://doi.org/10.3390/pharmaceutics13111979
4. Mabate, B., **Daub, C.D.**, Malgas, S., Pletschke, B.I., & Edkins, A.L. (2023). Comparative Analyses of Fucoidans from South African Brown Seaweeds that Inhibit Adhesion, Migration, and Long-Term Survival of Colorectal Cancer Cells. *Marine Drugs*, 21: 203. https://doi.org/10.3390/md2104020
5. Mabate, B., **Daub, C.D.**, Malgas, S., & Pletschke, B.I. (2024). Characterisation of *Sargassum elegans* Fucoidans Extracted using Different Technologies: Linking their Structure to α-Glucosidase Inhibition. *Algal Research*, 103885. https://doi.org/10.1016/j.algal.2024.103885
6. **Daub, C.D.**, Michaels, A., Mabate, B., Mkabayi, L., Edkins, A.L., & Pletschke, B.I. (2025). Exploring the Inhibitory Potential of Sodium Alginate against Digestive Enzymes Linked to Obesity and Type 2 Diabetes. *Molecules,* 30(5): 1155; https://doi.org/10.3390/molecules30051155

b. Topical paper:

1. Mabate, B., **Daub, C.D**., Malgas, S., & Pletschke, B.I. (2020). Kelp extracts and their pharmaceutical properties. *Atlas of Science.* (https://atlasofscience.org/kelp-extracts-andtheir-pharmaceutical-properties/#more-30415)

c. Conference presentations

1. Mabate, B., **Daub, C.D.**, Malgas, S., Edkins, A. L., & Pletschke, B. I. Relevance of brown seaweed fucoidans as therapeutics for Type 2 diabetes mellitus (T2DM) and cancer progression. The South African Society of Biochemistry and Molecular Biology conference (SASBMB) (Online). University of Pretoria from the 23-26 January 2022. (Oral Presentation)

2. Mabate, B., **Daub, C.D.**, Edkins, A. L., & Pletschke, B. Relevance of brown seaweed fucoidans as therapeutics for Type-2 diabetes mellitus (T2DM) and cancer progression. 24th International Seaweed Symposium (Online). Hobart, Tasmania and Online from the 19 – 24 February 2023. (Poster Presentation)

List of abbreviations

ANOVA	Analysis of variance
BSA	Bovine serum albumin
$CaCl_2$	Calcium chloride
CI	Cell index
CO_2	Carbon dioxide
CRC	Colorectal cancer
DMEM	Dulbecco's Modified Eagle's Medium
DMSO	Dimethylsulphoxide
DNS	3,5-Dinitrosalicylic acid
D_2O	Deuterium Oxide
ECM	Extracellular matrix
EDTA	Ethylenediaminetetraacetic Acid
FAK	Focal adhesion kinase
FTIR	Fourier-transform infrared spectroscopy
IC_{50}	Half maximal inhibitory concentration
HCl	Hydrochloric acid
HPLC	High performance liquid chromatography
MMP	Matrix Metalloproteinase
MOB1	Monopolar spindle-one-binder protein
mRNA	Messenger RNA
$NaCO_3$	Sodium carbonate
NaOH	Sodium hydroxide
NMR	Nuclear magnetic resonance
pAKT	Phosphorylated protein kinase B
PBS	Phosphate buffer saline
*p*NPG	*p*-nitrophenol-α-D-glucopyranoside
TMX	Tamoxifen
TGA	Thermogravimetric analysis
T2DM	Type 2 diabetes mellitus
UNT	Untreated
VEGF	Vascular endothelial growth factor
XRD	X-ray diffraction

List of symbols

α	Alpha
β	Beta
°C	Degree Celsius
g	Gram
h	Hour
kDa	Kilo Dalton
K_m	Michaelis constant
k_{cat}	Turnover number
mg	Milligram
$mg.ml^{-1}$	Milligram per millilitre
min	Minute
ml	Millilitre
µl	Microliter
µm	Micrometers
µmol	Micromole
mM	Milimolar
Mn	Number molecular weight
Mw	Molecular weight
$ng.ml^{-1}$	Nanogram per millilitre
nm	Nanometer
PDI	Polydispersity index
%	Percentage
$U.ml^{-1}$	Units of enzyme activity per millilitre
V_{max}	Maximum velocity
V	Volts
v/v	Volume per volume
w/v	Weight per volume
w/w	Weight per weight
× *g*	Relative centrifugal field

Chapter 1- General introduction and literature review

1.1 Introduction

Diabetes and cancer are two major public health concerns which, due to the current treatment regimens' limited efficacies and alarming side effects, negatively affect millions of people worldwide (Bradshaw Kaiser *et al.,* 2018; Siegel *et al.,* 2020). To lower the societal burden of these diseases, the pharmacological interventions for their treatment require drugs with higher clinical effectiveness and no undesirable side effects that may impact efficacy or compliance by patients. The synthetic development of novel therapeutic agents has been unable to design compounds that fill this gap (Atashrazm *et al.,* 2015). This has encouraged the search for natural sources of bioactive compounds with fewer side effects. Brown seaweeds are gaining wide attention as, due to their chemical and biological diversity, they contain numerous bioactive molecules (Holdt and Kraan, 2011). Given the latest advances and current knowledge gap, this project will evaluate the bioactivity potential of the less explored fucoidan and sodium alginate from South African seaweeds and explore their mechanisms of action.

1.2 Background to seaweeds

Seaweeds are multicellular photosynthetic plants that hold a key role in the food web and habitat of marine ecosystems and contribute to their biodiversity (Wernberg et al., 2019). They can be found along coastlines worldwide, spanning from warm tropical to icy cold polar regions (Subba Rao et al., 2018; Qin, 2018). Seaweeds represent an incredibly diverse taxonomic group, with approximately 11,000 different species documented worldwide (Msuya et al., 2022). The structure of seaweeds typically comprises a holdfast, anchoring it to the seabed or rocks, a stipe analogous to a terrestrial plant's stem, and a frond or blade resembling a leaf (Edwards et al., 2012). Seaweeds come in a variety of shapes, colours, and sizes. Classification of seaweed diversity has traditionally relied on factors such as habitat, pigment profile, morphology, anatomy, and reproductive structures (Abdel-Kareem and ElSaied, 2022). However, the taxonomic system is continuously being refined and updated as new genetic and structural data becomes available (Mattio et al., 2015). Presently, seaweeds are broadly grouped into three main categories based on their pigmentation: red seaweed

(Rhodophyta), green seaweed (Chlorophyta), and brown seaweed (Phaeophyceae) (Qin, 2018).

1.3 Current uses of seaweeds

Seaweeds from all three above-mentioned classifications have found applications for use for various purposes. They are commercially sold for direct human consumption. In Asia, seaweeds in the form of nori, kombu, wakame, and hijiki have been eaten as salads, soups, or as an added ingredient in multiple other dishes for millennia (Nagappan *et al.,* 2017; Leandro et al., 2020). These edible seaweeds are highly nutritious, boasting high protein content, along with vitamins, minerals, omega-3 and omega-6 unsaturated fatty acids, and dietary fiber (Leandro et al., 2020). Although seaweed consumption is relatively new in Western countries, it is steadily gaining popularity (Subba Rao et al., 2018). Furthermore, in certain parts of the world seaweeds are esteemed for their medicinal properties and are used in traditional Chinese and Japanese folk medicines (Leandro et al., 2020). In Western nations, seaweeds are mainly used in the production of various commodities such as cosmetics, fertilisers, organic manure, and additives in animal feed (Nagappan et al., 2017; Subba Rao et al., 2018). Additionally, seaweeds are valued for their functional components, such as agar, alginates, and carrageenan (Nagappan et al., 2017). These essential polysaccharides have found widespread applications across various industries including food, textile, paint, biotechnology, and biomedicine (Kraan et al., 2012). Moreover, ongoing research is investigating the beneficial properties of seaweed produced compounds (Leandro et al., 2020).

1.4 South Africa's seaweed resources and industry

The South African coastline is home to one of the richest and diverse seaweed flora, with a high degree of endemism (Bolton and Stegenga 2002). Of the country's diverse seaweed flora, the country's coast is colonised by more than 850 species, of which 101 are brown seaweed species (Msuya et al. 2022; Bolton and Stegenga 2002). The country's abundance of seaweed represents a reserve of species with considerable economic potential (Belattmania et al., 2020). The commercial exploitation of seaweeds in South Africa began in the 1950s and continues to this day (Amosu et al. 2013). In the past, South Africa mainly harvested the red seaweed *Gelidium pristoides* for agar production but also exported harvested seaweeds to Europe, North America, and Asia for alginate extraction (Msuya et al. 2022; Amosu et al. 2013). The country's

exploitation of seaweeds for these purposes has seen a decline over the past years (Rothman et al., 2020). Today, South Africa's seaweed industry largely consists of the harvesting of natural kelp stocks for the domestic use as abalone feed and the production of growth stimulants for the agricultural industry (Msuya et al. 2022; Rothman et al. 2020). The two species that form the base of the current industry are the kelp *Laminaria pallida* and, to a greater extent, *Ecklonia maxima* (Rothman et al. 2020). Commercial companies such as Afrikelp®, Basfoliar®, Kelpak® manufacture liquid fertilisers from *E. maxima* (Lötze and Hoffman, 2015). The South African seaweed industry, although valuable, remains an underdeveloped industry with a larger potential for exploitation in various market sectors (Msuya et al., 2022).

1.5 Brown seaweeds important metabolites

Brown seaweeds consist of polysaccharides (20–76% of dry weight), proteins (15–40% of dry weight), carotenoids, mineral ions (36% of dry weight), omega-3 fatty acids, and low levels of lipids, along with a high content of bioactive molecules (Kumar and Brown, 2013; Pádua et al., 2015). Brown seaweeds exhibit a remarkable ability to adapt and thrive in fluctuating marine environments through the production of chemical compounds. The content of seaweed metabolites is quite variable and depends largely on the species, geographical area, and season (Salehi et al., 2019). Their abundant functional compounds include both primary metabolites, such as proteins, polysaccharides, and lipids, as well as secondary metabolites, which include phenolic compounds, sterols, terpenes, small peptides, and halogenated compounds (Rosa *et al.,* 2020; Khalid et al*.,* 2018). Compounds like fucoidan, alginate, fucoxanthin, laminarin, and phlorotannins have demonstrated diverse bioactivities such as anti-inflammatory, neuroprotective, anti-cancer, anti-obesity, anti-diabetic, anti-viral, and anti-microbial activities (Lomartire and Gonçalves, 2022).

1.6 Fucoidan

Fucoidan is found in the intracellular tissue of the mucilaginous matrix of the cell walls of certain marine invertebrates, including sea cucumbers and sea urchins, as well as brown seaweeds (Rhein-Knudsen et al., 2023; Ponce and Stortz, 2020). In seaweed, fucoidan functions as a cell wall reinforcement molecule, strengthening and stabilising the cell wall by cross-linking cellulose and alginates. Additionally, fucoidan promotes cellular hydration, ensuring the seaweed's protection against desiccation during low tides (Ponce and Stortz, 2020).

Fucoidans, also known as sulphated fucans or fucosan, are heterogenous polysaccharides containing L-fucose and sulphate esters (Jayawardena et al., 2022). Their composition and structure vary based on factors such as source of seaweed species, environmental conditions, and method of extraction (Rhein-Knudsen et al., 2023). In addition to fucose, fucoidan may contain other monomeric sugar constituents to varying degrees. These include D-glucose, D-galactose, D-mannose, D-xylose, L-arabinose, and L-rhamnose (Fitton et al., 2015). Additionally, acetyl groups and uronic acid are often components of the fucoidan polymer (Jayawardena et al., 2022). Examples of the chemical composition of various fucoidans are summarised in Table 1.1 below.

Table 1.1: Chemical compositions of some known fucoidans

Brown seaweed	Chemical composition
Laminaria japonica	fucose, xylose, galactose, glucuronic acid, sulphate
Fucus vesiculosus	fucose, xylose, galactose, arabinose, sulphate
Fucus evanescens C.Ag.	fucose, sulphate, acetate
Fucus distichus	fucose, sulphate, acetate
Fucus serratus L.	fucose, sulphate, acetate
Lessonia vadosa	fucose, sulphate
Macrocytis pyrifera	fucose, galactose, sulphate
Pelvetia wrightii	fucose, galactose, sulphate
Undaria pinnatifida	fucose, galactose, sulphate
Ascophyllum nodosum	fucose, xylose, glucuronic acid, sulphate
Himanthalia lorea and Bifurcaria bifurcate	fucose, xylose, glucuronic acid, sulphate
Padina pavonia	fucose, xylose, mannose, glucose, galactose, sulphate
Laminaria angustata	fucose, galactose, sulphate
Ecklonia kurome	fucose, galactose, mannose, xylose, glucuronic acid, sulphate
Ecklonia radiata	fucose, xylose, galactose, arabinose, sulphate
Sargassum stenophyllum	fucose, galactose, mannose, glucuronic acid, glucose, xylose, sulphate
Adenocytis utricularis	fucose, galactose, mannose, sulphate
Hizikia fusiforme	fucose, galactose, mannose, xylose, glucuronic acid, sulphate
Dictyota menstrualis	fucose, xylose, uronic acid, galactose, sulphate
Spatoglossum schroederi	fucose, xylose, galactose, sulphate
Alaria esculenta	fucose, xylose, galactose, uronic acid

(Adapted from Li et al., 2008; Fitton et al., 2015)

The monomeric units of fucoidans link together through diverse glycosidic linkages, leading to the formation of a straight and/or branched-chain polysaccharide backbone. These structures are characterised by sulphate substitutions, which impart a negative charge to fucoidan, and exhibit a broad molecular weight distribution, spanning from less than 10 kDa to around 10,000 kDa (Zayed et al., 2020). Variations in the

constituent monosaccharides, glycosidic linkages, sulphate group positions, and molecular weight are the reasons why fucoidans exhibit structural diversity (Wang et al., 2020). Fucoidans are generally categorised as either homofucans or heterofucans based on their backbone composition (Rhein-Kudsen et al., 2023). Homofucans are further divided into two main types based on their skeletal structure. Type 1 consists exclusively of α-(1→3)-linked L-fucose residues, sulphated at C-2 and C-4, while Type 2 features alternating combinations of α-(1→3)- and α-(1→4)-linked L-fucose residues, sulphated at C-2 and C-4, and occasional sulphation at C-3 (Figure 1.1A and B) (Wang et al., 2020; Zayed et al., 2020; Sichert et al., 2021). The structural feature of a linear α-(1→3)-linked L-fucose unit backbone with multiple branching points was observed in fucoidans from *Ecklonia kurome* and *Chorda filum*, with sulphate groups mainly occupying the C-4 position, while some acetyl groups were found on the α-(1→3)-linked L-fucose residues (Li et al., 2008). Fucoidans derived from the order Fucales, such as *Ascophyllum nodosum*, *Fucus vesiculosus*, *Fucus evanscens*, and *Fucus serratus*, exhibit a backbone composed of α-(1→3)-linked L-fucose and α-(1→4)-linked L-fucose residues, with sulphate groups located at the C-2 and C-4 positions (Cumashi et al., 2007; Zhang et al., 2020). In contrast, heterofucans are characterised by a backbone composed of non-fucose units such as β-(1→6)-linked D-galactose or β-(1→3)-linked D-glucuronic acid, with fucose side branches and unique sulphation (Rhein-Knudsen et al., 2023; Sichert et al., 2021; Bilan and Usov, 2008). The fucoidan extracted from *Sargassum fusiforme* has a remarkably intricate fucose-free backbone structure, with a core chain of alternating units of α-(1→2)-linked D-mannopyranose and β-(1→4)-linked D-glucuronic acid, alongside a minor portion of 4-linked β-(1→4)-linked D-galactose and branched chains of L-fucose, D-galactose, D-mannose and D-xylose (Bilan and Usov, 2008). Similarly, fucoidan sourced from *Sargassum stenophyllum* displays a unique backbone structure comprised of β-(1→6)-D-galactose and β-(1→2)-D-mannose residues and revealed sulphated galactose units (Wang et al., 2020). The variations in the reported structural properties of fucoidans from different brown seaweed species highlight the diversity and complexity of these compounds.

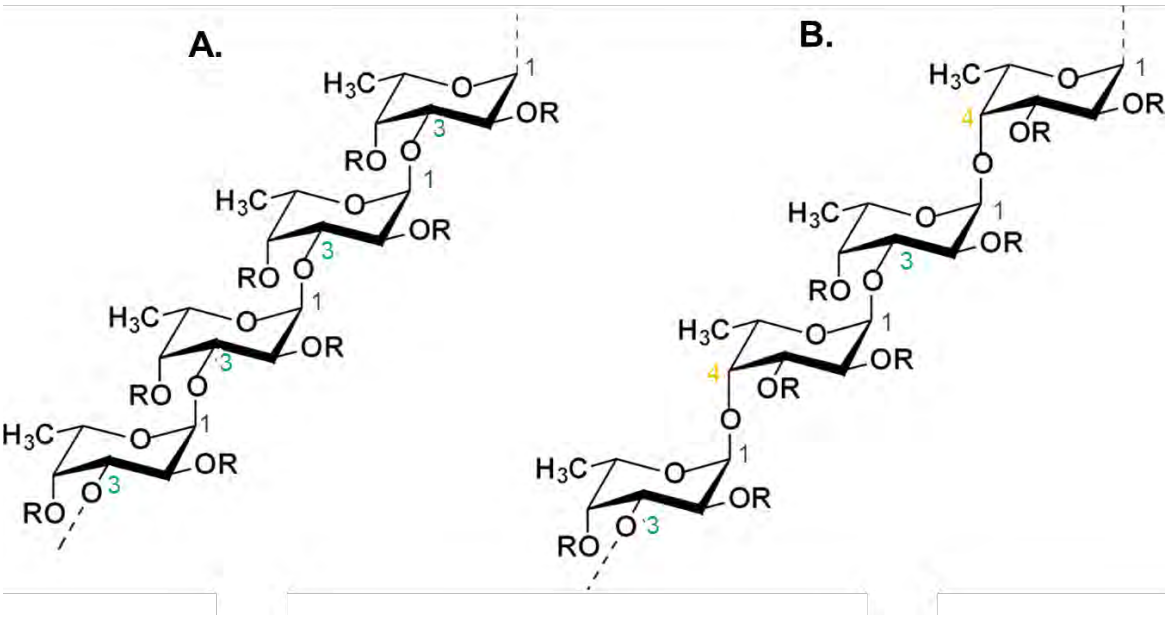

Figure 1.1: Structural model of the two major types of homofucose backbone structures. (A) Type 1 composed of repeating α-(1→3)-α-L-fucose residue backbone; (B) Type 2 containing alternating (1→3)- and (1→4)-linked α-L-fucose residues. R shows the potential places for attachment of carbohydrate (α-L-fucose, α-D-glucuronic acid, etc.) and noncarbohydrate (sulphate and acetyl groups) substituents. Adapted from Cumashi et al. (2007).

Fucoidan has attracted much attention from researchers due to its diverse array of biological activities, including anti-oxidant, anti-coagulant, anti-thrombotic, anti-inflammatory, anti-viral, anti-lipidemic, anti-metastatic, anti-diabetic and anti-cancer activities (Li *et al.,* 2008). It is currently marketed as a nutritional supplement and has gained regulatory approval in China, the US, and Europe. In recent years, the commercial presence of fucoidans in cosmetics, foods, and nutritional supplements has seen significant growth (Fitton et al., 2019). Fucoidan as of 2003 has been used as a certified drug to effectively treat renal diseases in China (Wang et al., 2019b). Furthermore, health authorities in both Canada and Australia have approved various listed medicines containing fucoidan extracts (Fitton et al., 2019). These extracts are also used for gut health, oral health, and anti-inflammatory purposes in humans, livestock and pets (Fitton et al., 2019). Many other promising applications related to the bioactivities of fucoidans have entered *in vivo* and clinical trial stages. In human clinical trials, the combination of fucoidan with anti-cancer drugs showed improvements in the rate of disease control among patients with metastatic colorectal cancer and extended the lifespan of patients with lung cancer (Hsu and Hwang, 2019). Additionally, independent clinical trials have noted that the oral intake and topical

treatment with a fucoidan cream improved the treatment of herpes (Fitton et al., 2019; Li et al., 2008). It is, therefore, expected that more fucoidan-based pharmaceuticals will be brought to market in the future.

1.7 Alginate

Alginate is the most abundant polysaccharide in brown seaweeds, comprising up to 40% of the dry matter (Rhein-Knudsen et al. 2017). Alginates are part of the structure of brown seaweed cell walls, where they exist in the form of divalent salts of alginic acid and form the intercellular gel matrix (Alba and Kontogiorgos, 2019). This provides flexibility and structural integrity to the seaweed, shielding it from potential harm when exposed to powerful seawater waves (Raus et al., 2021). While brown seaweeds are the primary source of alginate, bacteria of the *Azotobacter* and *Pseudomonas* genera can also synthesise alginates, albeit in an acetylated form (Mazéas et al., 2023). Several brown seaweed species, including *Ascophyllum, Durvillaea, Ecklonia, Laminaria, Lessonia, Macrocystis*, and certain *Sargassum* species, are utilised as sources for commercial alginate production, typically sodium alginate (Abka-Khajouei et al., 2022).

The alginate polysaccharide is composed of linear copolymers containing blocks of β-D-mannuronic (M) and α-L-guluronic acid (G) residues joined by (1→4) linkages, with attached free functional hydroxyl (OH) and carboxyl (COOH) groups (Neves et al., 2020). Figure 1.2 shows the position of both M and G in the structure of alginate. The mannuronic acid residues, connected by diequatorial linkages in the C-1 confirmation, form the M-blocks, which connect in a flat ribbon-like chain conformation (Figure 1.2). Conversely, the G-blocks consist of diaxially-linked guluronic acid residues in the C-4 confirmation, which hinder rotation around glycosidic bonds, giving them a more rigid structure. MG-blocks are composed of alternating axial–equatorial (GM) and equatorial–axial (MG) glycosidic bonds (Figure 1.2) (Williams and Phillips, 2004; Daemi and Barikani, 2012). The rigidity of the chemical linkages decreases in the order GG > MM > MG. Additionally, the structural sequences of alginate's M and G residues have a direct impact on their solubility due to their ion-binding capabilities (Williams and Phillips, 2004). It has been suggested that divalent cations such as Ca^{2+}, Na^{2+} and Mg^{2+} primarily crosslink with the carboxylate groups of the G residues and, to a lesser extent, with those of the M residues to form hydrogels. As such, alginates with a higher G block content form a stiffer hydrogel (Neves et al., 2020; Beuder and Braybrook,

2023). As a natural copolymer, the structural sequence (MM, GG, or MG), and proportions (M/G ratio) of D-mannuronic acid and L-guluronic acid vary widely in alginates extracted from different types of brown seaweeds (Neves et al., 2020). Consequently, the physical properties of alginate vary (Neves et al., 2020). Importantly, variations in the molecular weight of alginate affect its viscosity during gel preparation; higher molecular weight results in increased viscosity (Raus et al., 2021).

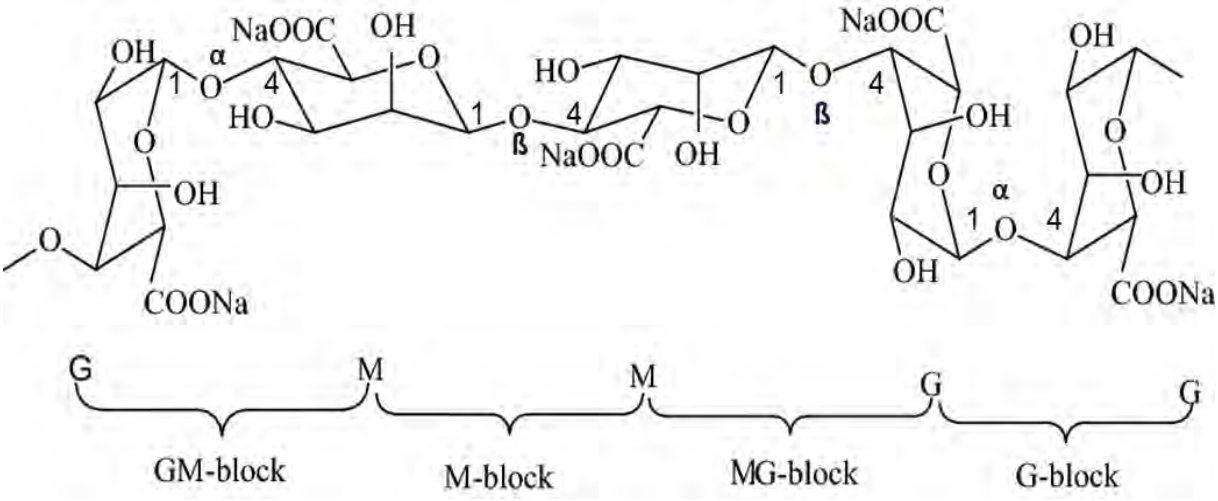

Figure 1.2: Molecular structural model of alginate (in its sodium alginate form) showing the various block structure components. Adapted from Raus et al. (2021) and Abka-Khajouei et al. (2022).

Due to its gelling ability alginate has found many applications as a thickening and stabilising agent in various industries, including the food, textile, cosmetics, painting or dye and pharmaceutical industries (Şahin, 2022; Fertha et al., 2017). Other fields of application for this biopolymer include biotechnology, bioengineering, biomedical, and clinical areas, including its use in wound dressings, heavy metal chelation, tissue engineering materials, nanoparticles (e.g. hydrogels, beads) for controlled drug delivery, 3D bio-printing matrices, prosthetics, dental moulds and impression materials and cell immobilisation (Hurtado et al., 2023). In biomedicine, alginate is frequently used in the form of a hydrogel. Commercial wound dressings based on sodium alginate and calcium alginate hydrogels, supplemented with additional components with favourable properties like anti-bacterial effects, have been developed to effectively treat dermal wounds (Raus et al., 2021). In tissue engineering, alginate-based biomaterials are being used for repairing both soft and hard tissues, such as skin, heart, bone, cartilage, and vascular tissue (Neves et al., 2020). Alginate and alginate composite hydrogels are also utilised as drug delivery carriers, encapsulating

compounds like insulin or diverse enzymes for release. They have also been investigated as a delivery vehicle for treating various diseases, including gastric reflux, colon disease, and cancer, among others (Hurtado et al., 2023).

1.8 Diabetes mellitus

Diabetes mellitus is a metabolic disorder of the carbohydrate metabolism where glucose is inefficiently used for energy and overproduced due to improper gluconeogenesis and glycogenolysis, leading to high glucose levels in the blood plasma, known as hyperglycaemia (American Diabetes Association, 2024). Diabetes mellitus is subdivided into several distinct types, of which type 1 (T1DM) and type 2 (T2DM) are the most common (American Diabetes Association, 2024). T1DM and T2DM are distinguished by the body's response to the blood sugar-lowering hormone insulin, which plays a central role in their pathophysiology (Sapra and Bhandari, 2023). In T1DM, there is an autoimmune destruction of the insulin-producing pancreatic beta cells, resulting in the inability to produce sufficient insulin. Consequently, the body cannot effectively lower its blood sugar levels. The onset of T1DM most commonly occurs in young children and adolescents (Sapra and Bhandari, 2023). In T2DM, it is the body's response to insulin that is impaired. In this type of diabetes, cells have developed insulin resistance, causing them to no longer take up sufficient amounts of glucose when stimulated by insulin. As a result, glucose remains in the blood, leading to an increase in blood glucose concentration. This type of diabetes is the most prevalent, representing 90% of all diabetes mellitus cases but is also preventable (Sapra and Bhandari, 2023).

1.8.1 Risk factors and pathophysiology of Type 2 diabetes

The onset of T2DM typically occurs later in life, but the rise in obesity among adolescents has contributed to an increase in T2DM among younger individuals (Sapra and Bhandari, 2023). There are several factors that contribute to the pathophysiological disturbances responsible for the impaired glucose homeostasis in T2DM (DeFronzo et al., 2015). Diet, obesity, and physical inactivity are known to be some of the primary factors contributing to this condition. However, increasing age and various genetic factors may also play a role (Kaul et al., 2013; American Diabetes Association, 2024). Progression of the disease occurs very slowly over many years, see Figure 1.3. Initially, the decreased insulin sensitivity of the key insulin-sensitive tissues (skeletal muscle, liver and adipose tissue) triggers hyperfunction of beta cells,

increasing insulin secretion to maintain normoglycemia. However, over time, the increased secretion of the beta cells fails to adequately compensate for cells acquiring insulin resistance. At the same time, beta cell function declines, ultimately resulting in insulin deficiency and the development of hyperglycaemia (Banday et al., 2020).

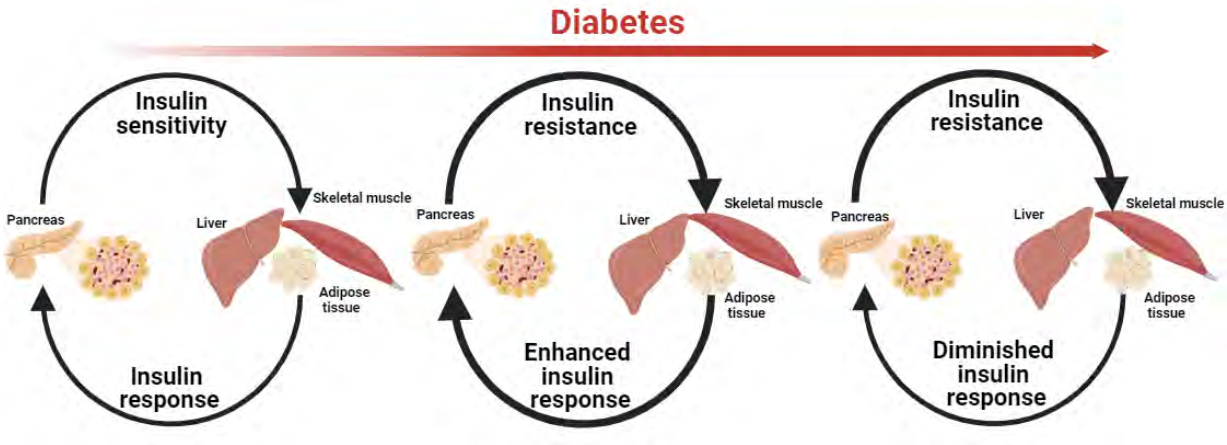

Figure 1.3: Pathogenesis of type 2 diabetes. The proposed sequence of events in the development of type 2 diabetes as described by Khan et al (2014).

The macronutrients ingested, particularly carbohydrates, contribute significantly to the onset of T2DM (Bonsembiante et al., 2021). Carbohydrates usually make up between 40% and 70% of our total caloric intake and serve as the primary sources of glucose in the body (Tappy, 2008). Consequently, blood glucose largely originates from the conversion of dietary carbohydrates into glucose during digestion (Bonsembiante et al., 2021).

1.8.2 Carbohydrate digestion and absorption

The carbohydrate sources sugar and starch (found in wheat, rice, maize, and potatoes), provide rapidly and slowly available glucose, respectively (Bonsembiante et al., 2021). Several specialised enzymes are employed in the human body to break down these starches into absorbable glucose (Lee et al., 2012). The first is salivary α-amylase, which initiates dietary starch digestion in the mouth. The salivary α-amylase hydrolyses internal α-(1,4) glycosidic bonds in starch molecules, producing linear malto-oligosaccharides and α-(1,6) branched oligosaccharides (α-limit dextrins). Amylase digestion is brief and incomplete due to its inability to hydrolyse α-(1,6) linkages, α-(1,4) linkages near branch points and terminal α-(1,4) linkages (Lee et al., 2012). The salivary α-amylase is deactivated by acid pH in the stomach, temporarily halting digestion. The produced oligosaccharides and some undigested carbohydrates

travel down the digestive tract to the small intestine, where the enzymatic digestion of carbohydrates recommences (Sanders, 2016).

In the small intestine, pancreatic α-amylase continues carbohydrate digestion in the same manner as salivary α-amylase, see Figure 1.4 (Sanders, 2016). The next stage of digestion (of the amylase-produced oligosaccharides and disaccharides) is carried out by mucosal α-glucosidases which are two brush border enzyme complexes: maltase-glucoamylase (MGAM) and sucrase-isomaltase (SI) (Lee et al., 2012). Each of the intestinal α-glucosidase complex enzymes breaks down the consumed starches further into simpler sugars or monosaccharides (e.g. glucose, galactose, and fructose). The MGAM continues to hydrolyse the α-1,4 glycosidic linkages from the non-reducing end of the α-amylase degraded starch molecules to release glucose from linear chains of glucose oligomers or polymers (Figure 1.4). SI can also cleave α-1,4 glycosidic linkages to release glucose. In addition, the N-terminal domain of SI cleaves the α-1,6 linkages, breaking down isomaltose and maltose into two glucose moieties, while the C-terminal domain of SI is able to cleave the α-(1,2) linkage of sucrose to release glucose (Lee et al., 2012; Dhital et al., 2013). The last major brush border complex, ß-glucosidase (lactase), hydrolyses the ß-(1,4) bond of lactose to release the monosaccharides, glucose and galactose (Sanders, 2016).

The released monosaccharide end products (mainly glucose) are absorbed by the cells (enterocytes) of the intestinal wall (Sanders, 2016). This absorption of the D-glucose and D-galactose monosaccharides from the intestinal lumen into enterocytes occurs through selective active transport via the Na^+/glucose cotransporter (SGLT1) (Figure 1.4), while fructose is passively transported via the GLUT5 transporter (Sanders, 2016). Once inside the enterocyte, the monosaccharides are then transported through the basolateral side of the cells through glucose transporters (GLUT2s) and released into the bloodstream (Figure 1.4). After absorption, glucose is transported by the circulatory system to target cells, where insulin-mediated/independent glucose uptake occurs, which, in the case of T2DM, does not occur sufficiently leading to hyperglycaemia (Lee et al., 2012). Carbohydrates that are not broken down by digestive enzymes and absorbed into the small intestine, such as resistant starch and dietary fibres, will proceed to the large intestine, where they undergo fermentation by microbes (Sanders, 2016).

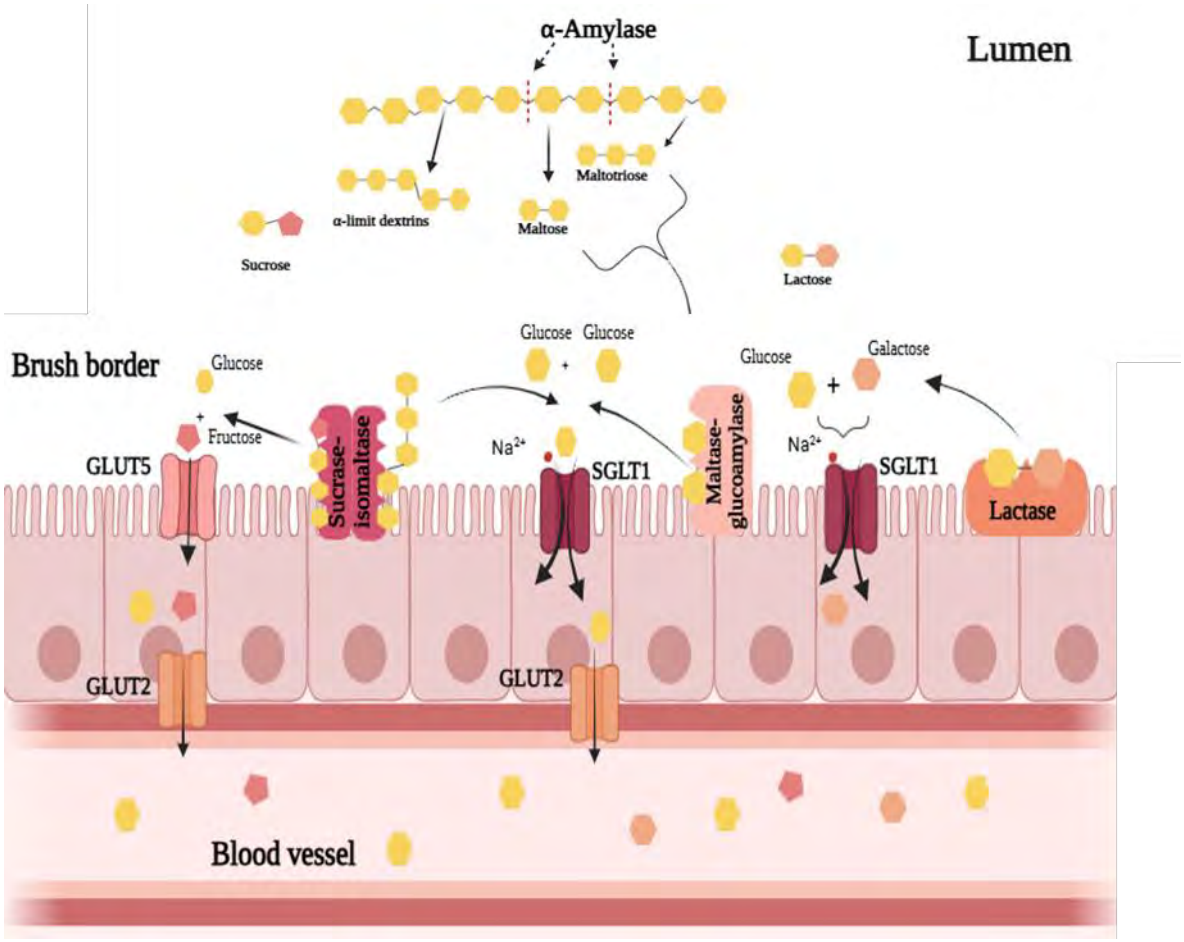

Figure 1.4: Carbohydrate digestion, absorption and transportation in the gastrointestinal tract. This schematic illustration provides a simplified representation of the enzymatic breakdown of carbohydrates into monosaccharides, alongside the crucial transporter molecules SGLT1, GLUT5, and GLUT2 involved in their absorption and subsequent transportation (Adapted from Boron and Boulpaep, 2017).

1.8.3 Management of hyperglycaemia in Type 2 diabetes

Left untreated T2DM chronic hyperglycaemia can lead to various diabetic complications, including immune system impairment, periodontal disease, retinopathy, nephropathy, somatic and autonomic neuropathy, cardiovascular diseases, and diabetic foot problems (Kaul et a., 2013). These detrimental symptoms and complications associated with diabetes can be prevented or delayed through rigorous glycaemic control. Advice on diet and lifestyle is often the first step in the treatment of T2DM. Dietary changes focusing on complex carbohydrates with a low glycaemic index in combination with increased physical activity and weight loss have proven beneficial in controlling high plasma glucose levels (Marín-Peñalver et al., 2016).

If dietary and lifestyle changes prove insufficient in managing glucose levels, oral hypoglycaemic medications are typically introduced. The current pharmacological

interventions to treat hyperglycaemia are numerous and include the use of different classes of oral anti-diabetic drugs including insulin secretagogues, insulin sensitisers, as well as α-amylase and α-glucosidase inhibitors (Cho et al., 2011; Lopes et al., 2017). The starch digestion role of α-amylases and α-glucosidases makes them the rate-limiting enzymes that determine the rate of digestion. Manipulation of their digestion rates allows for reduced glucose release from dietary starches and lowers postprandial blood glucose levels (Lee et al., 2012; Kumar et al., 2015). On this basis, inhibitors of pancreatic α-amylase and/or intestinal α-glucosidase are currently applied for T2DM regulation. Acarbose, a commercially available anti-diabetic agent, effectively inhibits both α-amylase and α-glucosidase and is employed to control blood glucose levels (Shan et al., 2016). Another prominent option is metformin, which ranks as the most frequently prescribed oral anti-diabetic medication. Its hypoglycaemic effects primarily stem from reducing hepatic gluconeogenesis to block the release of glucose from the liver, with a secondary effect of delaying intestinal nutrient absorption and promoting insulin-mediated glucose uptake in skeletal muscle to lower blood glucose (Nasri and Rafieian-Kopaei, 2014). Unfortunately, these treatments, like many others, can cause numerous gastrointestinal side effects, leading to irregular treatment adherence by T2DM patients, and is a major contributor to sub-optimal hyperglycaemia control (Cho et al., 2011; Kumar et al., 2015). Moreover, the Food and Drug Administration (FDA) has noted some safety concerns regarding another commonly used anti-diabetic agent, metformin (FDA, 2020).

Recently, glucagon-like peptide-1 (GLP-1) receptor agonists, such as semaglutide (marketed as Ozempic) and the dual glucose-dependent insulinotropic peptide (GIP) and GLP-1 receptor agonist tirzepatide (marketed under the name Mounjaro), have gained significant attention (Martins et al., 2024). These drugs work by mimicking incretin hormones, which help increase insulin secretion in response to glucose and reduce glucagon release, making them effective at improving blood sugar levels (Nauck and Müller, 2023; Boer and Holst, 2020). Additionally, their GLP-1 action slows gastric emptying, reduces postprandial glucose spikes, and promotes satiety, often leading to weight loss (Nauck and Müller, 2023; Boer and Holst, 2020). The combined effects of glucose regulation and appetite suppression have positioned these medications as promising advancements in managing type 2 diabetes mellitus (T2DM), particularly in individuals with obesity. Nonetheless, GLP-1 RAs like tirzepatide and semaglutide share similar gastrointestinal side effects with other anti-diabetic

medications, such as nausea, vomiting, and diarrhoea (Martins et al., 2024). Furthermore, they've also been linked to issues like anxiety, nervousness, and depression. On top of this, they are more expensive than other anti-diabetic treatments, and their recent surge in demand as diet medications has led to global shortages, making them more difficult to access (Martins et al., 2024). The pursuit of new treatments is, therefore, currently still underway, with a specific focus on natural products. These are favoured because of their apparent lack of side effects and their cost-effectiveness compared to synthetic hypoglycaemic analogues (Kumar et al., 2015).

1.8.4 Anti-diabetic relevance of fucoidan

Fucoidans, extracted from various species of brown seaweed, show promise in the treatment of diabetes, with research studies indicating various beneficial properties associated with these compounds for individuals living with this condition. For instance, many fucoidans have shown the ability to inhibit starch-degrading enzymes (such as α-amylase and α-glucosidase), consequently reducing blood glucose levels. In previous *in vitro* studies, fucoidan from *Turbinaria ornate* inhibited α-amylase, while fucoidans from *Sargassum ringgoldianum*, *Sargassum graminifolium* and *Sargassum honeri* inhibited α-glucosidase activity (Lakshmanasenthil et al., 2014; Shan et al., 2016). Other fucoidans, such as those from *Fucus vesiculosus*, *Ascophyllum nodosum* and *Sargassum wightii,* exhibited an inhibitory effect on both α-amylase and α-glucosidase activity (Kim et al., 2014; Shan et al., 2016; Vinoth Kumar et al., 2015). Many of these fucoidans have demonstrated significantly higher inhibitory potency against α-glucosidase compared to acarbose, the current therapeutic agent targeting these enzymes, with published studies reporting inhibition patterns occurring predominantly through competitive or mixed mechanisms (Mabate et al., 2021).

Furthermore, fucoidans, presumably based on their negative charge, have the capacity to slow down the post-digestion glucose absorption into the bloodstream through the small intestine by inhibiting the function of the Na+/glucose cotransporter 1 (SGLT1). Shan et al. (2020) demonstrated this for *Ascophyllum nodosum* fucoidan which inhibited glucose uptake in Caco-2 cells, a human intestinal epithelial cell line, by suppressing SGLT1 activity. Similarly, a study by Kim (2012) found that fucoidan extracted from *Ecklonia cava* inhibited glucose uptake in rat intestinal epithelial cells by downregulating SGLT1 expression. Moreover, fucoidans from *Cucumaria frondose*

and *Acaudina molpadioides* have demonstrated a positive effect on meeting the increasing demand for insulin in chronic hyperglycaemia, by increasing insulin production through the activation of the PI3K/PKB pathway and enhancing glucose uptake by muscle and fat tissue via the activation of glucose transporter 4 (GLUT4) translocation (Lu and Chen, 2022). Other studies have noted that fucoidan is able to inhibit dipeptidyl peptidase IV (DPP IV), an enzyme responsible for degrading incretin hormones that stimulate insulin secretion and decrease glucagon secretion (Mabate et al., 2021). Fucoidan has also been implicated in inhibiting protein tyrosine phosphatase 1B (PTP1B), a key enzyme involved in the negative regulation of the insulin-signalling pathway (Ali et al., 2017; Kasina and Baradhi, 2023). Also, treatment of mice with fucoidan from *Sargassum hemiphyllum* reported a positive effect on beta cell damage and loss, which may mitigate beta cell loss associated with T2DM progression (Yu et al., 2017).

1.8.5 Anti-diabetic relevance of sodium alginate

Alginate, as a major dietary fibre, also stands out for its acute hypoglycaemic effects - but, unlike fucoidan, mostly for its effect as an indigestible fibre. Within the gastric environment, sodium alginate fibres interact with protons and/or Ca^{2+} ions to form viscous fluids. Studies have credited the anti-diabetic effect of sodium alginate to its ability to increase digesta viscosity, which can delay gastric emptying and create a barrier between digesta and digestive enzymes, consequently slowing the digestion and absorption of ingested components such as glucose (Qiang et al., 2022; Giuntini et al., 2022). Several animal studies and human trials have reported potential anti-diabetic benefits of sodium alginates on this basis (Qiang et al., 2022). An early study by Torsdottir et al. (1991) demonstrated that adding sodium alginate to a meal of Type 2 diabetic patients significantly reduced the postprandial increase in blood glucose and serum insulin levels by 31% and 42%, respectively. Subsequent studies found that incorporating sodium alginate into food and beverages can positively affect the postprandial glucose level, insulin response and/or appetite in healthy adults (Giuntini et al., 2022). Some of the sodium alginates that showed effects beneficial to T2DM in human trials are listed in Table 1.2. Sodium alginate's ability to reduce blood glucose levels by inhibiting the starch-degrading enzymes α-amylase and α-glucosidase were reported in *in vitro* studies. Zaharudin *et al.* (2018) reported the inhibition of α-amylase by commercial alginates and alginates extracted from *Laminaria digitate* and *Undaria pinnatifida*. In contrast, sodium alginate derived from *Sargassum hystrix* was reported

to exhibit α-glucosidase inhibition potential, and in a subsequent *in vivo* study in rats demonstrated its ability to lower blood glucose levels (Samudra et al., 2017). Furthermore, a study by Szekalska et al. (2016) revealed that sodium alginate microspheres, utilised as a delivery system, enhance the hypoglycaemic effects of metformin hydrochloride, an orally administered anti-diabetic agent. These microspheres not only inhibited glucose uptake in *Saccharomyces cerevisiae* cells but also reduced α-amylase activity (Szekalska et al., 2016).

Table 1.2: Summary of human trials with sodium alginate and their reported glycaemic response

Study setup	Test subjects	Alginate source	Dose (g)	Test setup	Therapeutic effect	Publication
Randomised, placebo (as test meal) controlled, crossover design study	7 men with Type 2 diabetes	ND	5	Sodium alginate added to meal vs control meal	↓ AUC of blood glucose by 31% ↓ AUC of serum insulin by 42%	Torsdottir et al. (1991)
Randomised, double-blind, placebo-controlled, crossover design study	30 healthy adults	ND	3.75	Sodium alginate extract in glucose-based beverage vs. placebo glucose-based beverage with similar total dietary fiber level	↓ iAUC of blod glucose by 75%	Wolf et al. (2002)
Randomised, double-blind, placebo-controlled, crossover design study	48 healthy adults	ND	1.6	Sodium alginate and guar gum in a crispy bar vs. placebo crispy bar	↓ peak blood glucose by 30% ↓ iAUC of blood glucose by 33%	Williams et al. (2004)
Randomised, placebo-controlled, crossover design study	40 healthy men 20 in lower body fat group (< 16.10%); 20 in upper body fat group (≥ 16.10%)	ND	1.5	Drink with ionic-gelling sodium alginate formulation vs. drink with acid-gelling control	↓ peak blood glucose by 30% ↓ AUC of blood glucose by 52%	Harden et al. (2012)
Randomised, placebo-controlled, crossover design study	24 healthy adults	*Laminaria hyperborea*	8.13	Sodium alginate in chocolate milk vs placebo chocolate milk	↓ peak blood glucose by 38% ↓ peak serum insulin by 46% ↓ appetite by 134%	El Khoury et al. (2014)
Randomised, placebo-controlled, crossover design study	12 healthy adults	ND	0.625	Sodium alginate in sugar beverage containing soy protein isolate at pH 7 vs. control sugar beverage	↓ peak blood glucose by 53.2%. ↓ iAUC of blood glucose ↓ peak serum insulin	Huang et al. (2019)

*ND not disclosed; (AUC): area glycaemic under the curve; (iAUC): incremental glycaemic area under the curve

1.9 Cancer

Cancer is a multifactorial disease characterised by cells acquiring a growth and survival advantage, resulting in the uncontrolled division of abnormal cells (Atashrazm et al., 2015). It is often caused by genetic changes within cells, leading to the disruption of cellular pathways. This disruption causes cancer cells to function differently from normal cells (Atashrazm et al., 2015). Hanahan and Weinberg proposed eight fundamental characteristics commonly observed in cancer cells (Hanahan and Weinberg, 2011; Hanahan, 2022). These traits include the cells' ability to: (1) sustain their own growth signals, instructing the cells to grow and divide; (2) evade growth suppressors, permitting the cell to divide uncontrollably; (3) resist programmed cell death, ensuring cancer cells do not self-destruct; (4) enable replicative immortality, allowing cancer cells to divide indefinitely beyond a normal cell's limited proliferation potential; (5) promote the formation of their own blood vessels for oxygen and nutrient supply (angiogenesis); (6) activate the ability to invade and metastasise, allowing cancer cells to move to other organs and tissues to form new tumours; (7) reprogram cellular metabolism for energy production; and (8) avoid detection and destruction by the immune system. These hallmarks collectively contribute to the malignant behaviour of cancer cells and are central to the progression of cancer (Hanahan, 2022).

1.9.1 Cancer metastasis

The main cause of cancer-related deaths often stems not from the primary tumour itself but rather from the spread of cancer cells to other tissues and organs in the body, through a process known as metastasis. For metastasis to occur, cancer cells need to follow a series of sequential processes, as shown in Figure 1.5. Metastasis begins with local invasion, as individual cancer cells or cancer cell clusters detach from the primary tumour and acquire the ability to penetrate surrounding tissues by breaking through the basement membrane and extracellular matrix (ECM) (Fares et al., 2020; Martin et al., 2013). This process is facilitated by the activation or suppression of proteins involved in controlling migration and invasion (Martin et al., 2013). Subsequently, cancer cells may intravasate into nearby blood or lymphatic vessels, allowing them to enter the circulation and travel to new tumour sites (Fares et al., 2020; Jin et al., 2022). Once in the bloodstream or lymphatic system, cancer cells may become trapped in small capillaries within distant organs forcing them to extravasate into the surrounding tissue (Fares et al., 2020). The predominant form of extravasation involves paracellular migration, where tumour cells migrate between two endothelial

cells. Throughout this process, various ligands and receptors, such as selectins, cadherins, and integrins, play crucial roles in facilitating adhesion between the tumour cell and the endothelial cells (Castaneda et al., 2022). Upon extravasation, cancer cells colonise and establish micrometastases, small clusters of cancer cells that may remain dormant or progress into clinically detectable macrometastases by proliferation (Castaneda et al., 2022; Fares et al., 2020). This whole process is facilitated by angiogenesis, the formation of new blood vessels to sustain cancer cells, tumour growth and progression (Martin et al., 2013). Ultimately, metastasis leads to the formation of secondary tumours in distant tissues or organs, spreading cancer throughout the body and worsening the patient's prognosis (Castaneda et al., 2022). Over 90% of cancer-related deaths are attributed to metastasis, which is particularly lethal due to the systemic and pervasive nature of secondary tumours, as well as their increased resistance to drugs (Fares et al., 2020; Jin et al., 2022).

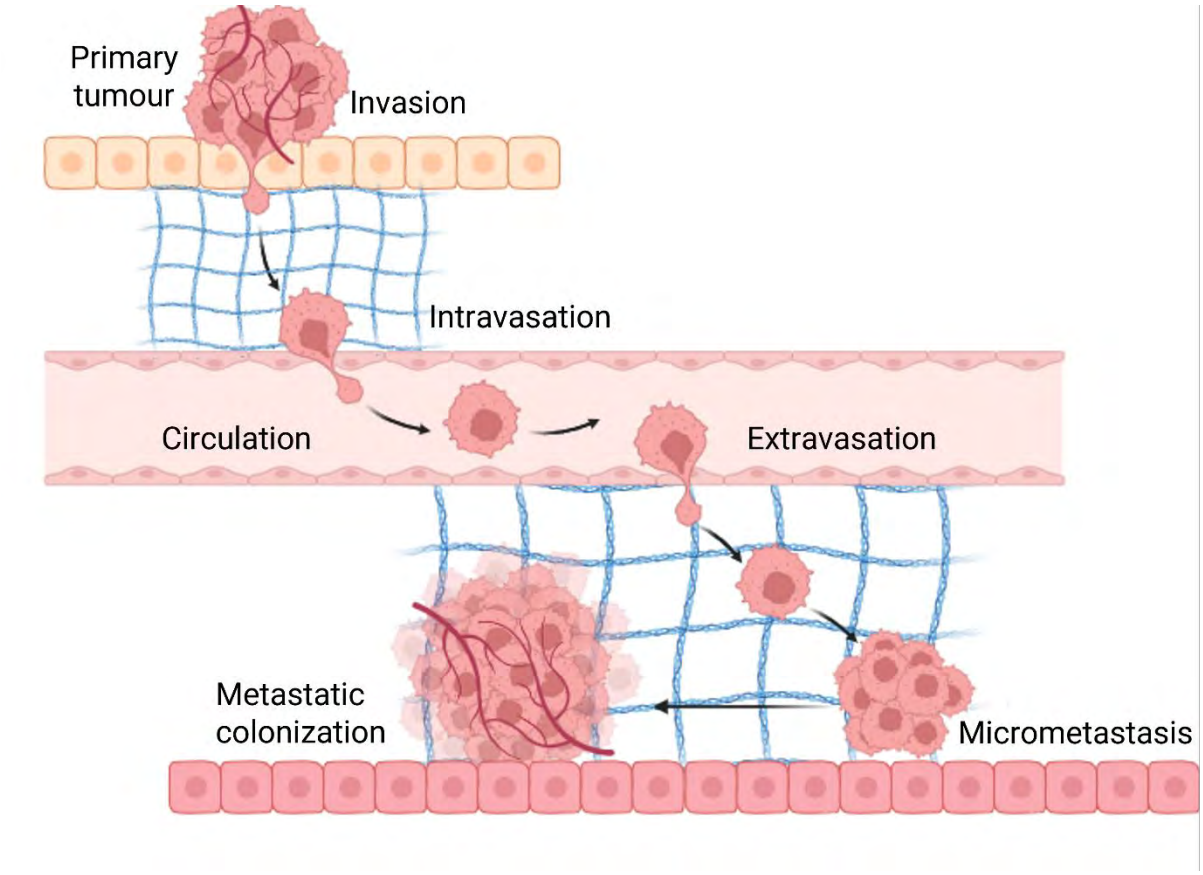

Figure 1.5: Graphic representation of the metastasis multistep process. The steps of metastasis include invasion, intravasation, circulation, extravasation, and colonization (Adapted from Fares et al., 2020).

1.9.2 Epithelial-mesenchymal Transition

During the initiation of metastasis, epithelial cancer cells undergo an epithelial-to-mesenchymal transition (EMT), a reversible process enabling cancer cells to engage in the metastatic cascade (Liu et al., 2021; Datta et al., 2021). EMT involves the loss of epithelial cell characteristics, including cell-cell adhesions mediated by tight, adherens, and gap junctions, as well as polarity, while acquiring a mesenchymal phenotype marked by increased migratory and invasive capabilities (Datta et al., 2021). Various signalling pathways, such as TGF-β, Wnt/β-catenin, and NOTCH, along with transcription factors like Snail, Slug, ZEB1/2, and Twist, orchestrate the downregulation of epithelial markers (e.g., E-cadherin) and the upregulation of mesenchymal markers (e.g., N-cadherin, vimentin) (Hsu et al., 2013; Liu et al., 2021).

Cadherins play a central role in facilitating adhesion at adherens junctions, cell-cell, or cell-matrix adhesive junctions by interacting with microfilaments through catenins (Martin et al., 2013). E-cadherin and N-cadherin play opposing roles in EMT: E-cadherin downregulation disrupts adherens and tight junctions, causing the loss of cell-cell adhesion and epithelial structure disruption, while N-cadherin upregulation reduces cell-cell adhesion, promoting interactions with other cells or the extracellular matrix, facilitating cell migration and invasion (Loh et al., 2019; Liu et al., 2021). Linked to the loss of E-cadherin, is the often-concurrent movement of β-catenin, which when no longer bound to E-cadherin, moves to the nucleus, where it further facilitates the transition toward a mesenchymal phenotype during EMT (Kalluri and Weinberg, 2009).

The cytoskeleton, crucial for maintaining cell structure and facilitating movement, also undergoes significant changes during EMT (Datta et al., 2021). Actin, as a key cytoskeletal component, undergoes remodelling closely linked to EMT (Datta et al., 2021). Vimentin, the expression of which increases during EMT, serves as a mesenchymal marker associated with poor prognosis in various cancers, including prostate, breast, melanoma, and colorectal cancers (Datta et al., 2021). The upregulation of vimentin facilitates the adoption of a more motile and invasive phenotype by cells, as it establishes the front-rear polarity essential for the efficient migration of tumour cells (Datta et al., 2021). Furthermore, vimentin promotes cell invasion by modulating the E-cadherin/β-catenin complex (Liu et al., 2021).

EMT also involves the restructuring of the cell's attachment to the ECM (Datta et al., 2021). Integrins, as cell surface receptors, mediate cell adhesion to the ECM and

undergo significant expression pattern changes during EMT (Martin et al., 2013; Lamouille et al., 2014). Epithelial cells downregulate certain integrins associated with cell-cell adhesion and basement membrane interaction, while upregulating others, facilitating interactions with ECM components in the tumour microenvironment, promoting cell detachment and invasion (Lamouille et al., 2014). Additionally, matrix metalloproteinases (MMPs), including MMP2 and MMP9, contribute to ECM remodelling by degrading various ECM components (Lamouille et al., 2014). MMP upregulation during EMT increases ECM degradation, facilitating cancer cell detachment from the primary tumour and invasion into surrounding tissues (Lamouille et al., 2014).

1.9.3 Role of Wnt/ ß-catenin pathway in the metastasis of cancer

One of the key pathways implicated in EMT is the Wnt/β-catenin signalling pathway. Overactivation of this pathway participates in EMT by upregulating the expression of EMT-related transcription factors (He and Gan, 2023). This pathway is involved in various cellular processes, including cell proliferation, differentiation, migration and polarity (Shah and Kazi, 2022; Liu et al., 2022). Central to this pathway is β-catenin, a key protein that regulates gene expression in response to Wnt signalling (Shah and Kazi, 2022). In the absence of Wnt ligands, β-catenin levels are kept low through a destruction complex composed of APC (adenomatous polyposis coli), axin, glycogen synthase kinase 3β (GSK-3β), and casein kinase 1 (CK1) (Liu et al., 2022; Shang et al., 2017). This complex phosphorylates β-catenin, targeting it for ubiquitination and proteasomal degradation (Shang et al., 2017). However, upon activation of this pathway the Wnt ligand binds to its receptor complex, inhibiting the destruction complex, resulting in the accumulation of non-phosphorylated β-catenin in the cytoplasm (Zhao et al., 2022; Shang et al., 2017). Subsequently, β-catenin translocates into the nucleus, where it interacts with T-cell factor/lymphoid enhancer factor (TCF/LEF) transcription factors to activate the transcription of Wnt target genes (Zhao et al., 2022; Shang et al., 2017).

Mutations in either the APC or β-catenin gene commonly occur in various cancers, especially in most colon cancers (Kaler et al., 2012). Loss-of-function mutations in APC, impair its ability to facilitate the degradation of β-catenin, resulting in β-catenin accumulation and the activation of Wnt signalling. Similarly, gain-of-function mutations in β-catenin can lead to β-catenin stabilisation and nuclear translocation even in the

absence of Wnt ligands. These mutations disrupt the balance of the β-catenin/Wnt pathway, contributing to oncogenesis and tumour progression in various types of cancers (Kaler et al., 2012; Liu et al., 2022).

1.9.4 Hippo pathway

The Hippo pathway acts as a tumour suppressor pathway, serving as a primary mechanism for controlling cell growth, regulating tissue expansion, and determining organ size by constraining cell proliferation (Zinatizadeh et al., 2021). Emerging evidence suggests that the Hippo pathway also influences EMT (Loh et al., 2019; Akrida et al., 2022). At the heart of the Hippo pathway lies a group of key proteins that regulate the activity of YAP (yes-associated protein) and TAZ (transcriptional coactivator with PDZ-binding motif), two important factors in cell growth and tissue development. When the Hippo pathway is active, these proteins phosphorylate YAP/TAZ, sequestering them in the cytoplasm and preventing their entry into the nucleus, where they would typically activate genes involved in cell proliferation and survival (Han, 2019). These proteins include MST1/2 (mammalian Ste20-like protein kinase 1/2) and LATS1/2 (large tumour suppressor kinase 1/2), which act as protein kinases to control the pathway. MOB 1 (monopolar spindle-one-binder protein) is also a crucial player in this process, acting as a central signal transducer (Gundogdu and Hergovich, 2019). When the Hippo pathway is activated, MST1/2 phosphorylate LATS1/2 and MOB1, forming an active MOB1/LATS complex. This complex then works to phosphorylate YAP/TAZ, preventing them from entering the cell nucleus and performing their functions. Additionally, NDR1/2 kinases, similar to LATS1/2, can also phosphorylate YAP1, keeping it in the cytoplasm. These proteins, including MOB1, LATS1/2, and NDR1/2, are directly influenced by MST1/2, forming a core network within the Hippo pathway (Gundogdu and Hergovich, 2019). Mutations and changes in the expression levels of key components in the Hippo pathway have been associated with promoting the migration, invasion, and malignancy of cancer cells (Han, 2019).

1.9.5 Cancer therapies

Current cancer therapies, consisting of a diverse array of treatment modalities, including chemotherapy, radiation therapy, surgery, or combinations thereof, are used to treat various types of cancers (Senthilkumar et al., 2013). Chemotherapy stands out as the main method in cancer management, targeting rapidly proliferating cancer cells and aberrant cellular mechanisms commonly observed in malignancies (Atashrazm et

al., 2015). However, the non-specific cytotoxicity of chemotherapy agents poses significant challenges, resulting in collateral damage to normal cells and consequential adverse events (Atashrazm et al., 2015). These limitations necessitate cautious dosage management, thereby often constraining treatment efficacy. Despite therapeutic advances, including immunotherapy, the prevention of metastasis and cancer recurrence remains a challenge, highlighting the ongoing need for innovative therapeutic strategies with improved efficacy and reduced toxicity (Ganesh and Massagué, 2021). In response to the shortcomings of conventional therapies, investigations into alternative treatment modalities have gained momentum. Among these, natural bioactive compounds, such as the polysaccharides fucoidan and sodium alginate, have emerged as promising candidates, offering potential therapeutic benefits while mitigating adverse effects (Senthilkumar et al., 2013).

1.9.6 Fucoidan's anti-cancer relevance

Fucoidan's anti-cancer mechanism has been reported to predominantly involve four key aspects: (1) halting of cell cycle progression, (2) triggering of apoptosis, (3) preventing angiogenesis and (4) inhibition of migration, invasion and metastasis (Jin et al., 2022; Zahariev et al., 2023).

The treatment of cancerous cells with fucoidans has been shown to induce cell cycle arrest at various stages and through different mechanisms of action, such as affecting the proper function of cyclins and cyclin-dependent kinases (CDKs) that regulate the cell cycle (Atashrazm *et al.,* 2015). Fucoidan caused hepatocellular carcinoma cell lines to accumulate in the G2/M phase of the cell cycle, whereas HUT-102 cells accumulated in the G1/S phase (Senthilkumar *et al.,* 2013). *F. vesiculosus* fucoidan down-regulated cyclin D1 and CDK4 resulting in G0/G1 arrest in cholangiocarcinoma CL-6 cells (Chantree et al., 2021). In addition, *F. vesiculosus* fucoidan arrested the HCT116 cell cycle at the G1 phase through the inhibition of CDK activity, mediated by the binding of CDK inhibitor proteins p21 and p27 to cyclin/CDK complexes, independent of alterations in G1 phase-associated cyclins and CDK proteins and irrespective of p53 status (Park et al., 2017).

The induction of apoptosis by fucoidan was demonstrated in multiple cancer cell lines. These studies showed that fucoidan induces apoptotic signals for the extrinsic and/ or intrinsic apoptotic pathways of various cancer types by activating or altering the expression of key apoptotic molecules, including mitochondria-associated proteins,

transcription factors, proteases and various cell cycle regulatory proteins (Lee et al., 2014). A study co-culturing *F. vesiculosus* fucoidan with HT-29 and HCT116 colon carcinoma cell lines revealed fucoidan-induced apoptosis in these cells, marked by caspase-3, -7, -8, and -9 activation, chromatin condensation, and PARP cleavage (Kim et al., 2010). This indicated the fucoidan's potential to induce apoptosis via both death receptor-mediated and mitochondria-mediated apoptotic pathways in HT-29 and HCT116 cell lines (Kim et al., 2010). In contrast, Zhang et al. (2011) showed that fucoidan from *Cladosiphon okamuranus* induced caspase-independent apoptosis in MCF-7 human breast cancer cells by up-regulating the expression of pro-apoptotic proteins Bax and Bad, and down-regulating the expression of anti-apoptotic proteins Bcl-2 and Bcl-x indicating fucoidan's modulation by a mitochondria-mediated apoptotic pathway.

Fucoidan exhibits anti-angiogenic properties primarily by inhibiting the binding of vascular endothelial growth factor (VEGF) to its cell membrane receptors (Zahariev et al., 2023; Jin et al., 2022). Fucoidan derived from *Undaria pinnatifida* effectively suppressed angiogenesis by downregulating the expression of VEGF-A in human umbilical vein endothelial cells (HUVEC) (Liu et al., 2012). Similarly, fucoidan extracted from *Sargassum thunbergii* significantly inhibited angiogenesis in HUVEC cells by attenuating MMP-2 activity and modulating VEGF/hypoxia-inducible factor-1α (HIF-1α) signaling (Hsu and Hwang, 2019). Furthermore, *in vitro* and *in vivo* studies have observed inhibition of angiogenesis with fucoidan from *F. vesiculosus*, which reduced the number of microvessels in a mouse breast cancer model using 4T1 cells (Atashrazm et al., 2015).

In addition, fucoidans have been shown to be capable of acting as potent inhibitors of the metastasis process, exerting their effects by impeding critical steps such as cell migration and colony formation, which play a key role in the process of tumour metastasis (Zahariev et al., 2023; Jin et al., 2022). Treatment with fucoidan sourced from *Padina boryana* effectively inhibited colony formation in colorectal carcinoma cells, DLD-1 and HCT116, showcasing its potential as a therapeutic agent against metastasis (Arumugam et al., 2019). The migration and invasion of tumour cells is intricately linked to the activity of matrix metalloproteinases (MMPs), which facilitate the degradation of ECM proteins (Zahariev et al., 2023). In this context, fucoidan treatment has demonstrated promising results in inhibiting the migration and invasion

of the 5637 bladder cancer cell line by downregulating the expression of MMP-9, a process mediated through the suppression of AP-1 and NF-κB binding activity (Cho et al., 2014). Fucoidan derived from *F. vesiculosus* exhibited significant inhibition of migration in HT-29 human colon cancer cells by targeting the PI3/Akt/mTOR/p70S6K1 pathway and suppressing MMP-2 expression (Han et al., 2015). In addition, studies involving highly metastatic MDA-MDB-231 breast cancer cells revealed that exposure to fucoidan inhibited the cells' ability to attach to platelets, which is crucial as platelets facilitate tumour cell migration (Atashrazm *et al.,* 2015).

1.9.7 The anti-cancer relevance of sodium alginate

Current emerging studies are extensively assessing sodium alginate as a delivery vehicle for chemotherapeutic agents in order to improve targeted delivery to cancer cells. The various delivery methods include the production of alginate hydrogels, tablets, capsules, liposomes, nanoparticles and microspheres (Shaikh et al., 2022). In this application, sodium alginate has been shown to be able to function as a carrier for targeted delivery, ensuring the selective uptake by tumour cells (Shaikh et al., 2022). Alginate has also been tested in combination with various other compounds to form sodium alginate/ZnO hydrogel beads to deliver curcumin in sodium alginate (SA)–polyvinyl alcohol (PVA)–bovine serum albumin (BSA) coated Fe3O4 nanoparticles to deliver the anti-cancer drug doxorubicin (Prabha and Raj, 2017; Wang et al., 2019). Furthermore, sodium alginate has been reported to have profound wound healing properties and has therefore found many uses, including as a wound powder, in pure form, or mixed with other drugs (Łabowska et al., 2019). Recently, alginate oligosaccharide (AOS) prepared from sodium alginate using alginate lyase showed anti-tumour activity on osteosarcoma cells (Chen et al., 2017). Also, in an *in vivo* study, a sodium alginate isolate from *Colpomenia sinuosa* significantly inhibited HCT116 colon cancer cell viability by accumulating cells in the sub-G1 phase and inducing apoptosis (Al Monla et al., 2022). Therefore, suggesting the potential anti-cancer activity of alginates.

Chapter 2- Research motivation, hypothesis and aims of study

2.1 Research motivation

Diabetes and cancer are chronic diseases that impose significant burdens on millions of individuals worldwide. As of 2024, the global prevalence of diabetes is estimated to affect 537 million people (Kumar et al., 2024). Notably, South Africa stands as the African country with the highest prevalence of diabetes (Thant et al., 2023). According to the International Diabetes Federation's 2021 report, 4.2 million adults in South Africa are living with diabetes, with half of them unaware of their condition (Thant et al., 2023). Cancer is recognised as one of the leading causes of illness and death. The most recent global cancer statistics reported 19.3 million cases and 10 million cancer-related deaths for the year 2020 (Chhikara and Parang, 2022). With cancer incidence inevitably on the rise, projections estimate that by 2030, there will be approximately 26 million new cancer cases and 17 million cancer-related deaths annually (Thun et al., 2010).

The limitations of the current pharmacological interventions for managing these diseases are numerous, and as a result, efforts are being made to develop therapies that are better tolerated and possess superior therapeutic properties. (Bradshaw Kaiser *et al.,* 2018; Siegel *et al.,* 2020). The emerging evidence of the therapeutic benefits of natural products has led to the widespread screening of various seaweed extracts for their potential to display anti-diabetic and anti-cancer properties (Holdt and Kraan, 2011). However, current studies often prioritise the rapid identification of compounds with promising activities - without an in-depth look into the mechanisms of action that underpin these favourable bioactivities.

Studies investigating compounds for the management of diabetes largely focus on their ability to inhibit the carbohydrate-digesting enzyme α-glucosidase. However, as noted by Attjioui et al. (2021), the standard α-glucosidase assay does not differentiate between the inhibition of its subtypes, maltase and sucrase, which play distinct roles in glucose release depending on the dietary carbohydrate composition. As individual diets and, therefore, the intake of sucrose and maltose vary, such differentiation may influence the effectiveness of an α-glucosidase inhibitor (Attjioui et al., 2021). In cancer treatment, cytotoxicity remains one of the most significant challenges associated with the use of chemotherapeutic agents (Atashrazm et al., 2015). To develop treatments effectively, an understanding of their mechanisms of action is integral to ensuring the

safety and effectiveness of compounds. Therefore, further investigations into seaweed-derived bioactive compounds remain important.

The natural compounds under investigation in this study, namely fucoidan and alginate, have demonstrated significant potential as anti-diabetic and anti-cancer agents, without any accompanying undesirable side effects. Most studies exploring the therapeutic potential of brown seaweed extracts have focused on species from China, Japan, and New Zealand. Consequently, South African seaweed extracts remain largely unexplored in this context.

2.2 Hypothesis

Fucoidans and alginates extracted from selected South African brown seaweeds exhibit inhibitory activity against key carbohydrate-hydrolysing enzymes relevant to T2DM and suppress colorectal cancer cell viability.

2.3 Aim

To identify South African seaweed extracted fucoidans and sodium alginates with anti-diabetic and anti-cancer activity and to investigate the mechanisms of action underpinning the pharmacological effects displayed by these compounds.

2.4 Objectives

To achieve this aim, the following objectives were set:

- To extract fucoidan and sodium alginate.
- To characterise the key chemical and structural features of the compounds.
- To evaluate the anti-diabetic activities of fucoidan and sodium alginate by investigating their ability to inhibit the key dietary starch-digesting enzymes (α-amylase, α-glucosidase, maltase and sucrase).
- To investigate the anti-cancer properties of the fucoidan and sodium alginate extracts on HCT116 colorectal human cancer cells.
- To identify some of the mechanisms of action of the extracts.

2.5 Thesis outline

- **Chapter 1** provides the general introduction and literature review introducing the global health challenges posed by T2DM and cancer. It highlights the need for novel treatment strategies and introduces fucoidan and sodium alginate, as

potential therapeutic agents. The chapter also reviews existing literature evaluating the bioactivity of these compounds in diabetes and cancer.

- **Chapter 2** presents the research motivation, hypothesis, and aims. It highlights the rationale for studying fucoidan and sodium alginate and outlines the key research objectives.
- **Chapter 3** focuses on the characterisation of the extracted fucoidans and sodium alginates using colorimetric and structural methods. This chapter details the chemical composition, structural features, identity confirmation, and purity assessment of the extracts.
- **Chapter 4** investigates the anti-diabetic activity of fucoidans and sodium alginates, focusing on their inhibition of key carbohydrate-digesting enzymes involved in T2DM management. The chapter discusses the significant enzyme inhibition results, compares efficacy with the commercial drug acarbose, and provides insights into the inhibition mechanisms using enzyme kinetics analysis.
- **Chapter 5** evaluates the anti-cancer activities of fucoidans and sodium alginates in human colorectal cancer cells (HCT116). The chapter investigates the effects of these compounds on various cellular processes critical to cancer progression, such as cell viability, proliferation, adhesion, migration, spheroid formation, and colony formation. Additionally, a more in-depth analysis of how selected fucoidans modulate key cancer-related pathways and signalling molecules is provided.
- **Chapter 6** presents the general discussion, future perspectives, and concluding remarks of this study.

Chapter 3- Extraction and partial characterisation of fucoidans and sodium alginates from South African brown seaweeds

3.1 Introduction

Fucoidan and alginate are some of the major polysaccharides in seaweeds that are of great commercial and research interest due to their desirable physicochemical characteristics and bioactive properties (Lorbeer et al., 2017). One of the most commonly accepted facts in the field is that the chemical structures of these polysaccharides determine their physical, chemical and biochemical properties and their biological activities (Dobrinčić *et al.,* 2020; Abka-Khajouei et al., 2022).

Fucoidans, even though they are now a well-known group of biopolymers, are commonly still described as sulphated polysaccharides consisting of predominantly L-fucose with a smaller proportion of 'other' monosaccharides. More recent studies recognise the chemical and structural diversity of fucoidans and that fucoidan may contain substantial amounts of 'other' monosaccharides such as D-galactose, D-glucose, D-mannose and D-xylose (Kopplin et al., 2018). As such, the term "fucoidan" now describes fucose-containing sulphated polysaccharides, including those of heterogeneous composition (i.e., fucogalactans, fucoglucuronans and xylofucoglucuromannans) (Kopplin et al., 2018; Kloareg et al., 2021). The heterogenous composition and resulting complex structure of fucoidans make it extremely difficult to fully elucidate the structural features of fucoidans (Zayed at al., 2020). Fundamentally, fucoidans are characterised by their monosaccharide composition, glycosidic linkages, branching, molecular weight and degree of sulphation and acetylation (Zayed at al., 2020).

Alginate, on the other hand, refers to the salt from of alginic acid and is a less complex linear anionic polysaccharide. The extraction of alginate using an alkaline medium such as sodium carbonate converts the seaweeds alginic acid into the sodium salt form of alginic acid known as sodium alginate (Wang et al., 2018). The main structure of sodium alginate is comprised of β-D-mannuronic acid (M) and α-L-guluronic acid (G) monomers. The ratio and arrangement of the M and G monomers in sodium alginate varies between species and is random with blocks of repeating M monomers (MM blocks), repeating G monomers (GG blocks), and mixed M and G monomers (MG/ MG blocks). Furthermore, the alginate polymer has abundant free hydroxyl and carboxyl

groups distributed along its backbone chain, that facilitate bonding between alginate molecules, which are also involved in the alginate-water interaction (Wang et al., 2018; Abka-Khajouei et al., 2022). The composition (M/G ratio) and sequence (arrangement of MM, MG, GG and GM blocks), in conjunction with its molecular weight, have an impact on the structure forming and functional properties of alginate. These factors are also crucial in determining the rheological properties of alginates. Structural and compositional information on sodium alginate can easily be obtained using a series of complementary approaches, i.e., NMR, FTIR, and uronic acid analysis (Abka-Khajouei et al., 2022).

To date, the natural seaweed population in South Africa represents one of the more unstudied marine habitats, with numerous species yet to be assessed for their bioactive potential. In this chapter, the content and composition of fucoidans and sodium alginates from four species of brown seaweeds were assessed, using solvent extraction methods, followed by basic biochemical assays and more complex analyses (chromatography, spectroscopy). The species were selected based on both availability and opportunity: *E. maxima* was included due to its large-scale commercial use and assured supply, while *E. radiata*, *S. elegans* and *S. cymosum* were collected opportunistically from the nearby coastline. This combination enabled the inclusion of a commercially relevant species while also assessing underexplored local species.

3.2 Objectives

The objectives of the experiments performed in this chapter were to:

- Extract fucoidan and sodium alginate from selected South African brown seaweeds; and
- Characterise the chemical composition and structural features of the extracted fucoidans and sodium alginates.

3.3 Materials and Methods

3.3.1 Materials

The commercial fucoidan from *Fucus vesiculosus* (Cat. No. F5631) and sodium alginate (Cat No. W201502) were purchased from Sigma Aldrich (St. Louis, MO, USA). The analytical kits used in this study were purchased from Megazyme^{TM} (Bray, WC, Ireland). All other reagents used in these experiments were purchased from Sigma-

Aldrich, MERCK (Darmstadt, HE, Germany), Fluka (Munich, BY, Germany) and Megazyme™ (Bray, WC, Ireland) (see Appendix Table A1).

3.3.2 Seaweed sampling and processing

The brown seaweed species *Ecklonia radiata*, *Sargassum elegans* and *Sargassum cymosum* were harvested from three separate coastal locations in the Eastern Cape, South Africa: Middle beach (-33° 41' 42.0102" E; 26° 40' 1.7436" S), Kelly's beach (-33° 36' 37.1442" S; 26° 53' 26.073" E) and Bonza Bay beach (-32° 58' 48.9648" S; 27° 57' 32.9292" E), respectively (Figure 3.1). *E. radiata* was collected as beach-cast, while *S. elegans* and *S. cymosum* were harvested from rockpools in the intertidal zone. The seaweeds were identified based on morphology by Professor John Bolton from the Department of Biological Sciences at the University of Cape Town. *Ecklonia maxima* was kindly donated by the HIK-Abalone Farm located in Hermanus, Western Cape, South Africa. The harvested seaweeds were transported on ice to the laboratory for processing. Seaweeds to be processed immediately were rinsed thoroughly with distilled water and oven-dried for 72 hours at 50 °C. The dried seaweed was pulverized using a coffee grinder and stored at room temperature until use. The remainder of the fresh seaweed was stored at -20 °C.

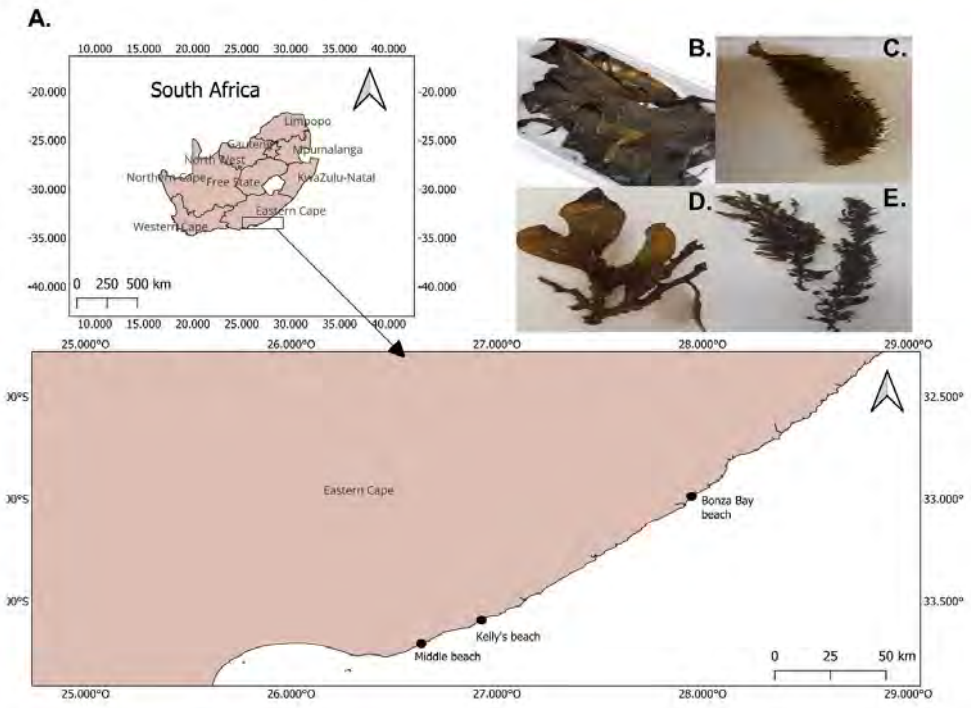

Figure 3.1: Sampling location and images of harvested seaweeds. (A) Map showing the sampling sites for *Ecklonia radiata*, *Sargassum elegans*, and *Sargassum cymosum* within the Eastern Cape province of South Africa. (B-E) Images of all brown seaweed species used in this study were taken shortly after harvesting and prior to processing. (B) *Ecklonia maxima*, (C) *Ecklonia radiata*, (D) *Sargassum elegans*, and (E) *Sargassum cymosum*.

3.3.3 Extraction of fucoidan

Fucoidan was extracted from *E. maxima*, *E. radiata*, *S. elegans* and *S. cymosum* using the hot water extraction described by Yang et al. (2008), with slight modifications. Briefly, the dried pulverized seaweeds were soaked in 85% (v/v) ethanol overnight to remove pigments. Fucoidan was extracted from dry depigmented seaweed (20 g) into 65°C distilled water (400 ml) over 6 hours. The fucoidan-containing supernatant was collected by centrifugation (5000 ×*g* for 20 minutes at 4°C) and incubated in 1% (w/v) $CaCl_2$ overnight at 4 °C to precipitate alginate. The precipitate was removed by centrifugation (5000 ×*g* for 20 minutes at 4°C). Ethanol [99% (v/v)] was added to the supernatant to a final concentration of 30% (v/v) and the solution was centrifuged as described previously to remove any remaining alginate and co extracted compounds. The collected supernatant was adjusted to a final ethanol concentration of 70% (v/v) and incubated overnight at 4°C to allow the fucoidan to precipitate. The fucoidan was collected by centrifugation at 10,000 ×*g* for 10 minutes at 4°C, washed with ethanol [99% (v/v)] followed by acetone and dried at ambient temperature overnight. The fucoidan yield (% w/w) was expressed relative to the seaweed's dry weight.

3.3.4 Extraction of sodium alginate

Sodium alginate was extracted from *E. maxima*, *E. radiata*, *S. elegans* and *S. cymosum* using an alkaline extraction method as described by Torres *et al.* (2007) and Fertah *et al.* (2014) with minor modifications. Dried pulverised seaweed samples were soaked in 2% (v/v) formaldehyde for 24 hours to eliminate pigments, washed with distilled water and incubated in 0.2 M HCl for a further 24 hours. After this, the samples were rewashed with distilled water, prior to being extracted under agitation at 40°C for 5 hours in 2% (w/v) sodium carbonate. Following the extraction, sodium alginate was precipitated with 80% (v/v) ethanol and collected by centrifugation (10,000 × *g* for 10 min). The collected precipitate was purified by filtration through a nylon membrane (0.45 µm pore size, Whatman International Ltd., Maidstone, UK), washed with ethanol, methanol and acetone, dried under ambient atmosphere and the extraction yield (% w/w) was expressed relative to the seaweed's dry weight.

3.3.5 Chemical characterisation of fucoidan and sodium alginate

3.3.5.1 Total protein content

The Bradford assay (Bradford, 1976) was used to determine the co-extracted protein content in the fucoidan and sodium alginate extracts. Briefly, 25 µl of extracts (1 mg.ml^{-}

^{1}) and bovine serum albumin (BSA) standards were mixed with 230 µl of Bradford's reagent. The reaction was incubated at room temperature for 20 minutes and the absorbance was read at 595 nm with an Epoch™ 2 microplate reader (BioTek with Gen 5™ software), and the protein concentrations were determined using the BSA (bovine serum albumin) standard curve (see Appendix Figure B1).

3.3.5.2 Total phenolic content

The Folin–Ciocalteu method, described by Malgas et al. (2016), was used to determine the total phenolic content. The hydrolysed extracts at 1 mg.ml^{-1} (10 µl) were incubated in 180 µl of distilled water and 20 µl of Folin–Ciocalteu reagent for 10 minutes at room temperature. Thereafter, 50 µl of 2 M sodium carbonate was added and the reactions were covered and incubated for a further 30 minutes at 37°C before reading absorbance at 765 nm using an Epoch™ 2 microplate reader (BioTek with Gen 5™ software). The total phenolic content was interpolated using a gallic acid standard curve (see Appendix Figure B2).

3.3.5.3 Total carbohydrate content

Fucoidan extracts were assessed for total carbohydrate content following the phenol-sulphuric acid method developed by Dubois et al. (1956). Briefly, to a volume of 100 µl of fucoidan (1 mg.ml^{-1}), 300 µl of concentrated sulphuric acid (97%) followed by 50 µl of 5% (w/v) phenol were added. The reaction was vortexed and heated at 90°C for 10 minutes. After cooling to room temperature, the absorbance was measured at 490 nm using an Epoch™ 2 microplate reader (BioTek with Gen 5™ software). The total carbohydrate content was determined using an L-fucose standard curve (see Appendix Figure B3).

3.3.5.4 Sulphate quantification

Fucoidan and alginate stock solutions (1 mg.ml^{-1}), prepared in 60% (v/v) formic acid, were hydrolysed overnight at 100°C. Following hydrolysis, samples were dried in a Centrivap (Vacutec) for 6 hours at 80°C. The dried samples were reconstituted to a concentration of 1 mg.ml^{-1} in dH_2O and assessed for sulphate content following the gelatine-barium method developed by Dodgson et al. (1961), with volumes scaled down for use in a microtiter plate. To 380 µl of 4% (w/v) trichloroacetic acid (TCA), 20 µl of fucoidan sample, followed by 100 µl of $BaCl_2$ reagent, was added. The reaction was mixed and incubated at room temperature for 20 minutes. The absorbance was

measured at 360 nm and the sulphate content interpolated using the sulphate (SO_4^{2-}) standard curve constructed with sodium sulphate (see Appendix Figure B4).

3.3.5.5 Acid hydrolysis of fucoidan and sodium alginate

Fucoidan and sodium alginate extracts (10 $mg.ml^{-1}$) were hydrolysed in 2 M trifluoroacetic acid (TFA) at 100°C for 6 and 10 hours, respectively. The hydrolysed samples were dried in a Centrivap (Vacutec Ltd., Roodepoort, South Africa) at 80°C for 6 hours and reconstituted to a concentration of 10 mg. ml^{-1} using dH_2O.

3.3.5.6 Total reducing sugar determination

The total reducing sugar content in the fucoidan extracts was measured using 3,5-dinitrosalicylic acid (DNS) method described by Miller (1959). Briefly, 150 µl of hydrolysed fucoidan (1 $mg.ml^{-1}$) was mixed with 300 µl of DNS reagent [1% (w/v) NaOH; 1% (w/v) dinitrosalicylic acid; 20% (w/v) sodium potassium tartrate; 0.2% (w/v) phenol and 0.05% (w/v) sodium metabisulphite]. The reactions were heated (Labnet AccuBlock™ digital dry bath) to 100°C for 6 minutes, then cooled on ice for 6 minutes, loaded on a 96 well plate and the absorbance was read at 540 nm (Epoch™ 2 spectrophotometer from BioTek with Gen 5™ software). Reducing sugars within the fucoidan extracts were quantified using a D-glucose standard curve (see Appendix Figure B5).

3.3.5.7 Total uronic acid determination

The uronic acid content within the hydrolysed fucoidan and sodium alginate extracts (1 $mg.ml^{-1}$) was determined according to the instructions of the microplate Megazyme™ assay kit (K-URONIC).

3.3.5.8 Monosaccharide composition analysis

Monosaccharide composition analysis was performed on a Shimadzu HPLC system (Shimadzu Corp, Kyoto, Japan) equipped with a refractive index detector (RID) using a Fortis Amino analytical column (4.6 x 150 mm) (Fortis Technologies Ltd., Neston, UK). The isocratic mobile phase consisted of HPLC grade acetonitrile and degassed H_2O (Milli-Q, MERCK) in a ratio of 3:1. The column temperature was set at 40°C and separation was performed within 15 minutes at a flow rate of 0.8 ml/min. All hydrolysed fucoidan samples (1 $mg.ml^{-1}$) and monosaccharide standards (D-arabinose, D-galactose, D-fructose, L-fucose, D-glucose and D-mannose) were injected using an

injection volume of 20 µl. The monosaccharides within the fucoidan were quantified using regression equations from established standard curves (see Appendix Table B1). The xylose content within the hydrolysed extracts (1 mg.ml^{-1}) was determined according to the microplate Megazyme^{TM} assay kit instructions (K-XYLOSE).

3.3.5.9 Mannuronic and guluronic acid determination

Mannuronic and guluronic acid in the hydrolysed sodium alginates were quantified using a Shimadzu HPLC system (Shimadzu Corp, Japan) equipped with a diode array detector (DAD), where chromatographic separation was achieved on a Hypersil Gold^{TM} Sax column (Phenomenex, Torrance, CA, U.S.A.) under ambient conditions. Elution was performed under isocratic conditions with a mobile phase of 50 mM phosphate buffer adjusted to pH 3.0 with ortho-phosphoric acid, at a flow rate of 0.8 ml/min over 10 min. The injection volume for the samples and standards was 10 µl and the UV absorption of the effluent was monitored at 214 nm. Standard curves for mannuronic and guluronic acid were constructed to determine the amounts of the respective uronic acids in the sodium alginate samples (see Appendix Figures B7 and B8).

3.3.6 Determination of molecular properties of fucoidan and sodium alginate

3.3.6.1 Molecular weight determination

The molecular weights of the fucoidans and sodium alginates were determined using high-performance size exclusion chromatography (HPSEC) with a refractive index detector (HPLC-RID). Chromatographic separation was achieved using a Shodex OHpak SB-806M HQ (8.0mmI.D. x 300mm) column (Showa Denko, Tokyo, Japan) with 0.1 M $NaNO_3$ aq.as the mobile phase over 25 minutes at a flow rate of 0.5 ml/min. The column temperature was set at 30°C. An injection volume of 20 µl was used for all samples, as well as for the pullulan standards (Shodex, Tokyo, Japan), which were used to construct the Log M_W vs. retention time curve for molecular weight determination (see Appendix Figure B9). The number molecular weight (Mn), molecular weight (Mw), and polydispersity index (PDI) were calculated as follows (Zayed et al., 2020):

$$Mn = \frac{\sum N_i M_i}{\sum Ni}$$

$$Mw = \frac{\sum N_i M_i^2}{\sum N_i M_i}$$

$$PDI = \frac{Mw}{Mn}$$

where M_i represents the molecular weight of a chain, and N_i denotes the number of chains with that molecular weight.

3.3.6.2 Thermogravimetric analysis (TGA)

Thermogravimetric analysis (TGA) was performed on a Pyris Diamond model thermogravimetric analyser (PerkinElmer®, Waltham, MA, USA). Briefly, in an aluminium crucible, ~ 4 mg of sample powder was heated from 30 °C to 800 °C at a heating rate of 30 °C/min with a continuous supply of nitrogen (20 ml/min). A separate run using an empty aluminium crucible was conducted for baseline correction. The weight loss relative to the temperature increase was plotted as TGA curves and the degradation rates at different temperatures were plotted as differential thermogravimetric (DTG) curves.

3.3.6.3 Kinematic viscosity determination

The kinematic viscosities of 1% (w/v) solutions of fucoidan and sodium alginate in dH_2O were measured using a semi-micro glass capillary viscometer of capillary diameter size 50 (Cannon-Manning (State College, PA, USA) at 25°C. Samples were equilibrated to the required temperature for 30 min before taking measurements. An average of no fewer than four readings was taken using two separately prepared replicates of the different samples. Distilled water was run as a control. To obtain the kinematic viscosity in mm^2 /s (cSt) the efflux time in seconds was multiplied by the viscometer constant (K= 0.003992) using the following equation:

$$viscosity = \text{viscometer constant (K)x time (s)}$$

3.3.7 Structural characterisation of fucoidan and sodium alginate

3.3.7.1 Fourier transform infrared spectrometer (FT-IR) analysis

Infrared spectra of the fucoidan and sodium alginate extracts were recorded on a Spectrum 100 FT-IR spectrometer system (*PerkinElmer*®, Waltham, MA, USA) equipped with a ZnSe (zinc selenide) ATR crystal. Each sample was pressed uniformly and tightly against the sample spotting surface using a spring-loaded anvil. FT-IR spectra were obtained by averaging four scans from 4000 to 600 cm^{-1} with a resolution of 4 cm^{-1}. Baseline and ATR corrections for penetration depth and frequency variations were performed using Spectrum™ One software (version 1.2.1) system (*PerkinElmer*®, Waltham, MA, USA).

3.3.7.2 Nuclear magnetic resonance (NMR) analysis

The fucoidan and sodium alginate samples were dissolved in D_2O at 10 mg.ml^{-1} and insolubilised particles were removed by centrifugation at 13,000 ×*g* for 2 min. The ^{1}H NMR spectra were recorded at 70°C using a Bruker Avance III (Fällanden, ZH, Switzerland) 600 MHz NMR spectrometer (with a cryoprobe for variable-temperature measurements) equipped with TopSpin NMR software, version 3.6.5 (Bruker, Billerica, MA, USA). The block structure and M/G ratio of the sodium alginates was calculated from the area under the ^{1}H NMR signal peaks denoted as (I-III) according to the calculation proposed by Grasdalen et al. (1979) using the following equations:

$$FG = AI/(AII + AIII)$$

$$FM = 1 - FG$$

$$FGG = AIII/(AII + AIII)$$

$$FGM = FG - FGG$$

$$FMM = FM - FGM$$

$$M/G = FM/FG$$

3.3.7.3 X-ray diffraction (XRD) analysis

The crystallinity of the extracts was determined by X-ray diffraction using Cu K radiation (1.5405 Å, nickel filter) on a Bruker D8® Discover equipped with a proportional counter. The samples were scanned from 2θ of 5 to 60º with a step size of 0.02º. The determination time was 0.02º per second.

3.4 Results and Discussion

3.4.1 Fucoidan and sodium alginate extraction yield

Solvent extraction methods were employed to extract fucoidan and sodium alginate from the four South African seaweeds. The obtained fucoidan and sodium alginate yields (expressed as a percentage of seaweed dry weight) are shown in Figure 3.2. The *Ecklonia* species gave higher yields of fucoidan of between 3-6% (w/w) compared to the *Sargassum* species, which yielded less than 2% (w/w). The fucoidan extraction yields for the *Ecklonia* species were close to those reported by Mabate et al., 2023 and Lorbeer et al., 2015 for *E. maxima* (5.4%) and *E. radiata* (3.75%), respectively. The

lower yields obtained for the *Sargassum* species are not surprising and fall into the general range of 0.63-4.3% (w/w) yields reported for fucoidans isolated from *Sargassum* species (Husni et al., 2022; García-Ríos et al., 2012).

The sodium alginate yields obtained from these seaweeds were considerably higher, with values of around 40% (w/w) - see Figure 3.2. The *Ecklonia* species yields were comparable, but marginally lower by around 3-9%, than the alginate yields obtained from the two *Sargassum* species. Since the alginates were extracted via the alkaline extraction method, the results obtained agreed well with those yields reported in the literature for these species (Belattmania et al., 2020; Lorbeer et al., 2015; Filippo-Herrera et al., 2018). Given the relatively high yields of fucoidans and alginates (exceeding 2%, even for those derived from *Sargassum*), supply challenges commonly associated with marine-derived compounds may be less of a concern if any of these were developed for therapeutic use.

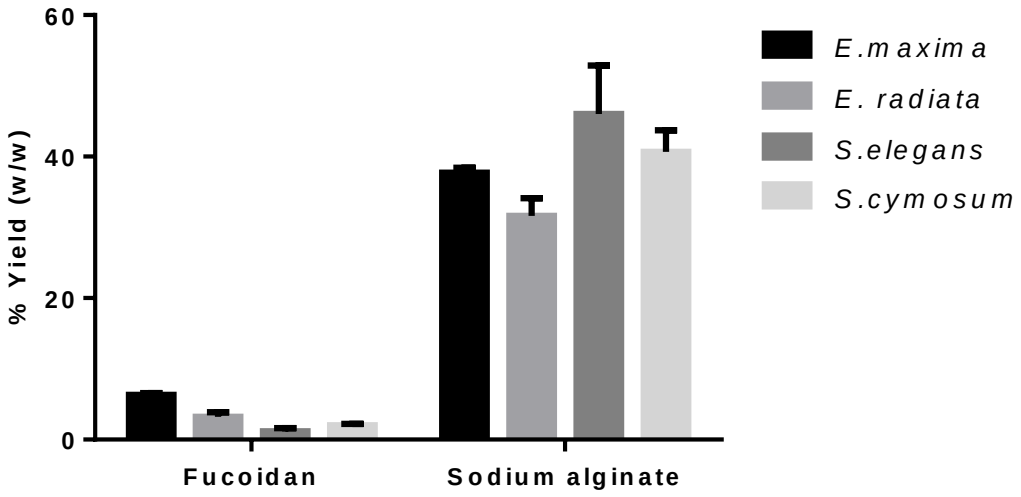

Figure 3.2: Fucoidan and sodium alginate extraction yields as a percentage of seaweed biomass dry weight. The bars represent the yields in terms of means ± SD from 3 technical replicates (n=3).

3.4.2 Chemical composition of the fucoidans

The chemical composition of the fucoidans extracted from the South African brown seaweeds is presented in Table 3.1, along with the commercial fucoidan from *Fucus vesiculosus* (a well-studied variant), which was included as a positive control. As can be seen in Table 3.1, fucoidans consisted mainly of carbohydrates and sulphate groups. Among these fucoidans, the *Ecklonia* species derived fucoidans were found to

have a high total carbohydrate content (>90%) compared to that detected in the commercial fucoidan (43%) and *Sargassum* species fucoidans (<39%). In contrast, sulphate content analysis showed that the commercial and *Sargassum* sp. fucoidan were highly sulphated, while the *Ecklonia* sp. reported lower sulphate content. The sulphate content of *E. radiata*'s was particularly low, at less than 4%. Of the highly sulphated fucoidans, *S. cymosum* fucoidan reported the highest sulphate content of 38.85%, followed by the commercial, *S. elegans* and *E. maxima* fucoidans that contained about 25%, 20% and 16%, respectively (Table 3.1). Previous studies on the composition of fucoidans from numerous brown seaweeds have reported results of total carbohydrate (22-59%) and sulphate content (4-48%) similar to those reported in this study (Lorbeer et al., 2017; Ponce and Stortz, 2020). In addition, the total carbohydrate content in the *Ecklonia* species was only slightly higher than the highest total carbohydrate content for fucoidan reported in literature, which was about 87% (Sanniyasi et al., 2023).

To obtain a more detailed chemical profile of these fucoidans, the content of specific monosaccharides was determined using HPLC analysis following 2 M TFA hydrolysis. The detection and separation profiles of the monosaccharide standards are shown in Appendix Figure B6. The monosaccharide compositions of the fucoidans are listed in Table 3.1 and showed a notable difference in the relative proportions of the various monosaccharides within the fucoidans. The commercial fucoidan was predominantly composed of L-fucose (51.50%) and L-arabinose (30.45%) with an appreciable amount of D-galactose (9.14%) and minor amounts of D-glucose (<5%) and D-xylose (<1%). This composition aligns with the findings of Bittkau and colleagues (2020), who reported that fucoidan from *Fucus vesiculosus* is predominantly composed of L-fucose, with the remainder consisting of a mixture of D-galactose, D-glucose, D-mannose, and D-xylose. Similar to the commercial fucoidan, the fucoidans from the *Sargassum* species consisted mainly of L-fucose (>48%). However, instead of L-arabinose, which is still detected in appreciable amounts, they contain D-galactose (>15%) as a prominent monosaccharide along with minor amounts of D-fructose (~5%), D-glucose (~3%) and D-xylose (<1%). On the other hand, the *Ecklonia* species fucoidans reported D-glucose and L-fucose as the principal constitutive monosaccharides, with D-glucose being the more predominant of the two sugars, see Table 3.1. While the non-fucose content of *E. radiata* fucoidan mainly consisted of glucose (76.03%), *E. maxima,* in addition to 35.10% D-glucose, contained 12.14% D-galactose and 16.03% D-mannose.

Despite the consensus view in the literature that L-fucose is the main monosaccharide in fucoidans, these monosaccharide profiles are consistent with those reported by January et al. (2019) and Lorbeer et al. (2015), for *E. maxima* and *E. radiata,* respectively, as well as other fucoidans (Li et al., 2023).

The main contaminants in seaweed-extracted fucoidans are other cell wall constituents, including proteins, phenolics, and alginates (Zhang et al., 2020). Quantification of protein, phenolic, and uronic acid content (Table 3.1) revealed that these contaminants were present at low concentrations, with their combined total being less than 6% across all fucoidans. All extracts contained small amounts of phenolics (<2%), while proteins were found in low quantities (<4%) in the *F. vesiculosus* and *Ecklonia* spp. fucoidans but were absent in the *Sargassum* spp. fucoidans. Additionally, uronic acid levels, which can indicate alginate contamination, were also low (<2%) in all extracts, suggesting negligible alginate content.

Table 3.1: Chemical composition profiles of the fucoidan extracts and commercial *F. vesiculosus* fucoidan

Fucoidan source	Total carbohydrate[a] (%)	Total RS[a] (%)	Protein[a] (%)	Phenolic[a] (%)	Sul[a] (%)	Total uronic acid[a]	Monosaccharide composition (%)						
							Ara[b]	Fruc[b]	Fuc[b]	Gal[b]	Glc[b]	Man[b]	Xyl[b]
***F. vesiculosus* (control)**	43.87 ± 0.40	13.33 ± 0.23	1.68 ± 0.42	1.76 ± 0.06	25.07 ± 0.55	1.72 ± 0.28	30.45 ± 1.79	ND	51.50 ± 2.01	9.14 ± 1.48	5.46 ± 0.15	ND	0.13 ± 0.02
E. maxima	92.70 ± 3.32	33.25 ± 0.71	4.33 ± 0.38	0.34 ± 0.06	15.97 ± 1.37	0.65 ± 0.23	ND	ND	30.80 ± 1.86	12.14 ± 1.03	35.10 ± 0.47	16.03 ± 0.72	0.14 ± 0.01
E. radiata	96.64 ± 1.51	50.68 ± 0.35	3.18 ± 0.74	0.71 ± 0.03	3.81 ± 0.28	1.33 ± 0.04	ND	3.21 ± 0.20	20.73 ± 2.14	3.21 ± 0.20	76.03 ± 1.53	ND	0.21 ± 0.01
S. elegans	39.93 ± 2.78	16.57 ± 0.21	ND	2.18 ± 0.13	19.87 ± 0.60	1.48 ± 0.29	9.45 ± 0.12	4.96 ± 0.31	57.39 ± 1.23	24.89 ± 0.96	3.25 ± 0.07	ND	0.61 ± 0.11
S. cymosum	16.22 ± 0.48	10.48 ± 0.01	ND	2.01 ± 0.12	38.85 ± 2.77	0.62 ± 0.19	15.45 ± 0.55	5.16 ± 0.00	48.16 ± 1.11	16.83 ± 0.23	3.96 ± 0.46	ND	0.29 ± 0.15

* RS, reducing sugar; Sul, Sulphate; Arab, L- arabinose; Fruc, D-fructose; Fuc, L-fucose; Gal, D-galactose; Glc, D-glucose; Man, D-mannose; Xyl, D-xylose; [a] percentage composition of fucoidan (w/w); [b] percentage composition of fucoidans' sugar content (w/w); ND: Not detected. The data values represent the means ± SD of technical replicates (n=3).

3.4.3 Chemical composition profiles of sodium alginates

Chemical composition analysis evaluated the quality of the sodium alginates extracted from the two *Ecklonia* and two *Sargassum* species. As is evident from the results in Table 3.2, the chemical composition of the sodium alginate extracts closely reflect that of the commercial alginate (Sigma Aldrich). The extracts consisted mainly of the uronic acids D-mannuronic and L-guluronic acid that comprise alginate. The amounts of total uronic acid content (25-39%) in the tested alginates, despite appearing low when compared to that obtained (>49%) for the commercial alginate in this study, are comparable to the total uronic acid content of 27 and 29% reported in the literature for the species *L. digitata* and *M. pyrifera* which are commercially exploited for alginate (Rhein-Knudsen et al. 2017). The M/G ratios of the commercial and extracted sodium alginates were found to be greater than 1, indicating a dominance of D-mannuronic acid over L-guluronic acid (Belattmania et al. 2020). The relative abundance of the D-mannuronic to L-guluronic acid content was similar between the extracts as indicated by their M/G ratios (Table 3.2). These ratios were similar to data available in the literature for the same species of alginate-producing seaweeds. The M/G ratio of *E. radiata* (3.28) was high, compared to that reported for alginate extracted from *E. radiata* collected from Australia (1.18 - 1.59), However, the M/G ratio noted for the commercial alginate falls within the M/G ratios noted previously for the same Sigma-Aldrich alginate (Belattmania et al. 2020; Lorbeer et al., 2017).

As alginates also occur in the highly complex matrices of cell walls and intercellular spaces, along with other carbohydrates (e.g., the sulphated fucose-based fucoidan as well as the glucose-based polysaccharides cellulose and laminarin), polyphenols and proteins; co-extraction of these is probable (Torres et al., 2007; Zayed et al.,2020). The level of impurities in the alginate extracts and the commercial alginate standard were similar (Table 3.2). As the chemical composition analysis revealed a low amount of L-fucose (>0.62%) and the absence of sulphate groups, the level of contamination of the alginate polysaccharides by fucoidan residues was assumed to be negligible. Furthermore, the low content of glucose (<1%) confirmed the absence of significant amounts of cellulose and laminarin. Moreover, other monosaccharides, protein (<1.54%) and phenolics (<0.08) were only present as minor components. This again implies that the sodium alginate extracts were relatively pure.

Table 3.2: Chemical profile of the sodium alginate extracts and commercial sodium alginate

Sodium alginate source	Total protein[a]	Total phenolics[a]	Total reducing sugar[a]	L- fucose[a]	D- glucose[a]	D- xylose[a]	Sul[a]	Total uronic acid[a]	D- mannuronic acid[b]	L- guluronic acid[b]	M/G ratio
Commercial (control)	1.37 ± 0.51	0.04 ± 0.00	3.75 ± 0.01	ND	0.29 ± 0.12	0.13 ± 0.04	ND	49.28 ± 0.37	53.61 ± 4.36	19.25 ± 2.51	2.78
E. maxima	1.54 ± 0.28	0.03 ± 0.00	3.84 ± 0.02	0.62 ± 0.17	0.47 ± 0.17	0.11 ± 0.05	ND	30.50 ± 1.06	75.83 ± 3.00	19.21 ± 3.22	3.95
E. radiata	0.88 ± 0.14	0.09 ± 0.02	4.78 ± 0.02	0.84 ± 0.29	0.72 ± 0.11	0.18 ± 0.04	ND	35.99 ± 5.96	54.24 ± 5.03	16.48 ± 1.79	3.28
S. elegans	1.42 ± 0.54	0.03 ± 0.01	2.86 ± 0.02	ND	0.43 ± 0.00	0.37 ± 0.07	ND	35.85 ± 2.81	70.50 ± 4.34	20.84 ± 1.27	3.39
S. cymosum	1.34 ± 0.55	0.02 ± 0.01	3.80 ± 0.01	ND	0.03 ± 0.06	0.27 ± 0.00	ND	25.97 ± 1.87	66.40 ± 5.06	19.32 ± 1.50	3.44

* [a] all values are given as percentage composition of sodium alginate per weight; [b] D-mannuronic acid and L-guluronic acid content as a percentage of total uronic acid content. The data values represent the means ± SD of technical replicates (n=3).

3.4.4 Molecular weight properties of the fucoidans and alginates

The molecular weight (Mw) distribution of the polysaccharides was analysed by HPSEC using a Mw standard calibration curve constructed from pullulan standards (see Appendix Figure B9). Table 3.3 shows the average molecular weight (Mw), the number average molecular weight (Mn), and the polydispersity index (PDI) of the fucoidans and sodium alginates. The Mw values, which provide an indication of the average size of the polysaccharides, indicated that the fucoidans ranged in Mw from 2.61 - 309.34 kDa. Based on the classification of fucoidans as low molecular weight (<10 kDa), medium weight molecular (10-10,000 kDa) or high molecular weight (>10,000 kDa) fucoidans, the Mw values of the *S. cymosum* fucoidan would be classified as a low molecular weight fucoidan, while the other fucoidans are regarded as medium molecular weight fucoidans (Senthilkumar et al., 2013). The PDI, as a measure of the ratio of Mw and Mn, reflects the size heterogeneity of these polymers, where a higher PDI denotes a more heterogenous distribution of the polymer's molecular weight (Dobrinčić et al., 2022). The PDI value of the fucoidans ranged from 1.00 to 6.86 in this study (Table 3.3), which match the PDI value range of 1 to 6.2 reported in literature for fucoidans (Dobrinčić et al., 2022). As is evident from the PDI values of >3, the *E. maxima* and *S. elegans* fucoidans consisted of molecular weight fractions that varied greatly in size (see Table 3.3). Interestingly, the *S. elegans* fucoidan contained a total number of four molecular weight fractions ranging in size from 371 kDa to 3.2 kDa, while the *E. maxima* fucoidan contained only two molecular weight fractions, the larger being 365 kDa in size, and the smaller fraction, 14 kDa. In contrast, the other fucoidans exhibited Mw fractions that were closely aligned with their reported average Mw values, showing less variation between fractions.

The extracted alginates were generally larger in size, with their Mw values ranging from 194.27 kDa to 304.24 kDa, while the commercial sodium alginate had a lower molecular weight of 78.49 kDa (Table 3.3). These values were within the range of reported sodium alginate Mw values of 48 – 756 kDa and compare well with the previously reported Mw value for the Sigma- Aldrich commercial alginate of 68 kDa (Galindo et al., 2017; Bojorges et al., 2023; Rhein-Knudsen et al., 2017). Although the extracts contained polydisperse macromolecules, as expected for alginate polymers, their size distribution was very narrow (PDI=1), indicating that structurally homogeneous sodium alginates were obtained for all investigated species. This

unusually low PDI indicates that the extraction procedure prevented the depolymerisation of the polysaccharides (Trica et al., 2019).

Table 3.3: Molecular properties and ash contents of the fucoidan and sodium alginate extracts from the brown seaweeds investigated and commercial standards

	Source	Mw (kDa)	Mn (kDa)	PDI (M_w/M_n)	Kinematic viscosity (cSt/s)	Ash content (%)
Fucoidan	*F. vesiculosus* (commercial)	78.67	78.65	1.00	1.18 ± 0.63	23.48
	E. maxima	207.38	30.35	6.86	1.43 ± 0.62	16.56
	E. radiata	10.03	9.58	1.05	1.08 ± 0.12	7.61
	S. elegans	309.34	88.24	3.51	1.09 ± 0.09	26.41
	S. cymosum	2.61	2.56	1.01	1.02 ± 0.02	61.31
Alginate	Commercial (commercial)	78.49	78.27	1.00	1.98 ± 0.02	22.38
	E. maxima	242.90	237.01	1.02	2.19 ± 0.02	43.46
	E. radiata	304.24	295.70	1.03	2.70 ± 0.04	30.92
	S. elegans	194.27	191.94	1.01	1.96 ± 0.05	36.29
	S. cymosum	259.04	257.82	1.00	1.42 ± 0.10	58.01

* The data values represent the means ± SD of technical replicates (n=3).

In addition, the kinematic viscosities of the fucoidans and sodium alginates when dissolved in water were measured (Table 3.3). The majority of the fucoidan solutions had a kinematic viscosity close to that of water, which had a kinematic viscosity of about 1.02 cSt/s. However, the *F. vesiculosus* and *E. maxima* fucoidan solutions were slightly more viscous, with cSt values of around 1.2 and 1.4, respectively. The sodium alginate solutions all reported a kinematic viscosity in the range of 2 cSt/s, apart from the *S. cymosum* solution which was slightly less viscous at 1.42 cSt. Furthermore, the total ash content was determined by measuring the residual mass following TGA analysis (Table 3.3). The elucidated ash content is a measurement of the inorganic material and mineral content (i.e. phosphates, carbonates and sulphates) present in the samples (Lakshmanan et al., 2022). Most of the fucoidan extracts had an ash content of around 20%. However, the *E. radiata* fucoidan had a lower ash content of around 8%, while that of the *S. cymosum* was, in comparison to the other fucoidans,

very high at around 61.31%. The chemical characterisation data provides insight into this, revealing a correlation between the sulphate contents and ash levels across the fucoidan extracts, which suggests that the elevated ash content may reflect a true high endogenous mineral content inherent to certain species. These results, for the most part, are consistent with the approximate ash content of 20% reported for most fucoidans, although higher ash contents of above 40% have also been reported (Mabate et al., 2023; Yu et al., 2021). The alginate extracts showed ash contents of above 30%, higher than the 22.38% found in the commercial alginate. Numerous factors can affect the natural mineral content contained in alginate extracts; some studies that have obtained comparably high ash contents have noted that this was most probably due to the presence of salt residues that were used for alginate precipitation (Iriyanti et al., 2019; Zhang et al., 2023; Flores-Hernández et al., 2021; Irianto et al., 2023). In this present study, sodium carbonate (Na_2CO_3) was used. Thus, adjusting the amount of sodium carbonate used in the extraction procedure may improve the overall ash content and should be investigated further. Nonetheless, certain species appear to inherently possess higher ash levels. To better understand the origin of this ash, comprehensive mineral profiling of the fucoidan and alginate extracts is recommended to characterise the specific inorganic constituents contributing to the overall ash content.

3.4.5 Structural analysis of fucoidan and sodium alginate

3.4.5.1 FT-IR analysis

The preliminary identification of the functional groups of the fucoidans and alginates was carried out by FT-IR analysis, collecting sample spectra in the range of 600-4000 cm^{-1}. Figure 3.3 depicts the FT-IR spectra of the fucoidan and alginate extracts, overlaid with that of the commercial standards. The spectra resulting from the extracts demonstrated peak patterns corresponding to those of the commercial standards, which were characteristic of the structural building blocks. The polysaccharide-specific broad band at 3400 cm^{-1}, assigned to O-H functional groups, and the characteristically small peak of aliphatic C–H at 2900 cm^{-1}, were present in all of the spectra (Kuczajowska-Zadrożna et al. 2020).

The fucoidan FTIR spectra in Figure 3.3A, show the primary absorptive peak at around 1033 to 1048 cm^{-1}, characteristic of the glycosidic linkage C–O–C in fucoidans (Wang and Chen, 2016). The bands present between 1440 and 1800 cm^{-1} indicate the

presence of the C=O stretching vibration of the carbonyl groups and O-acetyl groups (Zayed et al., 2020). Furthermore, the fucoidan spectra showed bands characteristic of the presence and pattern distribution of sulphate groups in fucoidan in the region of 1200-600 cm^{-1}. The band at 1218 cm^{-1}, assigned to the -S-O asymmetric stretching vibration of the sulphate group, is often used for detection of total sulphate esters in polysaccharides (Al Monla et al., 2022). This peak was much more pronounced in the fucoidan standard and *S. cymosum* fucoidan extract, compared to the *E. maxima* and *S. elegans* fucoidan extracts - and was almost absent in the fucoidan of *E. radiata*. This pattern was also observed during the chemical analysis (Table 3.1). The additional, small sulphate peaks at 840 and 820 cm^{-1}, assigned to general C–O–S stretching, denote substitutions of sulphate ester groups at the axial C-4 position of α-linked L-fucopyranose and the equatorial C-2/C-3 positions, respectively (Zayed at al., 2020). As was evident from Figure 3.3A, the *E. radiata*, *S. elegans* and *S. cymosum* fucoidans exhibited a small single peak around 840 cm^{-1}, indicating that the sulphates were substituted at the C-4 position. In contrast, the *F. vesiculosus* and *E. maxima* fucoidans displayed peaks of varying intensities at 840 cm^{-1} and 820 cm^{-1}, indicating the 2/3,4 disubstitution of sulphate groups. The significantly more pronounced peak for *F. vesiculosus* at 840 cm^{-1}, accordingly, indicates that the sulphate substitution is primarily at the C-4 position, which is consistent with the observation of Ale et al., (2011). The final peak at 628 cm^{-1} attributed to the asymmetric and symmetric O=S=O deformation of sulphates, was most pronounced in *S. cymosum* (Synytsya et al., 2010).

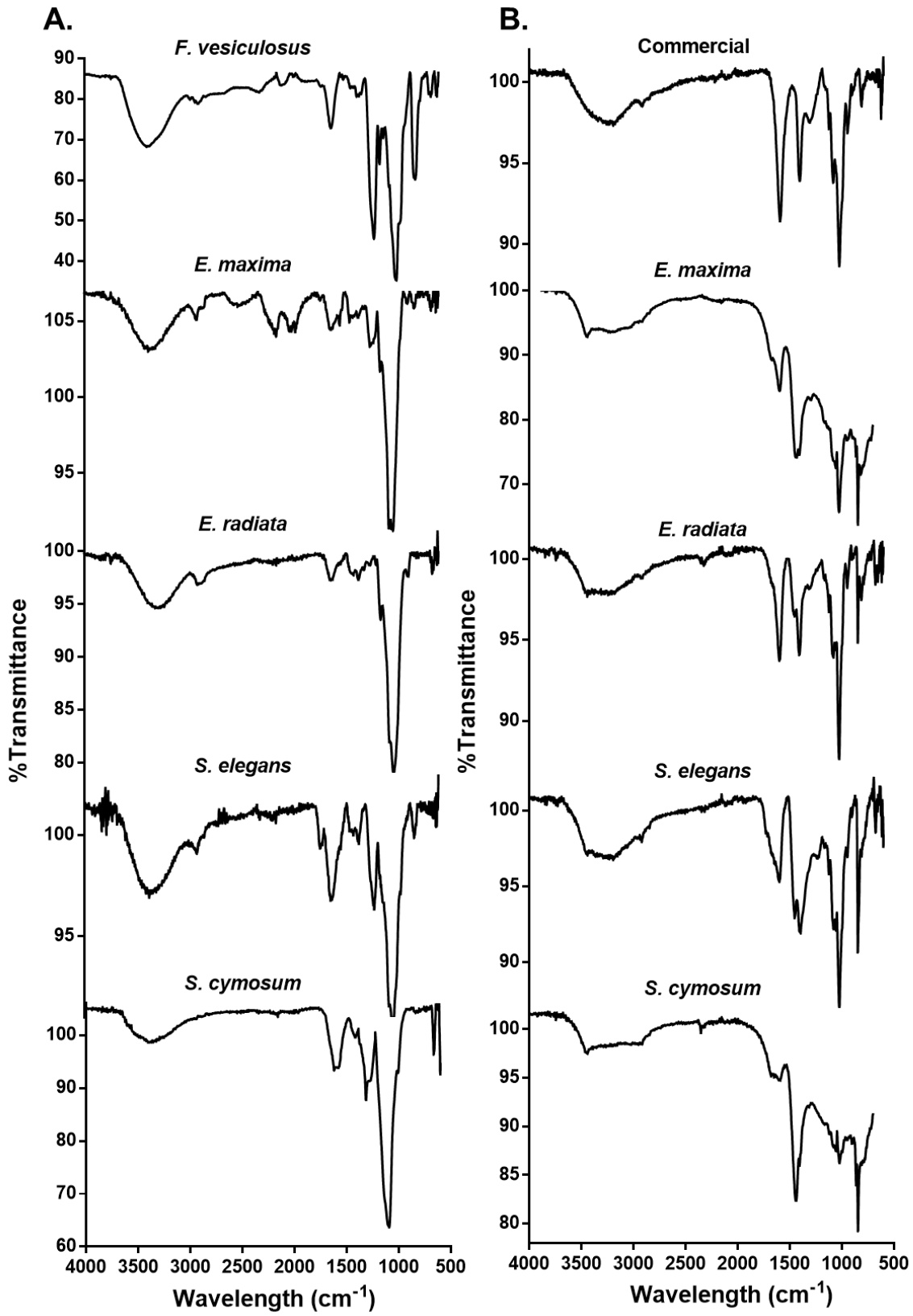

Figure 3.3: Overlay of FT-IR spectra of the (A) fucoidan and (B) sodium alginate extracts and the commercial standards (Sigma Aldrich) in the range of 600 - 4000 cm^{-1}.

The FT-IR spectra of the sodium alginates (Figure 3.3B) showed two strong bands at 1650 and 1460 cm^{-1} that are attributed to the asymmetric and symmetric stretching vibrations of carboxylate groups (O-C-O) in a sodium alginate molecule (Rhein-Knudsen et al. 2017; Kuczajowska-Zadrożna et al. 2020). The bands at 1100 cm^{-1} and 1020 cm^{-1} represent the C-O vibrations of pyranose rings with contributions from the deformation of C–C–H and C–O–H linkages of the mannuronic and guluronic acid units (Rhein-Knudsen et al. 2017; Rhimi et al. 2022). According to the literature, the band at 816 cm^{-1} is characteristic of the flexion vibration of mannuronic acid residues (Fertha et al. 2017; Belattmania et al. 2020). The prominence of this band is indicative of a significant mannuronic acid content, which is in accordance with the results obtained during the chemical composition analysis (Table 3.2). Furthermore, the absence of a signal around 1200 cm^{-1} typical of sulphate groups (S=O stretching), a characteristic of fucoidan and other sulphated polysaccharides, further confirmed the purity of the sodium alginates and the absence of fucoidan as a contaminant, in the extracted alginates (Kokova et al. 2023).

3.4.5.2 ^{1}H NMR analysis

^{1}H NMR spectroscopy analysis was employed for the further investigation of the structural features of the fucoidans and alginates. The proton spectra of the fucoidans contained chemical shifts ranging from 1.6 to 5.4 ppm (Figure 3.4). Assignments were made based on previously published NMR data (Zayed et al., 2020; Lutifa et al., 2020; Ayrapetyan et al., 2021). The doublet signals at 1.5 and 1.7 ppm specific to the methyl protons (CH3) at the C6 position and those coupled to the neighbouring methyl proton (C5) of L-fucose monomers, were the most pronounced in the spectra of the *F. vesiculosus* and *S. elegans* fucoidans (Lutifa et al., 2020). The presence of small amounts of O-acetyl groups in all fucoidans is shown by the peak at 2.2 ppm (Ayrapetyan et al., 2021). Additionally, the signal at 2.8 ppm assigned to the presence of amino sugars indicates that in the fucoidan derived from *S. cymosum* an amino group replaced a hydroxyl group on some monosaccharides (Lutifa et al., 2020). The group of signals present in the range of 4.9–5.5 ppm and 3.7–4.4 ppm corresponds to those of the anomeric (H1) protons and carbohydrate ring protons (H2-H5) present in *α*-linked sugar monomers such as D-glucose, D-galactose, D-mannose and L-fucose (Ayrapetyan et al., 2021; Zayed et al., 2020). The peaks in this anomeric and ring proton region provide information on the presence and glycosidic linkage position of

attached sulphate groups and the varying monosaccharide patterns (Alwarsamy et al., 2016). Although no detailed assignment is available for these, the chemical characterisation and FTIR analysis provide some additional detail. Overall similarities in the structural features of these fucoidans can be deduced from these analyses. For one, the prominent appearance of these signals for the *Ecklonia* sp fucoidans are reflected in their chemical composition data, which indicated the highest total sugar contents amongst all the fucoidans. Furthermore, from this limited NMR study, it is clear that the complex heterogeneous fucoidan structures of *F. vesiculosus* and *S. elegans* differ in detail but showed strong similarities in their structural features. In the case of the other fucoidans, there were strong similarities between the spectra of the *Ecklonia* species, whereas the fucoidan from *S. cymosum* had a more distinct proton spectrum. However, *E. maxima* and *S. cymosum* shared the distinctive unidentifiable signals in the region of 2.9 to 3.1 ppm. Considering that the bioactivity of fucoidan is directly related to their structure, further investigations are warranted.

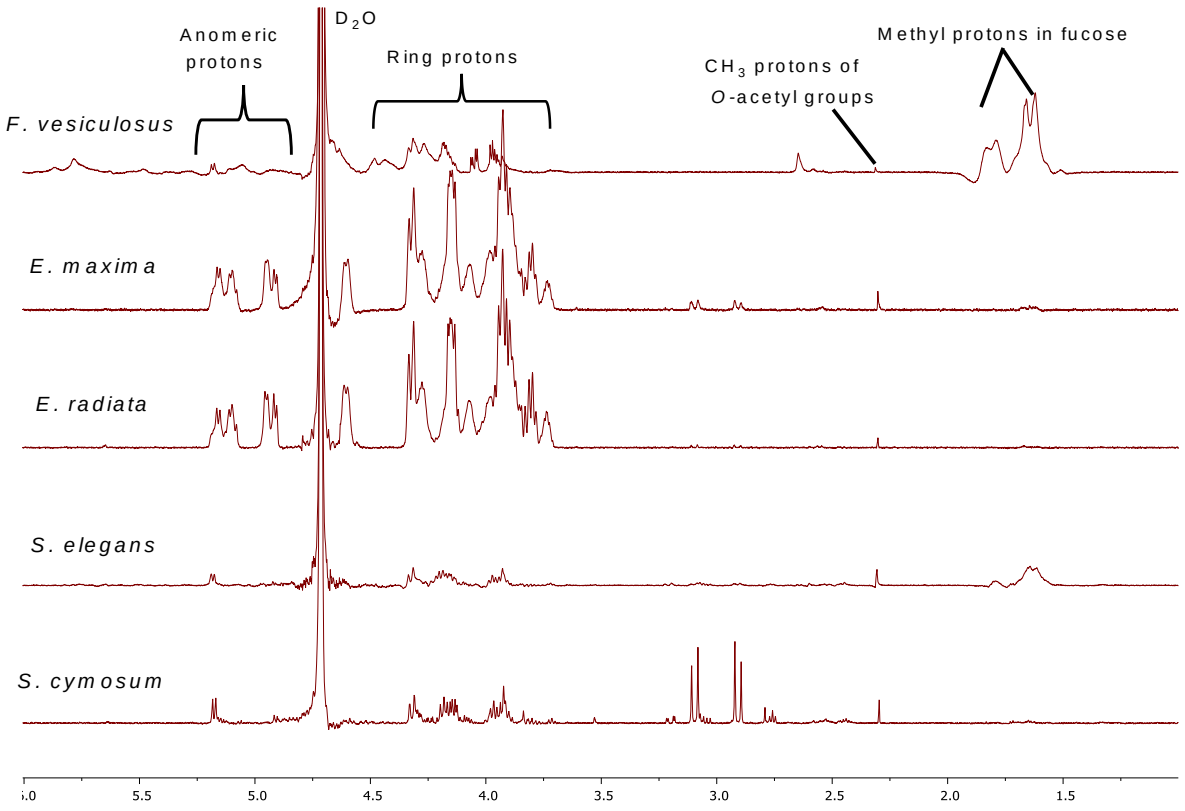

Figure 3.4: Stacked ^{1}H NMR spectra of *E. maxima*, *E. radiata*, *S. elegans*, *S. cymosum* fucoidans and the commercial standard *F. vesiculosus* fucoidan.

The ^{1}H NMR spectra of the sodium alginates showed clearly distinguishable signals of the monomer and block mannuronic (M) and guluronic acid (G) units (Figure 3.5). The

signal peaks representing the protons (H1 - H5) located at the different carbon positions on the uronic acids (M and G) were assigned as confirmed by literature (Bjerkan et al. 2004; Al Monla et al. 2022; Kokova et al. 2023). The mannuronic acid residue peaks, denoted as M1, M2, M3, M4 and M5, showed peak signals at 5.14 ppm, 4.45 ppm, 4.20 ppm, 4.27 ppm and 4.22 ppm, respectively. Furthermore, the spectrum showed the five typical L-guluronic acids residue peaks G1, G2, G3, G4 and G5 at 5.54 ppm, 4.45 ppm, 4.50 ppm, 4.62 ppm and 4.93 ppm, respectively.

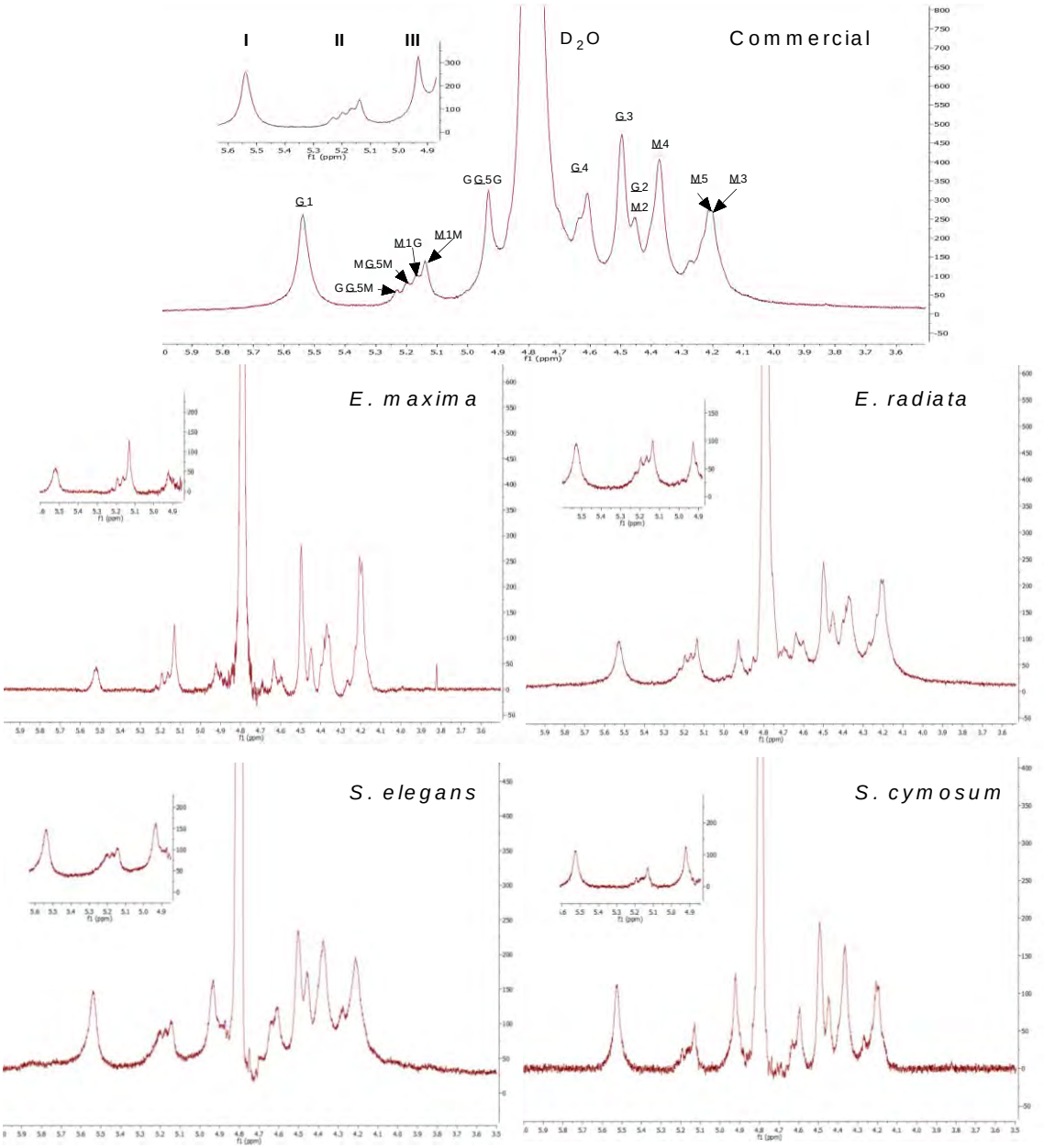

Figure 3.5: ^{1}H NMR spectra at 70°C of the commercial alginate and sodium alginates extracted from *Ecklonia* and *Sargassum* species. Expanded regions of the ^{1}H NMR spectrum show the signals marked I, II, and III used to calculate the M/G ratio as well as the frequency of the monad (F_G, F_M) and diad (F_{GG}, F_{MM}, F_{MG} or F_{GM}) sequence. Underlined M and G denote proton signals of the D-mannuronic acid and L-guluronic acid residues, respectively. Letters not underlined denote neighbouring residues along the copolymer chain. Numbers indicate which proton is responsible for the signal.

In addition to the peaks representing the individual M and G components, spectra showed diad and triad frequencies in the sodium alginate polymer chains. The signals at 5.24 ppm, 5.20 ppm and 4.93 ppm represent the H5 proton of a central G residue in the G-centered triads (GGM, MGM) and homopolymeric G blocks, respectively. The M-diad signals M1G at 5.17 ppm and M1M at 5.14 ppm denote the M residues neighbouring a G residue and another M residue (Fertha et al., 2017). From the area of the signals denoted as I, II and III, we calculated the ratio of the individual block structure components presented in Table 3.4, employing the equations adopted by Grasdalen et al. (1979). The M/G ratio values of the alginates were above 1, further indicating that these alginates have a higher fraction of mannuronic acid compared to guluronic acid. The lower M/G ratios reported here - compared to those detailed in Table 3.2 - can be attributed to differences in the analytical techniques. During hydrolysis, which is part of the HPLC sample preparation, G residues are released and subsequently decomposed from the alginate structure earlier than M residues (Lu et al., 2015). This early release and decomposition likely affected the M/G ratio determined via HPLC, leading to the higher reported values compared to those obtained through NMR, which does not require hydrolysis. Correlating to the overall higher M content, all alginates exhibited a higher mannuronic monad (FM) content than guluronic (FG), while the alternating block fractions (FMG and FGM) were present in low quantities (Table 3.4). Yet, the frequency of the guluronic diads (FGG) was higher in the *E. maxima*, *E. radiata* and *S. elegans* alginates compared to that of the mannuronic diads (FMM).

Table 3.4: Compositional data of the block structures of extracted and commercial alginates determined by NMR

Source	FG	FM	FMM	FGG	FMG=GM	M/G
Commercial	0.43	0.57	0.50	0.50	0.08	1.33
E. maxima	0.29	0.71	0.32	0.68	0.03	2.48
E. radiata	0.32	0.68	0.28	0.72	0.04	2.12
S. elegans	0.37	0.63	0.44	0.56	0.06	1.67
S. cymosum	0.45	0.55	0.57	0.43	0.11	1.21

3.4.5.3 Thermogravimetric analysis (TGA) of fucoidan and sodium alginate

The thermogravimetric analysis (TGA) was performed primarily to determine the ash content (Table 3.3), but it also highlighted some of the compositional differences between the extracts. The thermal behaviour of fucoidans showed a continuous weight loss with increasing temperature, demonstrating three distinctive decomposition stages denoted as x, y and z (Figure 3.6). The initial weight loss, denoted as x, of around 8-13% in the temperature range of 30 to 180°C, resulted from the loss of the freely bound and entrapped water molecules (Yang et al., 2022). These results indicated similar moisture contents amongst the fucoidans. Thereafter, the most significant weight loss was observed during the decomposition (y) stage, for the organic components of the fucoidan polymers. The greater weight loss (of between 41 and 52%) noted for the *Ecklonia* species, compared to that for the other three fucoidans, is related to the higher carbohydrate content within this species (Lakshmanan et al., 2022). Degradation of the organic contents of the fucoidans from *F. vesiculosus* (commercial standard) and the *Sargassum* species occurred earlier and, in the instance of the commercial fucoidan, also more rapidly than in the other fucoidans, as shown by the earlier and steeper slopes in the DTG graphs denoted y stage (Figure 3.6B). In the last decomposition stage (z) between 420°C and 800°C, the steady decomposition of carbonised residues occurred (Yang et al., 2022). At 800°C, the remaining percentage weight represents the ash content, which includes the phosphates, carbonates and sulphates present in the fucoidans (Lakshmanan et al., 2022). As mentioned previously, the high sulphate contents of the *Sargassum* species contributed to the high ash contents.

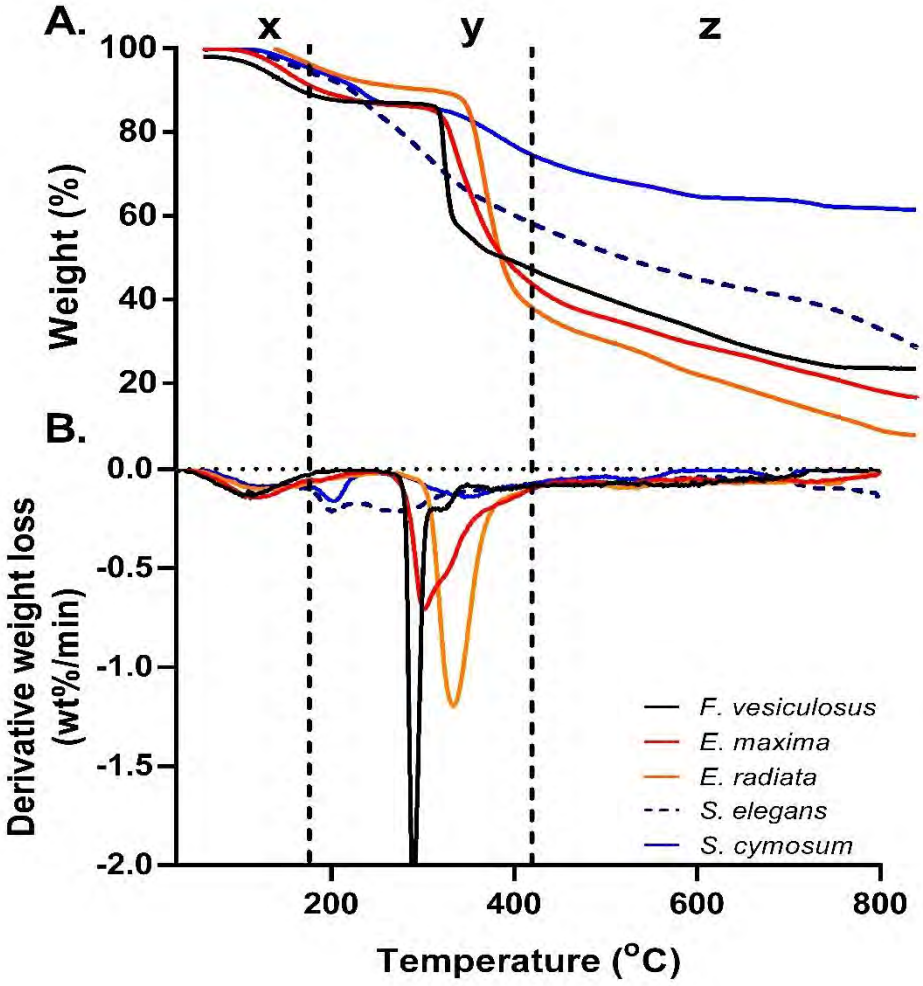

Figure 3.6: (A) Thermogravimetric (TGA) and (B) different thermogravimetric (DTG) analysis of the brown seaweed-derived fucoidans. The thermograms represent the fucoidans' percentage weight loss (TGA) and rate of weight loss (DTG) after continuous heating up to 800 °C.

The thermal degradation of the sodium alginates also occurred in three main degradation stages, as can be seen on the TGA and corresponding DTG thermograms in Figure 3.7. This thermal degradation profile compares to those of previously reported sodium alginates in literature (Zhang et al., 2023; Flores-Hernández et al., 2021). The sodium alginates lost between 8 and 17% of their weight, during the initial dehydration stage, denoted x. During the degradation of the alginate polymer, in the second stage marked y, the commercial alginate demonstrated a greater weight loss than the extracted sodium alginates, with *S. cymosum* only losing 18% of its sample mass, indicative of a lower alginate quality (purity) compared to that of the commercial alginate. In the last stage (z) which began at 440 °C and continued to 800 °C, the greatest loss in weight was seen on the thermograms for the *E. maxima* and *E. radiata*

samples, in the range of 580 - 660°C. Also previously mentioned, this weight loss is typically associated with the decomposition of excess Na_2CO_3 introduced during the alginate extractions' precipitation stage (Rowbotham et al., 2013, Da Silva Fernandes et al., 2018).

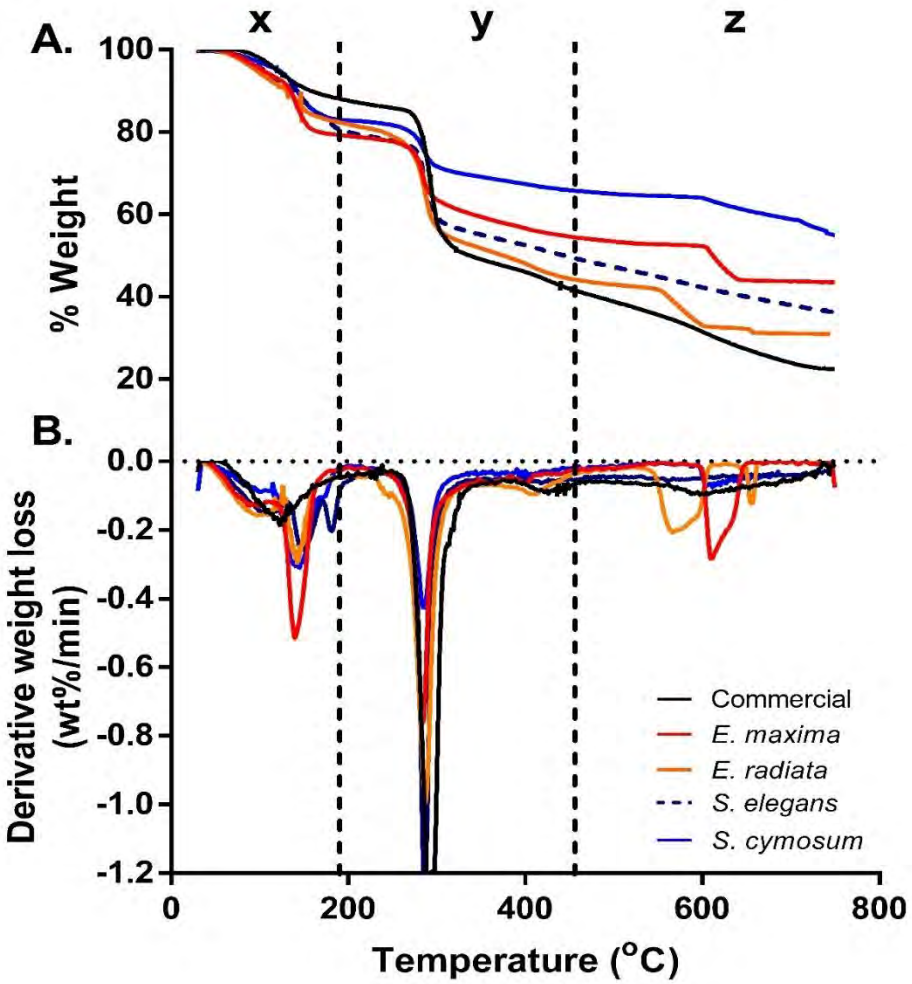

Figure 3.7: (A) Thermogravimetric (TGA) and (B) different thermogravimetric (DTG) analysis of the brown seaweed-derived sodium alginates. The thermograms represent the sodium alginate's percentage weight loss (TGA) and rate of weight loss (DTG) over the temperature range of 30 - 800°C after continuous heating up to 800 °C.

3.4.5.4 X-ray diffractometry (XRD) of the fucoidans and sodium alginates

The XRD profiles of the fucoidans and sodium alginates were obtained to investigate the microstructural differences between the various fucoidans and sodium alginates. The crystallinity of a polysaccharide depends on the degree of structural ordering within its molecular structure (Seidi et al., 2022). In general, a crystalline structure implies the

highly ordered arrangement of polysaccharide repeating units. Therefore, more complex and branched polysaccharides typically have a poor crystallisation capacity (Seidi et al., 2022). On an XRD spectrum the diffraction pattern of a crystalline structure contains many distinct peaks, while that of an amorphous structure contains only broad peaks. The diffractograms of the fucoidans (Figure 3.8) generally exhibited broad peaks at 2θ values of 13°and 22° as well as sharper peaks at 2θ values of 42°and 48°C. Furthermore, according to the interpretation of Saravana et al. (2016) of a similar peak pattern reported for fucoidan from *Saccharina japonica*, this confirmed that these fucoidans had a semi-crystalline structure. The sharper diffraction peaks seen in the *S. cymosum* fucoidan diffractogram also confirmed that it was more crystalline.

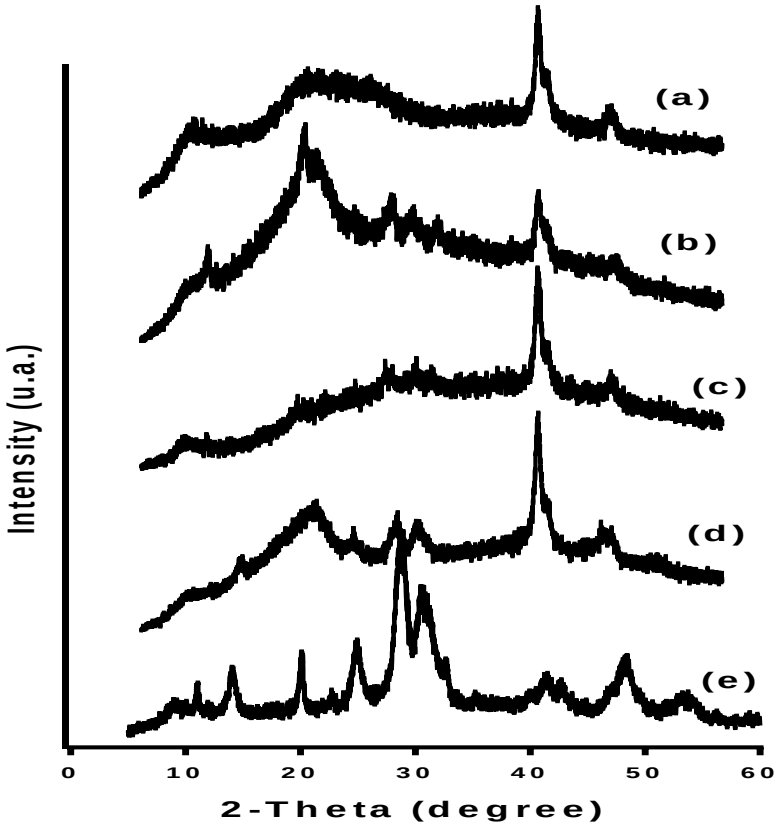

Figure 3.8: Xray diffraction spectra of (a) *F. vesiculosus*, (b) *E. maxima*, (c) *E. radiata*, (d) *S. elegans* and (e) *S. cymosum* fucoidans.

The XRD analysis of the sodium alginates, in Figure 3.9, showed the presence of peaks at 2θ values of 13°, 18°, 22°, 28°,29°, 32.5°, 34°, and 40°, respectively, that are characteristic of sodium alginate (Belattmania et al., 2018). The diffraction peaks at 13.5° and 22°, according to Belattmania and colleagues (2018), may correspond to the reflection of the (110) plane from the polyguluronate unit and (200) plane from the

polymannuronate unit, respectively. The additional unidentified crystalline peaks observed were also apparent in other studies (Belattmania et al., 2018; Hezma et al., 2023), but, based on the findings of dos Santos Araújo et al. (2019), these are suspected to be peaks arising from sodium carbonate. Overall, the XRD patterns of the alginates showed that sodium alginates had a semi-crystalline structure. This has been reported for sodium alginate before (Hezma et al., 2023).

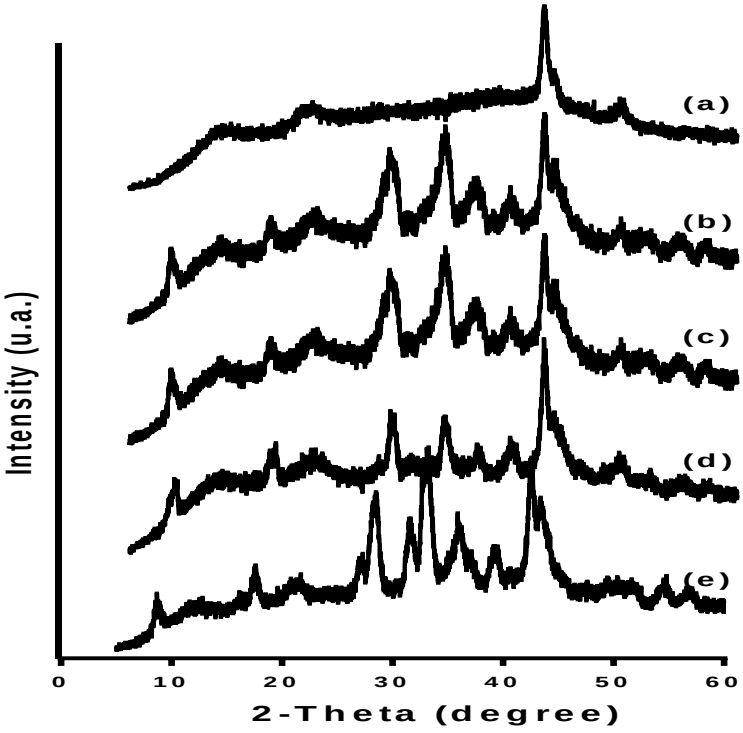

Figure 3.9: Xray diffraction spectra of the (a) commercial, (b) *E. maxima*, (c) *E. radiata*, (d) *S. elegans* and (e) *S. cymosum* sodium alginates.

3.5 Conclusion

In conclusion, extractions from the brown seaweeds, *Ecklonia* spp. and *Sargassum* spp. resulted in the isolation of fucoidans with yields of 3-6% and >2% of the dry weights of the seaweeds, respectively, and alginates with yields of around 40%. This work performed in this chapter showed that the extracts fulfilled the chemical and structural criteria for fucoidans and sodium alginates. The chemical composition and structural profiles revealed the heterogeneity of fucoidans among the two brown seaweed species, *Ecklonia* and *Sargassum*, where, most notably, the fucoidans derived from *Sargassum* spp. showed a high fucose and sulphate content, while in the *Ecklonia* spp. the principal sugar unit of the fucoidans was glucose, accompanied by a

lower fucose and sulphate content. Moreover, an investigation of the structures of these fucoidans indicated some similarities and differences, but further investigations are required in order to fully define these structural features. In addition, all the extracted sodium alginates displayed a mannuronic acid dominant composition (M/G ratio >1), medium MWs and low viscosities, and differences in their polymer chain arrangement. Overall, this chapter confirms the successful extraction of fucoidans and sodium alginates, with a validation of their purity and structural features. The moderate to high yields observed suggest that supply issues might be less of a concern. These findings establish a solid foundation for investigating their biological activities, which will be covered in the next two chapters.

Chapter 4- Inhibiting starch-degrading enzymes for the treatment of Type 2 Diabetes: exploring the potential of fucoidans and sodium alginates

4.1 Introduction

Diabetes mellitus is a metabolic disorder that is characterised by high levels of blood glucose that may become so drastic as to result in chronic hyperglycaemia (Vinoth Kumar *et al.,* 2015). This disease is classified as either Type 1 or Type 2 diabetes, with Type 2 accounting for ~ 90% of all diabetes cases. In T1DM, the body fails to produce insulin due to the autoimmune destruction of pancreatic cells. In contrast, T2DM is characterised by insulin resistance, where the body's cells become less responsive to the effects of insulin. Initially, the pancreas compensates by producing more insulin to maintain normal glucose homeostasis. However, over time, the pancreas becomes unable to sustain this increased insulin output, resulting in an insulin deficiency. As a result, glucose released from dietary carbohydrates fails to enter cells efficiently, leading to elevated glucose levels in the bloodstream. When inadequately controlled, untreated high levels of blood glucose can lead to several life-threatening consequences over time, which include damage to the blood vessels, the heart, eyes, kidneys and nerves (Lopes *et al.,* 2017). The pharmacological interventions to treat hyperglycaemia are numerous and include using different classes of oral anti-diabetic drugs (insulin secretagogues, insulin sensitisers, α-amylase and α-glucosidase inhibitors). These agents operate through two main therapeutic strategies: one compensates for insulin resistance and insufficient insulin secretion, thereby enhancing glucose uptake by cells and reducing blood glucose levels; the other delays the digestion and absorption of carbohydrates, limiting the postprandial rise in blood glucose.

Among these, the strategy of modulating digestion to slow glucose absorption is widely regarded as the preferred treatment approach (Attjioui *et al.,* 2021). The majority of the glucose entering the bloodstream stems from the ingestion of various starches that are hydrolysed into absorbable glucose by numerous enzymes located along the alimentary canal (Lee *et al.,* 2012; Attjioui *et al.,* 2021). α-Amylase, present in the saliva and pancreas, is initially responsible for the conversion of the starches (polysaccharides) into disaccharides, while α-glucosidases hydrolyse these

disaccharides (maltose, sucrose) to release absorbable glucose. There are four classes of α-glucosidases located in the small intestine's brush border membrane, namely maltase, glucoamylase, sucrase and isomaltase. These form two complexes maltase-glucoamylase (MGAM) and sucrase-isomaltase (SI), with different substrate specificities (Attjioui *et al.,* 2021). Each of the intestinal α-glucosidase complex enzymes breaks down the consumed starches further into simpler sugars or monosaccharides. Maltase is the major enzyme responsible for the digestion and absorption of dietary starch. Among these, maltase is the enzyme, to a larger extent, responsible for the digestion and absorption of dietary starch by releasing glucose units from maltose residues. In addition, sucrase hydrolyses sucrose to release glucose and fructose (Lee *et al.,* 2012; Attjioui *et al.,* 2021). By inhibiting these enzymes in the gastrointestinal tract, a reduction in postprandial glucose levels is achieved by reducing the liberation of glucose from oligosaccharides and disaccharides. Targeting the starch-degrading enzymes α-amylase and α-glucosidase is a well-established approach and has been an effective treatment strategy (Lakshmanasenthil *et al.*, 2014; Attjioui *et al.,* 2021).

4.2 Objectives

The objectives of this chapter were to:

- Identify the potential of the fucoidans and sodium alginates to inhibit the carbohydrate digestive enzymes (α-amylase, α-glucosidase, maltase and sucrase);
- Investigate the mode of enzyme inhibition of the fucoidans and/or alginates.

4.3 Materials and Methods

4.3.1 Materials

Acarbose (Cat. No. A8980), *F. vesiculosus* (Cat. No. F5631) and the commercial sodium alginate (Cat. No. W201502) were purchased from Sigma Aldrich. The carbohydrate-digesting enzymes; porcine pancreatic α-amylase (Cat. No. E-PANAA-9G), maltase (Cat. No. E-MALTS) and sucrase (Cat. No. E-SUCR), were purchased from Megazyme™**.** The commercial *Saccharomyces cerevisiae* α-glucosidase (Cat. No. G5003) was purchased from Sigma Aldrich. These enzymes were selected for their widespread use in the preliminary screening of digestive enzyme inhibitory activity. Although they differ structurally and mechanistically from the mammalian counterparts

involved in human digestion, they offer a reliable model for the initial evaluation of inhibitory potential. The remainder of the reagents and kits utilised in this study were of analytical grade and were purchased from Sigma-Aldrich, MERCK and Megazyme™.

4.3.2 α-Amylase inhibition assay

The inhibition of α-amylase (0.1 mg.ml^{-1}) in the presence of the test compounds (fucoidan and alginates) or positive control (acarbose), at various concentrations (0.1 – 1.0 mg.ml^{-1}), was assayed in a reaction volume of 400 µl using 2% (w/v) potato starch in 50 mM sodium phosphate buffer (pH 7.0) as the substrate. The reaction was allowed to occur at 37°C for 30 minutes with gentle agitation at 70 rpm. The reaction was then terminated by the addition of DNS reagent and the reducing sugars released were measured according to the DNS method (see section 3.3.5.6). Inhibitor controls were included to account for any reducing sugars released due to the thermal lysis of the inhibitors during the DNS assay. A control reaction was prepared using the same procedure, replacing the inhibitor with buffer. Inhibition was expressed as a relative percentage of the control according to the following formula:

$$\%Enzyme\ inhibition\ = \frac{(reducing\ sugars\ released\ by\ control\ -\ reducing\ sugars\ released\ by\ test\ reaction)}{reducing\ sugars\ released\ by\ control}\ x\ 100$$

4.3.3 α-Glucosidase inhibition assay

The inhibitory potential of the seaweed extracts (fucoidan and sodium alginate) [prepared in 50 mM sodium phosphate buffer (pH 7.0)] and positive control (acarbose) was assessed at various concentrations ranging from 0.1 - 1 mg.ml^{-1}. Their inhibition of α-glucosidase (0.625 µg.ml^{-1}) activity was investigated by monitoring the release of *p*-nitrophenol from the substate *p*-nitrophenyl-α-D-glucopyranoside (*p*NPG, 2.5 mM) in a reaction volume of 500 µl. The reaction was incubated at 37°C and the *p*-nitrophenol release was monitored in 1-minute intervals over 20 minutes at 405 nm (Epoch™ 2 spectrophotometer from Bio-Tek with Gen 5™ software). The absorbance readings were corrected for the absorbance contribution of the buffer, enzyme, substrate and respective inhibitors, respectively. The *p*-nitrophenol release was interpolated from the *p*-nitrophenol standard curve (see Appendix Figure B10). The control reaction was allowed to proceed using the same procedure replacing the inhibitor with buffer. The *α*-glucosidase inhibitory activity was calculated as percentage inhibition:

$$\%\ Enzyme\ inhibition\ = \frac{(p-nitrophenol\ released\ by\ control - p-nitrophenol\ \ released\ by\ test\ reaction)}{p-nitrophenol\ released\ by\ control}\ x\ 100$$

4.3.4 Maltase inhibition assay

The inhibitory activity of the test compounds (fucoidan and alginates) and positive control (acarbose) on maltase was determined by incubating the potential inhibitors at final concentrations ranging from 0.1 to 1.0 mg.ml^{-1}, with maltase (0.175 U.ml^{-1}) and isomaltotriose (15 mM) in a total reaction volume of 100 µl. The reaction was allowed to proceed for 30 minutes at 37°C. Following this, the enzymatic activity was terminated by incubation at 100°C for 10 minutes. The glucose released by the reaction mixture was determined by the glucose oxidase/peroxidase (GOPOD) kit according to the manufacturer's instructions using a glucose standard curve (see Appendix Figure B11). A control reaction monitored the activity of the enzyme without inhibitor. The percentage inhibition (%) was calculated using the following equation:

$$\%Enzyme\ inhibition\ = \frac{(glucose\ released\ by\ control - glucose\ realeased\ by\ test\ reaction)}{glucose\ released\ by\ control}\ x\ 100$$

4.3.5 Sucrase inhibition assay

The ability of the seaweed extracts (fucoidan and sodium alginate) and positive control (acarbose) to inhibit sucrase (0.001 U.ml^{-1}) activity was assayed for inhibitor concentrations from 0.1 – 1 mg.ml^{-1} using a fixed concentration of sucrose (10 mM) in a 100 µl total reaction volume. The reaction was incubated for 30 minutes at 37°C and then at 100°C for a further 10 minutes to terminate the reaction. The glucose released by the reaction mixture was determined by the glucose oxidase/peroxidase (GOPOD) kit according to the manufacturer's instructions using the glucose standard curve (see Appendix Figure B11). A control reaction monitored the activity of the enzyme without inhibitor. The percentage inhibition (%) was calculated using the following equation:

$$Enzyme\ inhibition\ \% = \frac{(glucose\ released\ by\ control - glucose\ realeased\ by\ test\ reaction)}{glucose\ released\ by\ control}\ x\ 100$$

4.3.6 Determination of IC_{50} values

Compounds which exhibited significant inhibition against α-glucosidase, maltase, and sucrase were screened using a broader concentration range (0.001-5 mg.ml^{-1}). The

IC_{50} value [defined as the concentration ($mg.ml^{-1}$) of each inhibitor required to inhibit half (50%) of the activity of the enzymes, was determined by nonlinear regression of the log-transformed inhibitor concentration (log [Inhibitor]) vs. the relative enzyme inhibition (% inhibition) at 2.5 mM *p*NPG,15 mM isomaltose and 10 mM sucrose using GraphPad Prism software (GraphPad Prism ver. 6, GraphPad Software, La Jolla, CA, USA).

4.3.7 EnzymeML kinetic analysis of α-glucosidase activity

Enzyme kinetic assays for α-glucosidase activity were conducted following the reaction conditions described in section 4.3.3, employing varying concentrations of pNPG (0.1, 0.25, 0.5, 1, 2.5, and 5 mM). Product formation data monitored over 20 minutes were extrapolated from the *p*-nitrophenol standard curve (see Appendix Figures B18 to B24), including appropriate controls. Mr Max Häußler (collaborator at Stuttgart University, Institute for Biochemistry and Technical Biochemistry) performed the enzyme kinetic analysis on this experimental data to identify the type of inhibition, utilising the software program EnzymeML (initial workflow outlined in Mr. Häußler master's thesis: Häußler, 2023). Briefly, the data was put into EnzymeML documents, accessed, modified, and generated using Python API PyEnzyme (Range et al., 2021), facilitating the integration of EnzymeML data into Python-driven data analysis workflows for kinetic parameter estimation. The datasets were evaluated against various kinetic models, including product and substrate inhibition models, as well as enzyme inactivation models. The estimated parameters (K_m, k_{cat}, and k_{cat}/K_m) for the assessed/fitted models were determined.

4.3.8 Kinetic analysis of maltase and sucrase

Kinetic assays for maltase and sucrase were conducted by maintaining the maltase and sucrase activity at 0.175 $U.ml^{-1}$ and 0.001 $U.ml^{-1}$, respectively. The enzyme activities in the absence and presence of the inhibitor were assayed at varying final concentrations of the maltose (2.5, 5, 10, 15, 20 and 25 mM) and sucrose (2.5, 5, 10, 15, 30 and 45 mM) substrates, as outlined in sections 4.3.4 and 4.3.5. The Michaelis–Menten inhibition constant, K_m, and the maximum rate, V_{max}, were determined using non-linear regression analysis with GraphPad Prism 6.0 software. The initial velocity data were used to draw Lineweaver-Burk plots, plotting 1/[S] on the X-axis and the 1/v values on the Y-axis.

4.3.9 Statistical analysis

Significant differences between the activities of the enzymes in the absence and presence of inhibitors were determined by one-way analysis of variance (ANOVA). The ANOVA test was performed using the data analysis feature in GraphPad Prism software version 6 (GraphPad Inc). The values were considered to be significantly different when $p < 0.05$.

4.4 Results and Discussion

4.4.1 Inhibitory effects of fucoidans and sodium alginates on α-amylase compared to acarbose

The ability of the seaweed-derived fucoidan and sodium alginate extracts to inhibit the degradation of potato starch by α-amylase was assessed by monitoring the release of reducing sugars using the DNS assay (Miller,1959). In Figure 4.1, the inhibitory potential of fucoidans and sodium alginate against porcine α-amylase was compared to that of the commercial anti-diabetic agent acarbose. While there was a direct relationship between the acarbose concentration and the inhibition of the enzyme (indicating a dose-dependent effect inhibiting up to 80% of the α-amylase activity), neither the fucoidans nor the sodium alginates displayed any significant inhibitory effect on the activity of α-amylase.

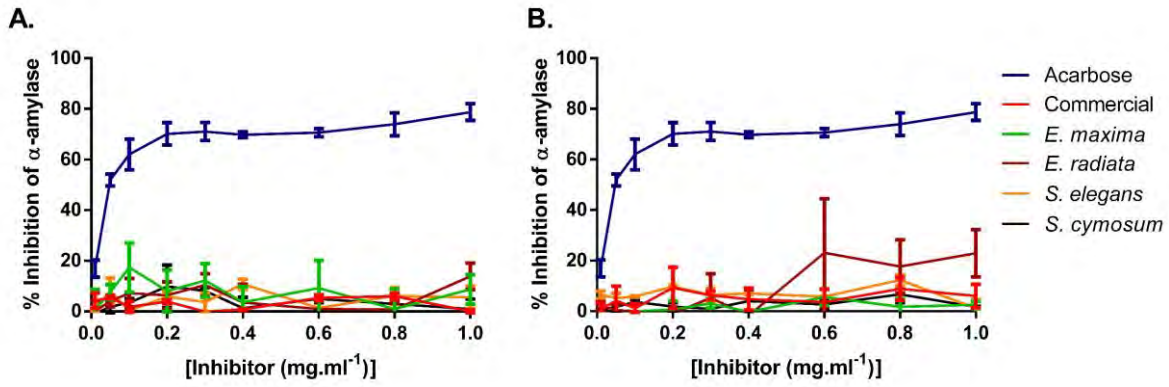

Figure 4.1: Inhibitory potential of acarbose compared to (A) fucoidans and (B) sodium alginates from the various brown seaweeds against α-amylase activity. Commercial fucoidan sourced from *F. vesiculosus*, source of the commercial sodium alginate unknown. The values are expressed as means ± SD (n=3).

The lack of inhibition of α-amylase activity observed for the fucoidan standard from *F. vesiculosus* was anticipated, as a previous study by Kim et al. (2014) demonstrated

that this fucoidan does not inhibit this enzyme. Similarly, previous studies (Daub et al., 2020; Mabate et al., 2021) in our laboratory revealed that fucoidans extracted from *E. radiata* and *E. maxima* also lack inhibitory effects on porcine α-amylase. Therefore, the lack of inhibition noted for the other fucoidans is not surprising. Likewise, all sodium alginates did not display any effect on α-amylase activity. There is limited literature available on the inhibitory effects of sodium alginates on α-amylase, so it's difficult to ascertain the reasons for their observed lack of inhibition. While acarbose, a known α-amylase inhibitor (Cho et al., 2011), inhibited the activity of this enzyme, it's worth noting that its apparent effectiveness decreased in a dose-dependent manner at concentrations above 0.3 $mg.ml^{-1}$ during our initial assessments. Further investigation revealed that acarbose is susceptible to thermolysis at temperatures above 95°C, as noted by Singla et al. (2016). Therefore, it was vital to correct for the increased amounts of reducing sugars being released from the thermolysis of acarbose during the sugar quantification step to ensure accurate reporting of its inhibitory potential. In contrast, the fucoidans and alginates were not susceptible to thermolysis (data not shown).

4.4.2 Inhibitory effects of fucoidans and sodium alginates on α-glucosidase compared to acarbose

Next, the fucoidans and sodium alginates were evaluated for their inhibitory potential against α-glucosidase, the enzyme responsible for further breaking down the oligosaccharides produced during starch digestion by α-amylase into glucose (Figure 4.2). For this assessment, a colourimetric assay using the synthetic model substrate *p*-nitrophenyl-α-D-glucopyranoside (pNPG) was employed. The results for the inhibitory effects of the fucoidans, as presented in Figure 4.2A, revealed that among the five fucoidans assessed, four exhibited higher maximal inhibitory effects against α-glucosidase, compared to acarbose, which achieved a maximal inhibition of 68.25% at 1 $mg.ml^{-1}$. Three of these fucoidans (from *F. vesiculosus*, *E. radiata*, and *S. elegans*) exhibited inhibitory effects of up to ~96% in a dose-dependent manner on α-glucosidase activity, achieving this level of inhibition at concentrations as low as 0.1 $mg.ml^{-1}$. The fourth fucoidan, from *E. maxima*, although it initially showed no inhibition of α-glucosidase at lower concentrations, surpassed the inhibitory effect of acarbose at 0.3 $mg.ml^{-1}$, reaching a maximal inhibition of 87.63%. The inhibitory potential of *S. cymosum* fucoidan was much lower (<40%), demonstrating a dose-dependent response, inhibiting α-glucosidase significantly ($p<0.05$) only at high concentrations exceeding 0.6 $mg.ml^{-1}$. In contrast to the majority of the fucoidans, the sodium alginates

(Figure 4.2B) exhibited weak and mostly insignificant inhibition in the concentration range assessed, with the degree of inhibition reaching only 26.28%. Overall, these findings highlight the strong inhibitory potential of fucoidans towards α-glucosidase (compared to sodium alginates), with many fucoidans exhibiting superior efficacy to acarbose.

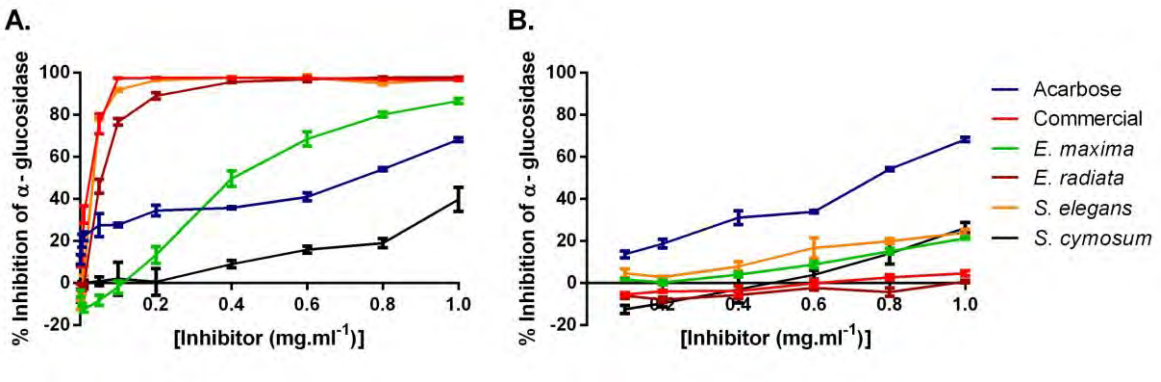

Figure 4.2: Inhibitory potential of acarbose compared to (A) fucoidans and (B) sodium alginates from various brown seaweeds against α-glucosidase activity. Commercial fucoidan sourced from *F. vesiculosus*, source of the commercial sodium alginate unknown. The values are expressed as means ± SD (n=3).

4.4.3 Inhibitory effects of fucoidans and sodium alginates on maltase compared to acarbose

Following the evaluation of α-glucosidase inhibition, we proceeded to assess maltase and sucrase inhibition each individually, to gain a more comprehensive understanding of how these seaweed extracts influence specific α-glucosidase enzymes involved in carbohydrate metabolism. The inhibition of maltase (Figure 4.3) showed that all fucoidan and sodium alginate extracts inhibited maltase to a varying degree. The maltase inhibitory effect of the five sodium alginate extracts, along with the *E. maxima* and S. *cymosum* fucoidans, was mild and irregular, with a maximum inhibition of between 20 and 40% ($p<0.05$) of the enzyme's activity, within the tested concentration range. In contrast, the other three fucoidans exhibited a greater effect on the enzyme, especially *E. radiata* and *S. elegans*, which displayed a higher inhibitory effect than acarbose (Figure 4.3A). At higher inhibitor concentrations, the *E. radiata* and *S. elegans* fucoidans displayed a maximal inhibitory effect (>85%), matching that of acarbose. Among all the inhibitors screened, only the commercial sodium alginate displayed no significant ($p<0.05$) inhibition.

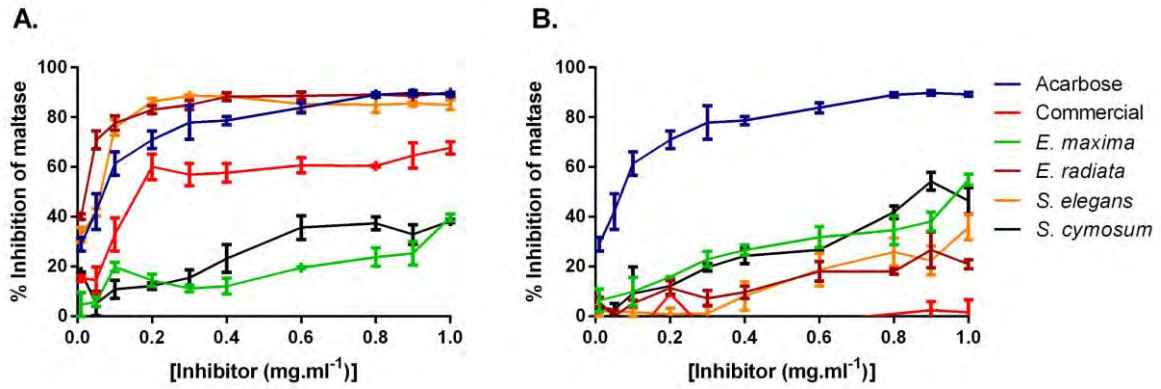

Figure 4.3: Inhibitory potential of acarbose compared to (A) fucoidans and (B) sodium alginates from various brown seaweeds against maltase activity. Commercial fucoidan sourced from *F. vesiculosus*, source of the commercial sodium alginate unknown. The values are expressed as means ± SD (n=3).

4.4.4 Inhibitory effects of fucoidans and sodium alginates on sucrase compared to acarbose

Lastly, we investigated the inhibitory effects of the fucoidans and sodium alginates on sucrase activity (Figure 4.4). The fucoidans from *F. vesiculosus* and *S. elegans* were the most potent inhibitors of sucrase (with over 90% inhibition), surpassing the efficacy of acarbose at all concentrations. *E. radiata* fucoidan also exhibited a notable inhibitory effect, reaching its maximal inhibitory effect of over 70% at 0.6 mg.ml^{-1}. However, *E. maxima* and *S. cymosum* fucoidan showed maximal inhibition of only around 30% ($p<0.05$). Interestingly, *E. maxima* and *E. radiata* fucoidan initially demonstrated some activation of the enzyme at lower concentrations before inhibiting sucrase activity at higher concentrations (Figure 4.4A). In contrast, the sodium alginates (Figure 4.4B) (except those from *E. maxima* and *S. cymosum*, which showed some limited inhibition of around 20% at 1 mg.ml^{-1} ($p<0.05$)) did not display any significant inhibition of sucrase activity.

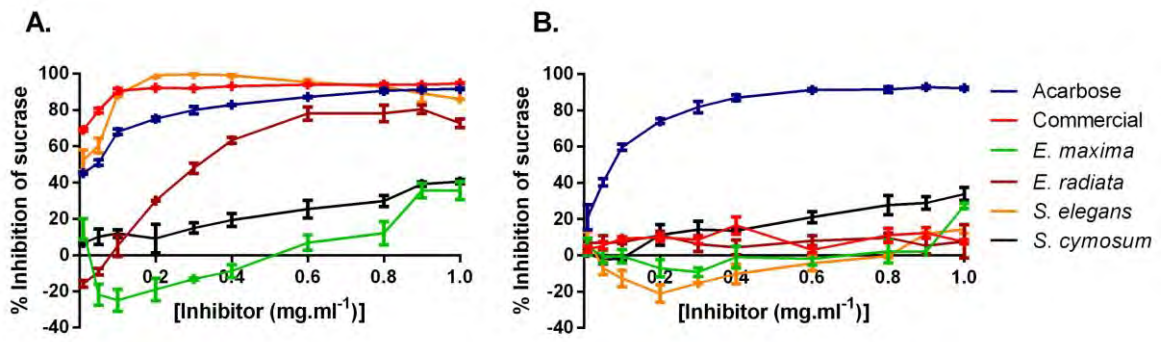

Figure 4.4: Inhibitory potential of acarbose compared to (A) fucoidans and (B) sodium alginates from various brown seaweeds against sucrase activity. Commercial fucoidan sourced from *F. vesiculosus*, source of the commercial sodium alginate unknown. The values are expressed as means ± SD (n=3).

4.4.5 Potency of fucoidan and sodium alginate extracts as inhibitors of α-amylase, α-glucosidase, maltase and sucrase

The half-maximal inhibitory concentrations (IC_{50}), reflecting the potency of enzyme inhibition, were determined to compare the efficacy of our inhibitors against α-amylase, α-glucosidase, maltase, and sucrase. The inhibitory effect of our compounds on these enzymes was assessed under the same conditions as above but covering a wider concentration range (0.001-5 $mg.ml^{-1}$). The IC_{50} values, depicted in Table 4.1 below, were derived from plots of the logarithm of inhibitor concentration versus percentage enzyme inhibition (see Appendix Figures B12 to 15).

As is evident from the absence of reported IC_{50} values for α-amylase in Table 4.1, neither the fucoidans nor the sodium alginates displayed significant inhibition of this enzyme, even across the broader concentration range. This selective inhibition is desirable, as strong α-amylase inhibition, such as that observed with acarbose, is often linked to gastrointestinal side effects (e.g., bloating, diarrhoea) due to undigested starch fermentation in the colon (Proença et al., 2019). In contrast, acarbose, the positive control, showed a stronger inhibition of α-amylase than the α-glucosidases (Table 4.1), consistent with previous studies (Mabate et al., 2021). Interestingly, the IC_{50} values revealed distinct inhibition patterns among the fucoidans from the various seaweed species across the three α-glucosidase enzymes: α-glucosidase, maltase and sucrase (Table 4.1). When comparing their α-glucosidase inhibitory potentials, it is evident that the fucoidans from *E. maxima*, *E. radiata*, and *S. elegans* surpassed acarbose in efficacy but did not exceed the efficacy of the commercial *F. vesiculosus*

fucoidan. *S. cymosum* fucoidan extract exhibited the lowest α-glucosidase inhibitory potential among the fucoidan samples tested; however, it still achieved 50% inhibition over an extended concentration range, unlike the sodium alginates. As further illustrated in Table 4.1, *E. maxima*, *E. radiata*, and *S. cymosum* fucoidans, along with sodium alginate extracts from *E. maxima* and *S. cymosum*, exhibited the selective inhibition of maltase rather than sucrase.

In contrast, commercial *F. vesiculosus* and *S. elegans* fucoidans appeared to be stronger inhibitors of sucrase compared to maltase. The strength of sucrase inhibition, as indicated by their IC_{50} values, followed the order: *F. vesiculosus* > *S. elegans* > *E. radiata* > Acarbose > *E. maxima* > *S. cymosum*. The inhibition of maltase activity by fucoidans decreased in the following order: *E. radiata* > *S. elegans* > Acarbose > *F. vesiculosus* > *E. maxima* > *S. cymosum*. The *E. radiata* and *S. elegans* fucoidans, therefore, appeared to be the most promising α-glucosidase inhibitors, given their particularly low IC_{50} values. While the higher inhibitory potency of *E. maxima* fucoidan, specifically against α-glucosidase activity compared to acarbose, would suggest it to be a good candidate, its relative lack of inhibition against maltase and sucrase may indicate a preference in specificity towards only the α-glucosidase enzyme.

Table 4.1: IC_{50} values for the inhibition of α-amylase, α-glucosidase, maltase and sucrase enzymes by acarbose and the different seaweed extracts

Compound	***IC_{50} (mg.ml^{-1})***			
	α-amylase	**α-glucosidase**	**maltase**	**sucrase**
Acarbose	0.051	0.714	0.108	0.130
Fucoidans				
F. vesiculosus	ND	0.021	0.161	0.056
E. maxima	ND	0.391	1.331	1.409
E. radiata	ND	0.049	0.045	0.112
S. elegans	ND	0.023	0.082	0.075
S. cymosum	ND	2.134	1.778	2.148
Sodium alginate				
E. maxima	ND	ND	1.026	ND
S. cymosum	ND	ND	0.876	ND

ND-Not detectable

Comparing the overall α-glucosidase, maltase, and sucrase IC_{50} values revealed a consistent trend: fucoidans from *F. vesiculosus*, *E. radiata*, and *S. elegans* exhibited stronger inhibitory effects on these enzymes compared to those from *E. maxima*, *S. cymosum*, and the sodium alginates. Numerous studies have highlighted the potent inhibitory activity of fucoidan extracts from various brown seaweed species against α-

glucosidase and a few studies also for the maltase, and sucrase enzymes - with reported IC_{50} values typically falling within the range of 0.137 to 0.536 $mg.ml^{-1}$ (Shan et al., 2016; Koh et al., 2020; Attjioui et al., 2021). By comparison, our fucoidans performed exceedingly well as inhibitors of these digestive enzymes and compare favourably to some of the most potent known fucoidans, for instance, *Ascophyllus nodusum* and *F. vesiculosus* fucoidans, which have been reported to exhibit IC_{50} values of 0.047 $mg.ml^{-1}$ and 0.049 $mg.ml^{-1}$ on α-glucosidase, respectively (Kim et al., 2014). Taken together, the fucoidans' strong and selective inhibition of α-glucosidase, maltase, and/or sucrase, paired with minimal α-amylase activity, closely matches the inhibition profile sought in next-generation antidiabetic agents.

Sodium alginates have been not well explored as inhibitors of carbohydrate-degrading enzymes, with limited studies conducted thus far. In our study, we observed inhibitory effects on maltase with sodium alginates derived from *E. maxima* and *S. cymosum*, demonstrating notable activity. While previous research by Nakamura et al. (2008) reported on the maltase inhibitory capacity of sodium alginate, specific IC_{50} values were not provided. Our findings can be compared to those of Samudra et al. (2017), who reported an IC_{50} of 1.55 $mg.ml^{-1}$ for a sodium alginate extract inhibiting α-glucosidase. Our study therefore represents the first comprehensive screening of various sodium alginates for their inhibitory potential against carbohydrate-degrading enzymes.

4.4.6 Exploring the kinetic inhibition mechanisms of α-glucosidase by fucoidans using kinetic modelling

To explore the mode of inhibition of α-glucosidase by fucoidans, we employed the traditional experimental procedure of measuring the enzyme activity at various substrate concentrations. Fucoidans, demonstrating higher inhibitory potencies than acarbose, including acarbose itself, were selected for an evaluation of their respective modes of inhibition. To identify their inhibition mechanism, we subjected the experimentally collected data to modelling using EnzymeML. The most appropriate model describing the inhibitor's mode of inhibition was determined by comparing the Akaike Information Criterion (AIC) values, which assess the relative quality of a model based on its goodness of fit. Controls of substrate, enzyme, and inhibitors were included throughout the experiment and were factored into the modelling process (see Appendix Figures B16-B19).

The parameter estimates for all evaluated kinetic models are provided in Tables 4.2-4.6 below, while the fitted inhibition models of the best fit are visualised in Appendix Figures B20 to B23. The models listed in Table 4.4 suggest that *E. maxima's* fucoidan inhibitory mechanism is best described by the competitive inhibition model, as evidenced by the lowest AIC. Acarbose and the fucoidans from *E. radiata*, *F. vesiculosus* and *S. elegans*, as inhibitors, exhibited the best fit with a competitive model featuring uncompetitive substrate inhibition and time-dependent enzyme inactivation. Consequently, the K_i value for uncompetitive binding is higher than that for competitive binding for acarbose and these fucoidans, indicating their lower affinity for the enzyme-substrate complex compared to the enzyme's active site.

Table 4.2: Estimated kinetic parameters for the models of α-glucosidase inhibition by acarbose

Model	AIC	RMSD	kcat (1/S)	Km (mM/L)	Ki uncompetitive (mg/L)	Ki competitive (mg/L)	Ki enzyme inactivation (1/S)	kcat/Km (1/s*1/mM/L)
Competitive inhibition with uncompetitive substrate inhibition and enzyme inactivation	-22251	0.003036	0.0292 ± 0.54%	0.2549 ± 1.23%	43.15 ± 4.62%	0.1550 ± 0.99%	0.0003 ± 2.63%	0.114 ± 1.34%
Competitive inhibition with enzyme inactivation	-21754	0.003458	0.0286 ± 0.41%	0.2026 ± 0.91%	-	0.1368 ± 1.01%	0.0003 ± 3.01%	0.131 ± 1.00%
Partially competitive inhibition with enzyme inactivation	-21751	0.003458	0.0286 ± 0.41%	0.2026 ± 0.92%	999.98 ± 940.14%	0.1367 ± 1.64%	0.0003 ± 3.02%	0.131 ± 1.01%
Competitive inhibition with uncompetitive substrate inhibition	-21129	0.004069	0.0256 ± 0.58%	0.2533 ± 1.65%	43.52 ± 6.25%	0.1543 ± 1.32%	-	0.101 ± 1.75%
Competitive inhibition	-20842	0.004387	0.0234 ± 0.21%	0.2016 ± 1.16%	-	0.1362 ± 1.29%	-	0.116 ± 1.18%
Partially competitive inhibition	-20839	0.004388	0.0234 ± 0.21%	0.2022 ± 1.14%	999.97 ± 1869%	0.1367 ± 2.09%	-	0.116 ± 1.16%
Uncompetitive inhibition with enzyme inactivation	-16202	0.014677	0.0314± 1.88%	0.6400 ± 2.60%	1.2771 ± 3.31%	-	0.0003 ± 13.04%	0.049 ± 3.21%
Uncompetitive inhibition	-16143	0.014914	0.0275± 1.00%	0.6388 ± 2.65%	1.2780 ± 3.37%	-	-	0.043 ± 2.83%
Irreversible Michaelis Menten with enzyme inactivation	-15104	0.019548	0.0251± 2.39%	0.6105 ± 3.28%	-	-	0.0003 ± 17.73%	0.041 ± 4.06%
Irreversible Michaelis Menten	-15073	0.019719	0.0221± 1.01%	0.6093 ± 3.32%	-	-	-	0.036 ± 3.47%

Table 4.3: Estimated kinetic parameters for the models of α-glucosidase inhibition by fucoidan from *F. vesiculosus*

Model	AIC	RMSD	kcat (1/S)	Km (mM/L)	Ki uncompetitive (mg/L)	Ki competitive (mg/L)	Ki enzyme inactivation (1/S)	kcat/Km (1/s*1/mM/L)
Competitive inhibition with uncompetitive substrate inhibition and enzyme inactivation	-15663	0.016881	0.0372 ± 3.56%	0.2949 ± 7.27%	19.71 ± 16.27%	0.0016 ± 5.18%	0.0006± 8.61%	0.126 ± 8.09%
Competitive inhibition with enzyme inactivation	-15613	0.017113	0.0312 ± 2.36%	0.1943 ± 4.88%	-	0.0012 ± 4.68%	0.0006 ± 8.76%	0.160 ± 5.42%
Partially competitive inhibition with enzyme inactivation	-15611	0.017114	0.0312 ± 2.36%	0.1950 ± 4.86%	999.98 ± 443.95%	0.0012 ± 4.80%	0.0006 ± 8.77%	0.160 ± 5.41%
Competitive inhibition with uncompetitive substrate inhibition	-15519	0.017536	0.0287 ± 3.00%	0.2966 ± 7.62%	19.28 ± 16.78%	0.0016 ± 5.36%	-	0.097 ± 8.19%
Competitive inhibition	-15474	0.017754	0.0239 ± 1.01%	0.1911 ± 5.14%	-	0.0012 ± 5.00%	-	0.125 ± 5.24%
Partially competitive inhibition	-15433	0.017935	0.0239 ± 1.05%	0.2333 ± 4.34%	946.28 ± 11742%	0.0015 ± 3.53%	-	0.103 ± 4.47%
Uncompetitive inhibition with enzyme inactivation	-15174	0.019184	0.0350 ± 2.71%	0.3772 ± 4.20%	0.0097 ± 2.85%	-	0.0006 ± 9.96%	0.093 ± 5.00%
Uncompetitive inhibition	-15066	0.019741	0.0269 ± 1.25%	0.3742 ± 4.34%	0.0096 ± 2.94%	-	-	0.072 ± 4.52%
Irreversible Michaelis Menten with enzyme inactivation	-12383	0.039706	0.0214 ± 6.32%	0.4946 ± 8.85%	-	-	0.0006 ± 20.77%	0.043 ± 10.88%
Irreversible Michaelis Menten	-12358	0.039980	0.0158 ± 2.58%	0.4929 ± 8.95%	-	-	-	0.032 ± 9.32%

Table 4.4: Estimated kinetic parameters for the models of α-glucosidase inhibition by fucoidan from *E. maxima*

Model	AIC	RMSD	kcat (1/S)	Km (mM/L)	Ki uncompetitive (mg/L)	Ki competitive (mg/L)	Ki enzyme inactivation (1/S)	kcat/Km (1/s*1/mM/L)
Competitive inhibition	-17476	0.010539	0.0232 ± 0.40%	0.1564 ± 2.67%	-	0.3121 ± 3.82%	-	0.148 ± 2.07%
Competitive inhibition with uncompetitive substrate inhibition	-17475	0.010538	0.0234 ± 1.05%	0.1602 ± 3.82%	458.62 ± 113.3%	0.3158 ± 4.07%	-	0.146 ± 3.96%
Partially competitive inhibition	-17473	0.010541	0.0232 ± 0.41%	0.1562 ± 2.68%	999.99 ± 339.75%	0.3111 ± 5.39%	-	0.149 ± 2.71%
Competitive inhibition with enzyme inactivation	-17459	0.010581	0.0242 ± 1.08%	0.1568 ± 2.68%	-	0.3130 ± 3.84%	0.0001 ± 66.29%	0.155 ± 2.89%
Competitive inhibition with uncompetitive substrate inhibition and enzyme inactivation	-17457	0.010581	0.0245 ± 1.38%	0.1625 ± 3.34%	304.26 ± 67.76%	0.3187 ± 3.87%	0.0001 ± 26.76%	0.151 ± 3.62%
Partially competitive inhibition with enzyme inactivation	-17455	0.010585	0.0242 ± 1.09%	0.1568 ± 2.69%	497.46 ± 643.49%	0.3124 ± 4.08%	0.0001 ± 74.83%	0.155 ± 2.91%
Uncompetitive inhibition	-16449	0.013770	0.0261 ± 0.74%	0.3479 ± 2.22%	2.5261 ± 3.97%	-	-	0.075 ± 2.34%
Uncompetitive inhibition with enzyme inactivation	-16440	0.013798	0.0273 ± 1.50%	0.3482 ± 2.22%	2.5283 ± 3.99%	-	0.0001 ± 48.12%	0.078 ± 2.68%
Irreversible Michaelis Menten	-15672	0.016867	0.0227 ± 0.65%	0.3258 ± 2.60%	-	-		0.070 ± 2.68%
Irreversible Michaelis Menten with enzyme inactivation	-15686	0.016885	0.0237 ± 1.74%	0.3261 ± 2.60%	-	-	0.0001 ± 11.30%	0.073 ± 3.13%

Table 4.5: Estimated kinetic parameters for the models of α-glucosidase inhibition by fucoidan from *E. radiata*

Model	AIC	RMSD	kcat (1/S)	Km (mM/L)	Ki uncompetitive (mg/L)	Ki competitive (mg/L)	Ki enzyme inactivation (1/S)	kcat/Km (1/s*1/mM/L)
Competitive inhibition with uncompetitive substrate inhibition and enzyme inactivation	-19020	0.007042	0.0378 ± 1.38%	0.3382 ± 2.84%	21.24 ± 6.61%	0.0166 ± 2.11%	0.0007 ± 3.09%	0.112 ± 3.16%
Competitive inhibition with enzyme inactivation	-18707	0.007645	0.0317 ± 0.92%	0.2263 ± 1.96%	-	0.0134 ± 2.09%	0.0007 ± 3.36%	0.140 ± 2.17%
Partially competitive inhibition with enzyme inactivation	-18704	0.007646	0.0317 ± 0.93%	0.2263 ± 1.96%	999.99 ± 684.34%	0.0134 ± 2.17%	0.0007 ± 3.38%	0.140 ± 2.17%
Competitive inhibition with uncompetitive substrate inhibition	-18097	0.008962	0.0289 ± 1.46%	0.3355 ± 3.64%	21.30 ± 8.46%	0.0164 ± 2.69%	-	0.086 ± 3.92%
Competitive inhibition	-17902	0.009434	0.0242 ± 0.48%	0.2243 ± 2.44%	-	0.0132 ± 2.59%	-	0.108 ± 2.49%
Partially competitive inhibition	-17899	0.009436	0.0242 ± 0.48%	0.2273 ± 2.38%	999.08 ± 23445%	0.0134 ± 3.49%	-	0.107 ± 2.43%
Uncompetitive inhibition with enzyme inactivation	-16064	0.015217	0.0381 ± 1.95%	0.6071 ± 2.77%	0.0922 ± 2.64%	-	0.0007 ± 6.66%	0.063 ± 3.38%
Uncompetitive inhibition	-15825	0.016201	0.0289 ± 1.04%	0.6052 ± 2.96%	0.0916 ± 2.81%	-	-	0.048 ± 3.14%
Irreversible Michaelis Menten with enzyme inactivation	-14034	0.025829	0.0284 ± 3.27%	0.6188 ± 4.51%	-	-	0.0007 ± 11.10%	0.046 ± 5.57%
Irreversible Michaelis Menten	-13945	0.026446	0.0213 ± 1.42%	0.6185 ± 4.64%	-	-	-	0.034 ± 4.85%

Table 4.6: Estimated kinetic parameters for the models of α-glucosidase inhibition by fucoidan from *S. elegans*

Model	AIC	RMSD	kcat (1/S)	Km (mM/L)	Ki uncompetitive (mg/L)	Ki competitive (mg/L)	Ki enzyme inactivation (1/S)	kcat/Km (1/s*1/mM/L)
Competitive inhibition with uncompetitive substrate inhibition and enzyme inactivation	-16438	0.013797	0.0318 ± 2.91%	0.2422 ± 6.08%	14.35 ± 10.42%	0.0042 ± 4.51%	0.0003 ± 15.85%	0.131 ± 6.74%
Competitive inhibition with uncompetitive substrate inhibition	-16398	0.013948	0.0283± 2.29%	0.2412 ± 6.16%	14.35 ± 10.55%	0.0041 ± 4.56%	-	0.117 ± 6.57%
Competitive inhibition with enzyme inactivation	-16296	0.014325	0.0255 ± 2.06%	0.1390 ± 4.57%	-	0.0028 ± 4.30%	0.0003 ± 16.60%	0.184 ± 5.01%
Partially competitive inhibition with enzyme inactivation	-16294	0.014326	0.0255 ± 2.06%	0.1390 ± 4.57%	999.99 ± 2174.8%	0.0028 ± 4.31%	0.0003 ± 16.62%	0.184 ± 5.02%
Competitive inhibition	-16260	0.014468	0.0227 ± 0.82%	0.1381 ± 4.64%	-	0.0028 ± 4.38%	-	0.164 ± 4.72%
Partially competitive inhibition	-16256	0.014472	0.0227 ± 0.81%	0.1427 ± 4.19%	907.27 ± 32310%	0.0029 ± 3.57%	-	0.159 ± 4.26%
Uncompetitive inhibition with enzyme inactivation	-15804	0.016282	0.0289 ± 2.93%	0.2860 ± 3.89%	0.0303 ± 2.34%	-	0.0003 ± 18.36%	0.101 ± 4.57%
Uncompetitive inhibition	-15775	0.016415	0.0256 ± 1.02%	0.2850 ± 3.93%	0.0303 ± 2.36%	-	-	0.090 ± 4.06%
Irreversible Michaelis Menten with enzyme inactivation	-12575	0.037771	0.0166 ± 6.29%	0.4095 ± 8.97%	-	-	0.0003 ± 43.09%	0.041 ± 10.96%
Irreversible Michaelis Menten	-12571	0.037828	0.0145 ± 2.46%	0.4092 ± 8.99%	-	-	-	0.035 ± 9.33%

It should be noted that EnzymeML significantly contributed to our study by facilitating the visualisation of measurement data alongside fitted kinetic models and identifying systematic deviations across all measured timepoints. It aided in detecting errors related to inhibitor, substrate, and enzyme concentrations, as well as temperature fluctuations, allowing us to address issues within the experimental design. However, in the case of the *F. vesiculosus* and *S. elegans* fitted data plots, systematic deviations between the model and the data persisted in the reactions with inhibitor concentrations of 0.1 and 0.15 $mg.ml^{-1}$ (see Appendix Figures B20 and B23). Notably, the inhibitor appeared to exert a stronger inhibitory effect than predicted by the model, suggesting a potential excess of inhibitor in the reactions compared to the specified concentrations. This discrepancy may stem from the inherent heterogeneity of our fucoidans, which occasionally resulted in variations even when preparing concentrations from the same stock. Despite encountering time constraints and unresolved technical issues with the photometer, which hindered the possibility of conducting additional experiments, the robust fit of the other concentrations to the model provided valuable insights. While we acknowledge this anomaly, we remain confident in our findings but recognise the need for further investigation to fully address this inconsistency.

In the context of our study, the application of EnzymeML proved most valuable in elucidating the individual inhibition mechanisms in more detail than traditional methods allowed for. Leveraging EnzymeML's modelling technique improved our understanding of the fucoidans' interaction with the enzymatic system under investigation. The characterisation of fucoidan from *E. maxima* revealed a competitive mode of inhibition, suggesting its ability to compete for occupancy of the enzyme's active site alongside the substrate and product (Koh et al., 2020), thereby decelerating enzymatic activity. In contrast, acarbose and the other fucoidans exhibited a mixed inhibition profile, combining competitive inhibition with uncompetitive substrate inhibition, indicating a more complex interaction mechanism. The K_i competitive value was smaller than the K_i uncompetitive value, which suggests that the binding affinity of these inhibitors to the α-glucosidase active site greatly exceeds that of the α-glucosidase-PNPG complex and they, therefore, predominantly acted as a competitive inhibitor. Interestingly, in addition to inhibition, we observed enzyme inactivation, which implies an additional inhibitory mechanism beyond mere binding to the enzyme or its enzyme-substrate complex. Enzyme inactivation can involve various mechanisms, including allosteric

modulation, induced conformational changes, covalent modification and competitive displacement or interference (Yadav et al., 2020). Our previous findings of direct interaction and conformational changes induced by these fucoidans support the possibility of induced conformational alterations leading to enzyme inactivation (Daub et al., 2020; Mabate et al., 2021). This suggests that fucoidans, as mixed inhibitors, may induce structural alterations in the α-glucosidase enzyme, also disrupting its catalytic function. While the mechanism of mixed inhibition by fucoidans has been reported previously (Mabate et al., 2021), this study, to the best of our knowledge, is the first to identify uncompetitive substrate inhibition and enzyme inactivation as elements of this mixed inhibition.

4.4.7 Exploring the kinetic inhibition mechanisms of maltase and sucrase by fucoidans

Next, inhibition kinetic studies of maltase and sucrase were performed relying on traditional Michaelis-Menten and Lineweaver-Burk plot analysis (Figures 4.5 and 4.6). Only the extracts showing significant inhibitory potential for the respective enzymes were investigated for their mode of inhibition. The Lineweaver-Burk double reciprocal plot of 1/v versus 1/[S] facilitated the initial identification of the mechanism of enzyme inhibition by acarbose and the fucoidans. For further confirmation of their mechanism of inhibition, Michaelis-Menten and Lineweaver-Burk plots were used to derive the kinetic parameters of the digestive enzymes. These analyses were conducted using GraphPad Prism 6.0 software (GraphPad Software, San Diego, CA, USA), and the results are summarised in Table 4.7.

The Lineweaver-Burk plot (Figure 4.5B) depicting the inhibition mechanism of acarbose on maltase showed straight lines sharing a y-intercept but differing in slopes and x-intercepts, indicating competitive inhibition of maltase (Pesaresi, 2023). The value of the Michaelis constant (K_m) decreased while the maximal reaction rate (V_{max}) remained unchanged (see Table 4.7), which is consistent with the characteristics of competitive inhibition (Koh et al., 2020). This finding agrees with existing literature, which widely reports the competitive inhibitory mode of acarbose (Shan *et al.,* 2016).

The inhibition mechanisms of maltase and sucrase by the *F. vesiculosus*, *E. radiata* and *S. elegans* fucoidans can be deduced from Figures 4.5B and 4.6B. Lineweaver-Burk plots for both enzymes in the presence of these fucoidans suggested that their inhibitions were of the mixed inhibition type (Adisakwattana et al., 2009, Pesaresi,

2023). Such inhibition is characterised by decreasing V_{max} and fluctuating K_m values. In the presence of the various fucoidans, there was a decrease in the value of V_{max}, while the K_m values of maltase predominantly increased (Table 4.7). Mixed inhibitors typically bind to both the free enzyme and the enzyme-substrate complex, but with varying affinities (Rouzbehan *et al.,* 2017). In this context, the K_m values of maltase from the fucoidans (Table 4.7) appeared to increase with increasing fucoidan concentration, indicating a preference for the free enzyme by the fucoidans classifying them as mixed-competitive inhibitors (Li et al., 2019). Furthermore, results from our kinetics analyses presented in Figure 4.6 and Table 4.7, indicated that acarbose acts as a mixed-competitive type inhibitor of sucrase. This form of inhibition, although rarely reported for acarbose, was noted in a study by Son and Lee (2013).

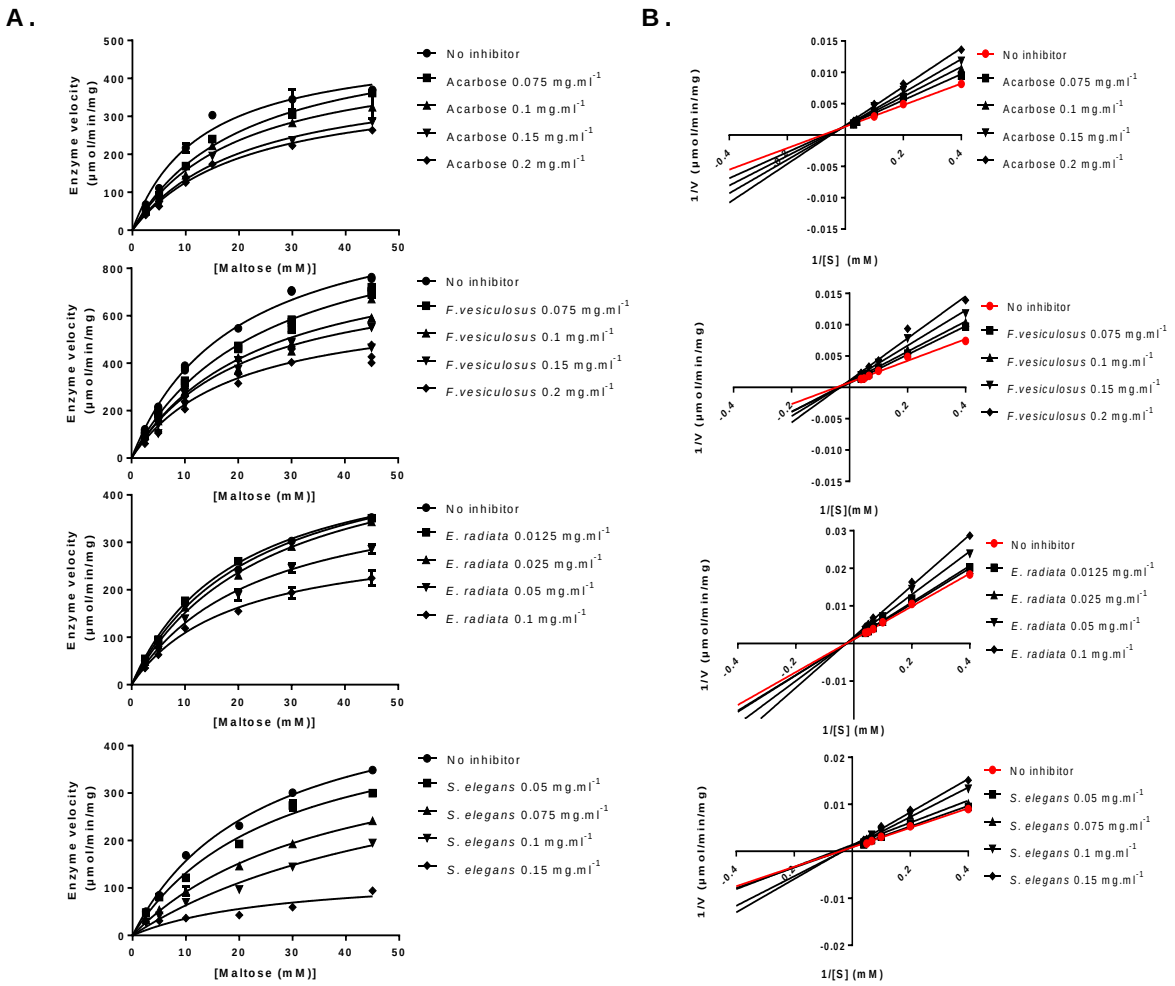

Figure 4.5: (A) Michaelis-Menten plots and (B) Lineweaver-Burk plots with maltase in the presence of the inhibitors acarbose and fucoidans.

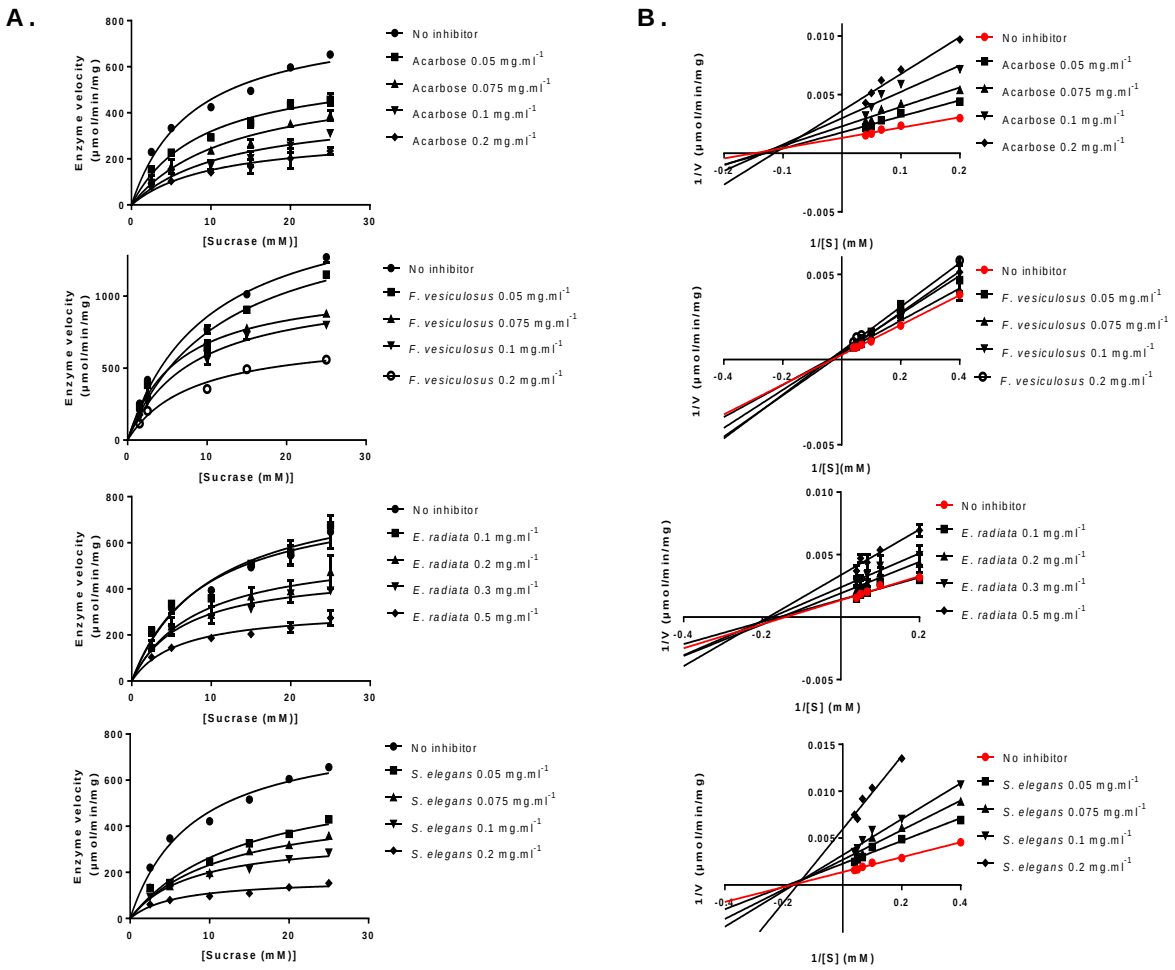

Figure 4.6: (A) Michaelis-Menten plots and (B) Lineweaver-Burk plots with sucrase in the presence of the inhibitors acarbose and fucoidans.

Table 4.7: K_m and V_{max} values and mechanism of inhibition of maltase and sucrase by acarbose and fucoidan extracts

Enzyme	Inhibitor ($mg.ml^{-1}$)	K_m	V_{max}	Type of inhibition
Maltase	[Acarbose]			Competitive
	No inhibitor	12.76	443	
	0.075	17.14	505	
	0.1	19.93	521	
	0.15	23.07	541	
	0.2	24.40	472	
	[*F. vesiculosus*]			Mixed
	No inhibitor	22.07	910	
	0.075	23.86	906	
	0.1	26.77	813	
	0.15	27.23	707	
	0.2	30.23	564	
	[*E. radiata*]			Mixed
	No inhibitor	22.69	529	
	0.0125	25.32	509	
	0.025	25.16	535	
	0.05	29.70	430	
	0.1	22.09	317	
	[*S. elegans*]			Mixed
	No inhibitor	17.09	533	
	0.0125	24.29	489	
	0.025	23.69	440	
	0.05	29.71	441	
	0.1	31.62	132	
Sucrase	[Acarbose]			Mixed
	No inhibitor	7.76	813	
	0.05	8.99	606	
	0.075	12.76	557	
	0.1	12.29	422	
	0.2	10.48	309	
	[*F. vesiculosus*]			Mixed
	No inhibitor	10.11	1222	
	0.025	9.87	1034	
	0.075	11.18	989	
	0.1	8.16	974	
	0.2	6.22	530	
	[*E. radiata*]			Mixed
	No inhibitor	8.84	815	
	0.1	9.89	867	
	0.2	8.16	580	
	0.3	6.51	482	
	0.5	7.01	312	
	[*S. elegans*]			Mixed
	No inhibitor	7.91	830	
	0.05	14.62	648	
	0.075	11.73	504	
	0.1	7.72	353	
	0.2	5.87	172	

When functioning as a competitive inhibitor, acarbose mimics the substrate of the enzyme, thereby competing for binding to the enzyme's active site (Proença et al., 2017). Unlike other forms of inhibition, competitive inhibition can be fully overcome by increasing the substrate concentration (Koh et al., 2020). Therefore, the mixed inhibition profiles observed for fucoidans in our study suggest a distinct advantage for their potential use, as it implies that their inhibitory activity would not be impeded by higher substrate concentrations. This is not the case for competitive inhibitors like acarbose, which may struggle to effectively compete at elevated substrate levels, necessitating larger doses when administered with meals (Rouzbehan et al., 2017). As our findings indicate a mixed inhibition pattern for fucoidans, fucoidans are expected to bind to the active sites of α-glucosidase enzymes. The structural resemblance of fucoidan molecules to biologically active mammalian glycans, as noted by Bilan and Usov (2008), further supports the notion that fucoidans are likely to interact with the active sites of these enzymes.

4.5 Conclusion

In conclusion, this chapter provides compelling *in vitro* evidence demonstrating that various South African brown seaweeds may serve as sources of potent α-glucosidase inhibitors. Our findings highlight the diverse inhibitory capabilities among brown seaweed species and extracts, with fucoidans clearly outperforming sodium alginates in inhibiting the carbohydrate digestive enzymes involved in postprandial glycaemia. Fucoidans strongly inhibited α-glucosidase, maltase, and sucrase activities, while α-amylase activity remained unaffected, an inhibition profile considered desirable due to the gastrointestinal issues associated with strong amylase inhibition. Among the fucoidans tested, those derived from *E. radiata* and *S. elegans* displayed particularly robust inhibition of these enzymes, surpassing the inhibition observed with the positive control acarbose. Moreover, our study reveals the selective and distinct inhibition profiles of the three major α-glucosidases by these fucoidans. Furthermore, we provided a detailed analysis of their kinetic inhibition patterns. The implementation of EnzymeML, a modern and versatile tool for enzyme kinetics analysis, enabled the accurate determination of the mode of inhibition of α-glucosidase by fucoidans. Our findings indicate that the fucoidans act as mixed inhibitors, with contributions from competitive inhibition, uncompetitive substrate inhibition and enzyme inactivation.

Traditional kinetic analysis of fucoidan extracts for sucrase and maltase suggests a mixed inhibition pattern that for maltase more closely resembled a competitive-like behaviour. This broader mixed inhibitory mechanism offers advantages over purely competitive inhibition, as its efficacy is less affected by dietary carbohydrate levels and remains consistent regardless of carbohydrate intake. In summary, the findings in this chapter offer valuable insights into the therapeutic potential of fucoidans from South African brown seaweeds as effective α-glucosidase inhibitors for managing postprandial glycaemia, for example in Type 2 Diabetes. Building on these promising results, the next chapter shifts the focus to exploring the anti-cancer activity of these fucoidans and sodium alginates.

Chapter 5- Evaluating anti-cancer potential: investigating the effects of fucoidans and sodium alginates on a colon cancer cell line

5.1 Introduction

Cancer is a complex, multifaceted disease characterised by the uncontrolled proliferation of abnormal cells leading to malignant tumour formation (Atashrazm et al., 2015). Among the various types of cancer, colorectal cancer (CRC) stands out for its widespread occurrence and significant global mortality rates. Globally, CRC ranks third in incidence but second in mortality (Han et al., 2022). With over 1.85 million new cases reported annually, accounting for 9.8% of total cancer diagnoses, CRC leads to an estimated 850,000 deaths yearly (Chhikara & Parang, 2023). Within the South African context, the incidence of CRC is projected to increase further, driven by factors such as urbanisation, rising obesity and diabetes prevalence (Lala et al., 2024). Most of the morbidity and mortality associated with CRC arises from metastatic disease (Rajput et al., 2008). While patients with early-stage disease typically undergo surgery without chemotherapy, those with advanced stages often receive adjuvant chemotherapy to reduce recurrence risk (Han et al., 2022). However, standard chemotherapy drugs like 5-fluorouracil (5-FU), commonly selected for CRC treatment, exhibit limited efficacy in advanced CRC, with monotherapy response rates of only 10-15%**.** Furthermore, chemotherapy is associated with varying degrees of side effects (Wang et al., 2022). In this study, 5-FU was selected as a positive control due to its widespread use in CRC treatment. Despite advancements in traditional toxic chemotherapeutics that have prolonged disease-free survival, the overall survival rates for patients with metastatic disease remain disappointingly low. Therefore, there is an urgent need for therapeutic strategies which prevent or suppress the progression to metastatic cancer, highlighting the critical importance of addressing this process as a therapeutic target (Han et al., 2022; Andersen et al., 2019).

Dysregulation of various cellular processes and signalling pathways contributes to the acquisition of metastatic traits by cancer. In the early stages of the metastatic cascade, cancer cells display a tendency to migrate and invade surrounding tissues, a crucial step in their journey to enter the bloodstream and spread to distant sites, facilitating metastasis (Massagué & Obenauf, 2016). Cells undergo dynamic changes in their cytoskeleton, particularly through the reorganisation of actin filaments, to facilitate

movement (Massagué & Obenauf, 2016). Cell adhesion molecules, such as integrins and cadherins, are essential in coordinating these migration events. Integrins, for instance, serve as cell-ECM adhesion receptors, bridging the actin cytoskeleton to the ECM and transmitting signals that modulate single-cell migration (Janiszewska et al., 2020). Meanwhile, cadherins mediate cell-cell adhesion through adherens junctions, facilitating the collective migration by enabling the coordinated movement of cell groups (Janiszewska et al., 2020).

Additionally, β-catenin, a key component of the cadherin-catenin complex, is involved in regulating cell-cell adhesion and functions as an effector in the activation of the Wnt/β-catenin signalling pathway that influences cell migration and invasion (Sato et al., 2001; Brabletz et al., 2001). The involvement of the Wnt/β-catenin signalling pathway in the proliferation, invasion, and metastasis of CRC cells has been well established.

The ECM normally acts as a barrier, impeding cell movement. However, cancer cells can breach this barrier with the help of enzymes known as matrix metalloproteinases (MMPs). Expressed on the cell surface, MMPs locally degrade ECM components, facilitating the loosening of the matrix structure for cancer cells to migrate through (Mustafa et al., 2022). This ECM breakdown allows cancer cells to invade surrounding tissues and join the bloodstream to spread to more distant sites (Mustafa et al., 2022). Consequently, during metastasis, cancer cells require the ability to grow independent of anchorage, to allow for proliferation and survival without substrate or ECM attachment, thereby facilitating metastasis by promoting survival in circulation (Sant and Johnston, 2017). The intermediate filament vimentin, acquired during EMT, strengthens a migrating cell's ability to withstand stress by creating an elastic meshwork that protects it against compressive and shear stress (Castaneda et al., 2022). As tumour metastasis is a hallmark of cancer, targeting fundamental metastatic processes presents a plausible strategy to alleviate tumour progression (Anderson et al., 2018).

Fucoidan and sodium alginate are both recognised for their diverse bioactive properties. As dietary fibres, they undergo minimal digestion in the upper gastrointestinal tract and accumulate in the lumen within the large intestine over extended periods of time (Zhang et al., 2022). Given their resistance to digestion, they may prove to be excellent candidates for the treatment of colon carcinogenesis, if they

exert anti-carcinogenic effects in the colon. Therefore, in this chapter, we screened the fucoidans and sodium alginates for their anti-cancer efficacy, using the HTC116 colon cancer cell line as a model system that fulfils the rate-limiting steps of local invasion and distant colony formation in metastasis (Rajput et al., 2008).

5.2 Objectives

The objectives of this chapter were to:

- Determine the cytotoxic effects of fucoidan and sodium alginate extracts on the HCT116 colon cancer cell line.
- Explore the effects of the fucoidan and sodium alginates on various cellular aspects, including tumour growth, adhesion, migration, invasion and anchor independent growth implicated in metastasis.
- Investigate the possible mechanisms that underpin these effects.

5.3 Materials and Methods

5.3.1 Materials

All experiments were performed using the HCT116 human colon cancer cell line purchased from the American Type Culture Collection (ATCC CCL-247). The analytical kits specific to each experiment are described in the methods section below. All reagents and antibodies, alongside their supplier information, are listed in Appendix Tables A1 and A2.

5.3.2 Cell culture maintenance

The cell line was cultured in Dulbecco's Modified Eagle's Medium (DMEM) with GlutaMAX™-I, 10% (v/v) fetal bovine serum (FBS), and 1% (v/v) penicillin, streptomycin and amphotericin (PSA), and was maintained at 37°C with 9% CO_2 in a humidified atmosphere.

5.3.3 Cytotoxicity screening

The sensitivity of the cell lines to fucoidan and sodium alginate extracts was assessed using the resazurin assay, as previously described by Mabate et al. (2023). Briefly, cells were seeded in DMEM growth medium into the wells of a 96 well plate at a density of 1 x 10^5 cells/well. The cells were allowed to adhere overnight before treatment with the extracts at various concentrations (0.00128 - 2500 $\mu g.ml^{-1}$). The plate was incubated at 37°C in an atmosphere of 9% CO_2 for 72 hours. Subsequently, resazurin

(0.54 mM) was added to each well and the plate was incubated for another 3 hours. Thereafter, fluorescent measurements (excitation = 560 nm and emission = 590 nm) were taken on a Synergy™ MX Microplate Reader (BioTek Instruments Inc., Winooski, VT, USA). All experiments were performed in triplicate. 5-Fluorouracil (5-FU) was included as a positive control. The half maximum response concentration (IC_{50}) was calculated by non-linear regression using Graph Pad Prism Software version 6.0 (GraphPad Inc., San Diego, CA, USA).

5.3.4 Cell proliferation

Cell proliferation was evaluated by resazurin assay. The untreated cells, alongside fucoidan and sodium alginate treated (100 – 500 $\mu g.ml^{-1}$) cells, were seeded at 6000 cells/well into 96 well plates for different periods of time (24, 48, 72 and 96 hours). The resazurin reduction assay was performed as outlined above (section 5.3.3).

5.3.5 Scratch assay to measure cell migration

The HCT116 cells were seeded onto 24 well plates at 7×10^5 cells/ml and grown to 100% confluence. After aspirating the medium, a wound was made by scratching the cells' monolayer with a sterile micropipette tip. Displaced cells were removed by washing with medium. Thereafter, fresh medium with and without treatments at various concentrations (0.1 – 0.5 $mg.ml^{-1}$) was added and plates were incubated for 24 hours. The wound area was imaged at 4x magnification using a Zeiss Primovert inverted light microscope (Carl Zeiss, Jena, Germany) at the time of initiation of the wound (t=0) and again after 6, 12 and 24 h of cell migration at the same position as the premigration images. The area of the wound was measured using Fiji/ImageJ software's wound healing plugin (Suarez-Arnedo et al., 2020) and cell migration was estimated by expressing % wound closure as wound area in relation to wound area at t=0 h.

5.3.6 Transwell migration assay to measure cell migration

Serum starved HCT116 cells in serum-free cell culture medium containing 0.1 % (w/v) bovine serum albumin (BSA) were seeded onto the top surface of 0.4 µm polycarbonate membrane transwell inserts in 6-well plates (CoStar, PID0522959) at a density of $1x10^6$ cells/well. The lower chambers of the transwell system were filled with 1 ml of medium containing 50 $ng.ml^{-1}$ vascular endothelial growth factor (VEGF), 25 µM tamoxifen (TMX) or 0.25 $mg.ml^{-1}$ fucoidan. For each treatment, replicate wells without transwell inserts were included to determine the percentage of total cells that migrated (control). The plates were incubated for 24 hours at 37°C in a 9% CO_2

atmosphere. After incubation, the non-migrated cells on the upper surface of the polycarbonate membranes were gently removed by scraping and rinsing the membranes to avoid damage. Migrated cells were quantified by staining the membranes with 50 ng/ml of 3-(4,5-dimethylthiazol-2-yl)-2,5-diphenyltetrazolium bromide (MTT) solution for 4 hours at 37°C. For wells without inserts, 600 µl of media was collected, centrifuged at 15,000 rpm for 1 minute, and the pellet was retained for solubilisation with 100% dimethyl sulfoxide (DMSO). For wells with inserts, the polycarbonate membranes were excised and solubilised in DMSO. The solubilised solution from all wells was centrifuged at 15,000 rpm for 1 minute, and the supernatant was collected. A 1:10 dilution of each treatment in DMSO was prepared, and 200 µl was transferred in triplicate into a 96-well plate. The absorbance at 540 nm was measured using a plate reader. Relative migration was calculated by normalising the absorbance of treatment groups to their corresponding control groups to account for differences in cell viability.

5.3.7 Cell adhesion

5.3.7.1 Cell adhesion: treatment at the time of seeding

Cells ($6x10^4$ cells/well) were seeded into wells of a 96 well plate with concurrent treatment with EDTA (0.25- 1.25 mM), fucoidan or sodium alginate (0.1-1 $mg.ml^{-1}$), and left to adhere over 8 hours under tissue culture conditions. Unattached cells were removed by aspirating the medium and washing thrice with sterile PBS [137 mM NaCl, 2.7 mM KCl, 10 mM Na2HPO4 and 2 mM KH_2PO_4, pH 7]. Adherent cells were fixed with methanol: acetic acid (3:1) for 15 min at room temperature. The fixative was discarded, and the cells were washed with dH_2O and blotted dry. Cells were stained with 0.1% (w/v) crystal violet dye at room temperature for 20 minutes with gentle agitation. The crystal violet stain was discarded, the wells washed four times with dH_2O and blotted dry. The stained cells were imaged using a Zeiss Primovert inverted light microscope (Carl Zeiss, Jena, Germany) at 10x magnification. After imaging, the crystal violet dye was solubilised overnight in 1% (w/v) SDS and the absorbance measured at 590 nm using the Epoch™ 2 Microplate Spectrophotometer (BioTek with Gen 5™ software)

5.3.7.2 Cell adhesion: seeding post-treatment

Cells seeded ($1x10^6$ cells/well) into the wells of a 12 well plate, containing EDTA (0.25 - 1.25 mM), fucoidan or sodium alginate at concentrations ranging from 0.1 - 1 $mg.ml^{-}$

^{1}, were allowed to adhere over 12 hours under tissue culture conditions. Non adherent cells were removed by washing thrice with PBS. The adherent treated and untreated cells were detached from the cell culture plate with trypsin, enumerated by trypan blue staining and seeded at a density of $6x10^4$ cells/well in a 96 well plate. The pre-treated cells were then allowed to adhere over 8 hours and cell adhesion was assessed as described in section 5.3.7.1 above.

5.3.7.3 De-adhesion of stably attached cells

To assess the detachment of cells in the presence of the various treatments (EDTA, fucoidan and sodium alginate), HCT116 cells were seeded, as for the other adhesion assays, at a density of $6x10^4$ cells/well into wells of a 96 well plate but left to fully adhere for 12 hours. Adherent cells were then left untreated or treated with EDTA (0.25 - 1.25 mM), fucoidan and sodium alginate at 0.1 - 1 $mg.ml^{-1}$. To quantify detachment, the cells were incubated for a further 8 hours, after which the detached cells were removed by three washes with PBS, and the adherent cells were stained, imaged, and quantified as described above in section 5.3.7.1.

5.3.7.4 Time-dependent cell adhesion

For this, the adhesion assays (section 5.3.7.1) were carried out using single concentrations of 0.05 $mg.ml^{-1}$ of fucoidan and sodium alginate. The cells ($6x10^4$ cells/well) were treated as noted above and incubated for 8 - 32 hours at 37°C, 9% CO_2. Plates were sampled at various time points and processed as outlined.

5.3.8 Immunofluorescent staining of monolayer cultures

HCT116 cells (20 x 10^4 cells/ml) were cultured on ethanol-sterilised glass coverslips overnight and treated as described in the figure captions. Cells on coverslips were washed with sterile PBS (137 mM NaCl, 10 mM Na_2HPO_4, 1.76 mM KH_2PO_4 2.7 mM KCl, pH 7.4), fixed with ice-cold methanol and air-dried. Following fixation, cells were permeabilised for 15 minutes with 0.1% (v/v) Triton X-100/PBS and blocked for 1 hour at room temperature using 1% (w/v) BSA in PBS-T (1% v/v Tween-20 in TBS). Cells were incubated with primary antibodies in 0.1% (w/v) BSA/TBS-T, washed twice with 0.1% (w/v) BSA/TBS and subsequently incubated with fluorescently conjugated species-matched secondary antibodies for 1 hour in the dark. Cells were washed again with 0.1% (w/v) BSA/TBS and nuclei were stained by a brief wash with Hoescht-33342 (1 µg/ml in dH_2O). The coverslips were mounted on to microscope slides using Dako

mounting medium. Images were captured on the Olympus BXM fluorescence microscope (Olympus life science, Tokyo, Japan) and analysed using ZEN blue software (Carl Zeiss, Jena, Germany) and ImageJ software 1.50i (NIH freeware). Antibodies and dilutions used are specified in Appendix Table A2. Colocalisation was performed using the Image J colocalisation plug-in (National Institutes of Health [NIH]).

5.3.9 Gelatin zymography

Cells seeded at a density of 1x 10^5 cells/ml in 12 well plates were grown to a confluency of 80%, after which the medium was replaced with serum-free DMEM, and the cultures were left untreated (control) or treated with 0.1 – 0.5 $mg.ml^{-1}$ fucoidan, 50 $ng.ml^{-1}$ VEGF or 25-125 mM TMX for 48 hours. Serum-free culture supernatant fractions were collected and clarified by centrifugation at 300 x*g,* and protein concentration was determined using the bicinchoninic acid (BCA) assay (Walker, 2009). Samples (10 µg total protein) mixed with non-reducing 2x Laemmli sample buffer without prior boiling were electrophoresed on 7.5% SDS-polyacrylamide gels containing 0.1% (w/v) gelatin at 150 V for 90 minutes. The gels were washed twice for 30 min in washing buffer [50 mM Tris- HCl, pH 7.5, 5 mM $CaCl_2$, 1 µM $ZnCl_2$, 2.5% Triton-X 100] to remove SDS and allow the protein to renature, and then immersed in developing buffer [50 mM Tris-HCl, pH 7.5, 5 mM $CaCl_2$, 1 µM $ZnCl_2$, 1% (v/v) Triton-X 100] for a 24-hour incubation at 37 °C. After that, the gels were stained with 0.5% (w/v) Coomassie Blue R250 in 40% (v/v) methanol and 10% (v/v) glacial acetic acid for 1 hour and subsequently destained (40% (v/v) methanol, 10% (v/v) acetic acid) until the desired contrast was achieved. The areas of gelatinolytic activities were visualised as transparent lysis zones against the blue stained background using a Chemi Doc™ XRS+ with Lab™ Software (BioRad, USA) and the bands' densities were measured using Image J (NIH freeware). A pre-stained broad range molecular weight marker (10-250 kDa) (BIOKÉ, Leiden, Netherlands) was run concurrently to approximate the molecular size of the bands displaying gelatinase activity. In addition, gelatin zymograms were run for the fucoidan extracts at various concentrations to ensure that no gelatin proteases were present within the extracts themselves. Parallel SDS-PAGE gels lacking gelatin, which had not been renatured or developed, were incubated directly in Coomassie stain to serve as a protein loading control.

5.3.10 Quantitative real-time PCR of MMP-9 and MMP-2

Total RNA was extracted from HCT116 cells (3x 10^6 cells/ml) left untreated and treated with fucoidan (0.25 mg.ml^{-1}) for 24 hours using a commercial kit (Direct-zol™ RNA Miniprep kit Cat. No. 2080 from Zymo Reasearch, Irvine, CA, USA) according to the manufacturer's instructions. The RNA was cleaned and concentrated using the RNA Clean and Concentrator^{TM}-5 kit (Cat. No. R1013/1014 from Zymo Research, Irvine, CA, USA) and equal amounts of total RNA concentration were converted to cDNA using the LunaScript RT SuperMix Kit (Cat. No. E3010 from Biolabs Inc., Cambridge, MA, USA). PCR primers for human MMP-9 and MMP-2 were as follows: MMP9 5′-TACCGAGAGAAAGCCTATT-3′ (sense) and 5′-CACCTGGTTCAACTCACT-3′ (antisense); MMP2 5′-CTTCCAAGTCTGGAGCGATGT-3′ (sense) and 5′-TACCGTCAAAGGGGTATCCAT-3′ (antisense). GAPDH (sense 5′-TGTAGTTGAGGTCAATGAAGGG -3′ and antisense 5′-ACATCGCTCAGACACCATG-3′) was used as the reference gene to nominalise expression between the different samples. Real time qPCR was performed on a CFX Connect Real-Time PCR Detection System (BioRad, USA) in a total volume of 20 µl using the Luna Universal qPCR Master Mix with 2 µl cDNA and 10 µM primers. The amplification conditions for the RT-qPCR were set as follow: 95°C for 1 min for one cycle, followed by 40 cycles of 95°C for 15 seconds and 60°C for 30 seconds. The relative quantification of mRNA abundance (ΔCt) was performed by nominalising MMP to GAPDH according to the equation ΔCt = Ct Target Gene - Ct Reference Gene and converting to normalised fold expression (ΔΔCt) relative to the control sample (untreated HCT116) according to the equation ΔΔCt = ΔCt Test - ΔCt Control (Dhanani et al., 2017). The amplification of a single PCR product was confirmed by melting curve analysis.

5.3.11 Fluorescent gelatin degradation assay

Coverslips were coated with 0.1 mg.ml^{-1} Oregon Green-488 conjugated gelatin and cross-linked with 0.5% glutaraldehyde as per the published protocol by Díaz (2013). Cells were seeded at a density of 20 x 10^4 cells/ml onto the OG-488-gelatin-coated glass coverslips and allowed to adhere overnight. Cells were left untreated or treated with 0.25 mg.ml^{-1} fucoidan (*E. maxima* and *S. cymosum*) for 24 hours at 37°C. After that, cells were fixed with freshly prepared 4% (w/v) paraformaldehyde and co-stained with Hoechst 33342 and Wheat Germ Agglutinin conjugated to Alexa Fluor 555 (WGA-555). Coverslips were prepared for fluorescent imaging, omitting the permeabilisation step, and imaged as described previously in section 5.3.8.

5.3.12 Spheroid formation

HCT116 spheroids were generated in agarose-coated 96 well plates. For plate coating, 1% (w/v) agarose stock solution was prepared in autoclaved dH_2O. The agarose was dissolved by heating, and 100 µl liquid agarose was dispensed into each well under sterile conditions. The coated plates were cooled to room temperature until a solid agarose layer was obtained. Cells were seeded at a density of 5000 cells/well and treated with various concentrations of EDTA (0.25 – 1.25 mM), fucoidan (0.01 - 1 $mg.ml^{-1}$) and sodium alginate (0.01 - 1 $mg.ml^{-1}$). Cells were allowed to aggregate undisturbed into spheroids over 3 days at 37°C in an atmosphere of 9% CO_2. On day 3, 50 µl of the old medium was supplemented by 40 µl of the fresh medium in each well and 10 µl treatment. Spheroids were imaged on days 3, 5 and 7 at 4X magnification. The spheroid area was measured by Fiji/ImageJ software.77 (NIH freeware).

5.3.13 Immunofluorescent staining of spheroids

After culturing the spheroids for 3 or 7 Days in agarose coated 96 well plates, as described in section 5.3.6, spheres were transferred to glass coverslips and fixed with ice cold methanol for 5 minutes. Then, immunofluorescent staining was performed, permeabilising the cells and incubating with the coverslips with antibodies as previously outlined in section 5.3.8.

5.3.14 Soft agar clonogenic assay

The soft agar colony formation assay was performed as previously described by Borowicz et al. (2014). In brief, 1x 10^4 cells, treated with 0.25 $mg.ml^{-1}$ fucoidan or sodium alginate or without treatment (control), were suspended in 1 ml DMEM (10% FBS, 1% GlutaMAX™-I, 1% PSA, 1% sodium pyruvate, 3.7 g/l sodium bicarbonate) containing 0.35% agarose and plated onto a DMEM base agar layer containing 0.5% agar in a 12 well plate. The cultures were maintained at 37°C in a 9% CO_2 incubator for 23 days and fed every 3 days with cell culture medium. The resulting colonies were stained with 0.05% crystal violet for 15 minutes, destained with autoclaved dH_2O and imaged using the ChemiDoc™ XRS+ imaging system (BioRad, USA). The number of colonies were counted using Fiji/Image J software.

5.3.15 Western blot analysis

The expression level of proteins in untreated and 24-hour fucoidan (*E. maxima* or *S. cymosum*) treated HCT116 cells was assessed by discontinuous Sodium Dodecyl Sulphate Polyacrylamide Gel Electrophoresis (SDS-PAGE) (Laemmli,1970) followed by Western blot analysis (Towbin et al., 1979) using standard modified protocols. Briefly, cells were washed with PBS and lysed in RIPA lysis buffer (1% (v/v) Igepal® CA-630, 0.5% (w/v) sodium deoxycholate, 0.15 M NaCl, 0.5% (w/v) SDS, 50 mM Tris, pH 8.0) supplemented with 1% (v/v) PIC (Protease inhibitor cocktail solution) for 15 min on ice using a plastic cell scraper. Total protein extracted was quantified using the BCA assay (section 5.3.9). Equal amounts of protein (50 µg) boiled in Laemmli sample buffer supplemented with 5% (v/v) β-mercaptoethanol for 5 minutes, were separated using a 4% (v/v) stacking gel (0.5 M Tris-Cl, pH 6.8) and either a 10 or 12% (v/v) resolving gel (1.5 M Tris-Cl, pH 8.8) electrophoresed at 120 V for 90 minutes in SDS-PAGE running buffer (0.25 mM Tris, 192 mM glycine, 1% (w/v) SDS, pH 8.3).

Resolved proteins were electro-transferred to a nitrocellulose membrane (Bio-Rad Laboratories, Hercules, CA, USA). Membranes were stained with Ponceau S stain (0.5% (w/v) Ponceau S, 1% (v/v) glacial acetic acid) to confirm protein transfer from the gel to the membrane. The membranes were blocked with 5% (w/v) BLOTTO in Tris-Buffered Saline (TBS; 50 mM Tris, 150 mM NaCl, pH 7.5) for 1 hour and probed with the indicated primary antibodies at 4°C overnight. The membranes were washed three times with TBST (TBS containing 1% (v/v) Tween 20) and incubated with species-matched HRP-conjugated secondary antibodies for 1 h at room temperature. After washing with TBST, the protein's chemiluminescent signal was developed with the Clarity Western Enhanced Chemiluminescence (ECL) substrate and detected using the ChemiDoc™ XRS+ imaging system (BioRad, USA). The intensity of the immunoreactive bands was analysed using ImageJ software 1.50i (NIH freeware) and normalised to the expression of GAPDH. Western blotting was used to explore the levels of pan-cadherin, β-catenin, p-β-catentin, p-Akt, FAK, p-FAK, MOB, p-MOB expressed in the HCT116 human colon cancer cells. Details on the antibodies used can be found in Appendix Table A2.

5.3.16 Statistical analysis

Data presented in this section were obtained from three technical replicates with values represented as mean ± standard deviation (SD), unless otherwise stated. Where relevant, one-way analysis of variance (ANOVA) was used to assess significant differences between the treated groups and controls. *P* values of less than 0.05 ($p < 0.05$) were considered statistically significant. The different levels of statistical significance are denoted by a different number of asterisks and are indicated as follows: ***p <0.001, **p <0.01, *p <0.05. All statistical analyses were performed using Graph Pad Prism Software version 6.0 (GraphPad Inc., San Diego, CA, USA).

5.4 Results and Discussion

5.4.1 Effect of fucoidan and sodium alginate treatment on HCT116 cell line viability

The effect of fucoidan and sodium alginate treatment on the viability of HCT116 colon cancer cells was examined using a standard resazurin assay and compared to the chemotherapeutic drug 5-fluorouracil (5-FU). The reduction in cell viability ascribable to the fucoidan and sodium alginate extracts was expressed as the percentage of viable cells remaining after treatment compared to the untreated control cells. The half-maximal inhibitory concentrations (IC_{50}) were determined using a non-linear regression equation in GraphPad Prism 6. The 5-FU treatment induced an expected significant dose-dependent reduction in cell viability, with an IC_{50} of 5.02 µM (see Appendix Figure B25). As shown in Figures 5.1A and 5.1B, none of the sodium alginate extracts or the fucoidan extracts from *E. radiata*, *S. elegans* and *S. cymosum* displayed any significant effect on the HCT116 cells viability (Figure 5.1.). However, treatment with *F. vesiculosus* and *E. maxima* fucoidan concentrations of 1250 µg.ml^{-1} and above significantly ($p < 0.001$) suppressed the viability of HCT116 cells in a dose-dependent manner (Figure 5.1A). The IC_{50} values of *F. vesiculosus* and *E. maxima* were predicted to be 1432 µg.ml^{-1} (R^2=0.972) and 1690 µg.ml^{-1} (R^2= 0.630), respectively (see Appendix Figure B25). This suggests that both fucoidans may be toxic to cells at high concentrations, however the poor fit of the survival curve for *E. maxima* means that this data must be interpreted with caution, as it is likely unreliable because we did not achieve a concentration that induced 100% cell death.

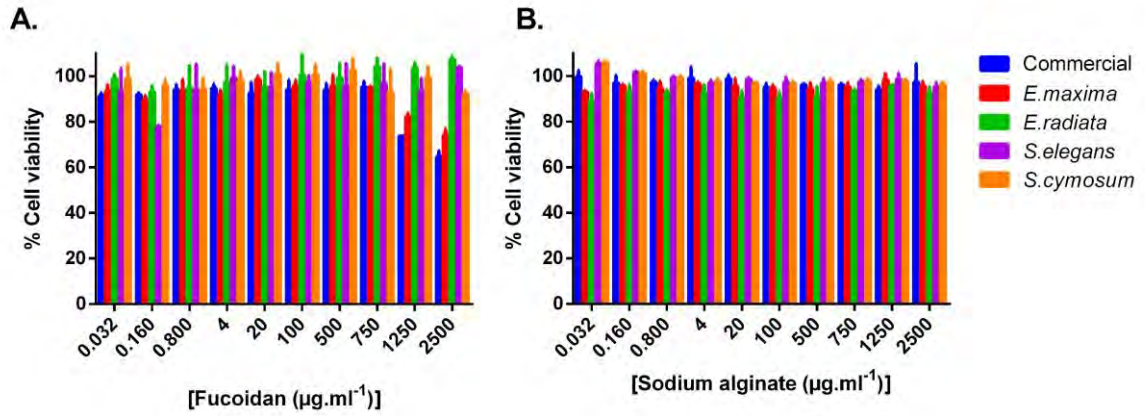

Figure 5.1: Cell viability of HCT116 cells following 72 hour treatment with (A) fucoidan and (B) sodium alginate extracts. % Cell viability was assessed by the resazurin assay in relation to untreated HCT116 cells**.** Commercial fucoidan sourced from *F. vesiculosus*, source of the commercial sodium alginate unknown. Values are represented as mean values ± SD (n=3).

Compared to 5-FU, the *F. vesiculosus* and *E. maxima* fucoidans were mildly cytotoxic towards the HCT116 cells. The observed lack of significant cytotoxicity in most of our fucoidan extracts, as well as all sodium alginate extracts, agrees with previous studies indicating their non-toxic nature (Bittkau et al., 2019; Gao et al., 2019; Lin et al., 2020; Mabate et al., 2023). Notably, previous studies have indicated that fucoidans lacking cytotoxic effects still exhibit inhibitory actions against carcinogenic activities, suggesting potential anti-cancer properties even without inducing cytotoxicity (Mabate et al., 2023). While some fucoidans showed activity at relatively high concentrations compared to conventional anticancer drugs (which typically act in the low µg/mL to ng/mL range), their modest potency could potentially be offset by their local delivery to the colon. However, the absence of a non-cancerous cell line in this study limits our ability to evaluate the selectivity and safety of these compounds. Therefore, all extracts were further tested to determine their effects on various cancer hallmark processes.

5.4.2 Effect of fucoidan and sodium alginate treatment on the cell proliferation of HCT116 cells

We proceeded to assess the effects of the extracts on the growth of HCT116 cells, employing the resazurin assay to monitor cell proliferation over a period of 96 hours. Cells were treated with non-toxic concentrations of fucoidan and sodium alginate ranging from 0.1 - 0.5 mg.ml^{-1}. The effects of the addition of the various fucoidans and sodium alginates on the proliferation of HCT116 cells were analysed by normalisation to untreated cells (taken as a 100%) as depicted in Figure 5.2.

Treatment of HCT116 cells with all concentrations of *E. maxima*, *S. elegans* and *S. cymosum* fucoidan (0.1, 0.25 and 0.5 $mg.ml^{-1}$) significantly inhibited the rate of proliferation compared with the untreated control after 96 hours by between 13 and 20% (Figure 5.2A). A treatment time of 72 hours and less, however, showed no significant effect on cell proliferation. In contrast, treatment with *E. radiata* fucoidan also affected cell proliferation after 96 hours. Compared to the untreated cells, *E. radiata* fucoidan, however, caused an increase in cell proliferation to 115.64 ± 4.34% and 122.29 ± 4.85%, when cells were treated with 0.25 $mg.ml^{-1}$ and 0.5 $mg.ml^{-1}$, respectively. Song et al. (2014), who also reported increased cell proliferation following fucoidan treatment, noted that high glucose levels could increase cell growth. It is, therefore, possible that the high glucose levels accounting for up to 76.03 ± 1.53% of the *E. radiata* fucoidan's composition played a role in the increased proliferation of HCT116 cells. Importantly, treatment with the various sodium alginates led to no significant changes in the proliferation of HCT116 cells (Figure 5.2B).

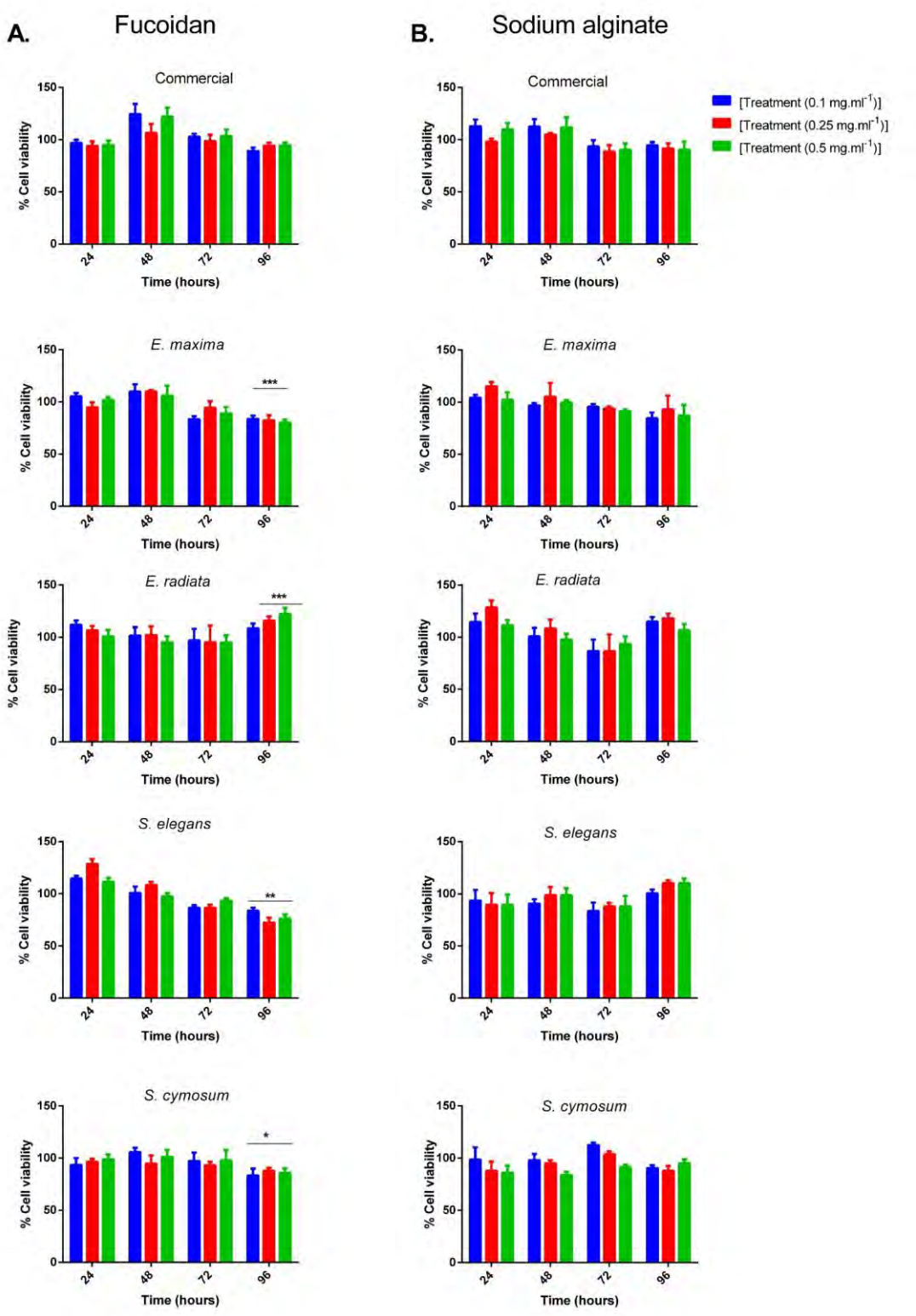

Figure 5.2: Dose-and time-dependent effects of (A) fucoidan and (B) sodium alginate treatment on the proliferation of HCT116 colon cancer cells. Cell proliferation of HCT116 cells incubated for 24 - 96 hours with various concentrations of fucoidan and sodium alginate was quantified by measuring the resorufin fluorescence intensities of cells. Commercial fucoidan sourced from *F. vesiculosus*, source of the commercial sodium alginate unknown. Values are expressed as the mean ± standard error of the mean (n>5) from three independent experiments (***p <0.001, **p <0.01, *p <0.05 vs. untreated cells).

The ability of fucoidans to inhibit proliferation, as seen in this study, has been reported in numerous cancer cell lines, including HepG2, CCD-25Sk, A549, DLD-1, T24 cells and HT29. The results of these previous *in vitro* studies have shown that fucoidan can exert anti-proliferation effects by arresting cell cycle progression, suppressing the activity of epidermal growth factor and/or affecting the expression of cell-cycle regulatory proteins (Arumugam et al., 2019; Lin et al., 2020; Song et al., 2014; Vishchuk et al., 2013). While the initial lack of proliferation inhibition by our fucoidans at earlier time points may suggest a delayed cytostatic effect, the eventual suppression of proliferation after prolonged treatment indicates a time-dependent response to fucoidan. This delayed effect may reflect the time required for fucoidan to exert its inhibitory effects on cell cycle progression or signalling pathways involved in cell proliferation (Lin et al., 2020). Prolonged delays in the later stages of cell cycle events, such as prolonged prometaphase duration during mitosis, have been shown to inhibit cancer cell proliferation (Colin et al., 2015). Cells can typically tolerate being held in mitosis for 12 - 48 hours before slippage into interphase occurs (Uetake and Sluder, 2010). The observed inhibition of proliferation after 72 hours could therefore possibly be due to fucoidan's interference with mitotic processes. In fact, fucoidan has been shown to suppress cancer cell proliferation by disrupting normal mitotic processes and modulating the cell cycle, particularly by arresting cells in the G1 or G2 phases (Lin et al., 2020), which may explain the delayed effects on cell growth observed in this study.

5.4.3 Effect of fucoidan and sodium alginate treatment on HCT116 cell migration

Cell migration is a process critical to both cancer development and tumour metastasis (Al-Menhali et al., 2014). To determine if the extracts affected the migratory capacity of HCT116 cells, the wound healing assay was performed initially. The HCT116 cells migration into a wound, created by scratching a confluent cell monolayer, was estimated with or without fucoidan at various concentrations (0.1, 0.25 and 0.5 $mg.ml^{-1}$) and time points (6, 12 and 24 hours). Figures 5.3A and 5.3B show the effect of treatment on migration after 24 hours calculated as percentage wound closure relative to wound area at 0 hours, as at this timepoint the greatest migration was observed. In addition, the proliferation assay indicated no significant differences in cell proliferation after 24 hours, meaning that wound closure was not due to the stimulation of cell growth (Figure 5.2). While the majority of the fucoidan and sodium alginate extracts did not affect the migratory capacity of HCT116 cells significantly at 24 hours, the cells

treated with *E. maxima* and *S. cymosum* fucoidan showed a dose-dependent reduction in migration that was significant at higher concentrations (Figure 5.3A). Notably, this decrease in migration was observed as early as 12 hours following fucoidan treatment (data not shown). An opposing trend was observed for *F. vesiculosus* fucoidan, which reduced wound area closure only at the lowest concentration (0.1 $mg.ml^{-1}$) tested – which was unexpected. This result could be indicative of a chemokine-like action. Chemokines typically guide cell migration through concentration gradients, with cells moving toward higher concentrations of the chemokine (Petrie & Aronin, 2017). However, when the concentration of the chemokine or related substances becomes too high, it can overwhelm the receptors on the migrating cells, resulting in the saturation or desensitisation of receptors causing reduced migration (Petrie & Aronin, 2017). In the case of *F. vesiculosus* fucoidan, this could explain why higher concentrations lose their ability to inhibit cell migration. This behaviour mirrors the way chemokines require an optimal concentration gradient for effective migration (Petrie & Aronin, 2017).

Our next objective was to confirm the reduced cell migratory effects of these fucoidans on HCT116 cells, by examining their effect on migration using the Boyden transwell migration assay. For this migration assay, the HCT116 cells were incubated for 48 hours in a transwell assay system, after which the number of live cells that had migrated through the membrane of the chamber was quantified by MTT assay. The results showed that fucoidan from *S. cymosum* fucoidan inhibited the migration of HCT116 cells in the transwell chamber by around 10% compared with the control group ($p < 0.03$) (Figure 5.3C). Interestingly, *E. maxima* fucoidan treated cells showed no significant effect on migration compared to untreated control cells (denoted as DMSO), contrary to the results of the previous wound healing assay. VEGF and TMX, included as positive controls, showed the expected effects on HCT116 cell migration (Figure 5.3C) Collectively, the data demonstrated that *S. cymosum* fucoidan suppressed the migratory properties of HCT116 colon cancer cells in the transwell assay, while *E. maxima* did not show similar effects.

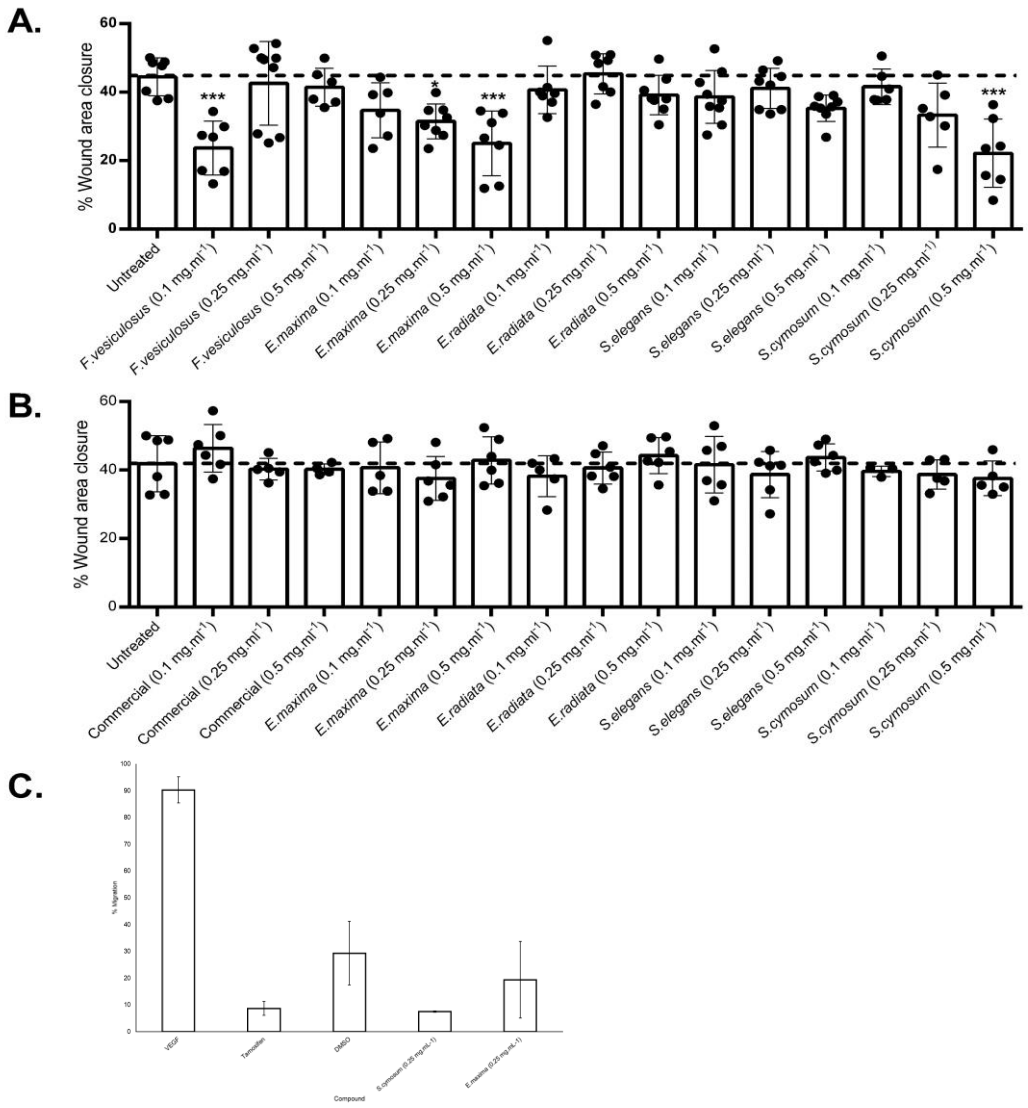

Figure 5.3: Effects of fucoidan and sodium alginate on the migration of HCT116 cells. Percentage of wound area closed by HCT116 migration following treatment with fucoidans (A) and sodium alginates (B) determined by scratch assay at 24 hours (n=9). (C) Quantification of migration in the transwell assay for HCT116 cells treated with 0.25 mg.ml^{-1} *E. maxima* or *S. cymosum* fucoidan, DMSO (vehicle control), 25 µM tamoxifen (TMX= positive control) and 50 ng/ml vascular endothelial growth factor (VEGF= positive control). Data are presented as mean ± SD (n=3). Statistical significance compared to migration of vehicle control treated HCT116 cells was determined using a one-way ANOVA in GraphPad Prism 6 (* $p<0.05$, ** $p<0.01$, *** $p < 0.001$, ns = not significant).

Overall, our findings suggest that fucoidan from *S. cymosum* inhibited both linear and transwell migration of HCT116 colon cancer cells, which is consistent with previous studies demonstrating the anti-migratory effects of fucoidan in various cancer cell lines (Li et al., 2016). In contrast, *E. maxima* fucoidan inhibited only linear migration, suggesting a different mechanism of action.

5.4.4 Effect of fucoidan and sodium alginate treatment on cell adhesion

Adhesion to the ECM is a dynamic intrinsic cellular process that plays a major role in the survival of cancer cells (Yayan et al., 2024). To investigate the effect the fucoidans and sodium alginates had on cell adhesion we examined the effect of these treatments on the cells' ability to attach the plate surface (Figure 5.4A), to re-adhere following treatment (Figure 5.4B) and to remain adherent to the plate surface upon treatment (Figure 5.4C).

As a control, EDTA, a metal ion chelator preventing cell adhesion, significantly reduced cell adhesion and led to cell detachment in a concentration-dependent manner at 2.5 mM and 5 mM (see Appendix Figure B26 A and C). The adhesion assays also showed that all fucoidans and sodium alginates reduced the attachment of HCT116 cells to the culture plate surface to some extent (Figure 5.4). However, significant differences were observed among the fucoidan and alginate treatments. The adhesion assays (Figure 5.4A) confirmed that treating cells at the time of seeding resulted in the strongest reduction in cell adhesion to the plate. While the fucoidans inhibited cell adhesion to a greater extent than the sodium alginates, a significant inhibition was noted for all treatments, albeit not at all concentrations ($p<0.05$) (Figure 5.4A). Notably, fucoidans from *F. vesiculosus*, *E. maxima*, and *S. elegans* were the most potent inhibitors, preventing up to 70% of seeded cells from adhering. This decrease in cell adhesion persisted even over longer periods, as assessment over 32 hours (Figure 5.4D) demonstrated that prolonged treatment further decreased cell adhesion.

Upon reseeding treated adherent cells after removal of the treatments through numerous washes, several cell treatments were able to resume inhibition of cellular adhesion (Figure 5.4B). Again, significant inhibition of adhesion was observed, particularly with *F. vesiculosus* and *E. maxima* fucoidans, although fucoidan from *S. elegans* as well as the commercial, *E. maxima* and *S. cymosum* sodium alginates also significantly reduced cell adhesion ($p<0.05$). These findings suggest a persistent negative effect of fucoidans and alginates on HCT116 cell adhesion, even after removal. However, it is important to note that cells treated with EDTA were able to re-adhere (see Appendix Figure B26B). Regarding the resistance of cells to detach from plate wells (de-adhesion), shown in Figure 5.4C, the data demonstrated that the commercial fucoidan and sodium alginate did not detach cells, while all fucoidan and alginate extracts, regardless of concentration, resulted in approximately 40% cell de-

adhesion. Visual imaging throughout confirmed the graphical representation of the effect on cell adhesion (Figure 5.4E).

There are three main stages to cell adhesion: the initial attachment, followed by the spreading of the cell body and lastly, the organisation of the actin cytoskeleton with the formation of focal adhesions (Murphy-Ullrich, 2001). The initial attachment of cells to the TC plastic was shown to be the most affected by the fucoidans and alginates (Figure 5.4A). This stage of adhesion is regulated by integrins that act as ties to the ECM (Murphy-Ullrich, 2001). Considering that fucoidans and alginates are anionic polysaccharides and integrins require cations such as Ca^{2+} or Mg^{2+} as a cofactor for adhesion, it is reasonable to suggest that this could have led to the reduced cell attachment observed above (Fuhrmann and Engler, 2015; Shi et al., 2023). However, Liu et al. (2005) noted that the inhibition of cell adhesion by fucoidan was not due to changes in integrin subunit expression, but rather due to fucoidan binding to fibronectin's heparin-binding domain. This binding prevents integrins on the cell surface from interacting with fibronectin, thereby disrupting cell adhesion. Since fucoidan is known to interact with attachment factors like fibronectin, it is plausible that in our experiments, fucoidan and/or sodium alginates interfered with attachment factors provided by FBS in the DMEM. These factors, including fibronectin and other ECM proteins, adsorb onto the culture surface and are essential for supporting cell adhesion and spreading (Bax, 2021). Consequently, if our treatments disrupted these interactions, this could have impaired the cells' ability to adhere to the surface during treatment.

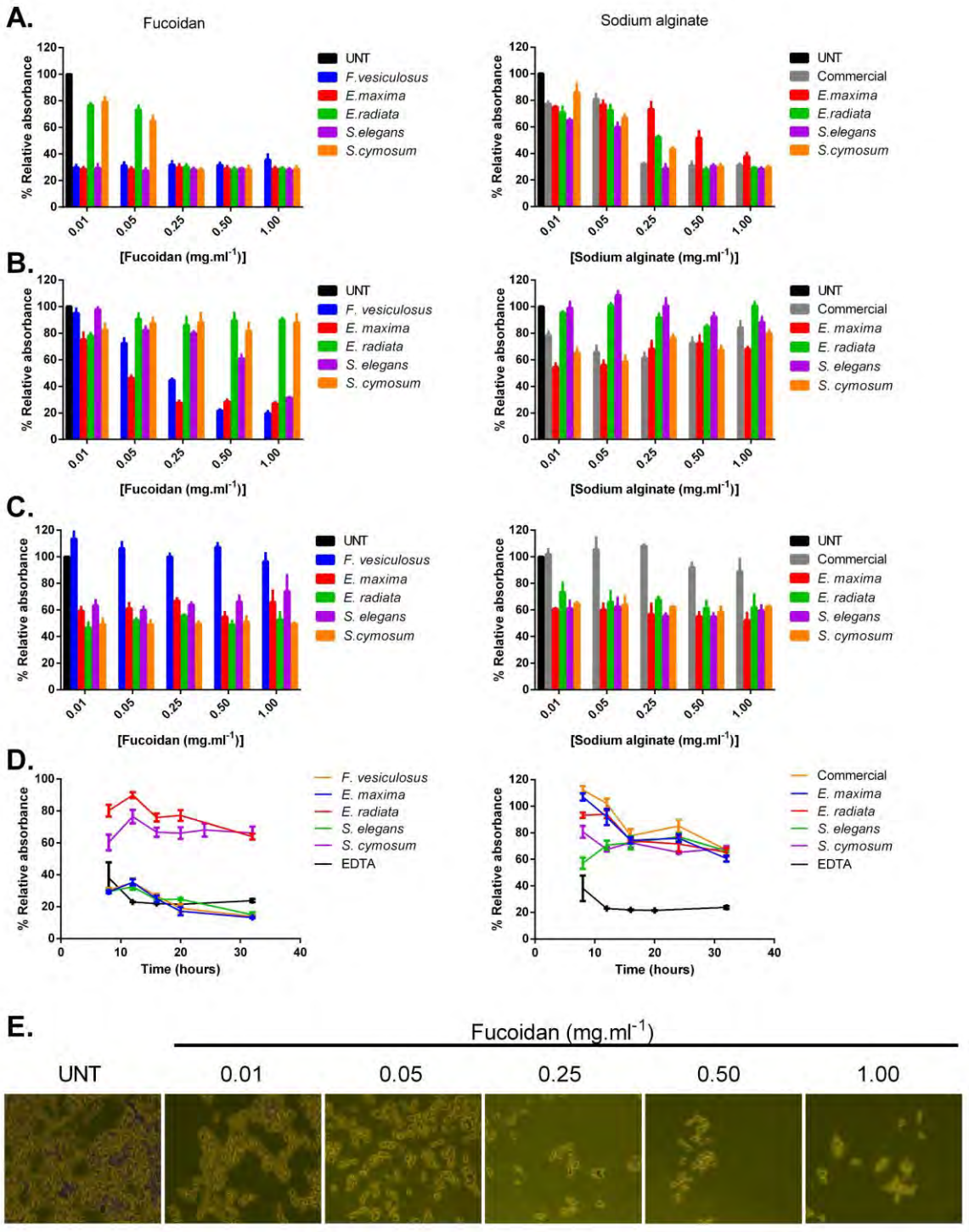

Figure 5.4: Fucoidans and sodium alginates reduce the adhesion of HCT116 cells. Quantification of the effect of fucoidan and sodium alginate treatments on HCT116 adhesion after 8 hours when; (A) cells were treated during seeding, (B) pre-treated adherent cells were reseeded, (C) treatments were added to already adhered cells. (D) Adhesion of HCT116 cells treated with 0.05 mg.ml^{-1} fucoidan or sodium alginate and 2.5 mM EDTA at the time of seeding when observed over 32 hours. Adhesion was measured by quantifying the SDS solubilised crystal violet stain inferred to the amount of adhered HCT116 cells and normalising to untreated cells (taken as a 100%). (E) A visual representation of crystal violet stained adhered untreated cells (UNT) and treated adhered HCT116 cells**.** Images were captured using the Zeiss Inverted light microscope with the 20x objective and represent triplicate independent experiments.

Nonetheless, the observation that some extracts inhibited cell adhesion to the plate surface even in their absence from the medium (Figure 5.4B) suggests that mechanisms other than attachment factor or cation sequestration may also be involved. Particularly since in the control reaction with EDTA it was apparent that once EDTA was removed from the medium cell adhesion was no longer inhibited (see Appendix Figure B26B). One possibility is that fucoidans and alginates bind to cell surfaces or are internalised, as supported by studies showing that these polymers can interact with cell membranes and be taken up by cells (Liu et al., 2005; Karthikeyan et al., 2023). If these molecules bind to adhesion-related surface receptors, they may form stable complexes that are not easily removed by washing, leading to a prolonged anti-adhesion effect. Studies on heparin and heparan sulphate, which share structural similarities with fucoidans, show that these molecules can bind directly to integrins (Ballut et al., 2012). Fucoidan itself has also been reported to bind several ECM proteins (Lin et al., 2020b). In addition to interactions with surface receptors, the internalisation of these polysaccharides could potentially alter intracellular signalling pathways, leading to the reprogramming of cell adhesion processes. This reprogramming may result in the reduced expression or impaired functionality of adhesion molecules or even generate a less adhesive phenotype (Smith, 2008). Studies have shown that fucoidan can interact with various cell surface receptors, triggering signalling changes that inhibit cell adhesion (Lin et al., 2020b). Therefore, direct cell interactions or intracellular signalling alterations induced by these polysaccharides might underlie the prolonged anti-adhesion effects observed, even in the apparent absence of the treatments.

Given the prominent role the cytoskeleton plays in maintaining and stabilising cell adhesion, changes to the expression and distribution of cytoskeletal components as a result of the treatments could have also led to reduced cell adhesion (Murphy-Ullrich, 2001). Indeed, the literature has reported changes to the polymerisation and organisation of actin following fucoidan treatment, together with an effect on cell adhesion (Zhang et al., 2018). The fact that we also noted that the fucoidan and alginate extracts caused the cells to actively detach from the plate surface, suggests that they stimulated the cells to detach themselves from the ECM. For cell detachment to occur, cells have to degrade the ECM, a process that is primarily managed by matrix metalloproteases (Zahariev et al., 2023). It remains to be investigated whether either of these cell adhesion mechanisms contributed to the inhibition of cell adhesion. It

should be emphasised that, considering the complexity of the cell adhesion process, we need to take into account that other targets of fucoidan and sodium alginate may be causing the observed effects. Additionally, the differential effects observed between our extracted fucoidans and alginates versus the commercial variants on cell de-adhesion (Figure 5C) raise the possibility that residual salts or chemicals used during our extraction process could have influenced our results. While these chemicals were carefully removed before testing, their potential contributions to the observed effects cannot be entirely ruled out. Future studies should include an analysis of residual extraction reagents to determine their potential impact on cell adhesion.

5.4.5 Fucoidan and sodium alginates effect on the HCT116 cells adhesion is not due to changes in cellular distribution of integrin β-1

After observing the significant impact of fucoidans and sodium alginates on cell adhesion, we investigated the potential role of integrin interactions in this process. Two fucoidans and two sodium alginates were selected for this, based on their differing effects on cell adhesion. Integrins function as heterodimers at the cell surface, mediating interactions with the ECM. Integrin β-1, the most common subunit in integrin heterodimer complexes, which associates with a variety of different α-subunits to form heterodimers that predominantly mediate attachment to the ECM, was selected for this analysis (Howe and Addison, 2012; Riopel et al., 2013). From Figure 5.5A, we observed an even punctate distribution pattern of the β1 integrin throughout the cell, with some accumulation at cell–cell contact sites in both the untreated and treated cells. Quantification of the occurrence frequency of these cell-cell contact sites, which we defined as strong cellular connections, showed that the sodium alginate treatments increased the occurrence of these slightly, while the fucoidan treatments did not (Figure 5.5B). In contrast, the EDTA control treatment, which blocks integrin-based adhesions by chelation of divalent cations, showed substantially rounded cells consistent with loss of cell adhesions. Consequently, the data suggests that the inhibition of cell adhesion resulting from the fucoidan and alginate treatments did not involve significant changes in the distribution of β1 integrin-based adhesion.

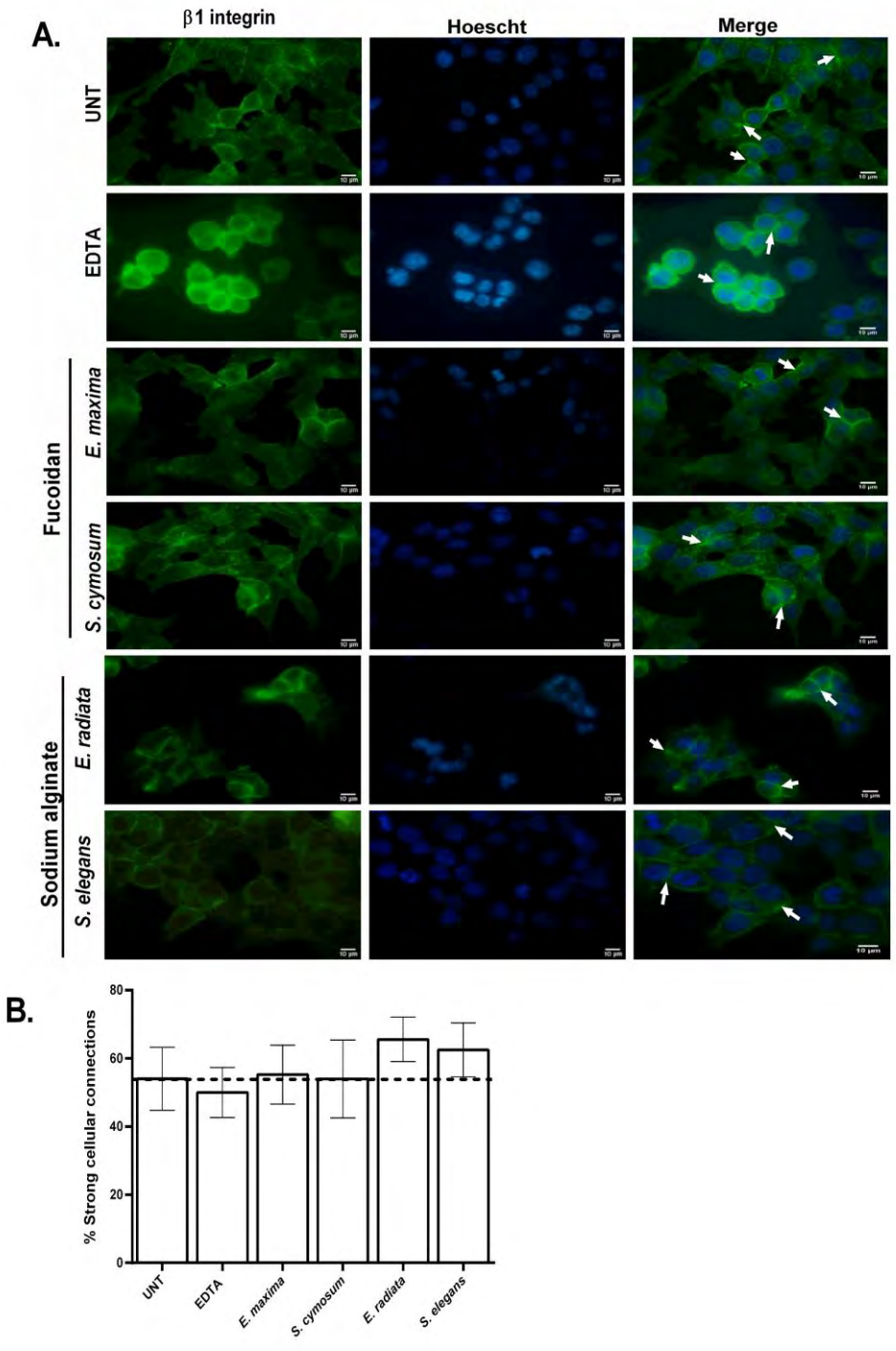

Figure 5.5: Expression of β1 integrin in untreated (UNT), EDTA, fucoidan and sodium alginate treated HCT116. (A) Immunofluorescence analysis of the localisation of the β1 integrin in untreated (UNT), (1 mM) EDTA, fucoidan and sodium alginate at 0.25 mg.ml^{-1} treated HCT116 cells. White arrows indicate selected areas of notable β1 integrin accumulation at cell–cell contact sites. Images were captured at 100x magnification and are representative of triplicate images captured from randomly selected fields. Scale bar represents 10 µm. (B) Quantification of the number of cells showing a high level of β1 integrin concentrated at cell-to-cell contact sites denoted as strong cellular connections and presented as a percentage of all cellular connections analysed. Analysis of the strong cellular connections was conducted using ImageJ cell counting analysis (n>62).

5.4.6 Effect of fucoidan and sodium alginate treatment on cytoskeletal organisation and cell morphology

Cell morphology and cytoskeleton dynamics play an important role in regulating both cell adhesion and migration processes. We therefore used fluorescence microscopy to assess the cell morphology and the organisation and distribution of the cytoskeletal actin and intermediate filament vimentin in HCT116 cells treated with fucoidan or sodium alginate (Kim et al., 2015; Klimaszewska-Wiśniewska et al., 2018). In Figure 5.6A, both untreated and treated cells exhibited a uniform distribution of actin and vimentin throughout the cytoplasm, with actin filaments appearing to be concentrated at points along the cell membrane. From the consistent intense staining of actin and vimentin in both the treated and untreated cells seen in Figure 5.6A, it was apparent that the treatments did not affect the polymerisation of vimentin or actin, which had previously been noted as a mechanism which was disrupted in treated HCT116 cells, causing them to lose their ability to adhere (Zhang et al., 2018).

Actin and vimentin, both major cytoskeletal components, form two coexisting separate networks that are mutually influenced by the disruption or reorganisation of either one of these networks (Esue et al., 2006). To assess for any changes in the organisation of these networks, we examined the colocalisation of actin and vimentin. The colocalisation analysis to quantify the level of colocalisation between actin and vimentin was conducted using ImageJ. Pearson's correlation coefficient, (Rr), ranges from -1 to 1, where -1 indicates total exclusion and +1 signifies perfect colocalisation. The Intensity Correlation Quotient (ICQ) value measures the synchronicity between the signals and if these vary together, with a value of -0.5 indicting segregated staining, a value of 0 represents random staining, and a value of 0.5 represents dependent staining (Li et al., 2004). The colocalisation analysis shown in Table 5.1 indicated that there was a high level of dependent colocalisation between actin and vimentin in HCT116 cells. As is evident from Table 5.1, the various treatments appeared to have no real effect on their colocalisation.

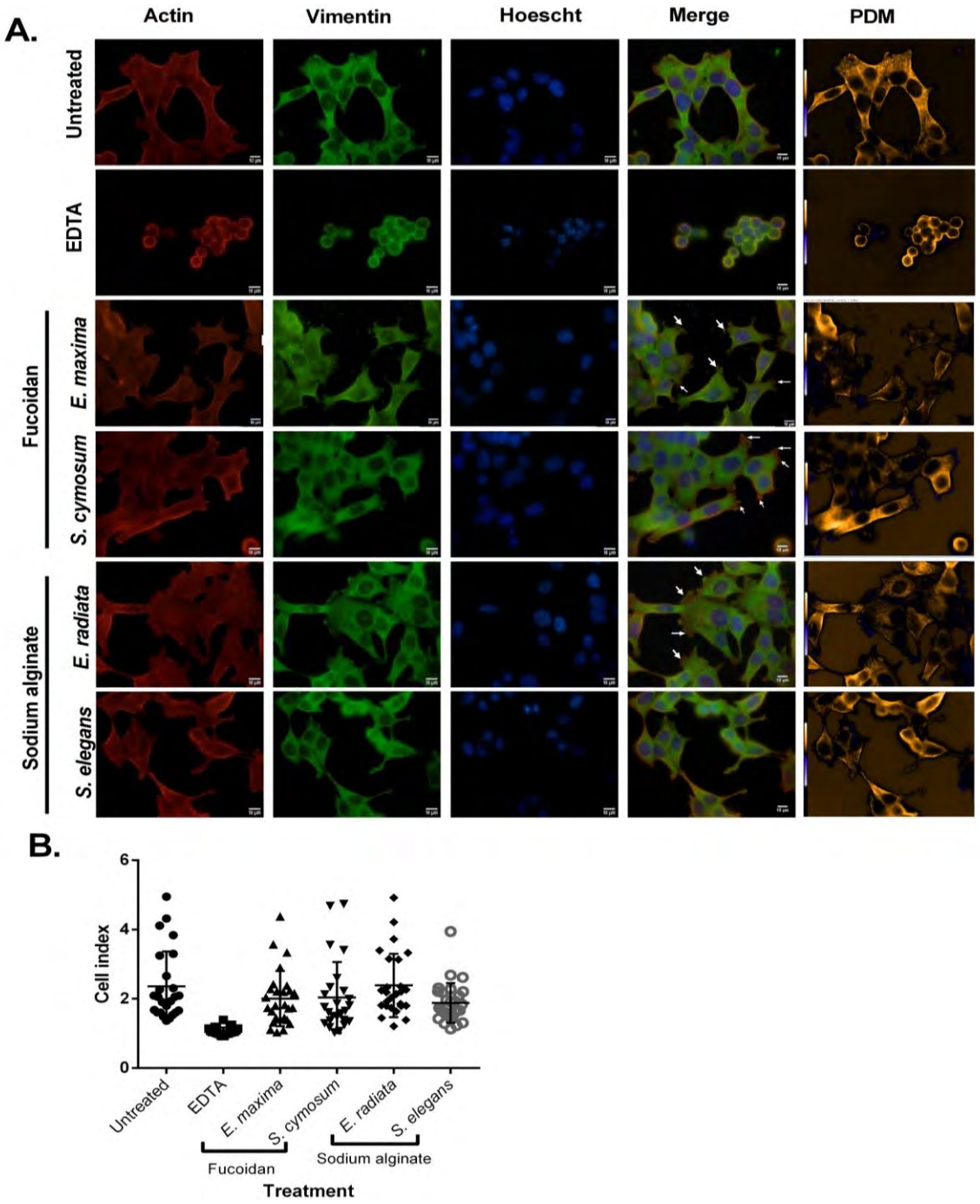

Figure 5.6: Effects of EDTA, fucoidans, and sodium alginates on the cell morphology and actin-vimentin cytoskeletal organisation of HCT116 cells. (A) Representative images of actin and vimentin distribution and colocalisation in HCT116 cells were obtained by fluorescence microscopy after 24 hours. Treatment with EDTA was performed at 2.5 mM, while fucoidan and sodium alginate treatment concentrations were 0.25 mg.ml^{-1}. The white arrows in indicate the locations of actin-rich pseudopodia and lamellipodia-like membrane ruffles, highlighting key morphological changes in the treated cells. The images represent images captured from four randomly selected fields at 100x magnification. Colocalisation analysis was conducted using ImageJ. PDM panels show colocalisation where an orange colour indicates colocalisation and blue indicates exclusion. Scale bars are 10 µm. (B) Graph showing the cell index of untreated and treated HCT116 cells. Cell index was quantified using ImageJ, based on individual cell measurements of length and width. The data represent individual values from a minimum of 25 cells per condition, with the mean ± SD shown. Cell index measurements of HCT116 cells were quantified using ImageJ.

Table 5.1. Colocalisation analysis for actin and vimentin in HCT116 cells. Analysis was performed using four independent frames. Data are presented as mean ± SD (n>25).

HCT116 cells treatment	Rr	R	ch1:ch2	ICQ
Untreated	0.871 ± 0.042	0.921± 0.027	0.964 ± 0.032	0.464 ± 0.010
EDTA	0.944 ± 0.014	0.960 ± 0.013	0.507 ± 0.098	0.412 ± 0.025
E. maxima fucoidan	0.792 ± 0.051	0.905 ± 0.013	0.962 ± 0.038	0.424 ± 0.017
S. cymosum fucoidan	0.910 ± 0.017	0.953 ± 0.005	0.818 ± 0.121	0.427 ± 0.013
E. radiata sodium alginate	0.862 ± 0.020	0.925 ± 0.019	0.967 ± 0.034	0.437 ± 0.018
S. elegans sodium alginate	0.882 ± 0.026	0.925 ± 0.012	0.721 ± 0.156	0.431 ± 0.018

While examining the cytoskeletal networks, we observed notable changes in the treated cells morphology that suggest altered cellular behaviour (Figure 5.6A). In the cells treated with *E. maxima* and *S. cymosum* fucoidan, distinct actin-rich pseudopodia were noted and are indicated with white arrows in Figure 5.6A. These finger-like projections are characteristic of amoeboid motility, which is typically associated with the more rapid and less adhesive movement of cells (Titus and Goodson, 2017). In contrast, cells treated with *E. radiata* sodium alginate showed the appearance of lamellipodia-like membrane ruffles filled with vimentin, also indicated by white arrows in Figure 5.6A. Supporting this observation, previous studies have shown that vimentin is localised within lamellipodia and plays a key role in their formation (Helfand et al., 2011). Lamellipodia are generally linked to slower, mesenchymal migration and require stronger adhesion to the extracellular matrix than amoeboid motility (Titus and Goodson, 2017). The appearance of these distinct morphological features in the treated cells would suggest a shift toward more migratory phenotypes (Titus and Goodson, 2017). Interestingly, despite the appearance of these migratory structures, we did not observe a corresponding increase in cell migration for either of these treatments (Figure 5.3). In fact, treatment with *E. maxima* fucoidan and *S. cymosum* fucoidan resulted in a decrease in cell migration. This would suggest that although fucoidan and sodium alginate treatments may promote cellular morphological changes associated with migration, the actual migratory capacity may be impaired or remain unaltered under these specific conditions.

To further assess the noted changes in cell morphology, we evaluated the cell shape changes using the cell index function, dividing the cell length by the cell width across multiple cells and images (Figure 5.6A). Cell index (CI) values close to 1 represent round cells, while values greater than 1 indicate a more elongated cell shape. HCT116 cells had lower cell index values when treated with EDTA (CI= 1.07 ± 0.11), compared to untreated cells (CI= 2.36 ± 1.01). This decrease in cell index values showed that the cells became more rounded in the presence of EDTA. No additional cell elongation was observed following treatment with *E. maxima* fucoidan (2.00 ± 0.78), *S. cymosum* fucoidan (2.04 ± 1.03), *E. radiata* sodium alginate (CI= 2.39 ± 0.92) and *S. elegans* sodium alginate (CI= 1.88 ± 0.57), as indicated by the CI values, which showed no significant difference compared to untreated cells. This suggests that, while pseudopodia and lamellipodia structures, typically associated with migration, were present, the CI values indicate a lack of significant elongation, meaning that the treated cells did not undergo the characteristic shape changes typically required for active migration (Schmidt and Friedl, 2009). Although the exact link between the morphological changes induced by these treatments and the alterations in HCT116 cell behaviours observed in other assays is unclear, it is evident that these behavioural changes are associated with the treatments affecting cell morphology rather than causing changes in cytoskeletal organisation.

5.4.7 *E. maxima* fucoidan enhances MMP-9 activity in HCT116 cells

Matrix metalloproteinases (MMPs) play a crucial role in degrading the ECM, which is essential for cellular migration and is implicated in tumour invasion and metastasis (Vinnakota et al., 2017). Given this role, the effects of *E. maxima* and *S. cymosum* fucoidans on cell adhesion and/or migration may involve changes in MMP activity. To explore this possibility, we analysed the impact of fucoidan on MMP activity and expression using three distinct methods, namely FITC-gelatin degradation, gelatin zymography, and real-time qPCR analysis.

We initially used the FITC-gelatin degradation assay to investigate ECM degradation by HCT116 cells treated with fucoidan. In this assay, cells were cultured on coverslips coated with fluorescent 488-Oregon Green conjugated gelatin, enabling visualisation of ECM degradation as dark spots. As depicted in Figure 5.7A, punctuate areas of gelatin degradation were observed adjacent to both the untreated and fucoidan-treated HCT116 cells. Notably, the areas of gelatin degradation appeared more pronounced in

cells treated with *E. maxima* fucoidan compared to untreated cells and *S. cymosum* fucoidan-treated cells. However, upon closer examination across multiple fields of view, we did not observe a statistically significant difference in the rate of occurrence of fluorescent ECM degradation between the untreated and *E. maxima* fucoidan-treated cells. This lack of clear differentiation prompted further investigation using gelatin zymography to achieve a more detailed assessment of MMP activity.

We next utilised gelatin zymography, which offers a more quantitative approach to assess the effect of fucoidan on MMP activity, particularly the secretion of MMP-2 and MMP-9 into the surrounding medium. These experiments were conducted without serum to eliminate any activity from MMPs in serum. HCT116 cells exhibited low basal levels of MMP-9 and MMP-2 secretion (Figure 5.7B). Interestingly, we observed a significant dose-dependent increase in MMP activity following treatment with *E. maxima* fucoidan (Figure 5.2B+C), while the MMP activity in *S. cymosum* fucoidan-treated cells remained unchanged (see Appendix Figure B27). The molecular size of the bands displaying enzymatic activity on the gelatin zymography corresponded to both the pro and active forms of MMP-9 and MMP-2 (Edwards et al., 2003). To ensure that the observed increase in MMP activity was not due to direct denaturation of gelatin by the *E. maxima* fucoidan, we performed gelatin zymography of the treatment concentrations of fucoidan. No degradation of gelatin was observed at any of the tested fucoidan concentrations, indicating that the increase in MMP activity was indeed attributed to the cells' response to treatment with *E. maxima* fucoidan (see Appendix Figure B27). In addition, positive (TMX) and (VEGF) controls were included in the analysis; however, no significant changes in MMP expressions were observed for either control in the HCT116 cell line (see Appendix Figure B27).

To elucidate the underlying mechanism for the observed apparent increase in MMP secretion, we conducted real-time PCR analysis to investigate the mRNA expression levels of MMP-9 and MMP-2 in response to *E. maxima* fucoidan treatment. We found that, in both the control and fucoidan-treated samples, MMP-9 was expressed, while transcripts for MMP-2 were not detectable in either the fucoidan-treated or control samples (data not shown). Specifically, treatment of HCT116 cells with *E. maxima* fucoidan led to a reduction in the level of MMP9 mRNA, whereas the abundance of MMP9 mRNA in *S. cymosum*-treated cells showed no significant change compared to untreated HCT116 cells (Figure 5.7C).

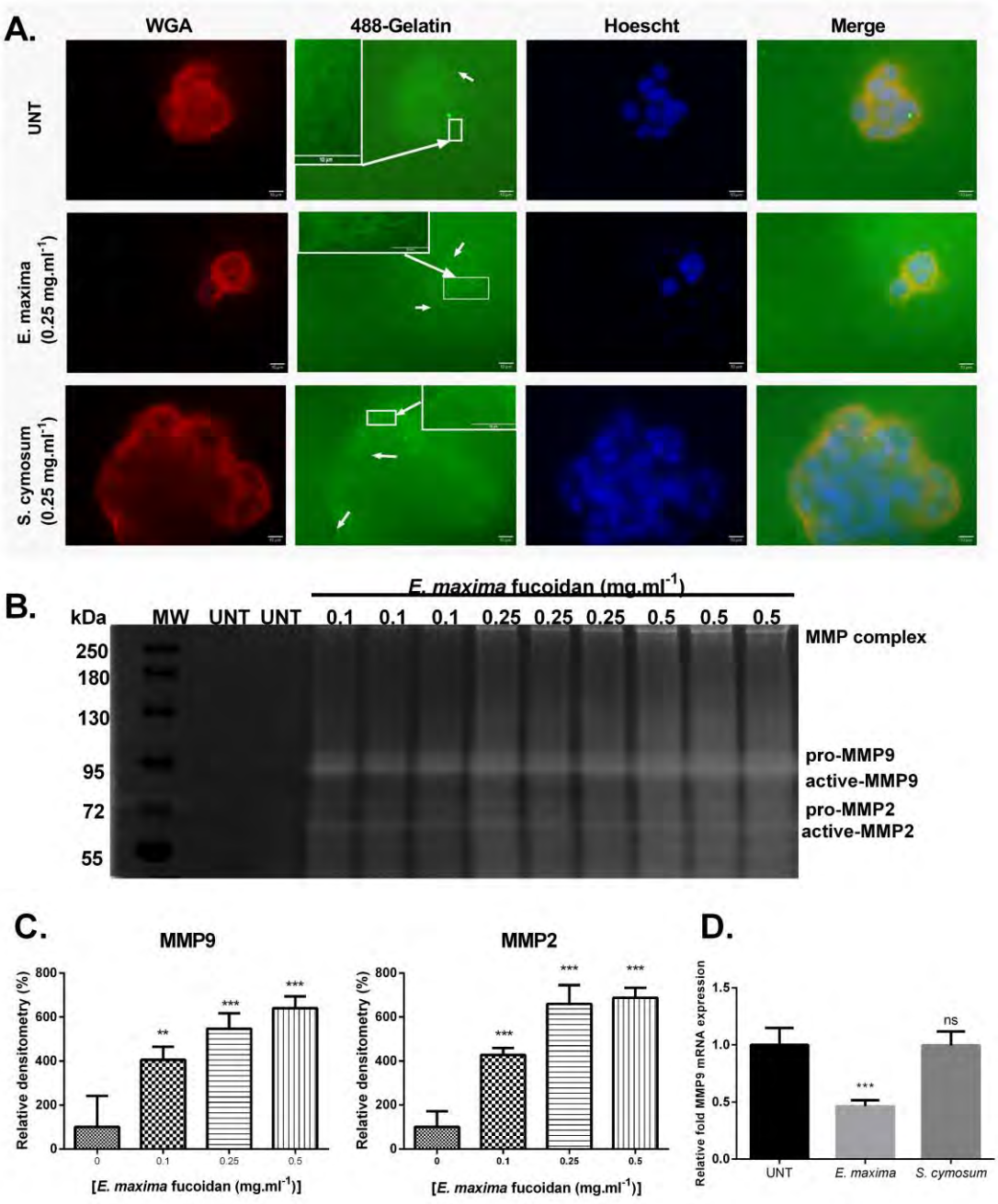

Figure 5.7: Gelatin degradation activity of HCT116 cells in response to *E. maxima* and *S. cymosum* fucoidans. (A) Representative images showing the gelatinase activity of untreated and fucoidan-treated cells plated on Oregon Green 488 conjugated gelatin for 24 hours. Nuclei were stained with Hoechst (blue) and the cell membrane was stained with WGA (red). The dark spots against the fluorescent background marked by white arrows represent areas of gelatin degradation. Representative fields of view are shown at 100x magnification with the scale bar = 10 µm. (B) Gelatin zymography of supernatants harvested from HCT116 cells treated with the indicated concentrations of fucoidan for 48 hours. (C) Quantification of the MMP band density using the ImageJ software relative to MMP expression of untreated HCT116 cells. Data are presented as mean ± SD (n=3). Statistical significance compared to control was determined using a one-way ANOVA in GraphPad Prism 6 (* $p<0.05$, ** $p<0.01$, *** $p < 0.001$, ns = not significant). (D) RT-qPCR analysis of the MMP-9 mRNA expression levels in untreated (UNT) and fucoidan treated HCT116 cells nominalised to GAPDH mRNA expression.

Given the elevated levels of active MMP-9 and MMP-2 identified in the gelatin zymography assay, the more specific holes observed in the gelatin matrix surrounding the *E. maxima* fucoidan-treated cells in the FITC-gelatin assay (Figure 5.7A) are potentially a result of localised gelatin degradation mediated by these enzymes. However, the resolution of the FITC-gelatin assay may have limited the accurate quantification of this degradation. Additionally, differences in assay durations - 24 hours for the FITC-gelatin assay versus 48 hours for zymography - could have impacted the observed results. Furthermore, it is also possible that other factors, such as the presence of regulatory mechanisms within the cellular environment, may have contributed to the observed variations between the degradation in the FITC-gelatin assay and gelatin zymography (Toth and Fridman, 2001). Notably, the decrease in MMP-9 mRNA levels suggests that *E. maxima* fucoidan regulates MMP-9 activity through post-translational mechanisms, such as influencing its secretion or activation. This regulatory effect has been previously reported in fucoidan-treated U937 cells by Sun et al. (2010).

It has to pointed out that despite the elevated MMP-9 and MMP-2 activity observed in zymography *E. maxima* fucoidan treatment inhibited HCT116 cell migration, a result that contradicts the typical association of MMP activity with enhanced migration (Vinnakota et al., 2017). This discrepancy could be explained by the activity of tissue inhibitors of metalloproteinases (TIMPs). While MMPs like MMP-9 and MMP-2 are typically associated with enhanced cell migration due to their role in degrading the extracellular matrix, TIMPs can regulate and inhibit MMP activity (Toth and Fridman, 2001). Notably, TIMP-2 has been shown to hinder the invasion and migration of HCT116 cells by regulating the activity of MMP-9 (Shoari et al., 2024). Gelatin zymography, while valuable, has the limitation of not accounting for tissue inhibitors of metalloproteinases (TIMPs) (Toth and Fridman, 2001). The denaturing conditions used in zymography, such as SDS during electrophoresis, dissociate MMP-TIMP complexes, allowing only the intrinsic MMP activity to be measured, without reflecting the regulatory effects of TIMPs on MMP function (Toth and Fridman, 2001). Senni et al. (2006) reported that fucoidan increases the association rates of MMPs with their specific inhibitors, TIMPs, suggesting a potential mechanism for this observed phenomenon. Considering the inhibitory effects of TIMPs on MMP activity, it is plausible that TIMPs could be limiting gelatin degradation despite the increased MMP levels induced by *E. maxima* fucoidan treatment. To investigate this, assays assessing

MMP-TIMP interactions, such as ELISA or Western blot analysis using antibodies specific to MMP-TIMP complexes (Sun et al., 2010; Ren et al., 2017), are necessary. Additionally, reverse zymography could be utilised to assess the activity of endogenous TIMPs, which would provide insights into the regulation of MMP activity and help confirm whether TIMPs are influencing the observed gelatin degradation (Ren et al., 2017).

5.4.8 Specific fucoidans and sodium alginates impact HCT116 cells anchorage-independent growth

The impact of the fucoidans and sodium alginates on the anchorage-independent colony formation ability of the HCT116 colon cancer cell line was evaluated using the soft agar assay, a well-established method for characterising this capability *in vitro* (Borowicz et al., 2014). The results revealed a notable reduction in the number of medium-to-large colonies following treatment with *E. maxima* fucoidan and *S. elegans* sodium alginate (Figure 5.A) by 51.35 ± 7.46% and 43.23 ± 7.63%, respectively, compared to the untreated cells (Figure 5.8B). Microscopy images in Figure 5.8C provide a magnified view of these reductions, offering a clearer illustration of the decrease in the number of medium-to-large colonies. Additionally, these magnified images also show a visible reduction in the number of small colonies in the treated groups. Together, the results indicate a significant ($p \leq 0.001$) degree of inhibition of colony formation by *E. maxima* fucoidan and *S. elegans* sodium alginate.

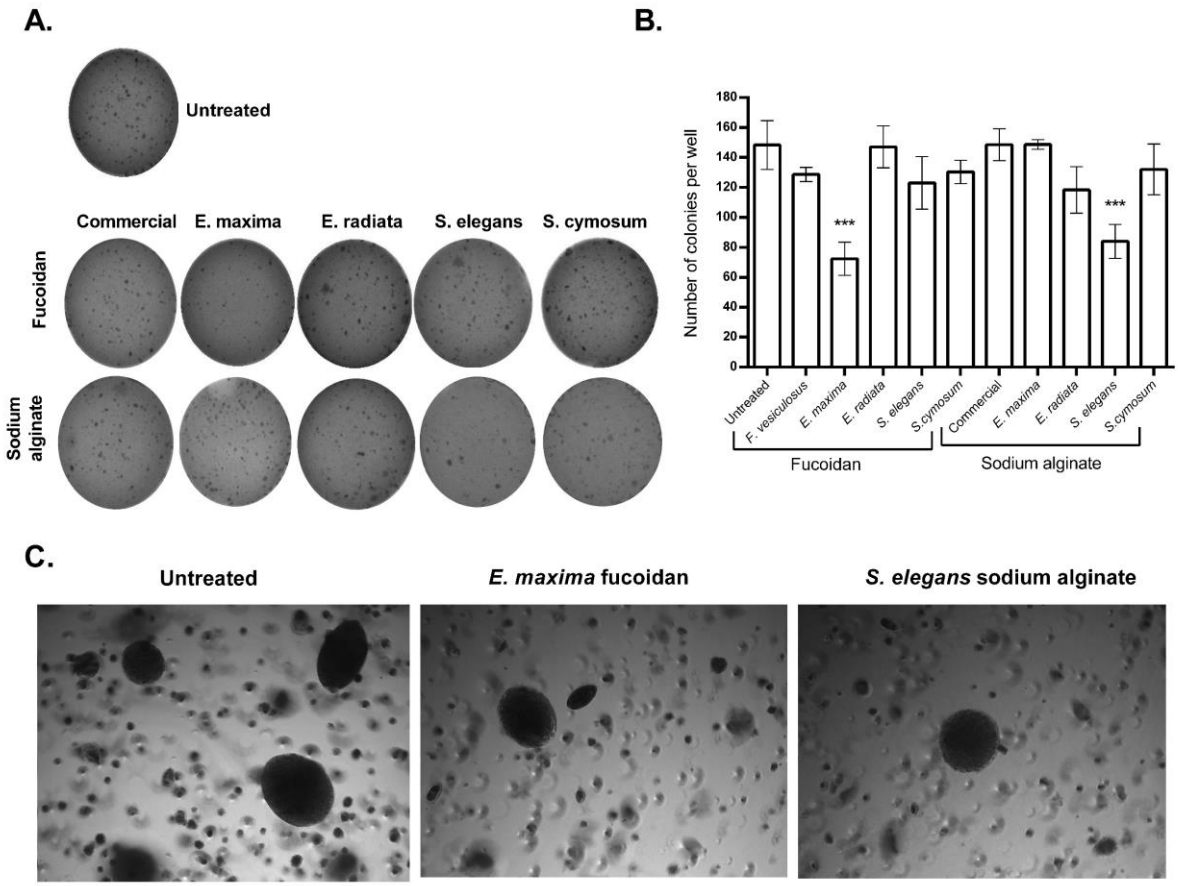

Figure 5.8: Effect of fucoidans and sodium alginates on the anchorage-independent growth of HCT116 cells in soft agar. (A) Images showing colony formation of HCT1116 cells in soft agar following treatment with the denoted fucoidan and sodium alginates at 0.25 mg.ml^{-1}. Images of plate wells were taken 21 days after seeding and are representative of three biological replicates. (B) Graphic representation of the total number of colonies classified as medium-large sized (>20 µm) colonies quantified using Image J. Data are presented as means ± SD (n=3). Statistical significance compared to untreated was determined using one-way ANOVA in GraphPad Prism 6 (*** $p < 0.001$). (C) Magnified light microscopy images taken with 4x objective showing that the formation of untreated and *E. maxima* fucoidan and *S. elegans* sodium alginate treatment reduced the formation of all sizes of colonies.

This observed decrease in the number of colonies following treatment with *E. maxima* fucoidan and *S. elegans* sodium alginate suggests an inhibitory effect on anchorage-independent growth of cancer cells. Anchorage-independent growth is a hallmark of carcinogenesis and is indicative of cancer cells transformed and malignant nature (Borowicz et al., 2014). Cancer cells with enhanced anchorage-independent growth are more likely to exhibit tumourgenic and metastatic potential (Mori et al., 2009). Therefore, the reduction in colony formation in response to these specific fucoidan and sodium alginate treatments indicates their ability to suppress this critical aspect of colon cancer cell behaviour. This finding is consistent with previous studies

demonstrating the anti-anchorage-independent growth properties of fucoidan on colon cancer cell lines (Usoltseva et al., 2018). The decrease in colony formation suggests that fucoidan interferes with the ability of these cancer cells to survive and proliferate independently of anchorage to the extracellular matrix, thereby potentially impeding tumour growth and metastasis.

5.4.9 Effects of fucoidan and sodium alginate treatment on spheroid formation

The colon cancer cells HCT116 were analysed for their spheroid formation capacity, alongside the fucoidans and alginates, in agarose-coated round bottom 96-well plates. This assay was selected as the self-assembly of the tumour spheroids predominantly depends on cell-cell interactions (Sant and Johnston, 2017). The spheroid morphology was investigated over seven days. After three days, untreated HCT116 cells had formed compact multicellular spheroids of regular round shape, that decreased in size over the next few days as the cells within the spheroid appeared to become more compacted (Figure 5.8B). Adherens junctions initiate and maintain cell-cell adhesion complexes and contain the Ca^{2+} required for the formation of tight junctions (Walzl et al., 2014). EDTA, included as a positive control, is a chelator of divalent cations and thus disrupts the establishment of close cell-cell interactions. Strikingly, spheroids treated with EDTA showed this loss in cell-cell interactions in a dose-dependent manner that prevailed over seven days, with further cell shedding shrinking the dense core spheroid over time (see Appendix Figure B28).

The initial screening of the fucoidans and sodium alginates identified *E. maxima* fucoidan as the sole treatment capable of disrupting spheroid formation (see Appendix Figure B28). Figure 5.9A showed that, during the cultivation of the spheroids with various concentrations of *E. maxima* fucoidan, there was a difference in the effect observed. At lower concentrations, cells were able to form compact spheroids by day 3 - these were indistinguishable from the untreated spheres but demonstrated cell detachment from the surface that progressed with time. In contrast, when treated with higher *E. maxima* fucoidan concentrations, the HCT116 cells formed less compact irregular aggregates by day 3 that compacted over time to form a spheroid core with a relatively large proportion of cells remaining unincorporated (Figure 5.9A). This resembled the observed effect noted after EDTA treatment (used as a positive control).

To confirm our observation that the fucoidan treatment hindered the formation of tight cell-cell contacts (like EDTA), we performed immunofluorescent staining of the cell

membrane with fluorescently labelled wheat germ agglutinin (WGA), a conventional marker of the plasma membrane and Golgi apparatus (Chazotte, 2011). To determine the role adherens junctions may have played, we co-stained for β-catenin which serves as an integral binding component of numerous adherens junction molecules (Valenta et al., 2012). Following treatment with *E. maxima* fucoidan and EDTA, the immunofluorescent images revealed detailed changes to the spheroid surface morphology, particularly in the cell surface shape, when compared to untreated control (Figure 5.9C). The untreated spheroid displayed cell-to-cell compactness and an overall condensed spherical morphology with an intact and smooth outer spheroid surface. However, upon exposure to EDTA or fucoidan, spheroids displayed irregular surface protrusions and an overall more heterogeneous spheroid surface shape. At the highest concentration of fucoidan treatment, a noticeable loss in cell-to-cell compactness within the spheroid structure was evident. This loss of compactness was characterised by outer cells appearing to leak from the spheroid, leading to increased intercellular spacing and reduced cohesion between adjacent cells within the structure. Interestingly, the localisation of the β-catenin protein in the spheroids was uneven and more intense on the surface of all spheroids (Fig 5.9C). However, from visual examination of these images, we were unable to discern any specific alterations in the expression or localisation of β-catenin within the spheroids. For a more detailed view of the individual cells within the spheroids, the cell membranes were stained with fluorescently labelled WGA during the process of spheroid formation (Figure 5.9D). From this, it was evident that cell-cell adhesion was densest within the core but diminished towards the periphery of fucoidan-treated spheroids. Taken together, these changes in spheroid morphology suggest a potential impact of fucoidan treatment on the spheroid's structural integrity and organisation of cells within the spheroid microenvironment. Notably, the observed alterations suggest a potential impact of fucoidan treatment on cell-cell adhesion dynamics within the spheroid structure.

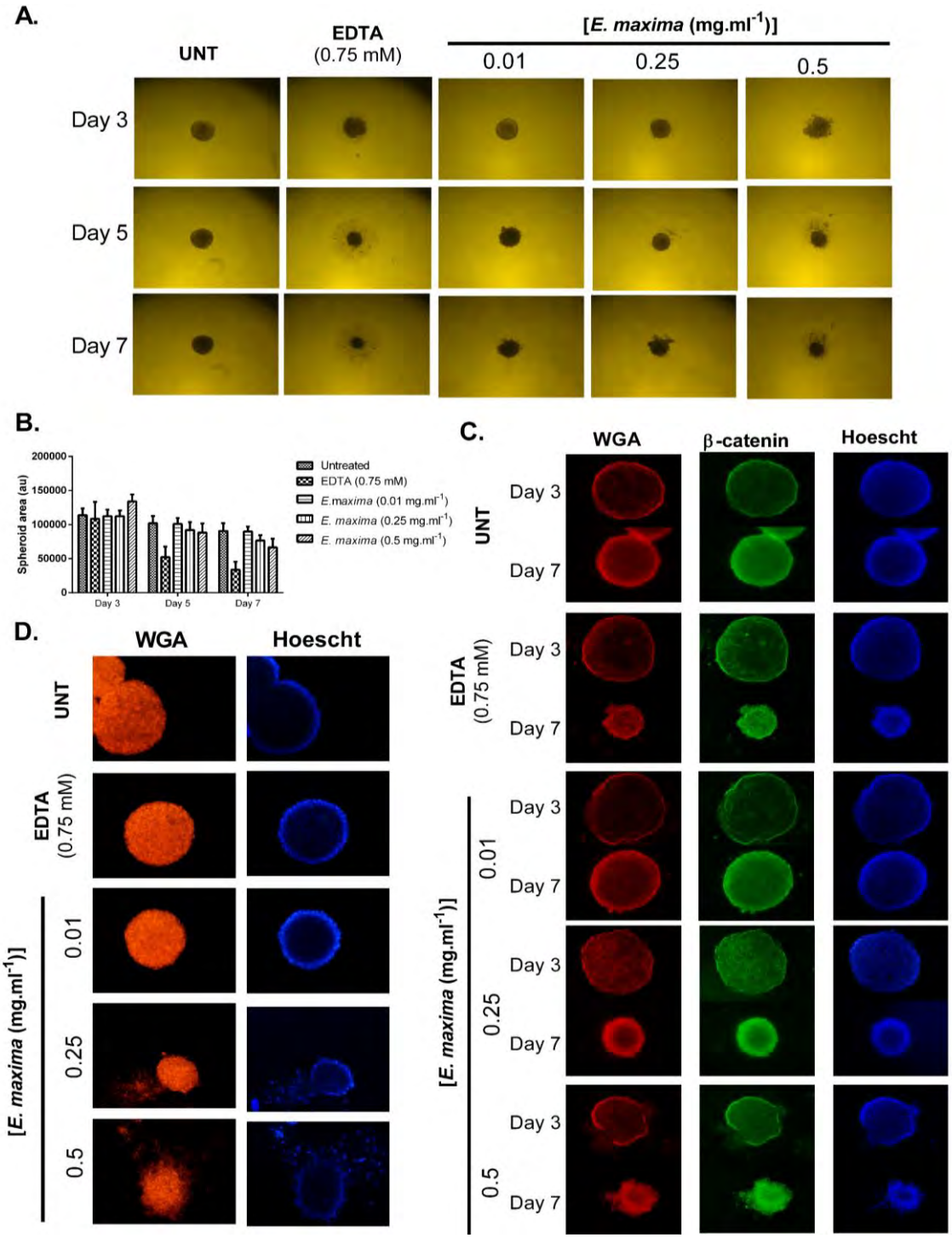

Figure 5.9: Effect of EDTA and *E. maxima* fucoidan treatment on the morphology of HCT116 tumour spheroids. (A) Brightfield images of the HCT116 spheroid morphology changes in response to EDTA and *E. maxima* fucoidan treatment over days 3 to 7. Images were captured using a Zeiss Inverted light microscope with the 4x objective and are representative of triplicate independent experiments (n=9). (B) Plot showing the changes of spheroid area on days 3, 5 and 7 quantified using Image J software. Depicted are mean values ± SD (n≥9). (C) Immunofluorescence images depicting the morphology of spheroids stained with Alexa-fluor 555 conjugated WGA (red) and β-catenin (green) on days 3 and 7 of spheroid formation, comparing untreated samples with those treated with either EDTA or fucoidan. Nuclei are stained with Hoechst 33352 (blue). These images represent data from at least 4 spheroids at 20x magnification. (D) Immunofluorescence images of spheroids formed in the presence of WGA (red) staining the individual cell membranes on day 7. Nuclei stained with Hoechst 33352 (blue). Images were captured at 20x magnification.

As a three-dimensional (3D) *in vitro* tumour model, spheroids offer valuable insights into cancer cell behaviour by more closely resembling aspects of *in vivo* tumour growth and its microenvironment (El Harane et al., 2023). Leveraging the HCT116 cell line's known ability to form tightly cohesive spheroids with pronounced three-dimensionality (Stadler et al., 2018), our study effectively evaluated the impact of *E. maxima* fucoidan treatments. While our investigation is among the first to explore fucoidan's effects on spheroid formation in this context, a study by Han et al. (2015) reported inhibition of sphere formation for HT-29 colon carcinoma cells by fucoidan in a time-dependent manner. As mentioned above, the self-assembly of spheroids relies on the establishment of close cell-cell interactions, which are primarily mediated by adherens junction proteins such as β1 integrin and cadherins and dependent on activation of signalling pathways, including β-catenin and actin-mediated cell-cell contacts (Ryu et al., 2019). As our previous examination in 2D culture, shown in Figures 5.5 and 5.6, demonstrated no changes in β1 integrin distribution or total actin expression, the observed effects in spheroid formation may suggest that alterations in cadherin or β-catenin expression play a more prominent role in driving these changes. However, it is important to acknowledge that the 3D spheroid microenvironment introduces factors not present in 2D cultures, and we did not assess β1 integrin or actin in 3D conditions. Furthermore, while we examined total actin expression, we did not investigate F-actin filament organization, which may be particularly relevant in 3D models.

5.4.10 Treating HCT116 cells with fucoidan results in the redistribution of β-catenin from the cytoplasm to the membrane and increases p-β-catenin levels

To investigate the potential role of β-catenin in HCT116 spheroid compactness, we assessed β-catenin subcellular localisation in 2D culture with fucoidan treatment. It is important to note that HCT116 cells are heterozygous for β-catenin, expressing one wild-type and one mutant oncogenic β-catenin. The mutant β-catenin escapes phosphorylation and degradation, leading to cytoplasmic accumulation and constitutive WNT/β-catenin pathway activation (Kaler et al., 2012). To understand β-catenin localisation, we co-stained the plasma membrane and Golgi apparatus with fluorescently labelled WGA.

This 2D immunofluorescence microscopy showed that untreated HCT116 cells predominantly exhibited β-catenin localisation in the Golgi, where it colocalised with WGA, with this strong signal visible in the PDM. A secondary localisation was observed

at the plasma membrane, while cytoplasmic and nuclear staining were minimal in comparison to these two primary sites (Figure 5.10A). In contrast, fucoidan-treated cells exhibited a noticeable increase in β-catenin localisation at the plasma membrane, as evidenced by the enhanced PDM signal in Figure 5.10A, where the membrane is now clearly visible in orange (indicated with white arrows). While the Golgi apparatus remained the primary site of β-catenin localisation, the enhanced membrane-associated signal suggests a redistribution of β-catenin in response to the treatment. Western blot analysis (Figure 5.10B), showed no significant changes in total β-catenin levels after fucoidan treatment, indicating that the observed increased membrane localisation was due to the recruitment of existing β-catenin pools rather than changes in expression levels. Notably, there was an increase in phosphorylated β-catenin (p-β-catenin) levels upon treatment. It is important to note that p-β-catenin and total β-catenin were measured on separate Western blots due to issues with the stripping buffer, which may limit direct comparisons between their levels.

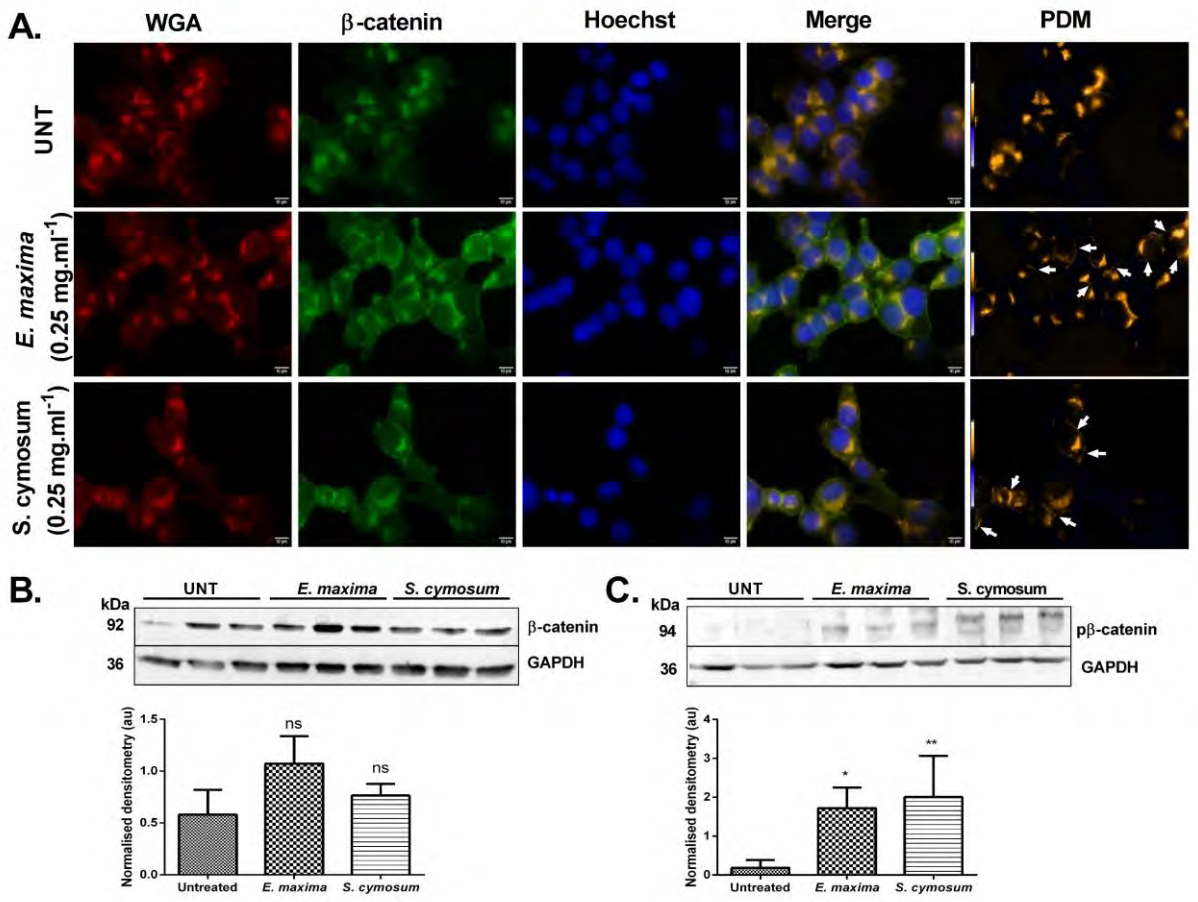

Figure 5.10: Effect of fucoidan on β-catenin localisation and the expression levels of β-catenin and p-β-catenin in untreated and fucoidan treated HCT116 cells. (A) Representative images showing the subcellular localisation of β-catenin (green) and the plasma membrane and Golgi apparatus marker Alexa fluor 555 conjugated WGA (red) for untreated and 0.25 mg.ml^{-1} fucoidan (from *E. maxima* or *S. cymosum*) treated HCT116 cells after 24 hours, as determined using fluorescence microscopy. Nuclei were stained with Hoechst 33352 (blue). White arrows mark the areas where the PMD signal in orange co-localises with β-catenin and WGA at the cell membrane. Images were captured at 100x magnification and are representative of triplicate images captured from randomly selected fields. Scale bar represents 10 µm. Colocalisation analysis was performed using ImageJ. (B) Western blot analysis of β-catenin and p-β-catenin expression in untreated HCT116 cells compared to those treated with 0.25 mg.ml^{-1} of fucoidan for 24 hours. The densitometry analysis represented with the western blots was determined using ImageJ. Statistical significance represents the difference between β-catenin levels in untreated and fucoidan-treated HCT116 cells, which was assessed by one-way ANOVA where * $p<0.05$ and ns = not significant.

Given the critical role of β-catenin in maintaining cell-cell adhesion at the membrane, where it links cadherins to the actin cytoskeleton (Valenta et al., 2012), the observed loss of spheroid compactness due to disrupted cell-cell adhesion (Figure 5) does not appear to be directly caused by β-catenin. However, the increased membrane localisation and elevated levels of phosphorylated β-catenin (p-β-catenin), could

suggest a potential modulation of the Wnt/β-catenin pathway activation status. Typically, phosphorylation of β-catenin leads to its inactivation and degradation, inhibiting its transcriptional activity in the Wnt/β-catenin signalling pathway (Kaler et al., 2012). The antibody used in this study specifically targets the phosphorylation sites at Ser33, Ser37, and Thr41, which are known to be phosphorylated by GSK3β and NEK2 (Shah et al., 2022). These phosphorylation events mark β-catenin for degradation via the ubiquitin-proteasome pathway and inhibit its nuclear translocation thereby preventing transcriptional activation of Wnt/β-catenin target genes (Shah et al., 2022). Although p-β-catenin and total β-catenin were analysed on separate gels due to technical limitations, the observed increase in p-β-catenin at these key sites suggests a potential shift towards β-catenin degradation. In line with our observations, Zhu et al. (2024) found that fucoidan treatment increased p-β-catenin levels and upregulated the expression of GSK-3β, while also decreasing total β-catenin levels, leading to a reduction in β-catenin accumulation in the nucleus. These findings support the idea that fucoidan may promote β-catenin degradation which could lead to a change in activation status of the Wnt/β-catenin signalling pathway. While the changes here are clearly not linked to the noted loss of cell-cell interactions in spheroids they might explain the inhibition of migration from *S. cymosum* and *E. maxima* treatments. As such, the inactivation of the Wnt pathway generally reduces cell migration by limiting pro-migratory gene expression (Shah and Kazi, 2022). However, additional assays investigating the cytoplasmic and nuclear distribution of β-catenin are required to fully confirm the impact these fucoidan treatments had on the activation status of the Wnt/β-catenin pathway in HCT116 cells.

5.4.11 Fucoidan increased cadherin expression levels and its recruitment to the cell membrane

Following the observed changes in β-catenin localisation and expression, we next assessed alterations in cadherin expression levels and localisation, as cadherins are the main binding partners of β-catenin in adherens junctions (Valenta et al., 2012; Benthani et al., 2018). The expression and localisation of cadherins in HCT116 cells were analysed by fluorescence microscopy and western blot analysis using a pan-cadherin antibody. To define where cadherins were localised, we again co-stained with the plasma membrane and Golgi apparatus marker WGA. In untreated HCT116 cells, cadherins were primarily localised in the Golgi apparatus, and, to a lesser extent, at the cell membrane (Figure 5.11A). Consistent with the increased β-catenin localisation

at the cell periphery, the addition of fucoidan also increased the cell membrane localisation of cadherins in both the *E. maxima*- and *S. cymosum*-fucoidan-treated cells. From the observed pan-cadherin expression levels, it was evident that this increase coincided with an overall increase in total cadherin protein levels (Figure 5.11B). Colocalisation analysis further highlighted this as the appearance of orange in the PDM images, which implies that colocalisation of WGA and pan-cadherin increased upon fucoidan treatment (Figure 5.11A).

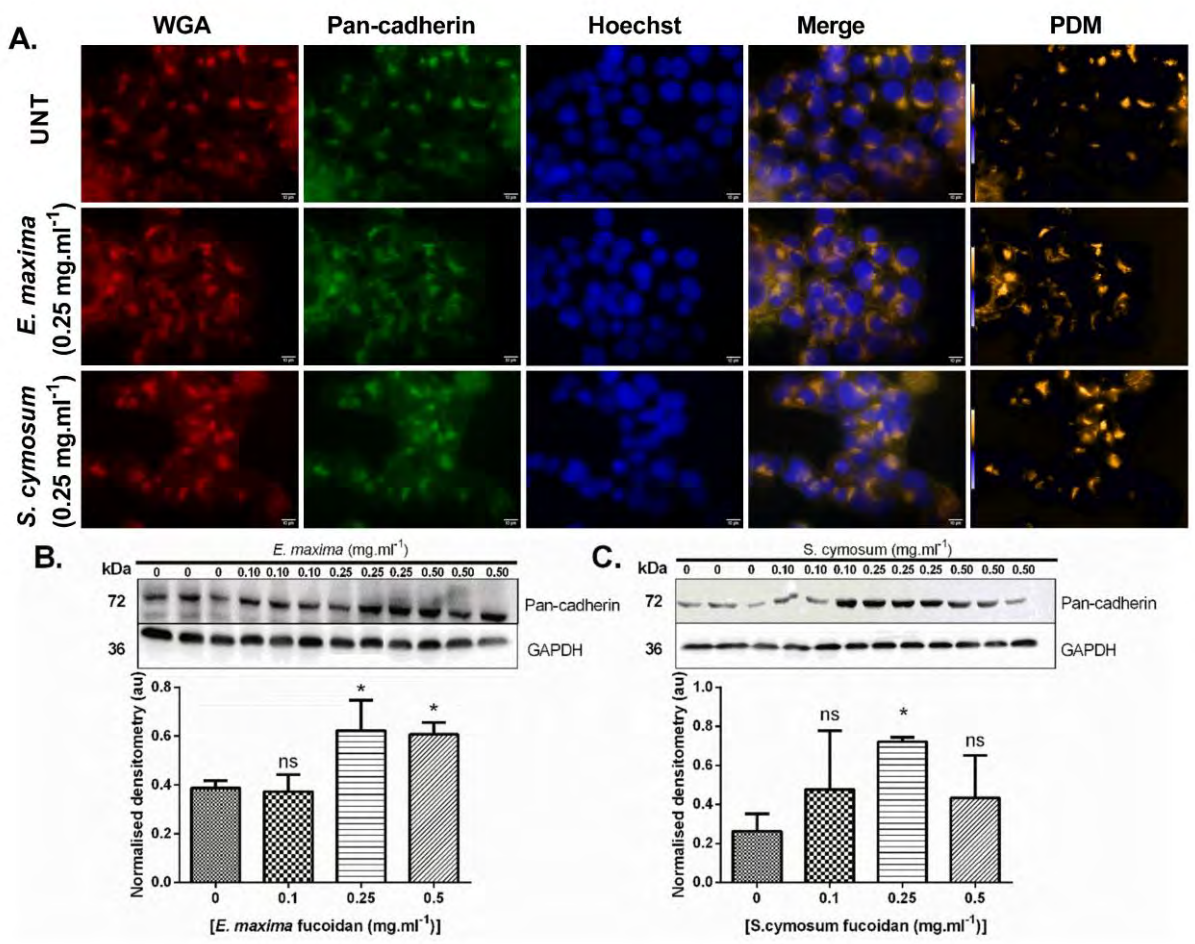

Figure 5.11: Fucoidan induced cadherin accumulation at the cell membrane and increased the cadherin expression levels in HCT116 colon cancer cell. (A) Representative images showing the subcellular localisation of pan-cadherin (green) and the plasma membrane and Golgi marker Alexa fluor 555 conjugated WGA (red) in untreated and 0.25 mg.ml^{-1} fucoidan (*E. maxima or S. cymosum*) 24 hour treated HCT116 cells determined using fluorescence microscopy. Nuclei were stained with Hoechst 33352 (blue). Images were captured at 100x magnification and are representative of triplicate images captured from randomly selected fields. Scale bar represents 10 µm. Colocalization analysis was done using ImageJ. (B) Western blot analysis of pan-cadherin expression in untreated and 24-hour fucoidan-treated HCT116 cells. The densitometry analysis represented alongside the western blots was determined using ImageJ. GAPDH was used as a loading control. Statistical significance represents the difference between pan-cadherin levels in untreated and fucoidan-treated HCT116 cells nominalised to GAPDH, which was assessed by one-way ANOVA where * $p<0.05$ and ns = not significant.

The HCT116 cell line expresses both epithelial E-cadherin and mesenchymal N-cadherin (Yue et al., 2018). With pan-cadherin detecting E-, N-, P-, and R-cadherin (George et al., 2022), the increase in pan-cadherin levels at the cell membrane raises questions about fucoidan affecting the balance between E-cadherin and N-cadherin expression. Given the known effects of fucoidans from *E. maxima* and *S. cymosum* on cell adhesion and migration, along with E-cadherin's association with epithelial characteristics and N-cadherin's role in increased migration and invasion (Loh et al., 2019), the observed decrease in migration might indicate a reduction in N-cadherin expression. While the increase in E-cadherin levels may appear contradictory to the observed reduction in cell-cell adherence observed during spheroid formation assay following treatment with *E. maxima* fucoidan, it's noteworthy that the loss of cell-cell adhesion in HCT116 spheroid formation is independent of E-cadherin expression and rather relies on P-cadherin (Stadler et al., 2018). In addition, the absence of E-cadherin can increase the free pool of β-catenin (Zhu et al., 2024) and a loss of E-cadherin in the HCT116 cell line is known to release β-catenin from the cell membrane (Kim et al., 2019). Since we observed an increase in β-catenin levels at the cell membrane along with cadherin levels, it is therefore unlikely that E-cadherin levels decreased. Instead, the elevated pan-cadherin levels at the cell membrane are likely due to an increase in E-cadherin expression, which may have compensated for the loss of P-cadherin. A shift in the cadherin balance, with an increase in E-cadherin expression and a reduction in P-cadherin, could explain the observed loss of cell-cell adhesion in the 3D spheroid model, as well as the increased pan-cadherin and β-catenin levels at the cell membrane. This would also be consistent with other studies indicating that fucoidan upregulates E-cadherin while downregulating N-cadherin protein levels (Chan et al., 2023). However, further studies focusing on the effects of fucoidan on E-cadherin, N-cadherin, and P-cadherin expression levels and their cellular distribution will be required to confirm this.

5.4.12 Alterations in cell signalling markers FAK, AKT, and MOB1 induced by fucoidan treatment

To begin to understand the potential mechanism underlying the observed anti-cancer-relevant effects of *E. maxima* and *S. cymsosum* fucoidan, we investigated the expression of some relevant cellular signalling pathway markers using western blot analysis (Figure 5.12). Protein kinase B (AKT) and focal adhesion kinase (FAK) have well known roles in modulating β-catenin signalling and cadherin-mediated cell

adhesion, with active AKT promoting β-catenin stability and nuclear translocation, and FAK influencing signalling mechanism linked to β-catenin and cadherin localisation at cell-cell junctions (Fang et al., 2007; Quadri, 2012). On the other hand, MOB1, as a key signalling molecule in the Hippo pathway, indirectly regulates β-catenin signalling by activating LATS1/2 kinases (Kim et al., 2016; Qin et al., 2023). LATS1/2 phosphorylates YAP/TAZ, leading to their inhibition and retention in the cytoplasm (Qin et al., 2023). Elevated levels of YAP/TAZ have been shown to bind β-catenin, suppressing its transcriptional activity without affecting its stability or degradation, suggesting that YAP/TAZ act as modulators of β-catenin. Notably, when Wnt signalling is inactivated, YAP/TAZ bind β-catenin as part of the destruction complex, promoting its phosphorylation and subsequent degradation (Qin et al., 2023). The activation of these pathways involves the phosphorylation of specific signalling intermediates; hence, we also evaluated their phosphorylation status. The western blot analysis revealed significant alterations in the phosphorylation status of AKT, FAK, and MOB following fucoidan treatment (Figure 5.12). Specifically, treatment with *E. maxima* fucoidan led to a significant increase in the levels of phosphorylated AKT (pAKT) at the Ser473 residue (Figure 5.12A). In contrast, treatment with *S. cymosum* fucoidan had no significant effect on pAKT levels. Due to the unavailability of an AKT antibody at the time of the study, it remained unclear whether total AKT levels were also upregulated or if the change was specific to pAKT. Levels of phosphorylated FAK (pFAK) at Tyr576/577 did not significantly change following *E. maxima* fucoidan treatment, but reduced following *S. cymosum* treatment, as shown in Figure 5.12C. However, the total levels of FAK remained unchanged following fucoidan treatment - therefore, the overall abundance of FAK protein was not affected (Figure 5.12B). This suggests that the proportion of total FAK that is phosphorylated at the specific site was reduced. Furthermore, we observed a significant increase in the phosphorylation of MOB1 (pMOB1) at Thr35 following *E. maxima* and *S. cymosum* fucoidan treatment, with unchanged total MOB levels, as is evident from Figures 5.12D and 5.12E, which suggests an increase in the proportion of MOB1 that is phosphorylated.

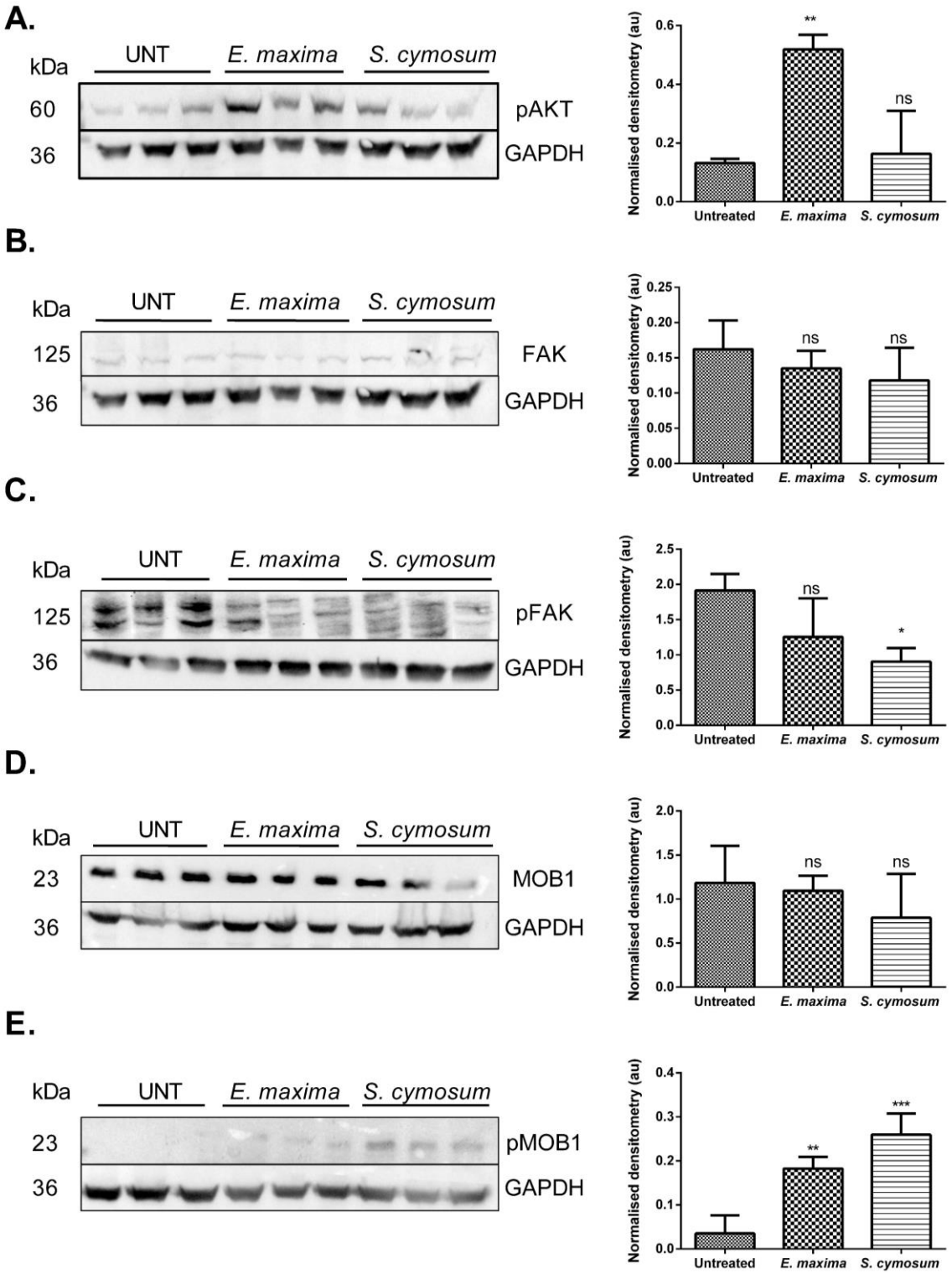

Figure 5.12: Fucoidan mediated effects on pAKT, FAK, pFAK, MOB and pMOB protein expression levels. After treating the HCT116 cells with 0.25 mg.ml^{-1} fucoidan from *E. maxima* or *S. cymosum* for 24 hours, whole cell lysates (50 µg) were analysed for expression level changes by western blot analysis using specific antibodies for (A) p-Akt, (B) FAK, (C) p-FAK, (D) MOB and (E) p-MOB. The densitometry analysis of the western blot bands presented alongside the western blots was performed using ImageJ software. GAPDH was used as a loading control. Statistical significance was determined by comparing the expression levels between untreated and fucoidan-treated HCT116 cells, normalised to GAPDH, using one-way ANOVA. Statistical significance levels are denoted as follows: * for $p < 0.05$, ** for $p < 0.01$, *** for $p < 0.001$, and ns for not significant.

The Akt signalling pathway is widely acknowledged for its critical involvement in tumour development and progression, typically associated with promoting cell growth and survival (Cho et al., 2014). Phosphorylation at the Ser473 residue of AKT is mediated by the mTORC2 complex (mammalian target of rapamycin complex 2) and is necessary for Akt's activation (Gulhati et al., 2009). Increased phosphorylation of Akt at Ser473 in colon cancer has been linked to more aggressive tumour behaviour and enhanced cell survival (Gulhati et al., 2009). Furthermore, the phosphorylation of AKT at this site has also been noted to correlate with the downregulation of membranous E-cadherin and β-catenin in nasopharyngeal carcinoma cells (Yip and Seow, 2012). Given these associations, it was unexpected that treatment with *E. maxima* fucoidan stimulated Akt phosphorylation. This outcome contradicts the anticipated decrease, considering the mild anti-proliferation and inhibited colony formation activity and increase in β-catenin and E- cadherin attributed to this fucoidan. While previous studies on fucoidan have often suggested Akt inhibition as a mechanism for decreasing cell growth and migration of cancer cells (Cho et al., 2014), insights from the study of Han et al. (2015) on fucoidan's effects in HT-29 colon cancer cells suggest the opposite. Han and co-workers linked Akt activation with fucoidan-induced inhibition of cell growth through G1-phase arrest, particularly via p21WAF1 expression. These contrasting literature results indicate a context-dependent role of Akt activation in mediating the anti-cancer effects of fucoidan. Considering this, the observed Akt activation could potentially underpin the anti-cancer activity of *E. maxima* fucoidan.

Furthermore, the above results suggest the potential involvement of focal adhesion kinase (FAK) in our fucoidan-mediated effects. Phosphorylation at Tyr576/577 is particularly crucial for FAK's full catalytic activity and this phosphorylation is achieved following Src binding and activation (Al-Ghabkari et al., 2019). Gayerd et al. (2018), demonstrated that Src-dependent FAK activation is required for E-cadherin relaxation and β-catenin nuclear translocation. When FAK is activated, it can phosphorylate β-catenin, leading to its dissociation from the cell membrane. This also causes E-cadherin to relax, which allows cells to detach from their neighbours - a crucial step in migration (Gayrard et al., 2018). The change in pFAK expression observed in this study therefore could have had implications for the localisation and expression of cadherins and β-catenin. We observed a notable decrease in the expression levels of pFAK following *S. cymosum* fucoidan treatment, while *E. maxima* fucoidan did not significantly affect pFAK expression. In the case of *E. maxima* fucoidan, where no

significant change in pFAK expression was noted, the upregulation of pan-cadherin and β-catenin at the cell membrane suggests that other signalling pathways might be involved. However, in the case of *S. cymosum* fucoidan, the reduction in pFAK levels, along with the observed increased cadherin and β-catenin (Figures 5.10A and 5.11A), may indicate that decreased pFAK activity contributed to the increased cadherin and β-catenin localisation at the membrane. Furthermore, Pei et al. (2017) found that downregulation of FAK promotes E-cadherin expression in melanoma cells, and that decreased E-cadherin expression facilitates cancer cell migration. In our study, both *E. maxima* and *S. cymosum* fucoidan treatments resulted in increased pan-cadherin expression at the cell membrane and inhibited migration. However, only *S. cymosum* fucoidan treatment was associated with reduced pFAK levels and decreased migration in the transwell assay. This could suggest that the inhibition of migration observed with *S. cymosum* fucoidan may be linked to the downregulation of pFAK, pointing to a reason for the different mechanisms of migration inhibition we observed between the two fucoidan treatments.

The increase in pMOB1 levels following *E. maxima* and *S. cymosum* fucoidan treatment may indicate a potential activation of the Hippo pathway, as phosphorylation of MOB1 at Thr35 (and Thr12) is a critical step in converting MOB1 from its autoinhibited form to an active state that binds and activates LATS1/2, which subsequently phosphorylates and retains YAP/TAZ in the cytoplasm, activating the pathway (Kim et al., 2016). This would agree with findings by Xue et al. (2020), who reported activation of the Hippo pathway with increased phosphorylation levels of both upstream and downstream effectors of MOB1 in colorectal cancer cells following fucoidan treatment. Furthermore, Xue et al. (2020) proposed that the activation of the Hippo pathway could suppress canonical Wnt/β-catenin signalling, through YAP-mediated β-catenin degradation. Given the observed increase in both pMOB1 and p-β-catenin levels following these fucoidan treatments, it could be speculated that these effects are linked, with increased pMOB1 levels potentially playing an indirect role in the noted β-catenin phosphorylation. Overall, these findings demonstrate that fucoidan treatment affects key signalling pathways in a complex and context-dependent manner. Different fucoidans result in the activation of different pathways key signals, which may explain the variation in anti-metastatic activities observed between them.

5.5 Conclusion

In conclusion, the findings of this chapter demonstrate that certain fucoidans and sodium alginates exhibit anti-cancer activities *in vitro* against HCT116 colon cancer cells by targeting essential cellular processes involved in metastasis. Our findings indicate that most of the fucoidan and sodium alginate extracts tested partially hinder the adhesion of HCT116 cells, a critical step in cancer cell migration and invasion. Of particular importance is the additional inhibition of anchorage-independent colony growth by *S. elegans* sodium alginate, suggesting its potential to impede the proliferation of detached cancer cells and hinder metastatic spread. However, *E. maxima* fucoidan stood out prominently in our study, showcasing a multifaceted inhibitory effect on various metastasis-related processes, including cell proliferation, cell adhesion, cell migration, spheroid formation, and anchorage-independent colony growth. These effects were associated with significant changes in the expression and/or cellular localisation of key markers, including changes such as increased β-catenin and cadherin expression, and a decrease in pMOB1, that could potentially contribute to the observed inhibition of certain cell metastatic processes. However, *E. maxima* fucoidan also led to increased expression of MMP2 and MMP9, accompanied by morphological changes suggestive of a more migratory phenotype, alongside elevated AKT phosphorylation. These alterations are typically associated with enhanced cell migration and invasion, indicating that the anti-metastatic effects of this fucoidan may involve complex and potentially opposing mechanisms. In addition, *S. cymosum* fucoidan demonstrated notable anti-cancer activity by inhibiting cell proliferation, cell adhesion and cell migration potentially through the suppression of the FAK pathway, modulating the Wnt/β-catenin pathway and inducing alterations in cadherin expression and increased phosphorylation of MOB1. Notably, the rise in pMOB1 may be indirectly connected to the increased levels of p-β-catenin. Overall, it is evident that these fucoidans affect the activation of key signalling markers in a complex and context-dependent manner, with different fucoidans inducing distinct changes in the activation of these markers to exert their anti-metastatic effects.

Chapter 6- General discussion, future perspectives and concluding remarks

In this study, we investigated the potential of fucoidans and sodium alginates derived from South African seaweeds as bioactive compounds for the treatment of cancer and diabetes. By examining the compositional attributes and biological activities of these compounds, we contributed to the expanding body of knowledge surrounding the bioactive potential of these compounds. Each of the chapters in this thesis focused on identifying specific aspects, such as the composition, structure, and bioactivities of these compounds, providing a foundation for a comprehensive overall discussion of the significance and relevance of these findings.

The extraction and characterisation of fucoidans and sodium alginates from the four selected South African brown seaweed species was a crucial first step in this study, ensuring the purity and identity of the polysaccharides for subsequent bioactivity screening. The extraction processes employed yielded relatively high-purity crude fucoidans and sodium alginates, with minimal contamination that could have interfered with subsequent bioactivity screening studies. This was followed by a thorough investigation of the chemical and structural characteristics of these compounds, recognising the crucial role of composition and structural features in understanding bioactivity. Previous studies have highlighted that the bioactivity of fucoidans is intricately linked to their diverse structural characteristics, such as monosaccharide composition, molecular weight, the presence of branches, and the content of sulphate and acetyl groups (Usoltseva et al., 2018).

Our analyses provided valuable insights, particularly into the monosaccharide compositional profiles, molecular weights, acetylation status, and sulphate contents of the fucoidans obtained (Chapter 3). We observed variations in some of these characteristics among the fucoidans, particularly with respect to their monosaccharide profiles and sulphate content. The monomeric composition of the *Ecklonia* and *Sargassum* fucoidans significantly differed with respect to L-fucose, D-glucose, and D-arabinose content, unlike the sulphate content, which was substantial in all but the *E. radiata* fucoidan. As higher fucose and/or sulphate contents did not necessarily lead to better bioactivity (Li et al., 2008), our data suggest that they may be necessary but not critical determinants of fucoidan bioactivity. In addition, a lower molecular weight did not seem to correlate with enhanced bioactivity (Li et al., 2008), as was evident by the

fact that *S. cymosum* fucoidan had the lowest molecular weight while *S. elegans* fucoidan displayed the highest. As all fucoidans were acetylated, it was challenging to draw conclusions regarding the effect of acetylation on bioactivity.

However, fully elucidating the structural features of the fucoidans posed challenges, particularly when using ^{1}H NMR spectroscopy, due to the complexity and overlapping signals inherent in this polysaccharide. Although the aim of our study was to decipher detailed structural differences, the ^{1}H NMR data presented limitations in drawing definitive conclusions. Nevertheless, our ^{1}H NMR findings underscore the substantial diversity in the compositional and structural complexity of bioactive seaweed fucoidans across these different species. Despite the challenges, the distinct signals observed in the 2.7 - 3.2 ppm region of the fucoidans from *E. maxima* and *S. cymosum* spectra were particularly interesting. These signals were noted in the fucoidans that exhibited less anti-diabetic but enhanced anti-cancer activity. This intriguing observation might suggest a potential link between the structural characteristics represented by these signals and the biological activities of these fucoidans. Future exploration of these structural motifs and their relationship with the observed bioactivities could provide valuable insights. While our study did not fully elucidate the precise structural details, it does emphasise the need for further investigation into the structure-function relationships of fucoidans.

The characterisation of the sodium alginate extracts in this study allowed us to elucidate their chemical composition and structural profiles. Using chemical analysis, FTIR spectroscopy, and NMR spectroscopy, we observed strong resemblances between the extracts and both the commercial sodium alginate and previously reported alginate compositions and structures (Belattmania et al. 2020; Lorbeer et al., 2017). Our investigations showed a notable predominance of D-mannuronic acid (M) over L-guluronic acid (G), with M/G ratio values spanning from 2.78 to 3.95. In addition, proton nuclear magnetic resonance spectroscopy provided insights into the heteropolymeric diads (MG, GM) and triads (GGM, MGM), outlining the sequential distribution of M and G within each species' alginate polymer. To the best of our knowledge this study marks the first characterisation of sodium alginate from *S. elegans* and *S. cymosum*, as well as the fucoidan from *S. cymosum*.

Carbohydrate digestion plays a pivotal role in the pathophysiology of Type 2 Diabetes Mellitus (T2DM), where dysregulated glucose metabolism results from impaired insulin

function or inadequate insulin production (Sapra and Bhandari, 2023; Bonsembiante et al., 2021). Enzymatic activity is central to carbohydrate digestion, making it a prime target for interventions which are aimed at managing hyperglycaemia (Lopes et al., 2017). In light of this, our study investigated the potential anti-diabetic activity of fucoidans and sodium alginates through the inhibition of key enzymes involved in carbohydrate digestion. In this study, the evaluated sodium alginate extracts demonstrated limited potential as inhibitors of the key glucose-liberating enzymes compared to the fucoidans extracted from the same seaweed species. While the decrease in postprandial blood glucose linked to sodium alginate intake is typically attributed to its viscosity, which slows intestinal glucose absorption, more recent studies have highlighted its additional potential to inhibit digestive enzymes such as α-glucosidase and/or α-amylase, thereby complementing its role in slowing glucose absorption (Torsdottir et al., 1991; Zaharudin et al., 2018). However, our findings suggest that the efficacy of sodium alginates as enzyme inhibitors may be less significant than previously proposed, indicating that their anti-diabetic potential may lie primarily in their viscosity-related mechanisms. Hence, despite our study concluding them as not having much potential in inhibiting enzymes as a mode of anti-diabetic activity, our sodium alginate extracts may still possess anti-diabetic activities that warrant further evaluation.

In contrast, selected fucoidans extracts were shown to have promising inhibition profiles, by inhibiting the α-glucosidases while sparing α-amylase activity. This specificity is crucial, as excessive α-amylase inhibition, as seen with medications like acarbose, can lead to undigested carbohydrates reaching the colon where their bacterial fermentation causes gastrointestinal discomfort (Proença et al., 2019). Furthermore, our study differentiated between sucrase and maltase inhibition, in addition to the traditional screening assay for α-glucosidase inhibition, which facilitated a deeper understanding of the inhibitory effects of our fucoidans on carbohydrate digestion. Targeting multiple α-glucosidase enzymes, given the variability in sucrose and maltose content in individuals' diets, could enhance the effectiveness of inhibiting postprandial hyperglycemia (Attjioui *et al.,* 2021). Therefore, the fucoidan extracts from *F. vesiculous*, *E. radiata*, and *S. elegans* that exhibited potent inhibition of all three enzymes—α-glucosidase, maltase, and sucrase— may hold the key for more effective regulation of postprandial glucose levels by these fucoidans compared to the other fucoidans, for example the fucoidan from *E. maxima*.

The determination of the type of enzyme inhibition is important in understanding the intricate interplay between the fucoidans and enzymes, that ultimately leads to them modulating enzyme activity. Our investigation revealed a spectrum of inhibition mechanisms among fucoidans sourced from different seaweed species. While fucoidan from *E. maxima* exhibited competitive inhibition, those from *E. radiata*, *S. elegans*, and *F. vesiculosus* demonstrated a mixed inhibition pattern for α-glucosidase, integrating elements of competitive, uncompetitive inhibition, and enzyme inactivation. Similarly, for maltase and sucrase, the mode of inhibition noted for fucoidan from *E. radiata*, *S. elegans*, and *F. vesiculosus* was also mixed in nature. This mixed mode of inhibition provides comprehensive control over enzyme activity, enabling the fucoidans to regulate the rate of carbohydrate digestion even in the presence of high substrate concentrations (Koh et al., 2020). Consequently, the enzyme inhibition profiles and mechanisms of these fucoidans confirm their ability to slow the rate of glucose release, offering promise in the management and prevention of hyperglycaemia (Vinoth Kumar et al., 2015).

The fucoidan and alginate extracts were also screened for their potential anti-cancer activity. Previous studies have demonstrated the broad spectrum of anti-cancer activities exhibited by fucoidan and sodium alginates (Jin et al., 2022; Chen et al., 2017). Given the significant metastatic potential of colon cancer cells, which contribute to approximately 90% of fatalities (Yue et al., 2018), our investigation focused on assessing the impact of these compounds *in vitro* on key metastasis-related cellular processes, such as cell adhesion, migration, spheroid formation, and anchorage-independent colony growth.

In our initial screening of the various fucoidans and sodium alginates extracts, we observed distinct activities across different cellular processes. The *S. cymosum* fucoidan showed potency by inhibiting HCT116 cell adhesion, proliferation as well as migration, while the *E. maxima* fucoidan showed superior activity by also disrupting spheroid formation and inhibiting anchorage-independent colony growth.

Notably, all fucoidan and sodium alginate extracts however demonstrated an inhibitory effect on cancer cell adhesion. This process, crucial for tumour cell migration and invasion, involves the coordinated action of the cytoskeleton and various adhesion molecules and receptors, such as integrins, selectins, glycoproteins, immunoglobulins, and proteoglycans (Kim et al., 2015b; Bendas and Borsig, 2012). In this study, we

found that the reduced cell adhesion observed with fucoidans and sodium alginates is not attributable to changes in the cytoskeleton or integrin β1 expression or distribution (Figure 5.4). While integrin β1 levels remained unchanged in our experiments, HCT116 cells express other major integrins, such as αvβ5 and αvβ4 (Bendas and Borsig, 2012; Jia et al., 2013), which may have been affected by our treatments. It would be valuable to explore whether these integrins undergo changes in expression or localisation following fucoidan treatment, as they could potentially contribute to the observed anti-adhesion effects.

Rather than altering integrin expression, our results suggest that these compounds play a role in preventing initial adhesion, inhibiting re-adhesion, and promoting detachment of cancer cells. This indicates that fucoidans and sodium alginates may interfere with cell-matrix interactions by disrupting both the initial attachment and subsequent adhesion processes. The observed anti-adhesion effects likely involve mechanisms beyond traditional integrin-mediated pathways. Specifically, we propose that fucoidans and sodium alginates could interfere with adhesion through direct interactions with extracellular matrix (ECM) proteins or by binding to specific cell surface receptors. Such interactions could trigger signalling pathways that modulate cell adhesion, including those involving Src kinase, Rho GTPase, FAK, and PI3K/Akt pathways (Brunton et al., 2004). Such reprogramming may involve reduced expression or impaired functionality of adhesion molecules or the induction of a less adhesive phenotype.

Migration inhibition was observed in cells treated with both *S. cymosum* and *E. maxima* fucoidans, through distinct mechanisms. *S. cymosum* fucoidan inhibited both linear and transwell migration, whereas *E. maxima* only impaired linear migration (Figure 5.3). It is worth noting that cells treated with both fucoidans exhibited actin-rich pseudopodia, characteristic of amoeboid motility (Titus and Goodson, 2017). Amoeboid migration is typically associated with rapid and less adhesive movement (Titus and Goodson, 2017) however, the observed inhibition of migration suggests that these pseudopodial structures were not functional for motility. While the inhibition of migration caused by these fucoidans could be in part linked to adhesion loss, the differences in their effects suggest that further distinct underlying mechanisms may be responsible.

Cell adhesion and migration are closely interconnected through focal adhesion turnover, a process regulated in part by focal adhesion kinase (FAK). The reduction in phosphorylated FAK (pFAK) levels observed in *S. cymosum*-treated cells suggests that its anti-adhesion and anti-migration effects are mediated via focal adhesion signalling. As a key component of integrin-mediated signalling, FAK phosphorylates multiple substrates and facilitates focal adhesion assembly and disassembly, thereby regulating cytoskeletal remodelling and traction force generation (Zhang et al., 2020). Its inhibition by *S. cymosum* fucoidan likely impaired focal adhesions, disrupting the integrin-ECM interactions required for directional migration. This is consistent with previous studies showing that FAK suppression limits cancer cell motility and promotes an anti-adhesive phenotype (Zhang et al., 2020).

In contrast, *E. maxima* fucoidan did not affect pFAK levels, suggesting that its anti-adhesion and migration effects are likely mediated through alternative pathways. The PI3K/AKT pathway plays a crucial role in regulating matrix metalloproteinase (MMP) expression in cancer cells, with elevated pAKT levels commonly being associated with increased MMP-2 and MMP-9 expression (Van Weelden et al., 2019). The increase in MMP-2 and MMP-9 following *E. maxima* fucoidan treatment is therfore likely linked to the corresponding rise in pAKT levels. However, the relationship between pAKT, MMP activity, and cancer progression is highly context-dependent, as fucoidans have shown contrasting effects on this pathway. For instance, fucoidan derived from *F. vesiculosus* inhibits migration and invasion by reducing MMP-2 expression and lowering pAKT levels (Van Weelden et al., 2019). In bladder cancer cell lines, fucoidan suppressed cell growth and migration despite an increase in pAKT, through the downregulation of MMP-9 expression (Van Weelden et al., 2019). Whereas, in colorectal cancer fucoidan treatment upregulated pAKT and induced G1-phase arrest, suppressing cell growth via p21WAF1 expression (Han et al., 2015). These findings suggest that elevated pAKT or MMP levels may not always correlate with enhanced migration or invasion, and may, in fact, contribute to anti-cancer effects depending on the broader regulatory context.

While MMPs are generally associated with promoting migration and invasion through ECM degradation, their activity is tightly regulated by tissue inhibitors of metalloproteinases (TIMPs). Fucoidans are known to upregulate TIMPs, counteracting MMP activity and preventing excessive ECM degradation that could drive invasive phenotypes (Zhang et al., 2020). Thus, the observed increase in MMP-2 and MMP-9

in our study may have been offset by TIMPs, resulting in an overall anti-migratory effect. This dual regulation of MMPs and TIMPs could also explain why *E. maxima* fucoidan treatment, despite enhancing MMP activity, did not promote migration or invasion. These findings underscore the complexity of the PI3K/AKT signalling pathway and its downstream effects. Instead of uniformly promoting a pro-migratory phenotype, the observed increase in pAKT and MMP activity following *E. maxima* fucoidan treatment may reflect a regulatory mechanism that inhibits migration or adhesion via ECM remodelling and adhesion reprogramming. This interpretation aligns with reports that AKT activation can lead to context-dependent outcomes, including anti-migratory effects when coupled with compensatory upregulation of TIMPs (Zhang et al., 2020; Van Weelden et al., 2019). Future studies should focus on quantifying TIMP expression in response to fucoidan treatment and further investigating the interplay between pAKT, MMPs, and TIMPs to fully understand their role in the anti-cancer effects of *E. maxima*.

The disruption of adhesion and migration may also be linked to changes in cell-cell adhesion molecules, such as cadherins and β-catenin (Janiszewska et al., 2020; Sato et al., 2001). The phosphorylation of β-catenin is often associated with the deactivation of the Wnt/β-catenin signaling pathway, which plays a critical role in regulating cell-cell adhesion and motility (Shah and Kazi, 2022). This pathways deactivation could have contributed to the observed loss of adhesion. The simultaneous increase in β-catenin and pan-cadherin at the membrane could reflect a compensatory response by the cells to maintain some level of adhesion, though it could also indicate a disrupted balance in adhesion dynamics, contributing to a less stable adhesion phenotype. Furthermore, the upregulation of p-MOB, a marker of Hippo pathway activation, suggests that the loss of adhesion may be linked to this pathway's activation. The Hippo pathway plays a pivotal role in regulating cell growth, differentiation, and migration. It exerts control over various cellular processes by modulating key transcriptional co-activators that influence genes involved in proliferation and motility. By suppressing excessive cell growth and migration, the Hippo pathway maintains tissue homeostasis under normal conditions (Fu et al., 2022). Taken together, these changes in the phosphorylation status of important markers of the Wnt/β-catenin and Hippo pathways likely contribute to the observed anti-adhesion and anti-migration effects.

Anchorage-independent growth and spheroid formation are also critical hallmarks of metastatic potential, enabling cancer cells to survive and proliferate in non-adherent environments (Borowicz et al., 2014; Mori et al., 2009). *E. maxima* fucoidan impaired both spheroid formation and anchorage-independent growth, suggesting its broader impact on tumorigenic behaviours. Spheroid formation relies on robust cell-cell and cell-ECM adhesion (El Harane et al., 2023), both of which were disrupted by *E. maxima*. Notably, the observed increase in β-catenin and pan-cadherin at the membrane appears contradictory, as these molecules are typically associated with stabilising adherens junctions (Martin et al., 2013; Valenta et al., 2012). The loss of P-cadherin, a known factor in the loss of cell-cell adhesion in HCT116 cells (Stadler et al., 2018), alongside potential compensation by E-cadherin at the membrane, could explain this contradiction. For now, it can only be speculated that the loss of P-cadherin at the membrane might be compensated by upregulation of E-cadherin or other cadherin family members. Thus, further investigation is needed to clarify this potential compensation. Additionally, the observed increase in phosphorylated β-catenin may reduce its transcriptional activity, potentially limiting the expression of genes necessary for anchorage-independent survival (Arensman et al., 2014). Furthermore, Hippo pathway activation, as indicated by increased pMOB, may further suppress anchorage-independent growth by inhibiting YAP/TAZ activity. YAP/TAZ are critical regulators of cell survival and proliferation in non-adherent conditions, and their inhibition could drive anoikis, a form of apoptosis induced by detachment from the ECM (Warren et al., 2018). Further experiments, such as quantifying YAP/TAZ activity, could help clarify the specific contributions of these signaling events.

The distinct fucoidan variants tested appear to activate different signalling cascades, which likely contribute to the observed variation in their anti-metastatic effects. Specifically, the activation of pathways such as Akt, FAK, and the Hippo pathway, along with their interplay with key markers like β-catenin and cadherins, suggests that fucoidan modulates cell behaviour of HCT116 cells through multiple mechanisms. While these observations provide valuable insights into the potential anti-cancer properties of fucoidan, further investigation is required to fully elucidate the exact molecular mechanisms at play. The continued exploration of these pathways will be crucial for understanding how fucoidans work.

While our study utilised a concentration range of 0.001–1 mg.ml^{-1} for fucoidans and sodium alginates, it is worth noting that these concentrations are lower than typical oral dosages used in medicinal products. For instance, adult single doses of sodium alginate typically range from 500 to 1000 mg, taken up to four times daily (Food Standards Agency & Food Standards Scotland, 2024), and clinical studies have demonstrated beneficial effects of fucoidans at doses of up to 4 g per day (Abe et al., 2013). The concentrations we tested fall within a range that could be comparable to amounts encountered through regular consumption, suggesting that the observed biological effects may be relevant for human applications.

In conclusion, this study demonstrated that South African seaweed extracts exhibit a range of biological activities relevant to the diabetes and cancer. Fucoidans extracted from *E. radiata* and *S. elegans* showed promise as potent enzyme inhibitors, effectively inhibiting key enzymes involved in carbohydrate digestion, including α-glucosidase, maltase and sucrase. The mechanisms of action were mixed, involving competitive inhibition, uncompetitive substrate inhibition, and enzyme inactivation—attributes that are highly desirable for anti-diabetic agents.

Additionally, fucoidans from *E. maxima* and *S. cymosum* exhibited notable anti-cancer effects by inhibiting critical processes involved in cancer metastasis. While a single underlying mechanism could not be identified, our findings suggest that the anti-cancer effects of *E. maxima* fucoidans may involve the modulation of MMP activity and AKT signalling, whereas *S. cymosum* fucoidan likely exert their effects through the suppression of focal adhesion kinase (FAK). Both fucoidans appear to interfere with key signalling pathways, including Wnt/β-catenin and the Hippo pathway, which are pivotal regulators of cell adhesion and migration. The combined effects on multiple key signalling markers and cell adhesion molecules are likely responsible for their anti-metastatic effects.

However, it is important to note that these findings are based solely on *in vitro* assays, and the lack of a non-cancerous cell line limits the evaluation of fucoidan selectivity and safety. Although the concentrations tested fall within ranges potentially achievable through human consumption, the translational relevance of these results should be interpreted cautiously. Future research should prioritise *in vivo* models to comprehensively assess both the anti-diabetic and anti-cancer efficacy and safety of these extracts. Moreover, detailed mechanistic studies are needed to identify specific

bioactivity markers. Overall, this study contributes to the growing body of evidence supporting the therapeutic potential of seaweed-derived polysaccharides and offers valuable insights into their mechanisms of action.

References

Abdel-Kareem, M.S., & ElSaied, A.F. (2022). Handbook of algae biofules, Chapter 2 - global seaweeds diversity, pp. 39-55, Elsevier, London. https://doi.org/10.1016/B978-0-12-823764-9.00001-7

Abe, S., Hiramatsu, K., Ichikawa, O., Kawamoto, H., Kasagi, T., Miki, Y., Kimura, T., & Ikeda, T. (2013). Safety Evaluation of Excessive Ingestion of Mozuku Fucoidan in Human. *Journal of food science*, *78*(4), T648–T651. https://doi.org/10.1111/j.1750-3841.2012.02966.x

Abka-Khajouei, R., Tounsi, L., Shahabi, N., Patel, A. K., Abdelkafi, S., & Michaud, P. (2022). Structures, Properties and Applications of Alginates. *Marine Drugs*, 20(6): 364. https://doi.org/10.3390/md20060364

Adisakwattana, S., Chantarasinlapin, P., Thammarat, H., & Yibchok-Anun, S. (2009). A Series of Cinnamic Acid Derivatives and their Inhibitory Activity on Intestinal α-Glucosidase. *Journal of Enzyme Inhibition and Medicinal Chemistry*, 24:5, 1194-1200, https://doi.org/10.1080/14756360902779326

Akrida, I., Bravou, V., & Papadaki, H. (2022). The Deadly Cross-talk between Hippo Hathway and Epithelial-Mesenchymal Transition (EMT) in Cancer. *Molecular Biology Reports*, 49(10): 10065–10076. https://doi.org/10.1007/s11033-022-07590-z

Alba, K., & Kontogiorgos, V. (2019). Seaweed Polysaccharides (Agar, Alginate Carrageenan), Encyclopedia of Food Chemistry, Academic Press, pp. 240-250, https://doi.org/10.1016/B978-0-08-100596-5.21587-4

Al Monla, R., Dassouki, Z., Sari-Chmayssem, N., Mawlawi, H., & Gali-Muhtasib, H. (2022). Fucoidan and Alginate from The Brown Algae *Colpomenia sinuosa* and Their Combination with Vitamin C Trigger Apoptosis in Colon Cancer. *Molecules*, 27(2):358. https://doi.org/10.3390/molecules27020358.

Ale, M. T., Maruyama, H., Tamauchi, H., Mikkelsen, J. D., & Meyer, A. S. (2011). Fucose-containing Sulfated Polysaccharides from Brown Seaweeds Inhibit Proliferation of Melanoma Cells and Induce Apoptosis by Activation of Caspase-3 *in vitro*. *Marine Drugs*, 9(12): 2605–2621. https://doi.org/10.3390/md9122605

Al-Ghabkari, A., Qasrawi, D.O., Alshehri, M., & Aru Narendran, A. (2019). Focal adhesion kinase (FAK) Phosphorylation is a Key Regulator of Embryonal Rhabdomyosarcoma (ERMS) Cell Viability and Migration. *Journal of Cancer Research and Clinical Oncology* 145: 1461–1469 https://doi.org/10.1007/s00432-019-02913-3

Ali, M. Y., Kim, D. H., Seong, S. H., Kim, H. R., Jung, H. A., & Choi, J. S. (2017). α-Glucosidase and Protein Tyrosine Phosphatase 1B Inhibitory Activity of

Plastoquinones from Marine Brown Alga *Sargassum serratifolium*. *Marine Drugs*, 15(12): 368. https://doi.org/10.3390/md15120368

Al-Menhali, A., Al-Rumaihi, A., Al-Mohammed, H., Al-Mazrooey, H., Al-Shamlan, M., AlJassim, M., Al-Korbi, N., & Eid, A. H. (2015). *Thymus vulgaris* (Thyme) Inhibits Proliferation, Adhesion, Migration, and Invasion of Human Colorectal Cancer Cells. *Journal of Medicinal Food*, 18(1): 54–59. https://doi.org/10.1089/jmf.2013.3121

Alwarsamy, M., Gooneratne, R., & Ravichandran, R. (2016). Effect of Fucoidan from *Turbinaria conoides* on Human Lung Adenocarcinoma Epithelial (A549) Cells. *Carbohydrate Polymers,* 152: 207–213. https://doi.org/10.1016/j.carbpol.2016.06.112

American Diabetes Association. (2024). Diagnosis and Classification of Diabetes: Standards of Care in Diabetes. *Diabetes Care,* 47 (Supplement 1): S20–S42. https://doi.org/10.2337/dc24-S002

Amosu, A.O., Robertson-Andersson, D.V., Maneveldt, G.W., Robert J. Anderson, R.J. & Bolton, J.J. (2013). South African Seaweed Aquaculture: A Sustainable Development Example for Other African Coastal Countries. *African Journal of Agricultural Research*, 8(43): 5260-5271. https://doi.org/10.5897/AJAR2013. 6994

Anderson, R.L., Balasas, T., Callaghan, J., Coombes, R.C., Evans, J., Hall, J.A., Kinrade, S., Jones, D., Jones, P.S., Jones, R., Marschall, J.F., Panico, M.B., Shaw, J.A., Steeg, P.S., Sullivan, M., Tong, W., Westwell, A.D., & Ritchie, J.W.A. (2019). A Framework for The Development of Effective Anti-Metastatic Agents. *Nature Reviews Clinical Oncology,* 16: 185–204. https://doi.org/10.1038/s41571-018-0134-8

Arensman, M. D., Kovochich, A. N., Kulikauskas, R. M., Lay, A. R., Yang, P. T., Li, X., Donahue, T., Major, M. B., Moon, R. T., Chien, A. J., & Dawson, D. W. (2014). WNT7B Mediates Autocrine Wnt/β-Catenin Signaling and Anchorage-Independent Growth in Pancreatic Adenocarcinoma. *Oncogene*, 33(7): 899–908.

Arumugam P., Arunkumar K., Sivakumar L., Murugan M., & Murugan K. (2019). Anticancer Effect of Fucoidan on Cell Proliferation, Cell Cycle Progression, Genetic Damage and Apoptotic Cell Death in HepG2 Cancer Cells. *Toxicology Reports*, 6: 556–563. https://doi.org/10.1016/j.toxrep.2019.06.005

Atashrazm, F., Lowenthal, R. M., Woods, G. M., Holloway, A. F., & Dickinson, J. L. (2015). Fucoidan and Cancer: A Multifunctional Molecule with Anti-Tumour Potential. *Marine Drugs*, 13(4): 2327–2346. https://doi.org/10.3390/md13042327

Attjioui, M., Ryan, S., Ristic, A., Higgins, T., Goñi, O., Gibney, E., Tierney, J., & O'Connell, S. (2021). Comparison of Edible Brown Algae Extracts for The Inhibition of Intestinal Carbohydrate Digestive Enzymes Involved in Glucose Release from the Diet. *Journal of Nutritional Science,* 10: E5. https://doi.org/10.1017/jns.2020.56

Ayrapetyan, O., Obluchinskaya, E., Zhurishkina, E., Skorik, Y., Lebedev, D., Kulminskaya, A., & Lapina, I. (2021). Antibacterial Properties of Fucoidans from the Brown Algae *Fucus vesiculosus L.* of the Barents Sea. *Biology*, 10(1): 67. https://doi.org/10.3390/biology10010067.

Bax, D. (2021). Appropriate Extracellular Matrix (ECM) Mimicking Surfaces Aid in The Establishment of Serum-Free Cell Culture Media (Master's thesis). Utrecht University. https://studenttheses.uu.nl/handle/20.500.12932/312

Belattmania, Z., Bentiss, F., Jama, C., Mustapha, B., Katif, C., Reani, A., & Sabour, B. (2018). Biosynthesis and Characterization of Silver Nanoparticles Using Sodium Alginate from the Invasive Macroalga *Sargassum muticum*. *BioNanoScience*, 8 (2): 617-623. https://doi.org/10.1007/s12668-018-0518-3

Belattmania, Z., Kaidi, S., El Atouani, S., Katif, C., Bentiss, F., Jama, C., Reani, A., Sabour, B., & Vasconcelos, V. (2020). Isolation and FTIR-ATR and 1H NMR Characterization of Alginates from the Main Alginophyte Species of the Atlantic Coast of Morocco. *Molecules, 25*(18): 4335. https://doi.org/10.3390/molecules25184335

Bendas, G., & Borsig, L. (2012). Cancer Cell Adhesion and Metastasis: Selectins, Integrins, and the Inhibitory Potential of Heparins. *International Journal of Cell Biology*, 2012: 676731. https://doi.org/10.1155/2012/676731

Benthani, F., Herrmann, D., Tran, P. N., Pangon, P.L., Lucas, M.C., Allam, A.H., Currey, N., Al-Sohaily, S., Giry-Laterriere, M. Warusavitarne, J., Timpson P., & Kohonen-Corish, M.R.J. (2018). 'MCC' Protein Interacts with E-Cadherin and β-Catenin Strengthening Cell–Cell Adhesion of HCT116 Colon Cancer Cells. *Oncogene,* 37**:** 663–672. https://doi.org/10.1016/j.jcmgh.2019.01.009

Berr, A. L., Wiese, K., Dos Santos, G., Koch, C. M., Anekalla, K. R., Kidd, M., Davis, J. M., Cheng, Y., Hu, Y. S., & Ridge, K. M. (2023). Vimentin is Required for Tumor Progression and Metastasis in a Mouse Model of Non-Small Cell Lung Cancer. *Oncogene*, 42(25): 2074–2087. https://doi.org/10.1038/s41388-023-02703-9

Beuder, S., & Braybrook, S.A. (2023). Brown algal Cell Walls and Development. *Seminars in Cell & Developmental Biology*, 134: 103-111. https://doi.org/10.1016/j.semcdb.2022.03.003

Bilan, M.I., & Usov, A.I. (2008). Structural Analysis of Fucoidans. *Natural Product Communications*, 3(10): 1639-1648. https://doi.org/10.1177/1934578X0800301011

Bittkau, K. S., Neupane, S., & Alban, S. (2020). Initial Evaluation of Six Different Brown Algae Species as Source for Crude Bioactive Fucoidans. *Algal Research*, 45: 101759.

Bittkau, K.S., Dörschmann, P., Blümel, M., Tasdemir, D., Roider, J., Klettner, A., & Alban S. (2019). Comparison of the Effects of Fucoidans on the Cell Viability of Tumor and Non-Tumor Cell Lines. *Marine Drugs*, 17(8):441. https://doi.org/10.3390/md17080441

Bjerkan, T.M., Bender, C.L., Ertesvåg, H., Drabløs, F., Fakhr, M.K., Preston, L.A., Skjåk-Bræk, G., & Valla, S. (2004). The *Pseudomonas syringae* Genome Encodes a Combined Mannuronan C-5-Epimerase and *O*-Acetylhydrolase, which Strongly Enhances the Predicted Gel-Forming Properties of Alginates. *The Journal of Biological Chemistry*, 279(28): 28920–28929. https://doi.org/10.1074/jbc.M313293200

Boer, G. A., & Holst, J. J. (2020). Incretin Hormones and Type 2 Diabetes-Mechanistic Insights and Therapeutic Approaches. *Biology*, *9*(12): 473. https://doi.org/10.3390/biology9120473

Bojorges, H., Martínez-Abad, A., Martínez-Sanz, M., Rodrigo, M.D., Vilaplana, F., López-Rubio, A., & José Fabra, M. (2023). Structural and Functional Properties of

Alginate Obtained by Means of High Hydrostatic Pressure-Assisted Extraction. *Carbohydrate Polymers*, 299: 120175, https://doi.org/10.1016/j.carbpol.2022.120175

Bolton, J. J., & Stegenga, H. (2002). Seaweed Species Diversity in South Africa. *South African Journal of Marine Science*, 24 (1): 9-18. https://doi.org/10.2989/025776102784528402

Bonsembiante, L., Targher, G., & Maffeis, C. (2021). Type 2 Diabetes and Dietary Carbohydrate Intake of Adolescents and Young Adults: What Is the Impact of Different Choices?. *Nutrients*, *13*(10): 3344. https://doi.org/10.3390/nu13103344.

Boron, W. F., & Boulpaep, E. L. (2017). Nutrient Digestion and Absorption. *Medical Physiology* (3rd ed., Chapter 45). Elsevier, London.

Borowicz, S., Van Scoyk, M., Avasarala, S., Karuppusamy Rathinam, M. K., Tauler, J., Bikkavilli, R. K., & Winn, R. A. (2014). The Soft Agar Colony Formation Assay. *Journal of Visualized Experiments: JoVE*, 92: e51998. https://doi.org/10.3791/51998

Brabletz, T., Jung, A., Reu, S., Prozner, M., Hlubek, F., Kunz-Schukghart, L., Knuechel, R., & Kirchner, T. (2001). Variable B-Catenin Expression in Colorectal Cancers Indicates Tumor Progression Driven by the Tumor Environment. *PNAS*, 98(18): 10356 –10361 www.pnas.orgycgiydoiy10.1073ypnas.171610498

Bradford, M. M. (1976). A Rapid and Sensitive Method for the Quantitation of Microgram Quantities of Protein Utilizing the Principle of Protein Dye Binding. *Analytical Biochemistry,* 72 (1-2): 248-254. https://doi.org/10.1016/0003-2697(76)90527-3

Bradshaw Kaiser, A., Zhang, N., & Van der Pluijm, W. (2018). Global Prevalence of Type 2 Diabetes over the Next Ten Years (2018-2028). *Diabetes*, 67 (Supplement 1): 202-LB. https://doi.org/10.2337/db18-202-LB

Brunton, V. G., MacPherson, I. R., & Frame, M. C. (2004). Cell Adhesion Receptors, Tyrosine Kinases and Actin Modulators: A Complex Three-Way Circuitry. *Biochimica et Biophysica Acta*, *1692*(2-3): 121–144. https://doi.org/10.1016/j.bbamcr.2004.04.010

Castaneda, M., den Hollander, P., Kuburich, N.A., Rosen, J.N., & Mani, S.A. (2022). Mechanisms of Cancer Metastasis, *Seminars in Cancer Biology*, 87:17-31. https://doi.org/10.1016/j.semcancer.2022.10.006

Chan, C. H., Deng, Y. H., Peng, B. Y., Chiang, P. C., Wu, L. A., Lee, Y. Y., Tsao, W., Mao, H. H., Wu, C. Y., & Deng, W. P. (2023). Anti-Colorectal Cancer Effects of Fucoidan Complex-Based Functional Beverage Through Retarding Proliferation, Cell Cycle and Epithelial-Mesenchymal Transition Signaling Pathways. *Integrative cancer therapies*, *22*: 15347354231213613. https://doi.org/10.1177/15347354231213613

Chantree, P., Na-Bangchang, K., & Martviset, P. (2021). Anticancer Activity of Fucoidan via Apoptosis and Cell Cycle Arrest on Cholangiocarcinoma Cell. *Asian Pacific journal of Cancer Prevention: APJCP*, 22(1): 209–217. https://doi.org/10.31557/APJCP.2021.22.1.209

Chazotte B. (2011). Labeling Membrane Glycoproteins or Glycolipids with Fluorescent Wheat Germ Agglutinin. *Cold Spring Harb Protocols*, 1(5):5623. https://doi.org/10.1101/pdb.prot5623

Chen, J., Hu, Y., Zhang, L., Wang, Y., Wang, S., Zhang, Y., Guo, H., Ji, D., & Wang, Y. (2017) Alginate Oligosaccharide DP5 Exhibits Antitumor Effects in Osteosarcoma Patients following Surgery. *Frontiers in Pharmacology*. 8:623. https://doi.org/10.3389/fphar.2017.00623

Chhikara, B.S., & Parang, K. (2023). Global Cancer Statistics 2022: The Trends Projection Analysis. *Chemical Biology Letters*, 10(1): 451. https://pubs.thesciencein.org/journal/index.php/cbl/article/view/451

Cho, M. L., Han, J. H., & You, S. G. (2011). Inhibitory Effects of Fucan Sulfates on Enzymatic Hydrolysis of Starch. *LWT- Food Science and Technology*, 44: 1164-1171. https://doi.org/10.1016/j.lwt.2010.09.019

Cho, T. M., Kim, W. J., & Moon, S. K. (2014). AKT Signaling is Involved in Fucoidan-Induced Inhibition of Growth and Migration of Human Bladder Cancer Cells. *Food and Chemical Toxicology*, 64: 344–352. https://doi.org/10.1016/j.fct.2013.12.009

Colin, D. J., Hain, K. O., Allan, L. A., & Clarke, P. R. (2015). Cellular Responses to a Prolonged Delay in Mitosis are Determined by a DNA Damage Response Controlled by Bcl-2 Family Proteins. *Open Biology*, *5*(3): 140156. https://doi.org/10.1098/rsob.140156

Cumashi, A., Ushakova, N.A., Preobrazhenskaya, M.E., D'Incecco, A., Piccoli, A., Totani, L., Tinari, N., Morozevich, G.E., Berman, A.E., Bilan, M.I., Usov, A.I., Ustyuzhanina, N.E., Grachev, A.A., Sanderson, C.J., Kelly, M., Rabinovich, G.A., Iacobelli, S., & Nifantiev, N.E. (2007). A Comparative Study of the Anti-Inflammatory, Anticoagulant, Antiangiogenic, and Antiadhesive Activities of Nine Different Fucoidans from Brown Seaweeds. *Glycobiology*, 17(5): 541–552. https://doi.org/10.1093/glycob/cwm014

da Silva Fernandes, R., de Moura, M.R., Glenn, G.M., & Aouada, F.A. (2018). Thermal, Microstructural, and Spectroscopic Analysis of Ca^{2+} Alginate/Clay Nanocomposite Hydrogel Beads. *Journal of Molecular Liquids,* 265: 327-336.https://doi.org/10.1016/j.molliq.2018.06.005

Daemi, H., & Barikani, M. (2012). Synthesis and Characterization of Calcium Alginate Nanoparticles, Sodium Homopolymannuronate Salt and its Calcium Nanoparticles. *Scientia Iranica*, 19 (6): 2023-2028. https://doi.org/10.1016/j.scient.2012.10.005

Datta, A., Deng, S., Gopal, V., Yap, K. C., Halim, C. E., Lye, M. L., Ong, M. S., Tan, T. Z., Sethi, G., Hooi, S. C., Kumar, A. P., & Yap, C. T. (2021). Cytoskeletal Dynamics in Epithelial-Mesenchymal Transition: Insights into Therapeutic Targets for Cancer Metastasis. *Cancers*, 13(8): 1882. https://doi.org/10.3390/cancers13081882

Daub, C. D., Mabate, B., Malgas, S., & Pletschke, B. I. (2020). Fucoidan from *Ecklonia maxima* is a Powerful Inhibitor of the Diabetes-related Enzyme, α-Glucosidase. *International Journal of Biological Macromolecules*, 151: 412–420. https://doi.org/10.1016/j.ijbiomac.2020.02.161

DeFronzo, R., Ferrannini, E., Groop, L., Henry, R.R., Herman, W.H., Host, J.J., Hu, F.B., Kahn, R., Raz, I., Shulman, G.I., Simonson, D.C., Testa, M.A., & Weiss, R. (2015). Type 2 Diabetes Mellitus. *Nature Reviews Disease Primers*, 1: 15019. https://doi.org/10.1038/nrdp.2015.19

Dhanani, K.C.H., Samson, W.J. & Edkins, A.L. (2017). Fibronectin is a Stress Responsive Gene Regulated by HSF1 in Response to Geldanamycin. *Scientific Reports,* 7: 17617. https://doi.org/10.1038/s41598-017-18061-y

Dhital, S., Lin, A. H., Hamaker, B. R., Gidley, M. J., & Muniandy, A. (2013). Mammalian Mucosal α-Glucosidases Coordinate with α-Amylase in the Initial Starch Hydrolysis Stage to Have a Role in Starch Digestion Beyond Glucogenesis. *PloS One*, 8(4): e62546. https://doi.org/10.1371/journal.pone.0062546

Díaz, B. (2013). Invadopodia Detection and Gelatin Degradation Assay. *Bio-Protocol*, 3(24): e997. https://doi.org/10.21769/BioProtoc.997

Dobrinčić, A., Zorić, Z., Pedisić, S., Repajić, M., Roje, M., Herceg, Z., Ćož-Rakovac, R., & Dragović-Uzelac, V. (2022). Application of Ultrasound-Assisted Extraction and Non-Thermal Plasma for *Fucus virsoides* and *Cystoseira barbata* Polysaccharides Pre-Treatment and Extraction. *Processes,* 10: 433. https://doi.org/10.3390/pr10020433

Dodgson, K. S. (1961). Determination of Inorganic Sulphate in Studies on the Enzymic and non-Enzymic Hydrolysis of Carbohydrate and Other Sulphate esters. *Biochemical Journal*, 78(2): 312–319. https://doi.org/10.1042/bj0780312

dos Santos Araújo, P., Belini, G.B., Mambrini, G.P., Yamaji, F.M., & Waldman, W.R. (2019). Thermal degradation of Calcium and Sodium Alginate: A Greener Synthesis Towards Calcium Oxide Micro/Nanoparticles*. International Journal of Biological Macromolecules*, 140: 749-760. https://doi.org/10.1016/j.ijbiomac.2019.08.103

Dubois, M., Gilles, K. A., Hamilton, J. K., Rebers, P. A. & Smith, F. (1956). Colorimetric Method for Determination of Sugars and Related Substances. *Analytical Chemistry*, 28 (3): 350-356. https://doi.org/10.1021/ac60111a017

Edwards, J. G., McLaren, J., Jones, J. L., Waller, D. A., & O'Byrne, K. J. (2003). Matrix Metalloproteinases 2 and 9 (Gelatinases A and B) Expression in Malignant Mesothelioma and Benign Pleura. *British Journal of Cancer*, 88(10):1553–1559. https://doi.org/10.1038/sj.bjc.6600920.

Edwards, M., Hanniffy, D., Heesch, S., Hernandez-Kantun, J., Miniz, M., Queguineur, B., Ratcliff, R., Soler-Vila, A., Wan, A. (2021). Macroalgae Fact-Sheets, in: A. Soler-Vila, M. Miniz (Eds.), Irish Seaweed Research Group, Ireland, 2012.

El Harane, S., Zidi, B., El Harane, N., Krause, K. H., Matthes, T., & Preynat-Seauve, O. (2023). Cancer Spheroids and Organoids as Novel Tools for Research and Therapy: State of the Art and Challenges to Guide Precision Medicine. *Cells*, 12(7): 1001. https://doi.org/10.3390/cells12071001

El Khoury, D., Goff, H.D., Berengut, S., Kubant, R., & Anderson, G.H. (2014). Effect of Sodium Alginate Addition to Chocolate Milk on Glycemia, Insulin, Appetite and Food Intake in Healthy Adult Men. Eu*ropean Journal of Clinical Nutrition*, 68: 613–618. https://doi.org/10.1038/ejcn.2014.53

Esue, O., Carson, A.A., Tseng, Y., & Wirtz, D. (2006). A Direct Interaction between Actin and Vimentin Filaments Mediated by the Tail Domain of Vimentin. *Journal of Biological Chemistry*, 281 (41): 30393-30399. https://doi.org/10.1074/jbc.M605452200

Fang, D., Hawke, D., Zheng, Y., Xia, Y., Meisenhelder, J., Nika, H., Mills, G. B., Kobayashi, R., Hunter, T., & Lu, Z. (2007). Phosphorylation of Beta-Catenin by AKT Promotes Beta-Catenin Transcriptional Activity. *The Journal of Biological Chemistry*, 282(15): 11221–11229. https://doi.org/10.1074/jbc.M611871200

Fares, J., Fares, M.Y., Khachfe, H.H. Salhab, H. A., & Fares, Y. (2020). Molecular Principles of Metastasis: A Hallmark of Cancer Revisited. S*ignal Transduction and Targeted Therapy,* 5(1): 28. https://doi.org/10.1038/s41392-020-0134-x

FDA, 2020. *U.S Food & Drug Administration*. [Online] Available at: https://www.fda.gov/news-events/press-announcements/fda-alerts-patients-and-health-care-professionals-nitrosamine-impurity-findings-certain-metformin [Accessed 12 November 2023].

Fertha, M., Belfkira, A., Dahmane, E.M., Taourirte, M., & Brouillette, F. (2017). Extraction and Characterization of Sodium Alginate from *Moroccan Laminaria* digitate Brown Seaweed. *Arabian Journal of Chemistry*, 10 (2): S3707-S3714. https://doi.org/10.1016/J.ARABJC.2014.05.003

Filippo-Herrera, D.A., Hernández-Carmona, G., Muñoz-Ochoa, M., Arvizu-Higuera, D.L., & Rodríguez-Montesinos, Y.E. (2018). Monthly Variation in the Chemical Composition and Biological Activity of *Sargassum horridum. Botanica Marina*, 61:91–102, https://doi.org/10.1515/bot-2017-0031

Fitton, J. H., Stringer, D. N., & Karpiniec, S. S. (2015). Therapies from Fucoidan: An Update. *Marine Drugs*, 13(9): 5920–5946. https://doi.org/10.3390/md13095920

Fitton, J.H., Stringer, D.N., Park, A.Y., & Karpiniec, S.S. (2019). Therapies from Fucoidan: New Developments. *Marine Drugs*, 17(10): 571. https://doi.org/10.3390/md17100571

Flores-Hernández, C.G., Cornejo-Villegas, M.L.A., Moreno-Martell, A., & Del Real, A. (2021). Synthesis of a Biodegradable Polymer of Poly (Sodium Alginate/Ethyl Acrylate). *Polymers,*13(4):504. https://doi.org/10.3390/polym13040504

Food Standards Agency & Food Standards Scotland. (2024). Safety Assessment on Product E 401 (Sodium Alginate) Used as a Surface Treatment in Entire Fruits and Vegetables (RP290). *FSA Research and Evidence*. https://doi.org/10.46756/001c.121793

Fuhrmann, A., & Engler, A. J. (2015). The Cytoskeleton Regulates Cell Attachment Strength. *Biophysical Journal*, 109(1): 57–65. https://doi.org/10.1016/j.bpj.2015.06.003

Fu, M., Hu, Y., Lan, T., Guan, K. L., Luo, T., & Luo, M. (2022). The Hippo Signalling Pathway and its Implications in Human Health and Diseases. *Signal Transduction and Targeted Therapy*, *7*(1): 376. https://doi.org/10.1038/s41392-022-01191-9

Galindo, E., Peña, C., Núñez, C., Segura, D., & Espín, G. (2007). Molecular and Bioengineering Strategies to Improve Alginate and Polydydroxyalkanoate Production by *Azotobacter vinelandii*. *Microbiological Cell Factories,* 6: 7. https://doi.org/10.1186/1475-2859-6-7

Ganesh, K., & Massagué, J. (2021). Targeting Metastatic Cancer. *Nature Medicine*, 27(1): 34–44. https://doi.org/10.1038/s41591-020-01195-4

Gao, Y-.Z., Chang, T-.X., & Wu, Y-.X. (2019). *In-Situ* Synthesis of Acylated Sodium Alginate-*g*-(Tetrahydrofuran5-*b*-Polyisobutylene) Terpolymer/Ag-NPs Nanocomposites. *Carbohydrate Polymers*, 219: 201-209. https://doi.org/10.1016/j.carbpol.2019.04.087

García-Ríos, V., Ríos-Leal, E., Robledo, D., & Freile-Pelegrin, Y. (2012). Polysaccharides Composition from Tropical Brown Seaweeds. *Phycological Research*, 60: 305-315. https://doi.org/10.1111/j.1440-1835.2012.00661

Gayrard, C., Bernaudin, C., Déjardin, T., Seiler, C., & Borghi, N. (2018). Src- and Confinement-Dependent FAK Activation Causes E-Cadherin Relaxation and β-Catenin Activity. *The Journal of Cell Biology*, *217*(3): 1063–1077. https://doi.org/10.1083/jcb.201706013

George, A., Sharma, R., Pfister, T., Abu-Asab, M., Hotaling, N., Bose, D., DeYoung, C., Chang, J., Adams, D. R., Cogliati, T., Bharti, K., & Brooks, B. P. (2022). *In vitro* Disease Modeling of Oculocutaneous Albinism Type 1 and 2 Using Human Induced Pluripotent Stem Cell-Derived Retinal Pigment Epithelium. *Stem Cell Reports*, 17(1): 173–186. https://doi.org/10.1016/j.stemcr.2021.11.016

Giuntini, E.B., Sardá, F.A.H., & de Menezes, E.W. (2022). The Effects of Soluble Dietary Fibers on Glycemic Response: An Overview and Futures Perspectives. *Foods*,11: 3934. https://doi.org/10.3390/foods11233934

Grasdalen, H., Larsen, B., & Smidsrød, O. (1979). A P.M.R. Study of the Composition and Sequence of Uronate Residues in Alginates. *Carbohydrate Research*, 68: 23-31, https://doi.org/10.1016/S0008-6215(00)84051-3

Gulhati, P., Cai, Q., Li, J., Liu, J., Rychahou, P. G., Qiu, S., Lee, E. Y., Silva, S. R., Bowen, K. A., Gao, T., & Evers, B. M. (2009). Targeted Inhibition of Mammalian Target of Rapamycin Signaling Inhibits Tumorigenesis of Colorectal Cancer. *Clinical Cancer Research*, 15(23): 7207–7216. https://doi.org/10.1158/1078-0432.CCR-09-1249

Gundogdu, R., & Hergovich, A. (2019). MOB (Mps one Binder) Proteins in the Hippo Pathway and Cancer. *Cells*, 8(6): 569. https://doi.org/10.3390/cells8060569

Gutschner, T., & Diederichs, S. (2012). The Hallmarks of Cancer: a Long Non-Coding RNA Point of View. *RNA Biology*, 9(6): 703–719. https://doi.org/10.4161/rna.20481

Han, N., Li, J., & Li, X. (2022). Natural Marine Products: Anti-Colorectal Cancer *In Vitro* and *In Vivo*. *Marine Drugs*, 20(6): 349. https://doi.org/10.3390/md20060349

Han, Y. (2019). Analysis of the Role of the Hippo Pathway in Cancer. *Journal of Translational Medicine,* 17: 116. https://doi.org/10.1186/s12967-019-1869-4

Han, Y.-S., Lee, J.H. & Lee, S.H. (2015). Fucoidan Inhibits the Migration and Proliferation of HT-29 Human Colon Cancer Cells via the Phosphoinositide-3 kinase/Akt/Mechanistic Target of Rapamycin Pathways. *Molecular Medicine Reports*, 2:3446-3452. https://doi.org/10.3892/mmr.2015.3804

Hanahan, D. (2022). Hallmarks of Cancer: New Dimensions. *Cancer Discov*ery, 12 (1): 31–46. https://doi.org/10.1158/2159-8290.CD-21-1059

Hanahan, D., & Weinberg, R. A. (2011). Hallmarks of Cancer: The Next Generation. *Cell*, 144: 646-674. https://doi.org/10.1016/j.cell.2011.02.013

Harden, C.J., Craig Richardson, J., Dettmar, P.W., Corfe, B.M., & Paxman, J.R. (2012). An Ionic-Gelling Alginate Drink Attenuates Postprandial Glycaemia in Males. *Journal of Functional Foods*, 4:122–128. https://doi.org/10.1016/j.jff.2011.09.002

Häußler, M. (2023). "From Raw Data to Kinetic Parameters: an EnzymeML-Based Workflow for Reproducible Enzyme Kinetics", [Masters thesis, University of Stuttgart], https://doi.org/10.18419/darus-3337, DaRUS, V1.

He, K., & Gan, W. J. (2023). Wnt/β-Catenin Signaling Pathway in the Development and Progression of Colorectal Cancer. *Cancer Management and Research*, 15: 435–448. https://doi.org/10.2147/CMAR.S411168

Helfand, B. T., Mendez, M. G., Murthy, S. N., Shumaker, D. K., Grin, B., Mahammad, S., Aebi, U., Wedig, T., Wu, Y. I., Hahn, K. M., Inagaki, M., Herrmann, H., & Goldman, R. D. (2011). Vimentin Organization Modulates the Formation of Lamellipodia. *Molecular Biology of he Cell*, 22(8): 1274–1289. https://doi.org/10.1091/mbc.E10-08-0699

He, X., Xue, M., Jiang, S., Li, W., Yu, J., & Xiang, S. (2019). Fucoidan Promotes Apoptosis and Inhibits EMT of Breast Cancer Cells. *Biological & Pharmaceutical Bulletin*, 42(3): 442–447. https://doi.org/10.1248/bpb.b18-00777

Hezma, A.M., Shaltout, W.A., Kabary, H.A., El-Bahy, G.S., & Abdelrazek, A.B. (2023). Fabrication, Characterization and Adsorption Investigation of Nano Zinc Oxide–Sodium Alginate Beads for Effective Removal of Chromium (VI) from Aqueous Solution. *The Journal of Inorganic and Organometallic Polymers and Materials,* 33: 1400–1408. https://doi.org/10.1007/s10904-023-02573-4

Holdt, S.L., & Kraan, S. (2011). Bioactive Compounds in Seaweed: Functional Food Applications and Legislation. *Journal of Applied Phycology*, 23(3): 543-597. https://doi.org/10.1007/s10811-010-9632-5

Howe, G. A., & Addison, C. L. (2012). β1 Integrin: an Emerging Player in the Modulation of Tumorigenesis and Response to Therapy. *Cell Adhesion & Migration*, 6(2): 71–77. https://doi.org/10.4161/cam.20077

Hsu, H. Y., & Hwang, P. A. (2019). Clinical Applications of Fucoidan in Translational Medicine for Adjuvant Cancer Therapy. *Clinical and Translational Medicine*, 8(1): 15. https://doi.org/10.1186/s40169-019-0234-

Hsu, H. Y., Lin, T. Y., Hwang, P. A., Tseng, L. M., Chen, R. H., Tsao, S. M., & Hsu, J. (2013). Fucoidan Induces Changes in the Epithelial to Mesenchymal Transition and Decreases Metastasis by Enhancing Ubiquitin-Dependent TGFβ Receptor Degradation in Breast Cancer. *Carcinogenesis*, 34(4): 874–884. https://doi.org/10.1093/carcin/bgs396

Huang, Z., Wang, Y., Shafer, R., Winn, N.C., Kanaley, J.A., & Vardhanabhuti, B. (2019). Glycemic Effects Following the Consumption of Mixed Soy Protein Isolate and Alginate Beverages in Healthy Adults. *Food & Function*, 10: 1718–1725. https://doi.org/10.1039/C8FO01627E

Hurtado, A., Aljabali, A. A. A., Mishra, V., Tambuwala, M. M., & Serrano-Aroca, Á. (2022). Alginate: Enhancement Strategies for Advanced Applications. *International Journal of Molecular Sciences*, 23(9): 4486. https://doi.org/10.3390/ijms23094486

Husni, A., Izmi, N., Ayunani, F. Z., Kartini, A., Husnayain, N., & Isnansetyo, A. (2022). Characteristics and Antioxidant Activity of Fucoidan from *Sargassum hystrix*: Effect of Extraction Method. *International Journal of Food Science*, *2022*: 3689724. https://doi.org/10.1155/2022/3689724

International Diabetes Federation. (2021). IDF Diabetes Atlas 10th edition. Available at: https://diabetesatlas.org/data/en/country/185/za.html. (Accessed 16 February 2024).

Irianto, H.E., Giyatmi, G., Fransiska, D., and Nuraelah, A. (2023). Physical and Chemical Characteristics of Alginate Extracted from *Sargassum sp*. IOP Conference Series: Earth and Environmental Science, https://doi.org/10.1088/1755-1315/1177/1/012029

Iriyanti, T., Wahid Wahab, A., & Bahar, R. (2019). Potential Na-Alginate Extraction from Brown Algae *Sargassum* sp. of the Mango Maturation Process. *Journal akta Kimia Indonesia,* 11(2): 17-27. https://doi.org/10.20956/ica.v11i2.6488

Janiszewska, M., Primi, M.C., & Izard, T. (2020). Cell Adhesion in Cancer: Beyond the Migration of Single Cells. *Journal of Biological Chemistry*, 295 (8): 2495-2505, https://doi.org/10.1074/jbc.REV119.007759.

January, G.G., Naidoo, R.K., Kirby-McCullough, B. & Bauerd, R. (2019). Assessing Methodologies for Fucoidan Extraction from South African Brown Algae. *Algal Research*, 40: 101517. http://doi.org/10.1016/j.algal.2019.101517

Jayawardena, T.U., Nagahawatta, D.P., Fernando, I.P.S., Kim, Y.-T., Kim, J.-S., Kim, W.-S., Lee, J.S., & Jeon, Y.-J. (2022). A Review on Fucoidan Structure, Extraction Techniques, and Its Role as an Immunomodulatory Agent. *Marine Drugs*. 20(12):755. https://doi.org/10.3390/md20120755

Jia, J., Starodub, A., Cushman, I., Liu, Y., Marshall, D. J., Hurwitz, H. I., & Nixon, A. B. (2013). Dual Inhibition of αV Integrins and Src Kinase Activity as a Combination Therapy Strategy for Colorectal Cancer. *Anti-Cancer Drugs*, 24(3): 237–250. https://doi.org/10.1097/CAD.0b013e32835d29fd

Jin, J.-O., Yadav, D., Madhwani, K., Puranik, N., Chavda, V., & Song, M. (2022). Seaweeds in the Oncology Arena: Anti-Cancer Potential of Fucoidan as a Drug—A Review. *Molecules*, 27(18): 6032. https://doi.org/10.3390/molecules27186032

Kaler P, Augenlicht L, Klampfer L. (2012). Activating Mutations in β-Catenin in Colon Cancer Cells Alter their Interaction with Macrophages; the Role of Snail. *PLoS One*, 7(9): e45462. https://doi.org/10.1371/journal.pone.0045462

Kalluri, R., & Weinberg, R. A. (2009). The Basics of Epithelial-Mesenchymal Transition. *The Journal of Clinical Investigation*, 119(6): 1420–1428. https://doi.org/10.1172/JCI39104

Karthikeyan, C., Varaprasad, K., Kim, S., Jangid, A.K., Lee, W., Hameed, A.S.H., & Kyobum, K. (2023). Size-Dependent Cellular Uptake of Sodium Alginate Passivated tin Dioxide Nanoparticles in Triple-Negative Breast Cancer Cells. *Journal of Industrial and Engineering Chemistry, 123: 476-487*, https://doi.org/10.1016/j.jiec.2023.04.001

Kasina, S.V.S.K., & Baradhi, K.M. Dipeptidyl Peptidase IV (DPP IV) Inhibitors. [Updated 2023 May 22]. In: StatPearls. Treasure Island (FL): StatPearls Publishing; 2024 Jan-. Available from: https://www.ncbi.nlm.nih.gov/books/NBK542331/

Kaul, K., Tarr, J.M., Ahmad, S.I., Kohner, E.M., & Chibber, R. (2013). Introduction to Diabetes Mellitus. In: Ahmad, S.I. (eds) Diabetes. Advances in Experimental Medicine and Biology, vol 771. Springer, New York, NY. https://doi.org/10.1007/978-1-4614-5441-0_1

Kahn, S. E., Cooper, M. E., & Del Prato, S. (2014). Pathophysiology and Treatment of Type 2 Diabetes: Perspectives on the Past, Present, and Future. *Lancet*, *383*(9922): 1068–1083. https://doi.org/10.1016/S0140-6736(13)62154-6

Khalid, S., Abbas, M., Saeed, F., Bader-Ul-Ain, H., & Suleria, H.A.R. (2018). Therapeutic Potential of Seaweed Bioactive Compounds. Therapeutic Potential of Seaweed Bioactive Compounds, Seaweed Biomaterials, p. 7-25, Sabyasachi Maiti, London, UK: IntechOpen. https://doi.org/10.5772/intechopen.74060

Kim, E. J., Park, S. Y., Lee, J. Y., & Park, J. H. (2010). Fucoidan Present in Brown Algae Induces Apoptosis of Human Colon Cancer Cells. *BMC Gastroenterology*, 10: 96. https://doi.org/10.1186/1471-230X-10-96

Kim H. K. (2012). *Ecklonia cava* Inhibits Glucose Absorption and Stimulates Insulin Secretion in Streptozotocin-Induced Diabetic Mice. *Evidence-based Complementary and Alternative Medicine*: 439294: 7. https://doi.org/10.1155/2012/439294

Kim, H., Ara, L., Won-Kyo, J., & Taeck, J. (2015). Effects of Fucoidan on Cell Morphology and Migration in Osteoblasts. *Food Science and Biotechnology*, 24: 699-704. https://doi.10.1007/s10068-015-0091-2

Kim, K.-T. Rioux, L.-E., & Turgeon, S. L. (2014). Alpha Amylase and Alpha-Glucosidase Inhibition is Differentially Modulated by Fucoidan Obtained from *Fucus vesiculosus* and *Ascophyllum nodosum*. *Phytochemistry*, 98: 27-33. https://doi.org/10.1016/j.phytochem.2013.12.003

Kim, N. G., & Gumbiner, B. M. (2015). Adhesion to Fibronectin Regulates Hippo Signaling via the FAK-Src-PI3K Pathway. *The Journal of Cell Biology*, 210(3): 503–515. https://doi.org/10.1083/jcb.201501025

Kim, S. Y., Tachioka, Y., Mori, T., & Hakoshima, T. (2016). Structural Basis for Autoinhibition and its Relief of MOB1 in the Hippo Pathway. *Scientific Reports*, *6*: 28488. https://doi.org/10.1038/srep28488

Kim, W. K., Kwon, Y., Jang, M., Park, M., Kim, J., Cho, S., Jang, D. G., Lee, W. B., Jung, S. H., Choi, H. J., Min, B. S., Il Kim, T., Hong, S. P., Paik, Y. K., & Kim, H. (2019). β-Catenin Activation Down-Regulates Cell-Cell Junction-Related Genes and Induces Epithelial-to-Mesenchymal Transition in Colorectal Cancers. *Scientific Reports*, 9(1): 18440. https://doi.org/10.1038/s41598-019-54890-9

Klimaszewska-Wiśniewska, A., Hałas-Wiśniewska, M., Grzanka, A., & Grzanka, D. (2018). Evaluation of Anti-Metastatic Potential of the Combination of Fisetin with Paclitaxel on A549 Non-Small Cell Lung Cancer Cells. *International Journal of Molecular Sciences*, 19(3): 661. https://doi.org/10.3390/ijms19030661

Kloareg, B., Badis, Y., Cock, J.M., & Michel, G. (2021). Role and Evolution of the Extracellular Matrix in the Acquisition of Complex Multicellularity in Eukaryotes: A Macroalgal Perspective. *Genes*, 12: 1059. https://doi.org/10.3390/genes12071059

Koh, H. S. A., Lu, J., & Zhou, W. (2020). Structural Dependence of Sulfated Polysaccharide for Diabetes Management: Fucoidan From *Undaria*

pinnatifida Inhibiting α-Glucosidase More Strongly Than α-Amylase and Amyloglucosidase. *Frontiers in Pharmacology*, *11*: 831. https://doi.org/10.3389/fphar.2020.00831

Kokova, V., Lukova, P., Baldzhieva, A., Katsarov, P., Delattre, C., Molinié, R., Petit, E., Elboutachfaiti, R., Murdjeva, M., & Apostolova, E. (2023). Extraction, Structural Characterization, and *In Vivo* Anti-Inflammatory Effect of Alginate from *Cystoseira crinita* (Desf.) borry Harvested in the Bulgarian Black Sea. *Marine Drugs*, 21(4):245. https://doi.org/10.3390/md21040245

Kopplin, G., Rokstad, A.M., Mélida, H., Bulone, V., Skjåk-Bræk, G., & Aachmann, F.L. (2018). Structural Characterization of Fucoidan from *Laminaria hyperborea*: Assessment of Coagulation and Inflammatory Properties and Their Structure−Function Relationship. *ACS Applied Biological Materials,* 1 (6): 1880−1892, https://doi.org/10.1021/acsabm.8b00436.

Kraan, S. (2012). Algal Polysaccharides, Novel Applications and Outlook, Chapter 22- Carbohydrates - Comprehensive Studies on Glycobiology and Glycotechnology. IntechOpen, pp. 489–532, https://doi.org/10.5772/51572

Kuczajowska-Zadrożna, M. Filipkowska, U., & Jóźwiak, T. (2020). Adsorption of Cu (II) and Cd (II) from Aqueous Solutions by Chitosan Immobilized in Alginate Beads. *Journal of Environmental Chemical Engineering*, 8 (4): 103878. https://doi.org/10.1016/j.jece.2020.103878

Kumar, A., Gangwar, R., Zargar, A.A., Kumar, R., & Sharma, A. (2024). Prevalence of Diabetes in India: A Review of IDF Diabetes Atlas 10th Edition. *Current Diabetes reviews*, 20(1): e130423215752. https://doi.org/10.2174/1573399819666230413094200.

Kumar, S. A., & Brown L. (2013). Seaweeds as Potential Therapeutic Interventions for the Metabolic Syndrome. *Reviews in Endocrine and Metabolic Disorders*, 14: (3), 299–308. https://doi.org/10.1007/s11154-013-9254-8

Kumar, T. V., Lakshmanasenthil, S., Geetharamani, D., Marudhupandi, T., Suja, G., & Suganya, P. (2015). Fucoidan- A α-D-Glucosidase Inhibitor from *Sargassum wightii* with Relevance to Type 2 Diabetes Mellitus Therapy. *International Journal of Biological Macromolecules*, 72: 1044-1047. https://doi.org/10.1016/j.ijbiomac.2014.10.013

Łabowska, B.M., Michalak, I., & Detyna, J. (2019). Methods of Extraction, Physicochemical Properties of Alginates and their Applications in Biomedical Field – A Review, *Open Chemistry*, *17*(1): 738-762. https://doi.org/10.1515/chem-2019-0077

Laemmli, U.K. (1970). Cleavage of Structural Proteins During the Assembly of the Head of Bacteriophage T4. *Nature*, 227: 680–685. https://doi.org/10.1038/227680a0

Lakshmanan, A., Balasubramanian, B., Maluventhen, V., Malaisamy, A., Baskaran, R., Liu, W.-C., & Arumugam, M. (2022). Extraction and Characterization of Fucoidan Derived from *Sargassum ilicifolium* and its Biomedical Potential with *in Silico* Molecular Docking. *Applied Sciences,* 12(24):13010. https://doi.org/10.3390/app122413010

Lakshmanasenthil, S., Vinoth Kumar, T., Geetharamanib, D., Marudhupandic, T., Sujaa, G., & Sindhua, N. S. (2014). Fucoidan—A Novel α-Amylase Inhibitor from

Turbinaria ornata with Relevance to NIDDM Therapy. *Biocatalysis and Agricultural Biotechnology*, 3: 66-70. https://doi.org/10.1016/j.bcab.2014.02.003

Lala, V. G., Mohamed, A., Tate, D. J., Seabi, N. M., & Mokgoko, D. (2024). Colorectal cancer screening: An update and South African perspective. *Wits Journal of Clinical Medicine, 6*(2): 95–102. https://doi.org/10.18772/26180197.2024.v6n2a7

Lamouille, S., Xu, J., & Derynck, R. (2014). Molecular Mechanisms of Epithelial-Mesenchymal Transition. *Nature Reviews Molecular Cell Biology*, 15(3): 178–196. https://doi.org/10.1038/nrm3758

Langers, A. M., Verspaget, H. W., Hawinkels, L. J., Kubben, F. J., van Duijn, W., van der Reijden, J. J., Hardwick, J. C., Hommes, D. W., & Sier, C. F. (2012). MMP-2 and MMP-9 in Normal Mucosa are Independently Associated with Outcome of Colorectal Cancer Patients. *British Journal of Cancer*, 106(9): 1495–1498. https://doi.org/10.1038/bjc.2012.80

Laronha, H., & Caldeira, J. (2020). Structure and Function of Human Matrix Metalloproteinases. *Cells*, 9(5): 1076. https://doi.org/10.3390/cells905107

Leandro, A., Pacheco, D., Cotas, J., Marques, J.C., Pereira, L., & Gonçalves, A.M.M. (2020). Seaweed's Bioactive Candidate Compounds to Food Industry and Global Food Security. *Life*,10(8):140. https://doi.org/10.3390/life10080140

Lee, B. H., Eskandari, R., Jones, K., Reddy, K. R., Quezada-Calvillo, R., Nichols, B. L., Rose, D. R., Hamaker, B. R., & Pinto, B. M. (2012). Modulation of Starch Digestion for Slow Glucose Release through "Toggling" of Activities of Mucosal α-Glucosidases. *The Journal of Biological Chemistry*, *287*(38): 31929–31938. https://doi.org/10.1074/jbc.M112.351858

Lee, H. E., Choi, E. S., Shin, J. A., Lee, S. O., Park, K. S., Cho, N. P., & Cho, S. D. (2014). Fucoidan Induces Caspase-Dependent Apoptosis in MC3 Human Mucoepidermoid Carcinoma Cells. *Experimental and Therapeutic Medicine*, *7*(1): 228–232. https://doi.org/10.3892/etm.2013.1368

Li, B., Lu, F., Wei, X., & Zhao, R. (2008). Fucoidan: Structure and Bioactivity. *Molecules*, 13(8): 1671-1695. https://doi.org/10.3390/molecules13081671

Li, Q., Lau, A., Morris, T. J., Guo, L., Fordyce, C. B., & Stanley, E. F. (2004). A syntaxin 1, Galpha(o), and N-Type Calcium Channel Complex at a Presynaptic Nerve Terminal: Analysis by Quantitative Immunocolocalization. *The Journal of Neuroscience: the Official Journal of the Society for Neuroscience*, *24*(16): 4070–4081. https://doi.org/10.1523/JNEUROSCI.0346-04.2004

Li, R., Zhou, Q-. J., Yang, R-.Y., Chen, S-.T., Ding, R., Liu, X-. F., Luo, L-. X., Xia, Q-.Y., Zhong, S-.Y., Qi, Y., & Williams, R.J. (2023). Determining the Potent Immunostimulation Potential Arising from the Heteropolysaccharide Structure of a Novel Fucoidan, Derived from *Sargassum Zhangii*. *Food Chemistry:* 18: 100712. https://doi.org/10.1016/j.fochx.2023.100712

Li, W.-T., Chuang, Y.-H., & Hsieh, J.-F. (2019). Characterization of Maltase and Sucrase Inhibitory Constituents from *Rhodiola crenulata*. *Foods*, 8(11):540. https://doi.org/10.3390/foods8110540

Lin, Y., Qi, X., Liu, H., Xue, K., Xu, S., & Tian, Z. (2020). The Anti-Cancer Effects of Fucoidan: a Review of Both *In Vivo* and *In Vitro* Investigations. *Cancer Cell International*, 20: 154-168. https://doi.org/10.1186/s12935-020-01233-8

Lin, Z., Tan, X., Zhang, Y., Li, F., Luo, P., & Liu, H. (2020b). Molecular Targets and Related Biologic Activities of Fucoidan: A Review. *Marine Drugs*, *18*(8), 376. https://doi.org/10.3390/md18080376

Liu, F., Wang, J., Chang, A. K., Liu, B., Yang, L., Li, Q., Wang, P., & Zou, X. (2012). Fucoidan Extract Derived from *Undaria pinnatifida* Inhibits Angiogenesis by Human Umbilical Vein Endothelial Cells. *Phytomedicine*, 19(8-9): 797–803. https://doi.org/10.1016/j.phymed.2012.03.015

Liu, J., Xiao, Q., Xiao, J. Niu, C., Li, Y., Zhang, X., Zhou, Z., Shu, G., & Yin, G. (2022). Wnt/β-Catenin Signalling: Function, Biological Mechanisms, and Therapeutic Opportunities. *Signal Transduction and Targeted Therapy,* 7: 3. https://doi.org/10.1038/s41392-021-00762-6

Liu, J.M., Bignon, J., Haroun-Bouhedja, F., Bittoun, P., Vassy, J., Fermandjian, S., Wdzieczak-Bakala, J., & Boisson-Vidal, C. (2005). Inhibitory Effect of Fucoidan on the Adhesion of Adenocarcinoma Cells to Fibronectin. *Anticancer Research*, 25: 2129-2134

Liu, M., Yang, J., Xu, B., & Zhang, X. (2021). Tumor Metastasis: Mechanistic Insights and Therapeutic Interventions. *Medcomm*, 2(4): 491-857.https://doi.org/10.1002/mco2.100

Loh, C. Y., Chai, J. Y., Tang, T. F., Wong, W. F., Sethi, G., Shanmugam, M. K., Chong, P. P., & Looi, C. Y. (2019). The E-Cadherin and N-Cadherin Switch in Epithelial-to-Mesenchymal Transition: Signaling, Therapeutic Implications, and Challenges. *Cells*, 8(10): 1118. https://doi.org/10.3390/cells8101118

Lomartire, S., & Gonçalves, A. M. M. (2022). An Overview of Potential Seaweed-Derived Bioactive Compounds for Pharmaceutical Applications. *Marine Drugs*, 20(2), 141. https://doi.org/10.3390/md20020141

Lopes, G., Andrade, P. B., & Valentão, P. (2016). Phlorotannins: Towards New Pharmacological Interventions for Diabetes Mellitus Type 2. *Molecules*, 22(1): 56. https://doi.org/10.3390/molecules22010056

Lorbeer, A., Charoensiddhi, S., Lahnstein, J., Lars, C., Franco, C., Bulone, V., & Zhang, W. (2017). Sequential Extraction and Characterization of Fucoidans and Alginates from *Ecklonia radiata, Macrocystis pyrifera, Durvillaea potatorum*, and *Seirococcus axillaris*. *Journal of Applied Phycology*, 29: 1515–1526. https://doi.org/10.1007/s10811-016-0990-5

Lorbeer, A.J., Lahnstein, J., Bulone, V., Nguyen, T., & Zhang, W. (2015). Multiple-Response Optimization of the Acidic Treatment of the Brown Alga *Ecklonia radiata* for the Sequential Extraction of Fucoidan and Alginate. *Bioresource Technology*, 197: 302-309, https://doi.org/10.1016/j.biortech.2015.08.103.

Lötze, E., & Hoffman, E. (2015). Nutrient Composition and Content of Various Biological Active Compounds of Three South African-Based Commercial Seaweed Biostimulants. *Journal of Applied Phycology*. 28: 1-8. https://doi.org/10.1007/s10811-015-0644-z

Lu, J., Yang, H., Hao, J., Wu, C., Liu, L., Xu, N., Linhardt, R.J., & Zhang, Z. (2015). Impact of Hydrolysis Conditions on the Detection of Mannuronic to Guluronic Acid Ratio in Alginate and its Derivatives. *Carbohydrate Polymers*, 122:180-188. https://doi.org/10.1016/j.carbpol.2015.01.008.

Lu, L.W., & Chen, J.-H. (2022). Seaweeds as Ingredients to Lower Glycemic Potency of Cereal Foods Synergistically—A Perspective. *Foods*, 11(5):714. https://doi.org/10.3390/foods11050714

Lutifa, F.N., Isnansetyo, A., Susidarti,R.A., & Nursid, M. (2020). Chemical Composition Diversity of Fucoidans Isolated from Three Tropical Brown Seaweeds (*Phaeophyceae*) Species. *Biodiversitas*, 21(7): 3170-3177. https://doi.org/10.13057/biodiv/d210739.

Mabate, B., Daub, C.D., Malgas, S., Pletschke, B.I., & Edkins, A.L. (2023). Comparative Analyses of Fucoidans from South African Brown Seaweeds That Inhibit Adhesion, Migration, and Long-Term Survival of Colorectal Cancer Cells. *Marine Drugs*, 21: 203. https://doi.org/10.3390/md2104020

Mabate, B., Daub, C.D., Malgas, S., Edkins, A.L., Pletschke, B.I. (2021). A Combination Approach in Inhibiting Type 2 Diabetes-Related Enzymes Using *Ecklonia radiata* Fucoidan and Acarbose. *Pharmaceutics*, 13(11):1979. https://doi.org/10.3390/pharmaceutics13111979

Malgas, S., van Dyk, J.S., Abboo, S., & Pletschke, B.I. (2016). The Inhibitory Effects of Various Substrate Pre-treatment By-Products and Wash Liquors on Mannanolytic Enzymes. *Journal of Molecular Catalysis B: Enzymatic*, 123: 132-140. https://doi.org/10.1016/j.molcatb.2015.11.014.

Marín-Peñalver, J. J., Martín-Timón, I., Sevillano-Collantes, C., & Del Cañizo-Gómez, F. J. (2016). Update on the Treatment of Type 2 Diabetes Mellitus. *World Journal of Diabetes*, 7(17): 354–395. https://doi.org/10.4239/wjd.v7.i17.354

Martin, T.A., Ye, L., Sanders, A.J., Lane, J., & Jiang, W.G. (2013). Cancer Invasion and Metastasis: Molecular and Cellular Perspective. In: Madame Curie Bioscience Database [Internet]. Austin (TX): Landes Bioscience; 2000-2013. Available from: https://www.ncbi.nlm.nih.gov/books/NBK164700/

Martins, A.C., de la Torre, B.G., & Albericio, F. (2024) Glucagon-Like Peptide-1 and Glucose-Dependent Insulinotropic Polypeptide Agonists for the Treatment of Obesity and Diabetes Mellitus. *Exploration of Drug Science*, 2:126–43. https://doi.org/10.37349/eds.2024.00039

Massagué, J., & Obenauf, A. C. (2016). Metastatic Colonization by Circulating Tumour Cells. *Nature*, 529(7586): 298–306. https://doi.org/10.1038/nature17038

Mattio, L., Anderson, R.J., & Bolton, J.J. (2015). A Revision of the Genus *Sargassum* (Fucales, Phaeophyceae) in South Africa. *South African Journal of Botany*, 98: 95-107. https://doi.org/10.1016/j.sajb.2015.02.008

Mazéas, L., Yonamine, R., Barbeyron, T., Henrissat, B., Drula, E., Terrapon, N., Nagasato, C., & Hervé, C. (2023). Assembly and Synthesis of the Extracellular Matrix in Brown Algae. *Seminars in Cell & Developmental Biology*, (134): 112-124. https://doi.org/10.1016/j.semcdb.2022.03.005

Miller, G.L. (1959). Use of Dinitrosalicylic Acid Reagent for Determination of Reducing Sugar. *Analytical Chemistry*, 31 (3): 426–428. https://doi.org/10.1021/ac60147a030

Mori, S., Chang, J., Andrechek, E., Matsumura, N., Baba, T., Yao, G., Kim, J., Gatza, M., Murphy, S., & Nevins, J. (2009). Anchorage-Independent Cell Growth Identifies Tumors with Metastatic Potential. *Oncogene,* 28: 2796-805. https://doi.org/10.1038/onc.2009.139

Msuya, F.E., Bolton, J., Pascal, F., Narrain, K., Nyonje, B., and Cottier-Cook, E.J. (2022). Seaweed Farming in Africa: Current Status and Future Potential. *Journal of Applied Phycology*, 34:985–1005, https://doi.org/10.1007/s10811-021-02676-w

Murphy-Ullrich J. E. (2001). The De-Adhesive Activity of Matricellular Proteins: is Intermediate Cell Adhesion an Adaptive State?. *The Journal of Clinical Investigation*, 107(7): 785–790. https://doi.org/10.1172/JCI12609

Mustafa, S., Koran S., & AlOmair, L. (2022). Insights Into the Role of Matrix Metalloproteinases in Cancer and its Various Therapeutic Aspects: A Review. *Frontiers in Molecular Biosciences,* 9: 96099. https://doi.org/10.3389/fmolb.2022.896099

Nauck, M. A., & Müller, T. D. (2023). Incretin Hormones and Type 2 Diabetes. *Diabetologia*, 66(10): 1780–1795. https://doi.org/10.1007/s00125-023-05956-x

Nagappan, H., Pee, P., Kee, S.H.Y., Ow, J.T., Yan, S.W., Chew, L.Y., & Kong, K.W. (2017). Malaysian Brown Seaweeds *Sargassum siliquosum* and *Sargassum polycystum*: Low density lipoprotein (LDL) Oxidation, Agiotension Converting Enzyme (ACE), α-Amylase, and α-Glucosidase Inhibition Activities. *Food Research International*, 99: 950-958. https://doi.org/10.1016/j.foodres.2017.01.023

Nakamura, S., Aki, M., Hashiguchi-Ishiguro, M., Ueda, S., & Oku, T. (2008). Inhibitory Effect of Depolymerized Sodium Alginate by Vibrio Alginolyticus SUN53 on Intestinal Brush Border Membrane Disaccharidase in Rat. *Journal of Japanese Association for Dietary Fiber Research*, 12(1): 9-15.

Nasri, H., & Rafieian-Kopaei, M. (2014). Metformin: Current Knowledge. *Journal of Research in Medical Sciences*, *19*(7): 658–664. https://doi.org/10.4103/JRMS.JRMS_62_24

Neves, M. I., Moroni, L., & Barrias, C. C. (2020). Modulating Alginate Hydrogels for Improved Biological Performance as Cellular 3D Microenvironments. *Frontiers in Bioengineering and Biotechnology*, 8: 665. https://doi.org/10.3389/fbioe.2020.00665

Pádua, D., Rocha, E., Gargiulo, D., & Ramos, A.A. (2015). Bioactive Compounds from Brown Seaweeds: Phloroglucinol, Fucoxanthin and Fucoidan as Promising Therapeutic Agents Against Breast Cancer. *Phytochemistry Letters*, 14: 91-98. https://0-doi.org.wam.seals.ac.za/10.1016/j.phytol.2015.09.007

Park, H. Y., Park, S. H., Jeong, J. W., Yoon, D., Han, M. H., Lee, D. S., Choi, G., Yim, M. J., Lee, J. M., Kim, D. H., Kim, G. Y., Choi, I. W., Kim, S., Kim, H. S., Cha, H. J., & Choi, Y. H. (2017). Induction of p53-Independent Apoptosis and G1 Cell Cycle Arrest by Fucoidan in HCT116 Human Colorectal Carcinoma Cells. *Marine Drugs*, 15(6): 154. https://doi.org/10.3390/md15060154

Pei, G., Lan, Y., Chen, D., Ji, L., & Hua, Z. C. (2017). FAK Regulates E-cadherin Expression via p-SrcY416/p-ERK1/2/p-Stat3Y705 and PPARγ/miR-125b/Stat3 Signaling Pathway in B16F10 Melanoma Cells. *Oncotarget*, 8(8): 13898–13908. https://doi.org/10.18632/oncotarget.14687

Pesaresi A. (2023). Mixed and Non-Competitive Enzyme Inhibition: Underlying Mechanisms and Mechanistic Irrelevance of the Formal Two-Site Model. *Journal of Enzyme Inhibition and Medicinal Chemistry*, 38(1): 2245168. https://doi.org/10.1080/14756366.2023.2245168

Petrie Aronin, C. E., Zhao, Y. M., Yoon, J. S., Morgan, N. Y., Prüstel, T., Germain, R. N., & Meier-Schellersheim, M. (2017). Migrating Myeloid Cells Sense Temporal Dynamics of Chemoattractant Concentrations. *Immunity*, *47*(5): 862–874.e3. https://doi.org/10.1016/j.immuni.2017.10.020

Ponce, N.A. & Stortz, C.A. (2020). A Comprehensive and Comparative Analysis of the Fucoidan Compositional Data Across the *Phaeophyceae. Frontiers in Plant Science*, 11: 556312. https://doi.org/10.3389/fpls.2020.556312

Prabha, G., & Raj, V. (2017). Sodium Alginate–Polyvinyl Alcohol–Bovin Serum Albumin Coated Fe3O4 Nanoparticles as Anticancer Drug Delivery Vehicle: Doxorubicin Loading and *In Vitro* Release Study and Cytotoxicity to HepG2 and L02 Cells. *Materials Science and Engineering: C*, 79: 410-422. https://doi.org/10.1016/j.msec.2017.04.075

Proença, C., Freitas, M., Ribeiro, D., Oliveira, E. F. T., Sousa, J. L. C., Tomé, S. M., Ramos, M. J., Silva, A. M. S., Fernandes, P. A., & Fernandes, E. (2017). α-Glucosidase Inhibition by Flavonoids: An *In Vitro* and *In Silico* Structure-Activity Relationship Study. *Journal of Enzyme Inhibition and Medicinal Chemistry*, *32*(1): 1216–1228. https://doi.org/10.1080/14756366.2017.1368503

Proença, C., Freitas, M., Ribeiro, D., Tomé, S.M., Oliveira, E.F.T., Viegas, M.F., Araújo, A.N., Ramos, M.J., Silva, A.M.S., Fernandes, P.A., & Fernandes, E. (2019). Evaluation of a Flavonoids Library for Inhibition of Pancreatic α-Amylase Towards a Structure–Activity Relationship. *Journal of Enzyme Inhibition and Medicinal Chemistry*, 34: 577-588, https://doi.org/10.1080/14756366.2018.1558221

Qiang, T., Wang, J., Jiang, L., & Xiong, K. (2022). Modulation of Hyperglycemia by Sodium Alginate is Associated With Changes of Serum Metabolite and Gut Microbiota in Mice. *Carbohydrate Polymers*, 291:119359. https://doi.org/10.1016/j.carbpol.2022.119359

Qin, Y. (2018). Bioactive Seaweeds for Food Applications: Natural Ingredients for Healthy Diets, pp. 6-10, Elsevier, London.

Qin, K., Yu, M., Fan, J., Wang, H., Zhao, P., Zhao, G., Zeng, W., Chen, C., Wang, Y., Wang, A., Schwartz, Z., Hong, J., Song, L., Wagstaff, W., Haydon, R. C., Luu, H. H., Ho, S. H., Strelzow, J., Reid, R. R., He, T. C., Shi, L. L. (2023). Canonical and Noncanonical Wnt Signaling: Multilayered Mediators, Signaling Mechanisms and Major Signaling Crosstalk. *Genes & Diseases*, 11(1): 103–134. https://doi.org/10.1016/j.gendis.2023.01.030

Quadri S. K. (2012). Cross Talk Between Focal Adhesion Kinase and Cadherins: Role in Regulating Endothelial Barrier Function. *Microvascular Research*, 83(1): 3–11. https://doi.org/10.1016/j.mvr.2011.08.001

Rajput, A., San Martin, I.D., Rose, R., Beko, A., LeVea, C., Sharratt, E., Mazurchuk, R., Hoffman, R.M., Brattain, M.G., & Wang, J. (2008). Characterization of HCT116 Human Colon Cancer Cells in an Orthotopic Model. *Journal of Surgical Research*, 147(2): 276-281, https://doi.org/10.1016/j.jss.2007.04.021

Range, J., Bergmann, F., & Swainston, N. (2021). PyEnzyme 1.1.0-Alpha (v1.1.0-alpha). *Zenodo*. https://doi.org/10.5281/zenodo.5021263

Raus, R.A., Wan Mohd Fazli Wan Nawawi, W.M.F.W., Nasaruddin, R.R. (2021). Alginate and Alginate Composites for Biomedical Applications. *Asian Journal of Pharmaceutical Sciences*, 16(3): 280-306. https://doi.org/10.1016/j.ajps.2020.10.001

Rhein-Knudsen, N., Ale, M.T., Ajalloueian, F., & Meyer, A.S. (2017). Characterization of Alginates from Ghanaian Brown Seaweeds: *Sargassum* spp. and *Padina* spp. *Food Hydrocolloids*, 71: 236-244. https://doi.org/10.1016/j.foodhyd.2017.05.016

Rhein-Knudsen, N., Reyes-Weiss, D., & Horn, S.J. (2023). Extraction of High Purity Fucoidans from Brown Seaweeds using Cellulases and Alginate Lyases, *International Journal of Biological Macromolecules*, 229: 199-209, https://doi.org/10.1016/j.ijbiomac.2022.12.261

Rhimi, A., Zlaoui, K., Horchani-Naifer, K. & Ennigrou, D.J. (2022). Characterization and Extraction of Sodium Alginate from Tunisian Algae: Synthesizing a Cross-Linked Ultrafiltration Membrane. *Iranian Polymer Journal*, 31: 367–382. https://doi.org/10.1007/s13726-021-01005-9

Riopel, M., Li, J., Liu, S., Leask, A., & Wang, R. (2013). *β*1 Integrin–Extracellular Matrix Interactions are Essential for Maintaining Exocrine Pancreas Architecture and Function. *Laboratory Investigation,* 93: 31–40. https://doi.org/10.1038/labinvest.2012.147

Rosa, G.P., Tavares, W.R., Sousa, P.M.C., Pagès, A.K., Seca, A.M.L., & Pinto, D.C.G. (2020). Seaweed Secondary Metabolites with Beneficial Health Effects: An Overview of Successes in *In Vivo* Studies and Clinical Trials. *Marine Drugs*, 18(1): 8. https://doi.org/10.3390/md18010008

Rothman, M., Anderson, R., Kandjengo, L., & Bolton, J. (2020). Trends in Seaweed Resource Use and Aquaculture in South Africa and Namibia over the Last 30 Years. *Botanica Marina*, 63 (4): 315-325. https://doi.org/10.1515/bot-2019-0074

Rouzbehan, S., Moein, S., Homaei, A., & Moein, M.R. (2017). Kinetics of α-Glucosidase Inhibition by Different Fractions of Three Species of Labiatae Extracts: a New Diabetes Treatment Model. *Pharmaceutical Biology*, 55:1, 1483-1488. https://doi.org/10.1080/13880209.2017.1306569

Rowbotham, J., Dyer, P., Greenwell, C., Selby, D., & Theodorou, M. (2013). Copper (II)-Mediated Thermolysis of Alginates: A Model Kinetic Study on the Influence of Metal Ions in the Thermochemical Processing of Macroalgae. *Interface Focus*, 3: 20120046. https://doi.org/10.1098/rsfs.2012.0046.

Ryu, N. E., Lee, S. H., & Park, H. (2019). Spheroid Culture System Methods and Applications for Mesenchymal Stem Cells. *Cells*, 8(12): 1620. https://doi.org/10.3390/cells8121620

Şahin, O. I. (2021). Polysaccharides Properties and Applications, Scrivener Publishing LLC, USA, pp. 28. https://doi.org/10.1002/9781119711414.ch4

Salehi, B., Sharifi-Rad, J., Seca, A. M. L., Pinto, D. C. G. A., Michalak, I., Trincone, A., Mishra, A. P., Nigam, M., Zam, W., & Martins, N. (2019). Current Trends on Seaweeds: Looking at Chemical Composition, Phytopharmacology, and Cosmetic Applications. *Molecules*, 24(22): 4182. https://doi.org/10.3390/molecules24224182

Samudra, A., Sani, F., & Husni, A. (2017). *In vitro* α-Glucosidase and *In Vivo* of Anti-Hyperglycemia Activity Extract of Alginate from the Brown Marine Algae *Sargassum hystrix*. *Journal of Pharmacy Research*, 11(8): 927-931.

Sanders, L. M. (2016). Carbohydrate: Digestion, Absorption and Metabolism. Encyclopedia of Food and Health (1st ed.). pp.643-646, Elsevier Ltd. http://doi.org/10.1016/B978-0-12-384947-2.00114- 8

Sanniyasi, E., Gopal, R., Damodharan, R., Arumugam, A., Kumar, M.S., Senthilkumar, N., & Anbalagan, M. (2023). *In Vitro* Anticancer Potential of Laminarin and Fucoidan from Brown Seaweeds. *Scientific Reports,* 13: 14452. https://doi.org/10.1038/s41598-023-41327-7

Sant, S., & Johnston, P. A. (2017). The Production of 3D Tumor Spheroids for Cancer Drug Discovery. Drug Discovery Today. *Technologies*, 23, 27–36. https://doi.org/10.1016/j.ddtec.2017.03.002

Sapra, A., & Bhandari, P. (2023). Diabetes. In: StatPearls [Internet]. Treasure Island (FL): StatPearls Publishing; 2024 Jan-. Available from: https://www.ncbi.nlm.nih.gov/books/NBK551501/

Saravana, P.S., Cho, Y-.J., Park, Y-.B., Woo, H-.C. & Chun, B.S. (2016). Structural, Antioxidant, and Emulsifying Activities of Fucoidan from *Saccharina japonica* Using Pressurized Liquid Extraction. *Carbohydrate Polymers*, 153: 518-525. https://doi.org/10.1016/j.carbpol.2016.08.014

Sato, H., Hasegawa, T., Kanai, Y., Tsutsumi, Y., Osamura, Y., Abe, Y., Sakai, H., & Hirohashi, S. (2001). Expression of Cadherins and their Undercoat Proteins (α-, β-, and γ-Catenins and P120) and Accumulation of β-Catenin with No Gene Mutations in Synovial Sarcoma. *Virchows Archive,* 438: 23–30. https://doi.org/10.1007/s004280000318

Schmidt, S., & Friedl, P. (2010). Interstitial Cell Migration: Integrin-Dependent and Alternative Adhesion Mechanisms. *Cell Tissue Research,* 339: 83–92. https://doi.org/10.1007/s00441-009-0892-9

Seidi, F., Yazdi, M.K., Jouyandeh, M., Habibzadeh, S., Munir,M.J., Vahabi, H., Bagheri, B., Rabiee, N., Zarrintaj, P., & Saeb, M.R. (2022). Crystalline Polysaccharides: A Review, Carbohydrate Polymers. *Carbohydrate Polymers*, 275:118624. https://doi.org/10.1016/j.carbpol.2021.118624.

Senni, K., Gueniche, F., Foucault-Bertaud, A., Igondjo-Tchen, S., Fioretti, F., Colliec-Jouault, S., Durand, P., Guezennec, J., Godeau, G., & Letourneur, D. (2006). Fucoidan a Sulfated Polysaccharide from Brown Algae is a Potent Modulator of Connective Tissue Proteolysis. *Archives of Biochemistry and Biophysics*, 445(1): 56–64. https://doi.org/10.1016/j.abb.2005.11.001

Senthilkumar, K., Manivasagan, P., Venkatesan, J., & Kim, S. K. (2013). Brown Seaweed Fucoidan: Biological Activity and Apoptosis, Growth Signaling Mechanism

in Cancer. *International Journal of Biological Macromolecules*, 60: 366–374. https://doi.org/10.1016/j.ijbiomac.2013.06.030

Shah, K., & Kazi, J. U. (2022). Phosphorylation-Dependent Regulation of WNT/Beta-Catenin Signaling. *Frontiers in Oncology*, *12*: 858782. https://doi.org/10.3389/fonc.2022.858782

Shaikh, M.A.J., Alharbi, K.S., Almalki, W.H., Imam, S.S., Albratty, M., Meraya, A.M., Alzarea, S.I., Kazmi, I., Al-Abbasi, F.A., Afzal, O., Alfawaz Altamimi, A.S., Singh, Y., Kumar Singh, S., Dua, K., & Gupta, G. (2022). Sodium Alginate Based Drug Delivery in Management of Breast Cancer, *Carbohydrate Polymers*, 292: 119689. https://doi.org/10.1016/j.carbpol.2022.119689

Shah, K., & Kazi, J. U. (2022). Phosphorylation-Dependent Regulation of WNT/Beta-Catenin Signaling. *Frontiers in Oncology*, *12*: 858782. https://doi.org/10.3389/fonc.2022.858782

Shan, X., Liu, X., Hao, J., Cai, C., Fan, F., Dun, Y., Zhao, X., Liu, X., Li, C., & Yu, G. (2016). *In Vitro* and *in Vivo* Hypoglycemic Effects of Brown Algal Fucoidans. *International Journal of Biological Macromolecules*, 82: 249-255. https://doi.org/10.1371/10.1016/j.ijbiomac.2015.11.036

Shan, X., Wang, X., Jiang, H., Cai, C., Hao, J., & Yu, G. (2020). Fucoidan from *Ascophyllum nodosum* Suppresses Postprandial Hyperglycemia by Inhibiting Na^+/Glucose Cotransporter 1 Activity. *Marine Drugs*, 18(9): 485. https://doi.org/10.3390/md18090485

Shang, S., Hua, F., & Hu, Z. W. (2017). The Regulation of β-Catenin Activity and Function in Cancer: Therapeutic Opportunities. *Oncotarget*, 8(20): 33972–33989. https://doi.org/10.18632/oncotarget.15687

Shi, F., Chang, Y., Shen, J., Chen, G., Xue, C. (2023). A Comparative Investigation of Anionic Polysaccharides (Sulfated Fucan, ι-Carrageenan, κ-Carrageenan, and Alginate) on the Fabrication, Stability, Rheology, and Digestion of Multilayer Emulsion. *Food Hydrocolloids*, 134:108081. https://doi.org/10.1016/j.foodhyd.2022.108081

Shoari, A., Ashja Ardalan, A., Dimes, A.M., Coban, M.A. (2024). Targeting Invasion: The Role of MMP-2 and MMP-9 Inhibition in Colorectal Cancer Therapy. *Biomolecules*, 15(1):35. https://doi.org/10.3390/biom15010035

Sichert, A., Le Gall, S., Klau, L. J., Laillet, B., Rogniaux, H., Aachmann, F. L., & Hehemann, J. H. (2021). Ion-Exchange Purification and Structural Characterization of Five Sulfated Fucoidans from Brown Algae. *Glycobiology*, 31(4): 352–357. https://doi.org/10.1093/glycob/cwaa064

Siegel, R.L., & Miller, K.D., & Jemal, A. (2020). Cancer Statistics, 2020. *CA A Cancer Journal for Clinicians*, 70 (1): 7-30, https://doi.org/10.3322/caac.21590

Singla, R.K., Singh, R., & Dubey, A.K. (2016). Important Aspects of Post-Prandial Antidiabetic Drug, Acarbose. *Current Topics in Medicinal Chemistry*, 16: 1-9. https://doi.org/10.2174/1568026616666160414123500

Son, H.U. & Lee, S.H., 2013. Comparison of α-Glucosidase Inhibition by *Cudrania tricuspidata* According to Harvesting Time. *Biomedical Reports*, 1: 624–628, https://doi.org/10.3892/br.2013.111.

Song, Y.S., Li, H., Balcos, M.C., Yun, H.Y., Baek, K.J., Kwon, N.S., Choi, H.R., Park, K.C., & Kim, D.S. (2014). Fucoidan Promotes the Reconstruction of Skin Equivalents. *Korean Journal of Physiology & Pharmacology*, 18(4):327-331. https://doi.org/10.4196/kjpp.2014.18.4.327

Stadler, M., Scherzer, M., Walter, S., Holzner, S., Pudelko, K., Riedl, A., Unger, C., Kramer, N., Weil, B., Neesen, J., Hengstschläger, M., & Dolznig, H. (2018). Exclusion from Spheroid Formation Identifies Loss of Essential Cell-Cell Adhesion Molecules in Colon Cancer Cells. *Scientific Reports,* 8:1151. https://doi.org/10.1038/s41598-018-19384-0

Suarez-Arnedo, A., Torres Figueroa, F., Clavijo, C., Arbeláez, P., Cruz, J. C., & Muñoz-Camargo, C. (2020). An image J Plugin for the High Throughput Image Analysis of *In Vitro* Scratch Wound Healing Assays. *PloS One*, 15(7): e0232565. https://doi.org/10.1371/journal.pone.0232565

Subba Rao, P.V., Periyasamy, C., Suresh Kumar, K., Srinivasa Rae, A., & Anantharaman, P. (2018). Bioprospecting of Algae, Chapter 6- Seaweeds: Distribution, Production and Uses, pp 59-72, Society for Plant Research.

Sun, J., Feng, A., Zhang, Y., Sun, S., Hu, W., Yang, M., Wei, F., & Qu, X. (2010). Fucoidan Increases TNF-Alpha-Induced MMP-9 Secretion in Monocytic Cell Line U937. *Inflammation,* 59(4): 271–276. https://doi.org/10.1007/s00011-009-0095-6

Sung, C. J., Wang, H. H., Sun, K. H., Hsieh, C. C., Huang, R., Sun, G. H., & Tang, S. J. (2022). Fucoidan from *Sargassum hemiphyllum* Inhibits the Stemness of Cancer Stem Cells and Epithelial-Mesenchymal Transitions in Bladder Cancer cells. *International Journal of Biological Macromolecules*, 221: 623–633. https://doi.org/10.1016/j.ijbiomac.2022.09.047

Synytsya, A., Kim, W-.J., Kim, S-.M., Pohl, R., Synytsya,A., Kvasnička, F., Čopíková, J., & Park, Y. (2010). Structure and Antitumour Activity of Fucoidan Isolated From Sporophyll of Korean Brown Seaweed *Undaria pinnatifida*. *Carbohydrate Polymers*, 81(1): 41-48. https://doi.org/10.1016/j.carbpol.2010.01.052

Szekalska, M., Wróblewska, M., Sosnowska, K., & Winnicka, K. (2016). Influence of Sodium Alginate on Hypoglycemic Activity of Metformin Hydrochloride in the Microspheres Obtained by the Spray Drying. *International Journal of Polymer Science,* 8635408: 12 pages. https://doi.org/10.1155/2016/8635408

Tappy, L. (2008). Basics in Clinical Nutrition: Carbohydrate Metabolism. *Journal of Clinical Nutrition and Metabolism*, 3: e192-195. http://doi.org/10.1016/j.eclnm.2008.06.010.

Thant, W.P., Mambimongo, M., Bataliack, S.M., Maina, W., Barango, P., Dangou, J.M., Karamagi, H., & Makubal, L.E. (2023). Analytical Fact Sheet March 2023: Diabetes, a silent killer in Africa. Integrated African Health Observatory. Available at: https://files.aho.afro.who.int/afahobckpcontainer/production/files/iAHO_Diabetes_Regional_Factsheet.pdf. (Accessed on 16 Feburary 2024).

Thun, M. J., DeLancey, J. O., Center, M. M., Jemal, A., & Ward, E. M. (2010). The Global Burden of Cancer: Priorities for Prevention. *Carcinogenesis*, 31(1): 100–110. https://doi.org/10.1093/carcin/bgp263

Titus, M. A., & Goodson, H. V. (2017). An Evolutionary Perspective on Cell Migration: Digging for the Roots of Amoeboid Motility. *The Journal of Cell Biology*, 216(6): 1509–1511. https://doi.org/10.1083/jcb.201704112

Torres, M. R., Sousa, A.P.A., Silva Filho, E.A.T., Melo, D.F., Feitosa, J.P.A., de Paula, R.C.M., & Lima, M.G.S. (2007). Extraction and Physicochemical Characterization of *Sargassum vulgare* Alginate from Brazil. *Carbohydrate Research*, 342: 2067-2074. https://doi.org/10.1016/j.carres.2007.05.022

Torsdottir, I., Alpsten, M., Holm, G., Sandberg, a S., & Tölli, J. (1991). A Small Dose of Soluble Alginate-Fiber Affects Postprandial Glycemia and Gastric Emptying in Humans with Diabetes. *The Journal of Nutrition*, 121(6): 795–799. https://doi.org/10.1093/jn/121.6.795

Toth, M., & Fridman, R. (2001). Assessment of Gelatinases (MMP-2 and MMP-9 by Gelatin Zymography. *Methods in Molecular Medicine*, 57: 163–174. https://doi.org/10.1385/1-59259-136-1:163

Towbin, H., Staehelin, T., & Gordon, J. (1979). Electrophoretic Transfer of Proteins from Polyacrylamide Gels to Nitrocellulose Sheets: Procedure and Some Applications. *Proceedings of the National Academy of Sciences*, 76: 4350-4354 https://doi.org/10.1073/pnas.76.9.435

Trica, B., Delattre, C., Gros, F., Ursu, A.V., Dobre, T., Djelveh, G., Michaud, P., & Oancea F. (2019). Extraction and Characterization of Alginate from an Edible Brown Seaweed (*Cystoseira barbata*) Harvested in the Romanian Black Sea. *Marine Drugs*, 17(7):405. https://doi.org/10.3390/md17070405

Uetake, Y., & Sluder, G. (2010). Prolonged Prometaphase Blocks Daughter Cell Proliferation Despite Normal Completion of Mitosis. *Current Biology: CB*, 20(18): 1666–1671. https://doi.org/10.1016/j.cub.2010.08.018

Usoltseva, R. V., Anastyuk, S. D., Ishina, I. A., Isakov, V. V., Zvyagintseva, T. N., Thinh, P. D., Zadorozhny, P. A., Dmitrenok, P. S., & Ermakova, S. P. (2018). Structural Characteristics and Anticancer Activity *In Vitro* of Fucoidan from Brown Alga *Padina boryana*. *Carbohydrate Polymers*, 184: 260–268. https://doi.org/10.1016/j.carbpol.2017.12.071

Valenta, T., Hausmann, G., & Basler, K. (2012). The Many Faces and Functions of β-Catenin. *The EMBO Journal*, 31(12): 2714–2736. https://doi.org/10.1038/emboj.2012.150

Van Weelden, G., Bobiński, M., Okła, K., Van Weelden, W.J., Romano, A., & Pijnenborg, J.M.A. (2019). Fucoidan Structure and Activity in Relation to Anti-Cancer Mechanisms. *Marine Drugs*, 17: 32. https://doi.org/10.3390/md17010032

Vinnakota, K., Zhang, Y., Selvanesan, B. C., Topi, G., Salim, T., Sand-Dejmek, J., Jönsson, G., & Sjölander, A. (2017). M2-like Macrophages Induce Colon Cancer Cell Invasion via Matrix Metalloproteinases. *Journal of Cellular Physiology*, 232(12): 3468–3480. https://doi.org/10.1002/jcp.25808

Vinoth Kumar, T. V., Lakshmanasenthil, S., Geetharamani, D., Marudhupandi, T., Suja, G., & Suganya, P. (2015). Fucoidan- A α-D-Glucosidase Inhibitor from *Sargassum wightii* with Relevance to Type 2 Diabetes Mellitus Therapy. *International*

Journal of Biological Macromolecules, 72: 1044-1047. https://doi.org/10.1016/j.ijbiomac.2014.10.013

Vishchuk, O.S., Ermakova, S.P., & Zvyagintseva, T.N. (2013). The Fucoidans from Brown Algae of Far-Eastern Seas: Anti-Tumor Activity and Structure-Function Relationship. *Food Chemistry*. 141(2):1211–1217. https://doi.org/10.1016/j.foodchem.2013.03.065

Walker, J.M. (2009). The Bicinchoninic Acid (BCA) Assay for Protein Quantitation. In: Walker, J.M. (eds) The Protein Protocols Handbook. Springer Protocols Handbooks. Humana Press, Totowa, NJ. https://doi.org/10.1385/0-89603-268-X:5

Walzl, A., Unger, C., Kramer, N., Unterleuthner, U., Scherzer, M., Hengstschläger, M., Schwanzer-Pfeiffer, D., Dolznig, H. (2014). The Resazurin Reduction Assay Can Distinguish Cytotoxic from Cytostatic Compounds in Spheroid Screening Assays: *SLAS Discovery*, 19(7): 1047-1059. https://doi.org/10.1177/1087057114532352

Wang, B., Wan, Y., Lee, X., Liu, T., Yu, Z., Huang, J., Ok, Y.S., Chen, J., & Gao, B. (2018). Alginate-Based Composites for Environmental Applications: A Critical Review. *Critical Reviews in Environmental Science and Technology*, 49: 1-39. https://doi.org/10.1080/10643389.2018.1547621.

Wang, C-. Y., & Chen, Y-. C. (2016). Extraction and Characterization of Fucoidan from Six Brown Macroalgae. *Journal of Marine Science and Technology*, 24(2):319-328. https://doi.org/10.6119/JMST-015-0521-3

Wang, H., Gong, X., Guo, X., Liu, C., Fan, Y-.Y., Zhang, J., Niu, B., & Li, W. (2019). Characterization, Release, and Antioxidant Activity of Curcumin-Loaded Sodium Alginate/ZnO Hydrogel Beads. *International Journal of Biological Macromolecules*, 121:1118-1125. https://doi.org/10.1016/j.ijbiomac.2018.10.121

Wang, J., Geng, L., Yue, Y., & Zhang, Q. (2019b). Progress in Molecular Biology and Translational Science, Chapter Six - Use of fucoidan to treat renal diseases: A review of 15 Years of Clinic Studies. *Academic Press*, pp. 95-111, https://doi.org/10.1016/bs.pmbts.2019.03.011

Wang, M., Liu, X., Chen, T., Cheng, X., Xiao, H., Meng, X., & Jiang, Y. (2022). Inhibition and Potential Treatment of Colorectal Cancer by Natural Compounds via Various Signaling pathways. *Frontiers in Oncology*, *12*:956793. https://doi.org/10.3389/fonc.2022.956793

Wang, S. H., Huang, C. Y., Chen, C. Y., Chang, C. C., Huang, C. Y., Dong, C. D., & Chang, J. S. (2020). Structure and Biological Activity Analysis of Fucoidan Isolated from *Sargassum siliquosum*. *ACS Omega*, 5(50): 32447–32455. https://doi.org/10.1021/acsomega.0c04591

Wang, S., & Basson, M. D. (2011). Akt Directly Regulates Focal Adhesion Kinase Through Association and Serine Phosphorylation: Implication for Pressure-Induced Colon Cancer Metastasis. *American Journal of Physiology. Cell Physiology*, 300(3): C657–C670. https://doi.org/10.1152/ajpcell.00377.2010

Warren, J. S. A., Xiao, Y., & Lamar, J. M. (2018). YAP/TAZ Activation as a Target for Treating Metastatic Cancer. *Cancers*, 10(4): 115. https://doi.org/10.3390/cancers10040115

Wernberg, T., Krumhansl, K., Filbee-Dexter, K., & Pedersen, M. F. (2019). Status and Trends for the World's Kelp Forests. In C. Sheppard (Ed.), World Seas: An Environmental Evaluation: Ecological Issues and Environmental Impacts,2 ed., Vol. 3, pp. 57-78. Academic Press, Cambridge.

Williams, J.A., Lai, C.-S., Corwin, H., Ma, Y., Maki, K.C., Garleb, K.A., Wolf, B.W. (2004). Inclusion of Guar Gum and Alginate into a Crispy Bar Improves Postprandial Glycemia in Humans. *The journal of Nutrition*, 134(4): 886–889. https://doi.org/10.1093/jn/134.4.886

Williams, P.A., & Phillips, G. O. (2004). Gums and Stabilisers for the Food Industry 12, pp. 84-86, Royal Society of Chemistry, Cambridge.

Wolf, B.W., Lai, C.-S., Kipnes, M.S., Ataya, D.G., Wheeler, K.B., Zinker, B.A., Garleb, K.A., & Firkins, J.L. (2002). Glycemic and Insulinemic Responses of Nondiabetic Healthy Adult Subjects to an Experimental Acid-Induced Viscosity Complex Incorporated into a Glucose Beverage. *Nutrition*, 18 (7): 621–626. https://doi.org/10.1016/S0899-9007(02)00750-5

Xue, M., Liang, H., Ji, X., Zhou, Z., Liu, Y., Sun, T., & Zhang, L. (2020). Effects of Fucoidan on Gut Flora and Tumor Prevention in 1,2-Dimethylhydrazine-Induced Colorectal Carcinogenesis. *The Journal of Nutritional Biochemistry*, 82: 108396. https://doi.org/10.1016/j.jnutbio.2020.108396

Yadav, J., Paragas, E., Korzekwa, K., Nagar, S. (2020). Time-dependent Enzyme Inactivation: Numerical Analyses of *In Vitro* Data and Prediction of Drug-Drug Interactions. Pharmacology & Therapeutics, 206: 107449, https://doi.org/10.1016/j.pharmthera.2019.107449.

Yang, C., Chung, D., & You, S. G. (2008). Determination of Physiochemical Properties of Sulphated Fucans from Sporophyll of *Undaria pinnatifida* using Light Scattering Technique. *Food Chemistry*, 111: 503-507. https://doi.org/10.1016/j.foodchem.2008.03.085

Yang, Y., Qi, Y., Adel, A., Ghena, M., Fahad, A., & El-Sayed, S. (2022). Potential of Marine Seaweeds for Bioactive Compounds: a Comprehensive Analysis of *Padina australis* Biomass. *International Journal of Marine Sciences*, 38: 1-10. https://doi.org/10.1007/s41208-022-00436-2

Yayan, J., Franke, KJ., Berger, M., Windisch, W., & Kurt Rasche, K. (2024). Adhesion, Metastasis, and Inhibition of Cancer Cells: a Comprehensive Review. *Molecular Biology Reports*, 51: 165. https://doi.org/10.1007/s11033-023-08920-5

Yip, W. K., & Seow, H. F. (2012). Activation of Phosphatidylinositol 3-Kinase/Akt Signaling by EGF Downregulates Membranous E-Cadherin and β-Catenin and Enhances Invasion in Nasopharyngeal Carcinoma Cells. *Cancer Letters*, 318(2): 162–172. https://doi.org/10.1016/j.canlet.2011.12.018

Yu, H., Gao, M., Ma, Y., Wang, L., Shen, Y., & Liu, X. (2018). Inhibition of Cell Migration by Focal Adhesion Kinase: Time-Dependent Difference in Integrin-Induced Signaling Between Endothelial and Hepatoblastoma Cells. *International Journal of Molecular Medicine*, 41(5): 2573–2588. https://doi.org/10.3892/ijmm.2018.3512

Yu, J., Li, Q., Wu, J., Yang, X., Yang, S., Zhu, W., Liu, Y., Tang, W., Nie, S., Hassouna, A., White, W. L., Zhao, Y., & Lu, J. (2021). Fucoidan Extracted from

Sporophyll of *Undaria pinnatifida* Grown in Weihai, China - Chemical Composition and Comparison of Antioxidant Activity of Different Molecular Weight Fractions. *Frontiers in Nutrition*, *8*: 636930. https://doi.org/10.3389/fnut.2021.636930

Yu, W.C., Chen, Y.L., Hwang, P.A., Chen, T.H., & Chou, T.C. (2017). Fucoidan Ameliorates Pancreatic β-Cell Death and Impaired Insulin Synthesis in Streptozotocin-Treated β Cells and Mice via a Sirt-1-Dependent Manner. *Molecular Nutrition & Food Research*, 61(10). https://doi.org/10.1002/mnfr.201700136.

Yue, B., Liu, C., Sun, H., Liu, M., Song, C., Cui, R., Qiu, S., & Zhong, M. (2018). A Positive Feed-Forward Loop between LncRNA-CYTOR and Wnt/β-Catenin Signaling Promotes Metastasis of Colon Cancer. *Molecular Therapy*, 26(5): 1287–1298. https://doi.org/10.1016/j.ymthe.2018.02.024

Zahariev, N., Katsarov, P., Lukova, P., & Pilicheva, B. (2023). Novel Fucoidan Pharmaceutical Formulations and Their Potential Application in Oncology-A Review. *Polymers*, 15(15): 3242. https://doi.org/10.3390/polym15153242

Zaharudin, N., Salmeán, A.A., & Dragsted, L.O. (2018). Inhibitory Effects of Edible Seaweeds, Polyphenolics and Alginates on the Activities on Porcine Pancreatic α-Amylase. *Food Chemistry*, 245: 1196-1203. https://doi.org/10.1016/j.foodchem.2017.11.027

Zayed, A., El-Aasr, M., Ibrahim, A. S., & Ulber, R. (2020). Fucoidan Characterization: Determination of Purity and Physicochemical and Chemical Properties. *Marine Drugs*, 18(11): 571. https://doi.org/10.3390/md18110571

Zhang, M., Chen, L., Liu, Y., Chen, M., Zhang, S., & Kong, D. (2020). Sea Cucumber Cucumaria Frondosa Fucoidan Inhibits Osteosarcoma Adhesion and Migration by Regulating Cytoskeleton Remodeling. *Oncology Reports*, 44(2): 469–476. https://doi.org/10.3892/or.2020.7614

Zhang, X., Chen, J., Shao, X., Li, H., Jiang, Y., Zhang, Y., & Yang, D. (2023). Structural and Physical Properties of Alginate Pretreated by High-Pressure Homogenization. *Polymers, 15 (15)*: 3225. https://doi.org/10.3390/polym15153225

Zhang, X., Su, C., Cao, C., Gong, G., Huang, L., Wang, Z., Song, S., & Zhu, B. (2022). Gut Microbiota of Individuals Could Be Balanced by a 14-Day Supplementation With *Laminaria japonica* and Differed in Metabolizing Alginate and Galactofucan. *Frontiers in Nutrition*, *9*: 881464. https://doi.org/10.3389/fnut.2022.881464

Zhang, X., Sui, T., Ma, Q., Shao, H., Hu, X., Sheng, H., Ma, Z., Luo, G. (2018). Cantharidin Suppresses HCT116 Colorectal Carcinoma Cell Proliferation and Migration by Changing the Cytoskeleton Structure, *Journal of Traditional Chinese Medical Sciences*, 5 (3): 302-309. https://doi.org/10.1016/j.jtcms.2018.07.004

Zhang, Z., Teruya, K., Eto, H., & Shirahata, S. (2011). Fucoidan Extract Induces Apoptosis in MCF-7 Cells via a Mechanism Involving the ROS-Dependent JNK Activation and Mitochondria-Mediated Pathways. *PloS one*, 6(11): e27441. https://doi.org/10.1371/journal.pone.0027441

Zhao, H., Ming, T., Tang, S., Ren, S., Yang, H., Liu, M., Tao, Q., & Xu, H. (2022). Wnt Signaling in Colorectal Cancer: Pathogenic Role and Therapeutic Target. *Molecular Cancer*, *21*(1): 144. https://doi.org/10.1186/s12943-022-01616-7

Zhu, Z., Luo, J., Li, L., Wang, D., Xu, Q., Teng, J., Zhou, J., Sun, L., Yu, N., & Zuo, D. (2024). Fucoidan Suppresses Proliferation and Epithelial-Mesenchymal Transition Process via Wnt/β-Catenin Signalling in Hemangioma. *Experimental Dermatology*, *33*(3): e15027. https://doi.org/10.1111/exd.15027

Zinatizadeh, M. R., Miri, S. R., Zarandi, P. K., Chalbatani, G. M., Rapôso, C., Mirzaei, H. R., Akbari, M. E., & Mahmoodzadeh, H. (2019). The Hippo Tumor Suppressor Pathway (YAP/TAZ/TEAD/MST/LATS) and EGFR-RAS-RAF-MEK in Cancer Metastasis. *Genes & Diseases*, 8(1): 48–60. https://doi.org/10.1016/j.gendis.2019.11.003

APPENDIX A: List of reagents and antibodies

Table A1: List of the reagents and kits utilised and their suppliers

Reagent name	Supplier (Catalogue number)
α-Amylase porcine pancreatic	Megazyme™ (E-PANAA)
Acarbose	Sigma-Aldrich (A8980)
Acetone	MERCK (8.22251.2500)
Acetonitrile	Sigma-Aldrich (34851)
Acrylamide/Bis solution	Biorad (1610148)
Ammonium persulphate (APS)	Sigma Aldrich (A3678)
Barium chloride dihydrate	Sigma-Aldrich (217565)
Bovine serum albumin (BSA)	Sigma (A7906)
Bradford reagent	Sigma (B6916)
Calcium chloride	Saarchem (1524920EM)
Clarity Western Enhanced Chemiluminescence substrate	Bio-Rad Laboratories (170506)
Coomassie Brilliant Blue R250	Merck (1.12553)
DAKO flourecent mounting medium	Agilent Technologies (S3023)
3,5-Dinitrosalicylic acid	Sigma (D0550)
D2O	Sigma-Aldrich (151882)
Ethanol	MERCK (8.18700)
5-Fluorouracil	Sigma-Aldrich (04541)
Formaldehyde	Sigma-Aldrich (47670)
Folin-Ciocalteu reagent	Sigma-Aldrich (F9252)
Formic acid	MERCK (1038392)
D-Fructose	
Fucoidan from *F. vesiculosus*	Sigma-Aldrich (F5631)
L-Fucose	Sigma (F2252)
L-Fucose kit	Megazyme™ (K-FUCOSE)
Gelatine	Fluka (48723)
Glacial acetic acid	Sigma-Aldrich (A6283)
α-Glucosidase from *Saccharomyces cerevisiae*	Sigma-Aldrich (G5003)
D-Glucose	Saarchem (2676020)

D-Glucuronic acid kit	Megazyme™ (K-URONIC)
Glutaraldehyde	Sigma (G5882)
GOPOD	Megazyme™ (K-GLUC)
Hoechst 333542	Sigma-Aldrich (875756-97-1)
Hydrochloric acid	MERCK (1047705)
Isomaltotriose	Megazyme™ (O-IMO3)
Luna Universal qPCR Master Mix	Biolabs Inc (M3003E)
Maltase	Megazyme™ (E-MALTS)
2-mercaptoethanol	Fluka (63700)
Methanol	Sigma-Aldrich (34860)
D-Mannose, D-Fructose & D-Glucose kit	Megazyme™ (K-MANGL)
Nuclease free water	Biolabs Inc (B1502A)
Phosphate buffered saline	Sigma-Aldrich (P4417)
Phenol	Sigma-Aldrich (P1037)
p-nitrophenol	Sigma (42,575-3)
p-nitrophenyl-α-D-glucopyranoside	Sigma (N1377)
Potato starch	Sigma (54501)
Protease inhibitor cocktail (PIC)	P8340-5ML
RIPA lysis buffer	Sigma-Aldrich (R0278)
Sodium alginate	*Sigma-Aldrich (W201502)*
Sodium azide	MERCK (8.22335)
Sodium borohydride	Sigma-Aldrich (452882)
Sodium carbonate	Sigma-Aldrich (223484)
Sodium chloride	Sigma-Aldrich (S9888)
Sodium dodecyl sulphate (SDS)	BDH biochemicals (301754)
Sodium hydroxide	MERCK (1.06469.1000)
Sodium metabisulfite	Sigma-Aldrich (255556)
Sodium phosphate dibasic	Sigma-Aldrich (71640)
Sodium sulphate	Saarchem (8525200EM)
Sucrase	Megazyme™ (E-SUCR)
Sucrose	MERCK (107651)
Sulphuric acid	Sigma (30743)

N,N,N′,N′-Tetramethylethylene diamine (TEMED)	Sigma (T22500)
Tris(hydroxymethyl)aminomethane	Sigma- Aldrich (252859)
Tween™ 20	Merck (Cat. No. 8.22184.0500)
Trichloroacetic acid	Sigma-Aldrich (T9159)
Triton X-100	Sigma-Aldrich (Cat. No. T-8787)
Trifluoroacetic acid	Sigma-Aldrich (T6508)
D-Xylose	Sigma (X3877)
D-Xylose kit	Megazyme™ (K-XYLOSE)
Zinc chloride	Sigma-Aldrich (208086)

Table A2: List of the antibodies detailing their supplier and individual experimental details

Antibody	Species	Type	Supplier (Catalogue number)	Experimental details*
Anti-human β-Actin [EPR21241]	Rabbit	Primary antibody	Abcam (ab213262)	F: 1:3000
Anti-human Vimentin [D21H3]	Rabbit	Primary antibody	Cell signalling technology (5741S)	F: 1:250
Anti-human Integrin β1 (ITGB1) [JB1B]	Mouse	Primary antibody	Santa Cruz Biotechnology (SC59829)	1:200
Alexa-Fluor-550 conjugated Wheat Germ Agglutinin	-	Directly conjugated	Invitrogen (W32464)	IF: 1:1000
Anti-human Pan-cadherin [C1821]	Mouse	Primary antibody	Sigma (047M4806V)	F: 1:200; WB: 1:1000
Anti-human β-Catenin [H-102]	Rabbit	Primary antibody	Santa Cruz Biotechnology (SC7199)	F: 1:200; WB: 1:500
Anti-human Phospho-β-Catenin [9561]	Rabbit	Primary antibody	Cell signalling technology (9561L)	WB: 1:1000
Anti-GAPDH antibody [EPR6256]	Rabbit	Loading control	Abcam (ab185059)	WB: 1:10 000
Anti-human Phospho-Akt [D9E]	Rabbit	Primary antibody	Cell signalling technology (4060L)	WB: 1:2000
Anti-human Phospho-FAK	Rabbit	Primary antibody	Cell signalling technology (3281S)	WB: 1:1000
Anti-human FAK	Rabbit	Primary antibody	Cell signalling technology (3285S)	WB: 1:1000

Anti-human Phospho-MOB1 [D2F10]	Rabbit	Primary antibody	Cell signalling technology (8699P)	WB: 1:1000
Anti-human MOB 1 [CST 3281S]	Rabbit	Primary antibody	Cell signalling technology (13730S)	WB: 1:1000
Anti-rabbit 488	Donkey	Fluorescent secondary antibody	Abcam (ab96891)	F: 1:500
Anti-rabbit DY550	Donkey	Fluorescent secondary antibody	Abcam (ab96892)	F: 1:500
Anti-mouse DY488	Donkey	Fluorescent secondary antibody	Abcam (ab96875)	F: 1:500
Anti-mouse DY550	Donkey	Fluorescent secondary antibody	Abcam (ab96876)	F: 1:500
HRP-conjugated anti-mouse	Donkey	Secondary antibody	Abcam (ab9702S)	WB: 1:5000
HRP-conjugated anti-rabbit	Donkey	Secondary antibody	Abcam (ab9706A)	WB: 1:10000

* WB= Western Blot Analysis, F= Fluorescence Microscopy

APPENDIX B: Supplementary results

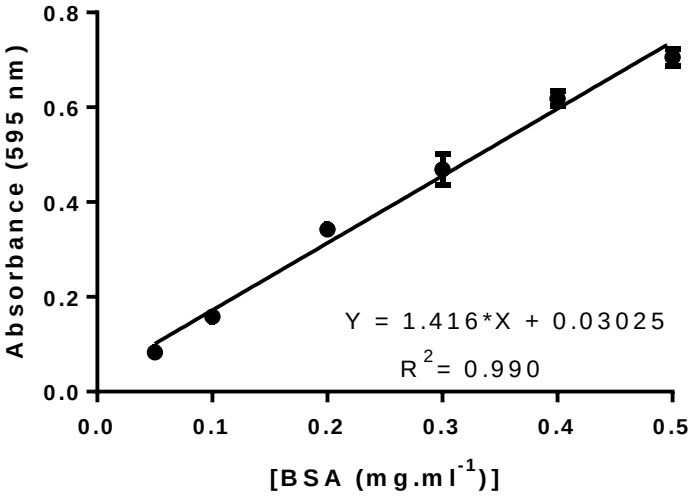

Figure B1: Protein standard curve constructed for the Bradford assay. Data points are presented as mean values ± SD (n=3).

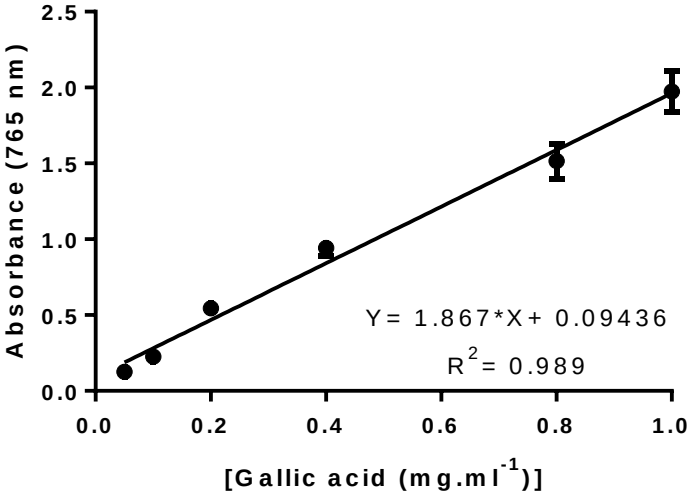

Figure B2: Phenolics (Gallic acid equivalents) standard curve for the Folin-Ciocalteu assay. Data points are presented as mean values ± SD (n=3).

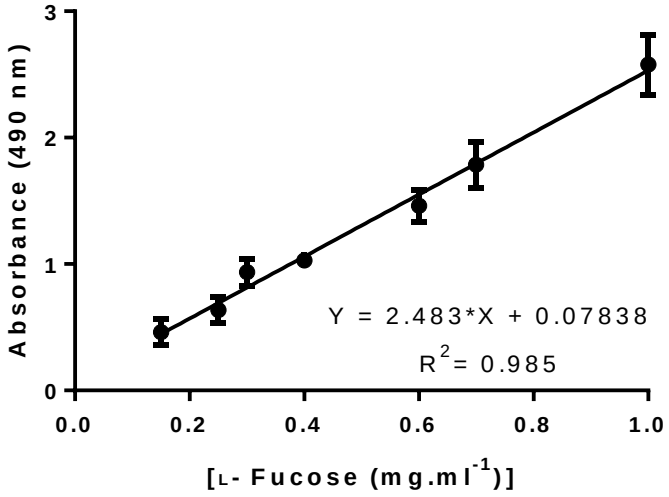

Figure B3: Total carbohydrate L-fucose standard curve for the phenol-sulphuric acid assay. Data points are presented as mean values ± SD (n=3).

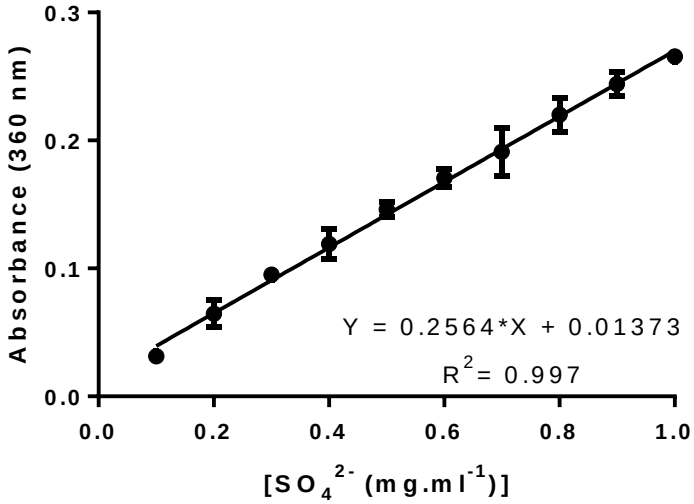

Figure B4: Sulphate standard curve for the gelatine-barium method. Data points are presented as mean values ± SD (n=3).

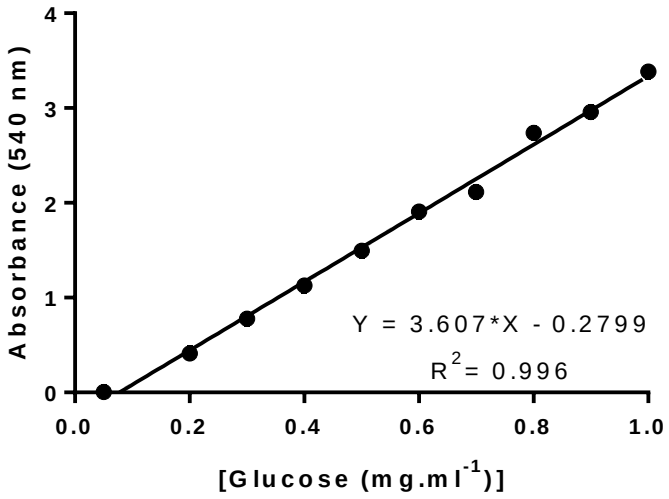

Figure B5: Total reducing sugar glucose standard curve for the DNS assay. Data points are presented as mean values ± SD (n=3).

Table B1: Linearity of sugar monomers analysed by HPLC- RID

Sugar monomer	Linearity range	Equation	Coefficient of determination (R^2)
Fucose	0.05 - 1	Y=154134*X-2140	0.99
Arabinose	0.05 - 1	Y=144338*X-12427	0.98
Fructose	0.05 - 1	Y=218176*X-963.1	0.99
Mannose	0.05 - 1	Y=129886*X-8856	0.99
Glucose	0.05 - 1	Y=185923*X+3973	0.99
Galactose	0.05 - 1	Y=114880*X-5812	0.99

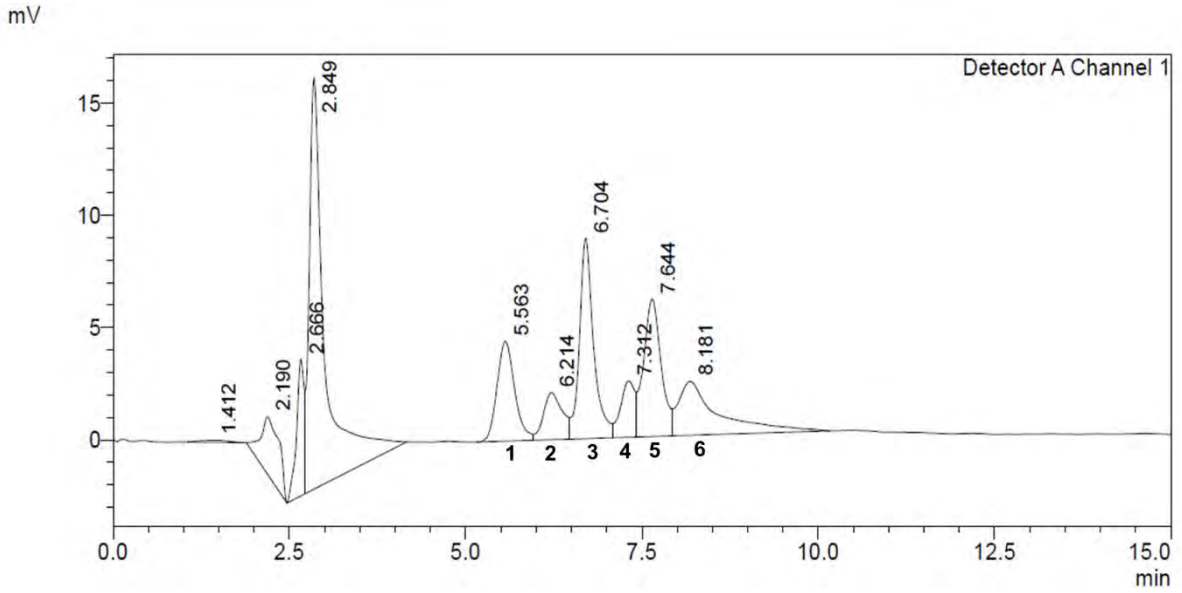

Figure B6: HPLC-RID chromatogram for the separation of the sugar monomer standards (0.5 mg/ml, injected 20 µl) on a Fortis Amino column. 1- fucose; 2- arabinose; 3- fructose; 4- mannose; 5- glucose; 6- galactose.

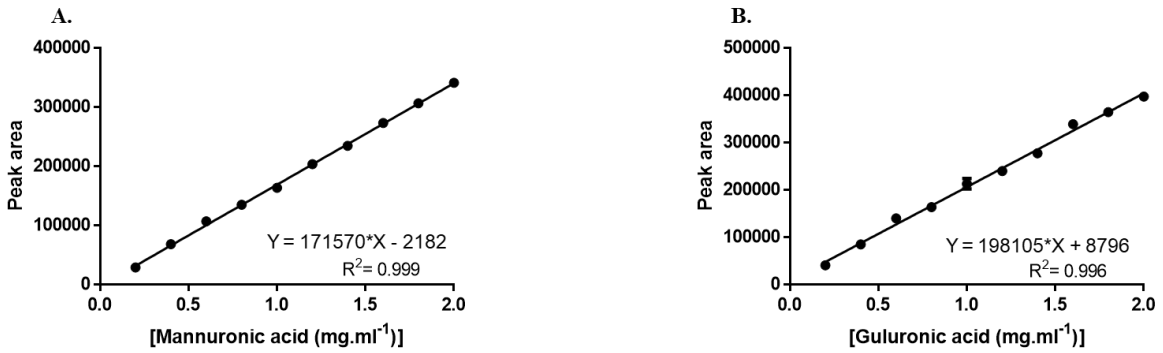

Figure B7: Standard curves of the (A) D-mannuronic acid and (B) L-guluronic acid standards analysed by HPLC-UV. Data points are presented as mean values ± SD (n=6).

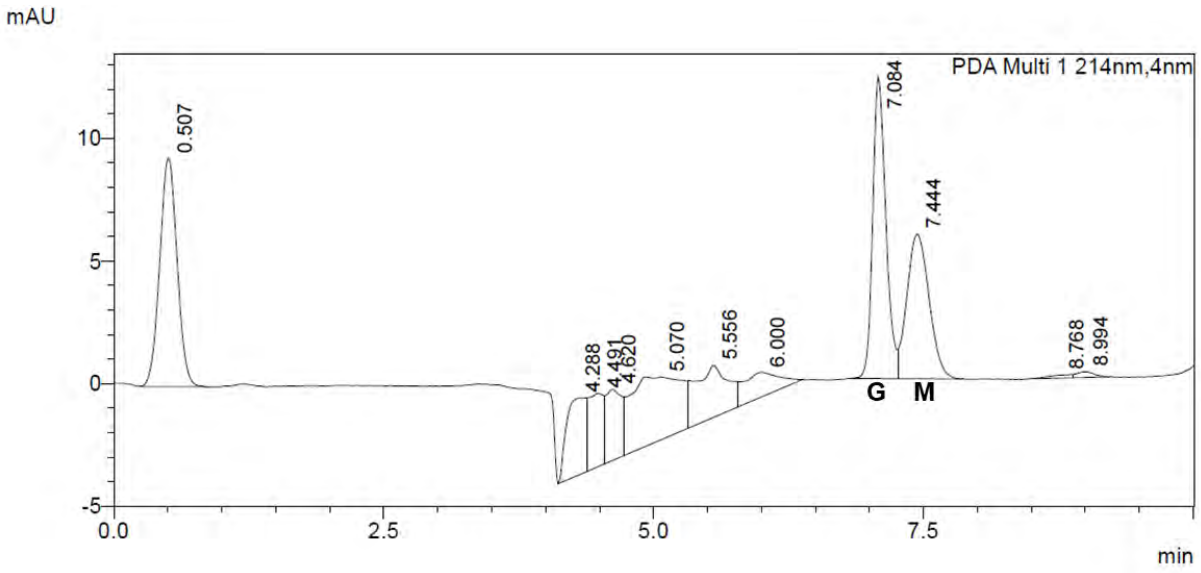

Figure B8: HPLC-UV chromatogram for the simultaneous detection of D-mannuronic acid (M) and L-guluronic acid (G). The chromatographic separation was performed using a Hypersil Gold™ Sax column.

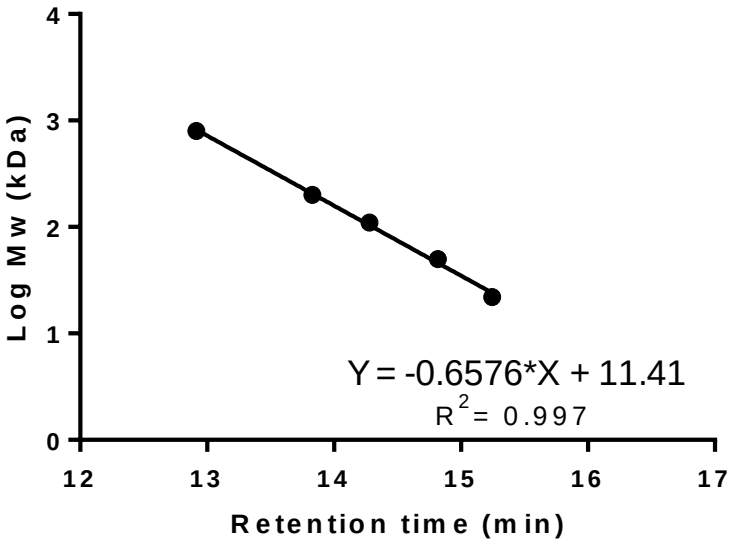

Figure B9: Calibration curve Log M_W vs. retention time for pullan standards using a Shodex OHpak SB-806M HQ (8.0 x 300 mm) column. Data points are presented as mean values ± SD (n=4).

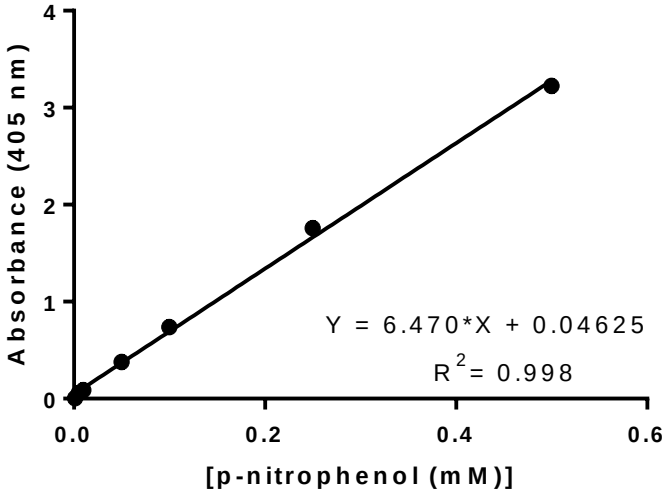

Figure B10: *p*-nitrophenol standard curve. Data points are presented as mean values ± SD (n=3).

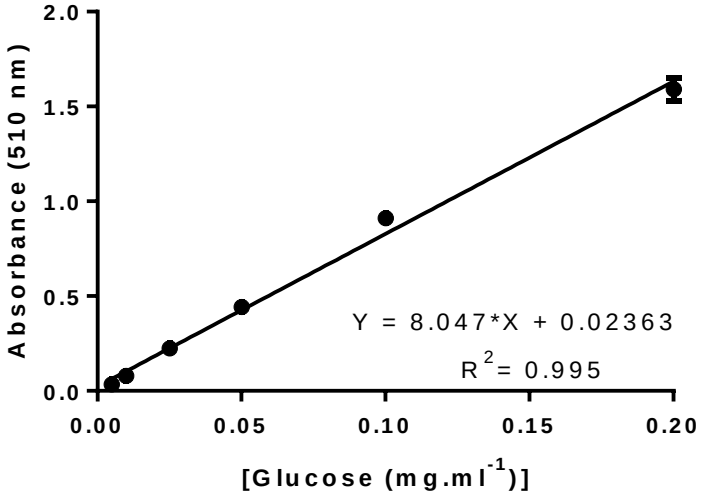

Figure B11: Glucose standard curve for the GOPOD assay. Data points are presented as mean values ± SD (n=3).

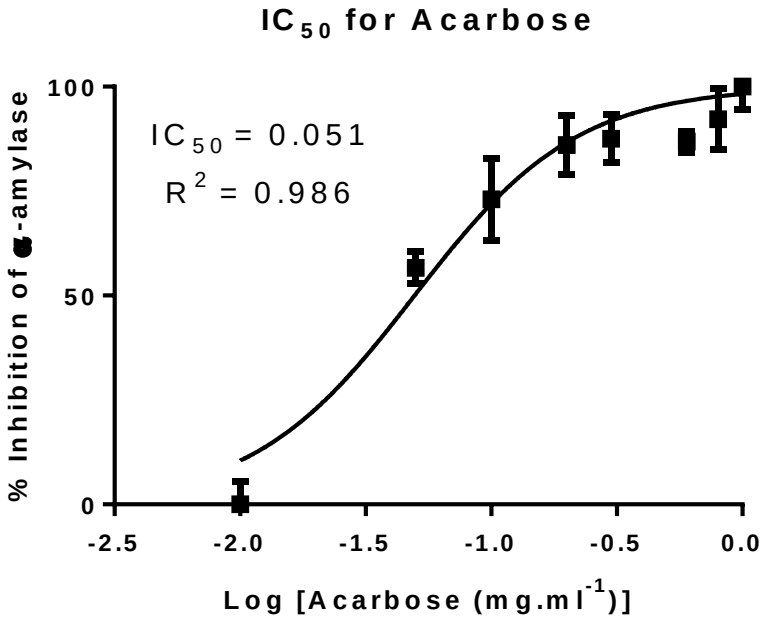

Figure B12: Dose response curves and IC_{50} values of α-amylase inhibition. Data points are presented as mean values ± SD (n=5).

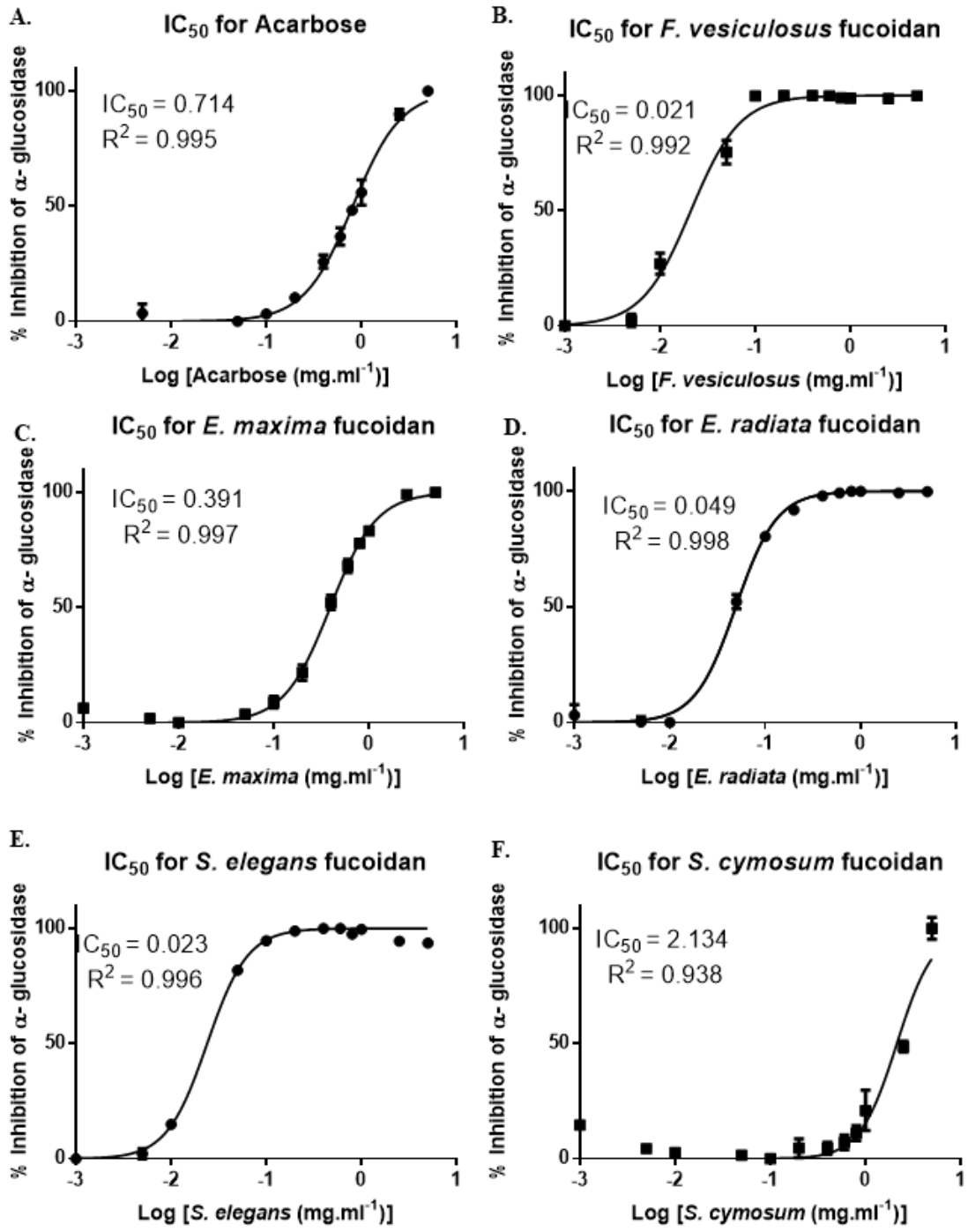

Figure B13: Dose-response curves and IC_{50} values of α-glucosidase inhibition. Data points are presented as mean values ± SD (n=3).

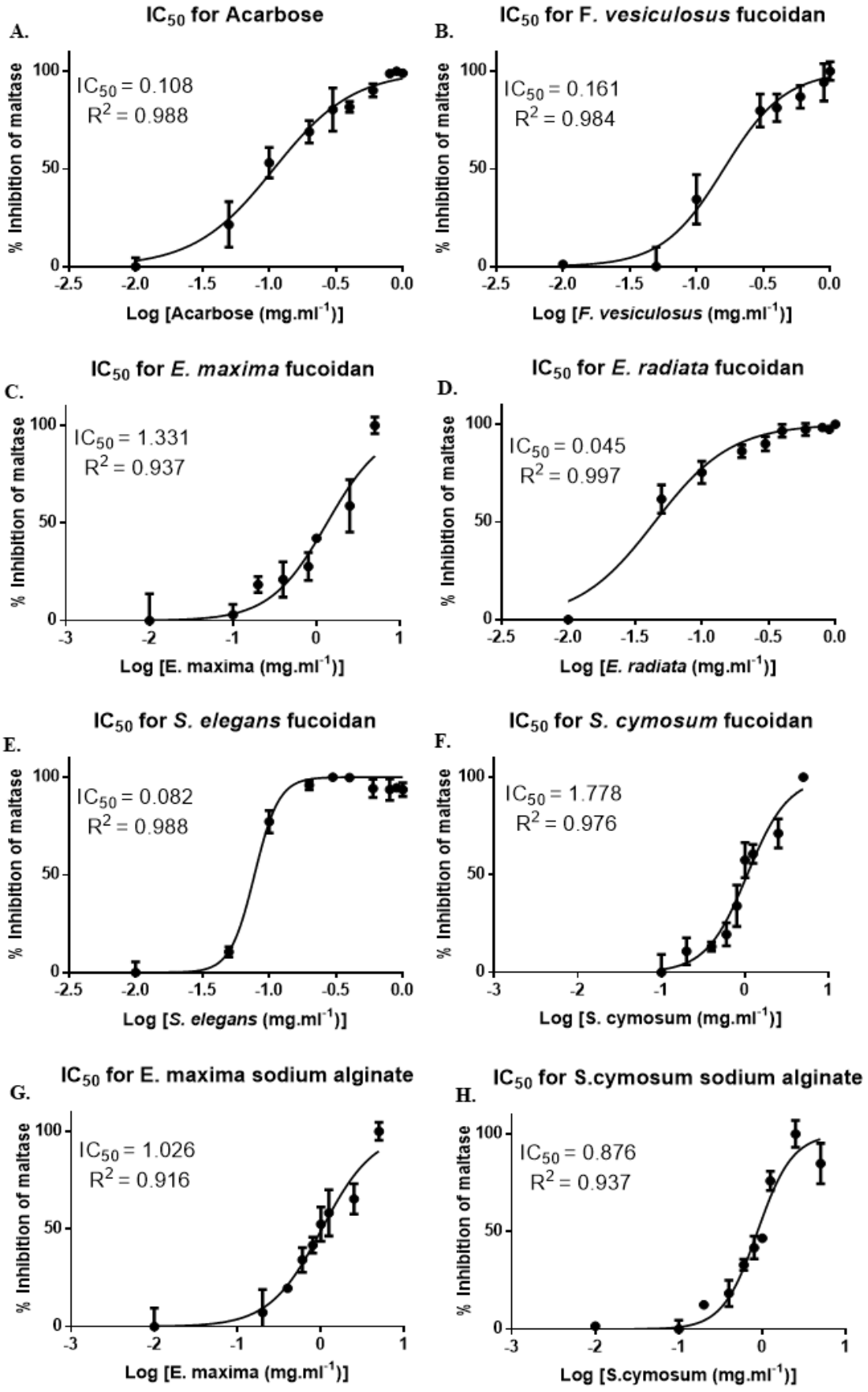

Figure B14: Dose-response curves and IC_{50} values of maltase inhibition. Data points are presented as mean values ± SD (n=3).

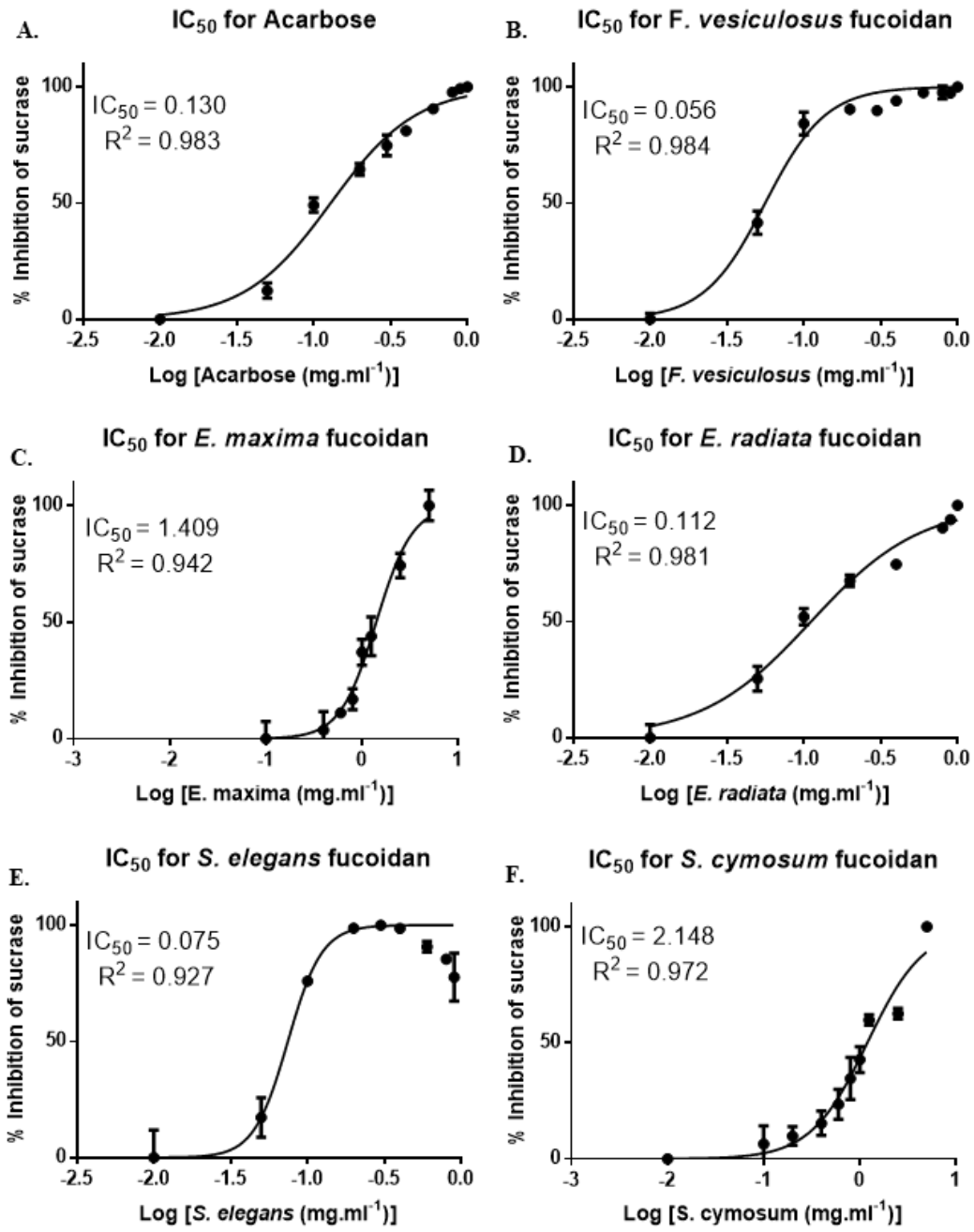

Figure B15: Dose-response curves and IC_{50} values of sucrase inhibition. Data points are presented as mean values ± SD (n=3).

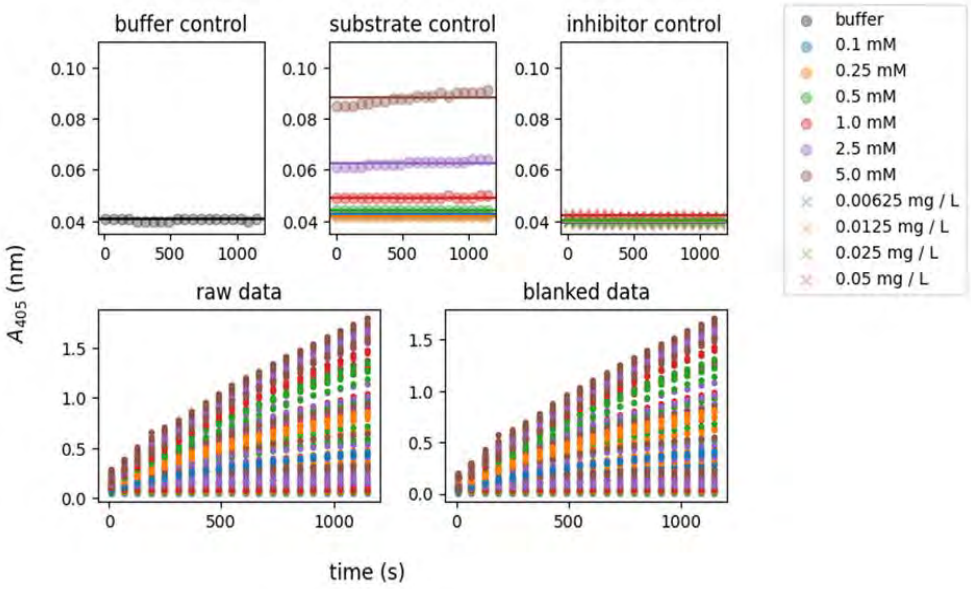

Figure B16: Time-course data illustrating the change in absorbance of the controls, as well as the uncorrected and corrected reactions for the six substrate concentrations and four inhibitor concentrations of the modelled reactions for *E. radiata* fucoidan. Each measurement consisted of three replicates.

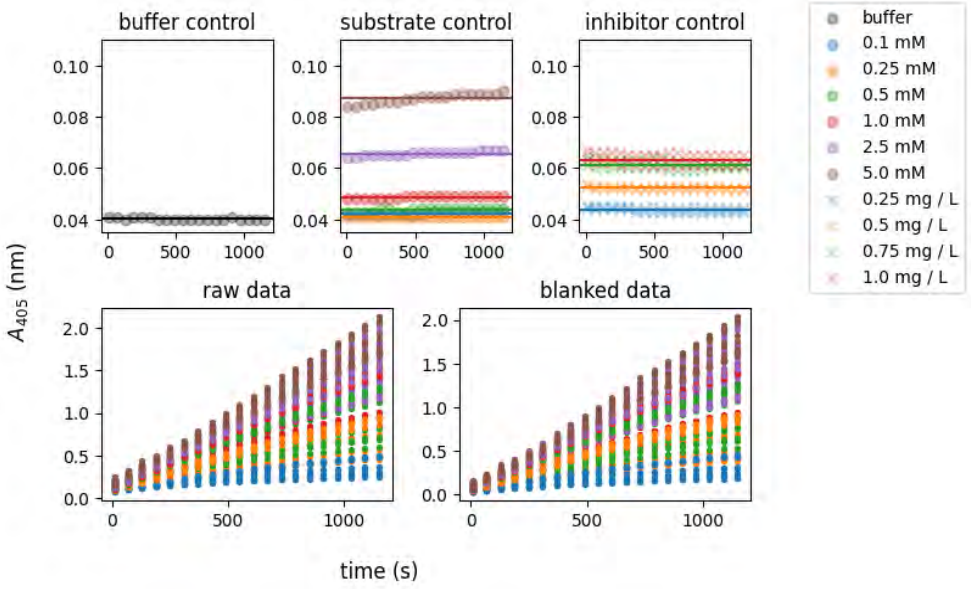

Figure B17: Time-course data illustrating the change in absorbance of the controls, as well as the uncorrected and corrected reactions for six substrate concentrations and four inhibitor concentrations of the modelled reactions for *E. maxima* fucoidan. Each measurement consisted of three replicates.

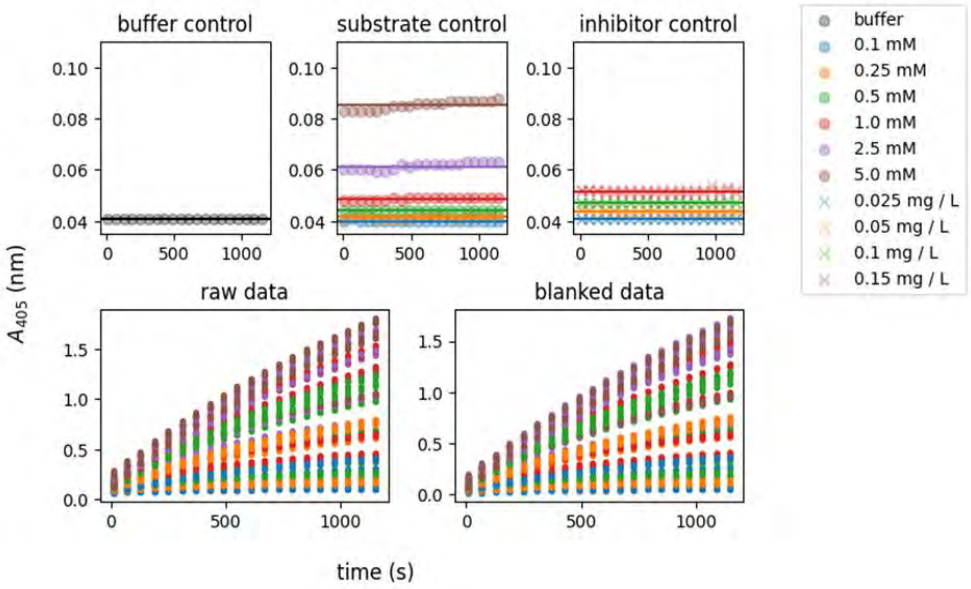

Figure B18: Time-course data illustrating the change in absorbance of the controls, as well as the uncorrected and corrected reactions for six substrate concentrations and four inhibitor concentrations of the modelled reactions for *E. radiata* fucoidan. Each measurement consisted of three replicates.

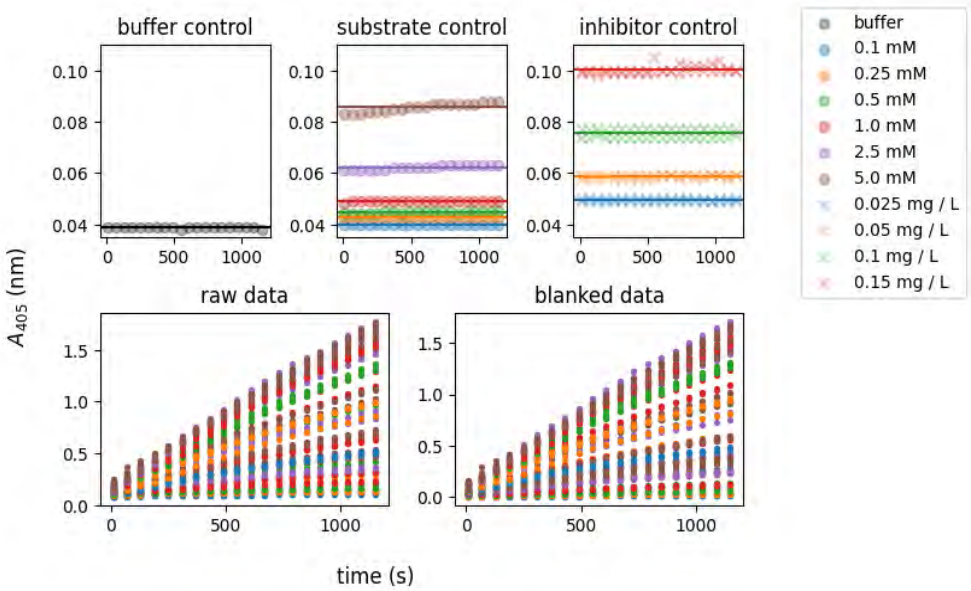

Figure B19: Time-course data illustrating the change in absorbance of the controls, as well as the uncorrected and corrected reactions for six substrate concentrations and four inhibitor concentrations of the modelled reactions for *S. elegans* fucoidan. Each measurement consisted of three replicates.

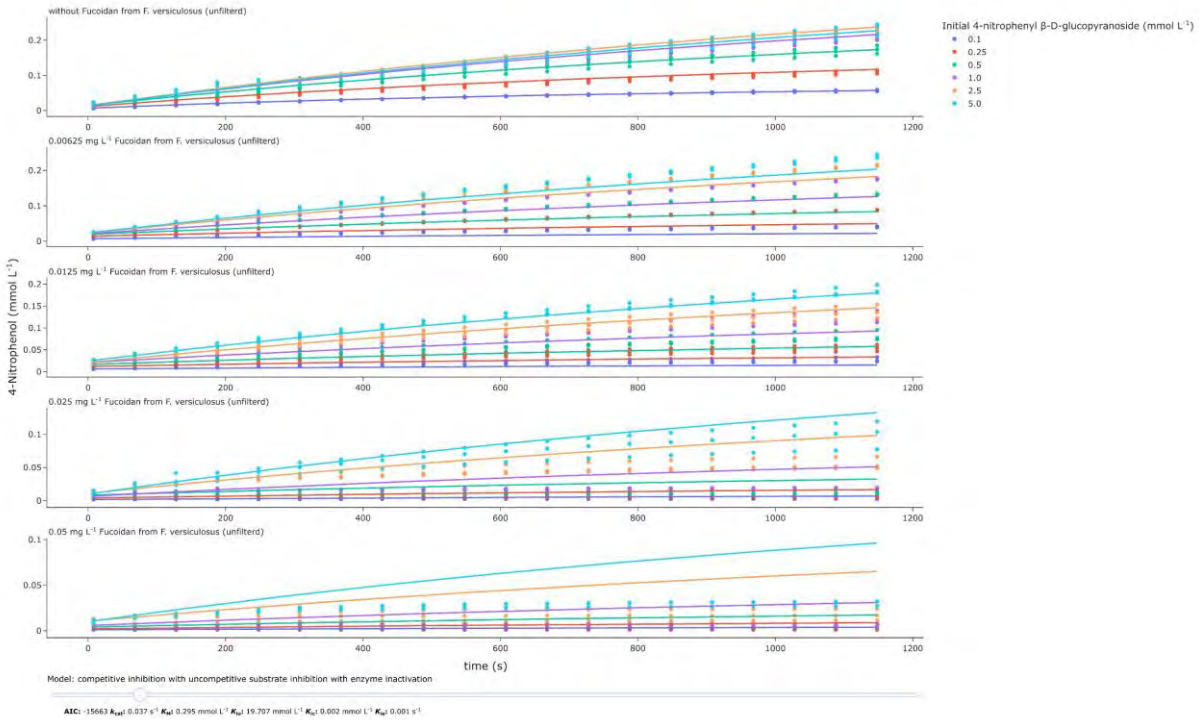

Figure B20: Measurement data set with and without *F. vesiculosus* inhibitor fitted against the kinetic model selected for parameter estimation of α-glucosidase reactions. Each measurement consisted of three replicates, with the data points representing each individual replicate shown.

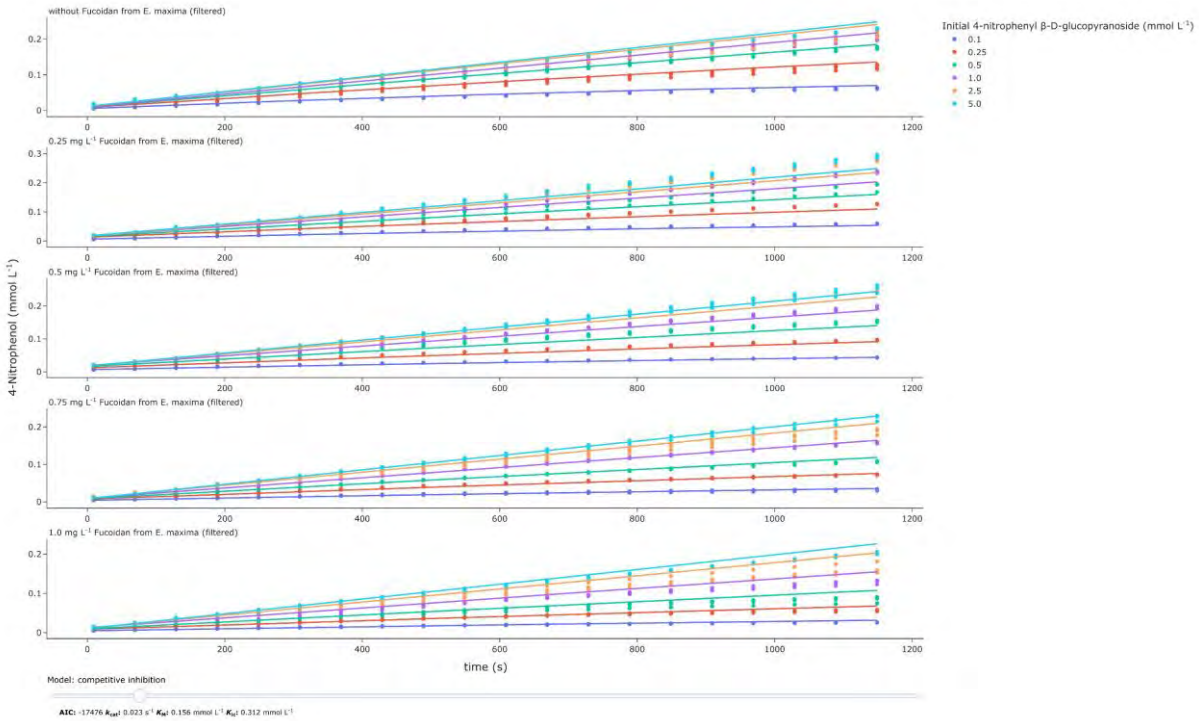

Figure B21: Measurement data set with and without *E. maxima* inhibitor fitted against the kinetic model selected for parameter estimation of α-glucosidase reactions. Each measurement consisted of three replicates, with the data points representing each individual replicate shown.

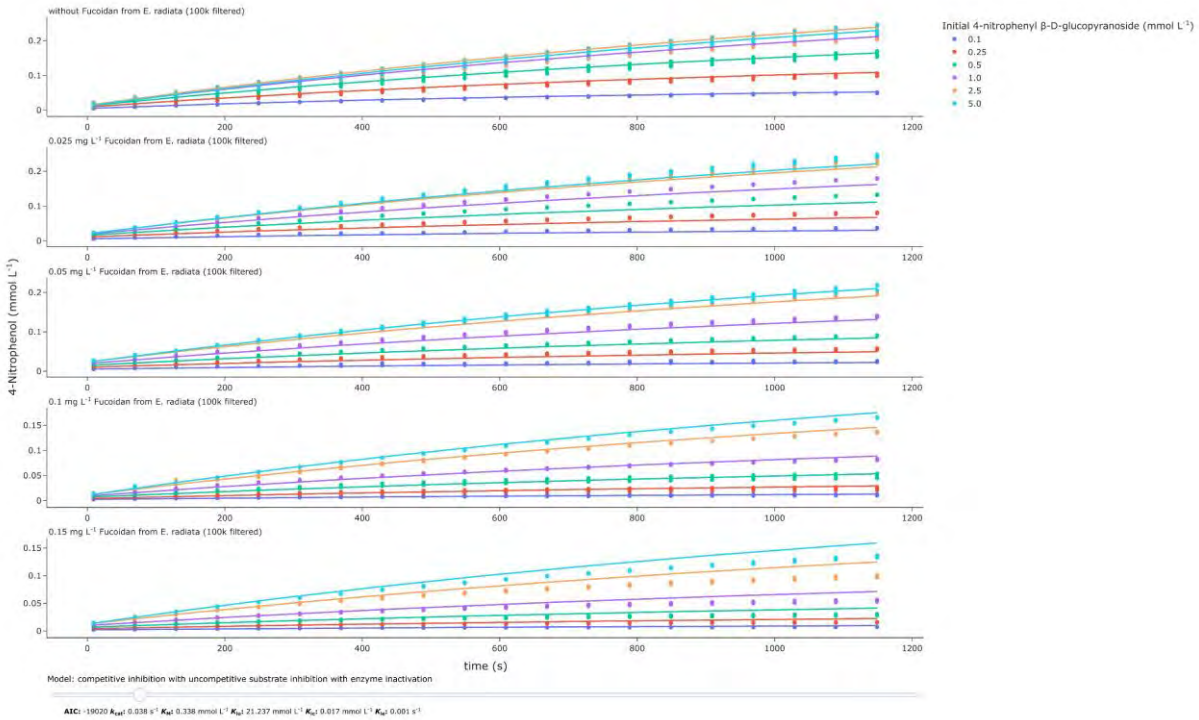

Figure B22: Measurement data set with and without *E. radiata* inhibitor fitted against the kinetic model selected for parameter estimation of α-glucosidase reactions. Each measurement consisted of three replicates, with the data points representing each individual replicate shown.

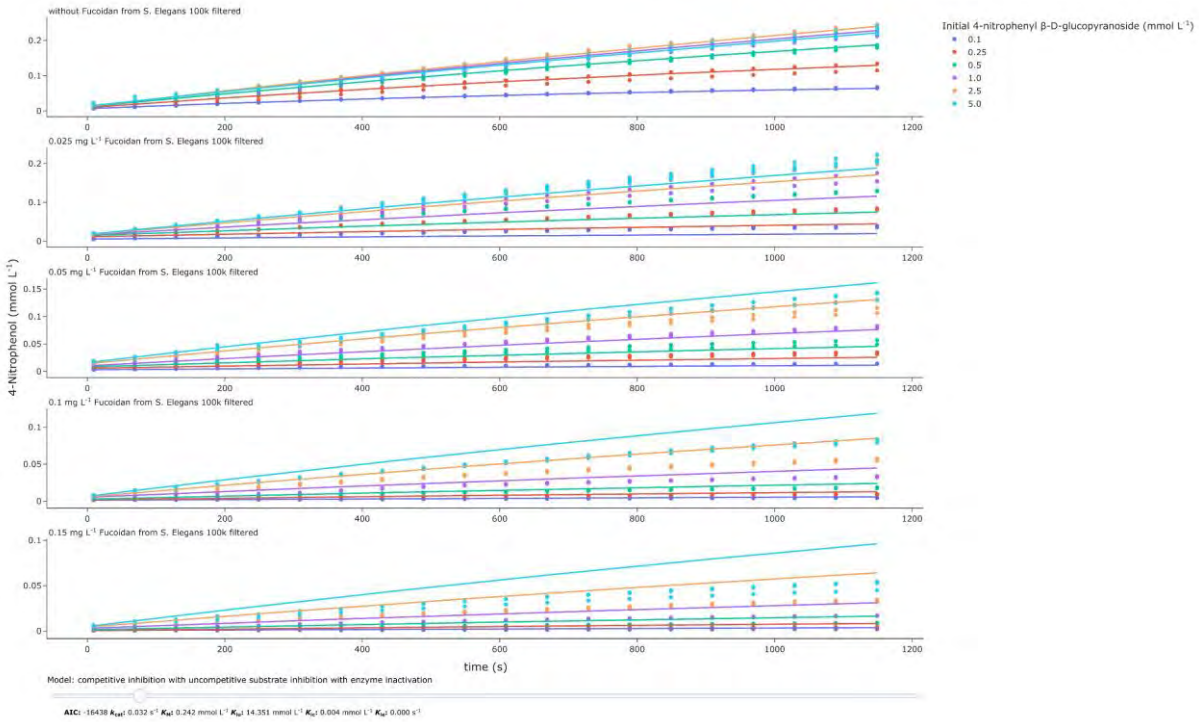

Figure B23: Measurement data set with and without *S. elegans* inhibitor fitted against the kinetic model selected for parameter estimation of α-glucosidase reactions. Each measurement consisted of three replicates, with the data points representing each individual replicate shown.

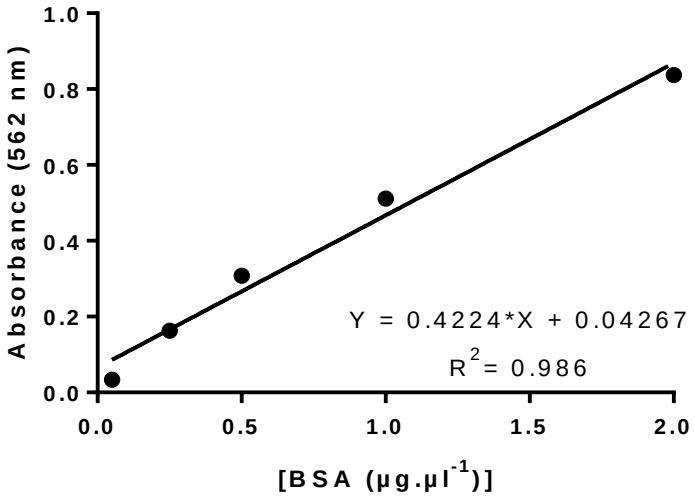

Figure B24: BSA standard curve for the BCA assay. Data points are presented as mean values ± SD (n=3).

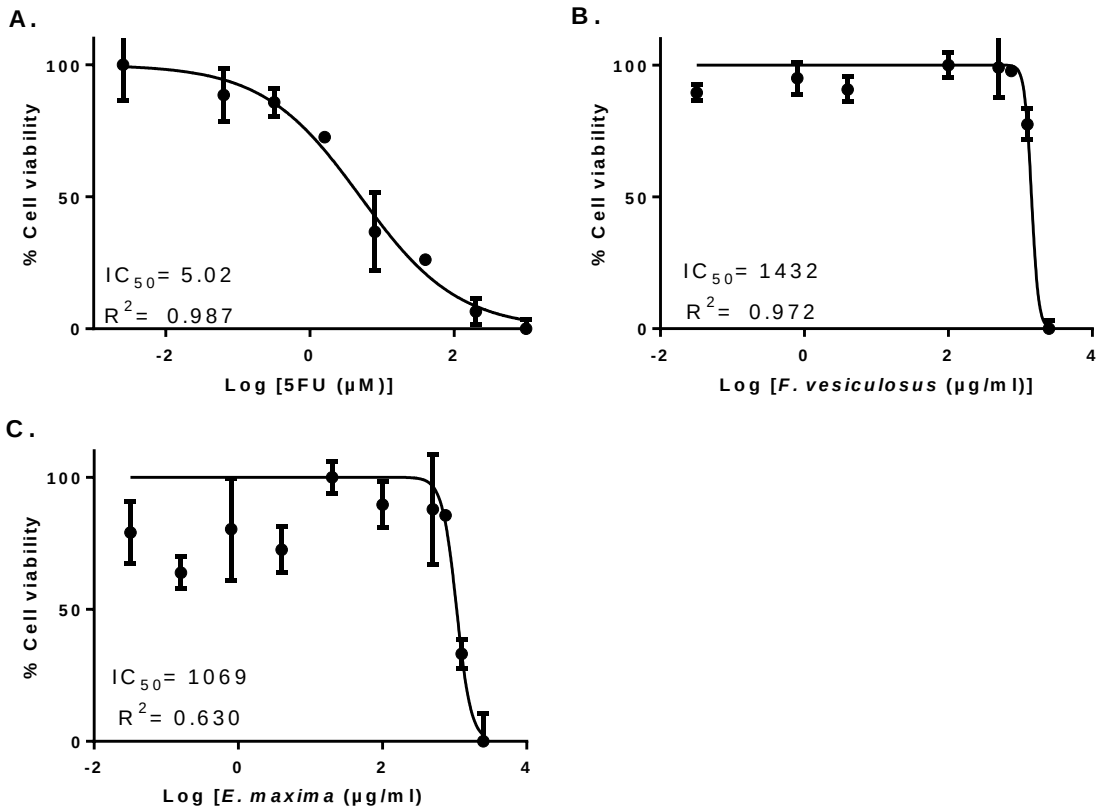

Figure B25: Dose response curves and IC_{50} values of the (A) positive control 5FU, (B) commercial fucoidan from *F. vesiculosus* and (C) *E. maxima* fucoidan. Data points are presented as mean values ± SD (n=3).

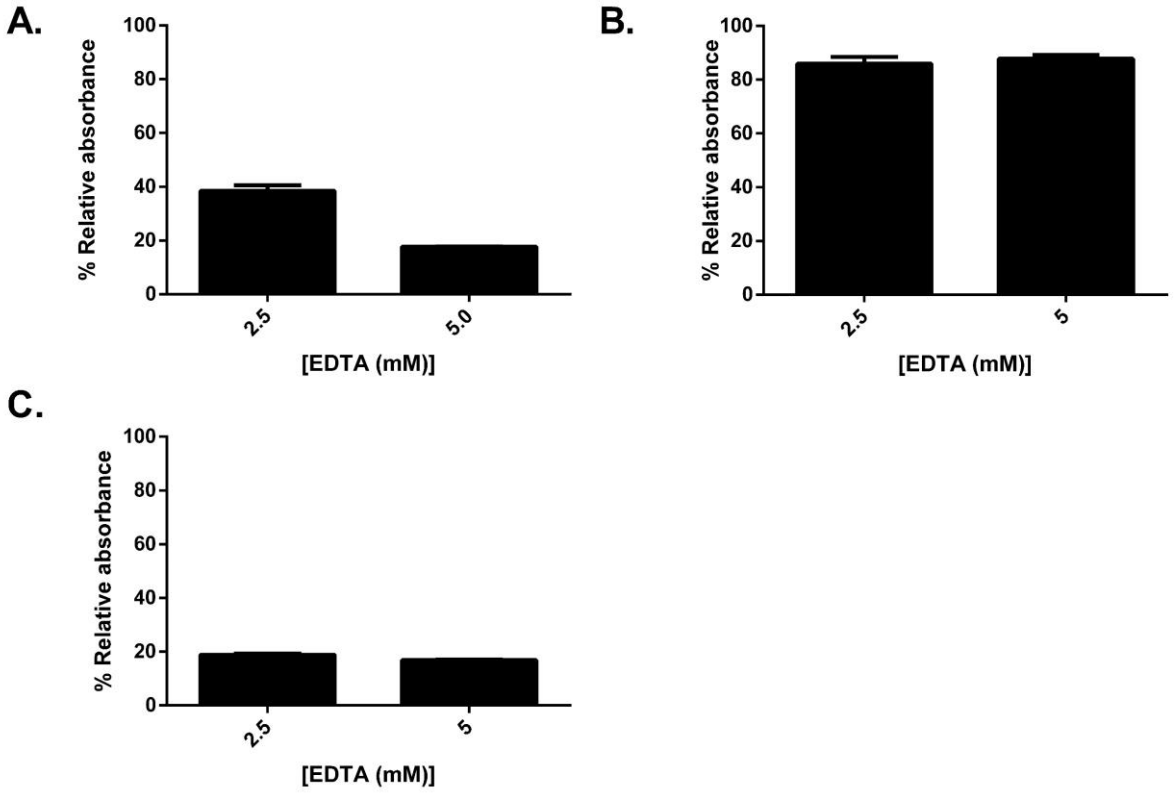

Figure B26: EDTA reduces the adhesion of HCT116 cells. Quantification of the effect of EDTA treatment on HCT116 adhesion after 8 hours when; (A) cells were treated during seeding, (B) pre-treated adherent cells were reseeded, (C) treatments were added to already adhered cells. Data points are presented as mean values ± SD (n=3).

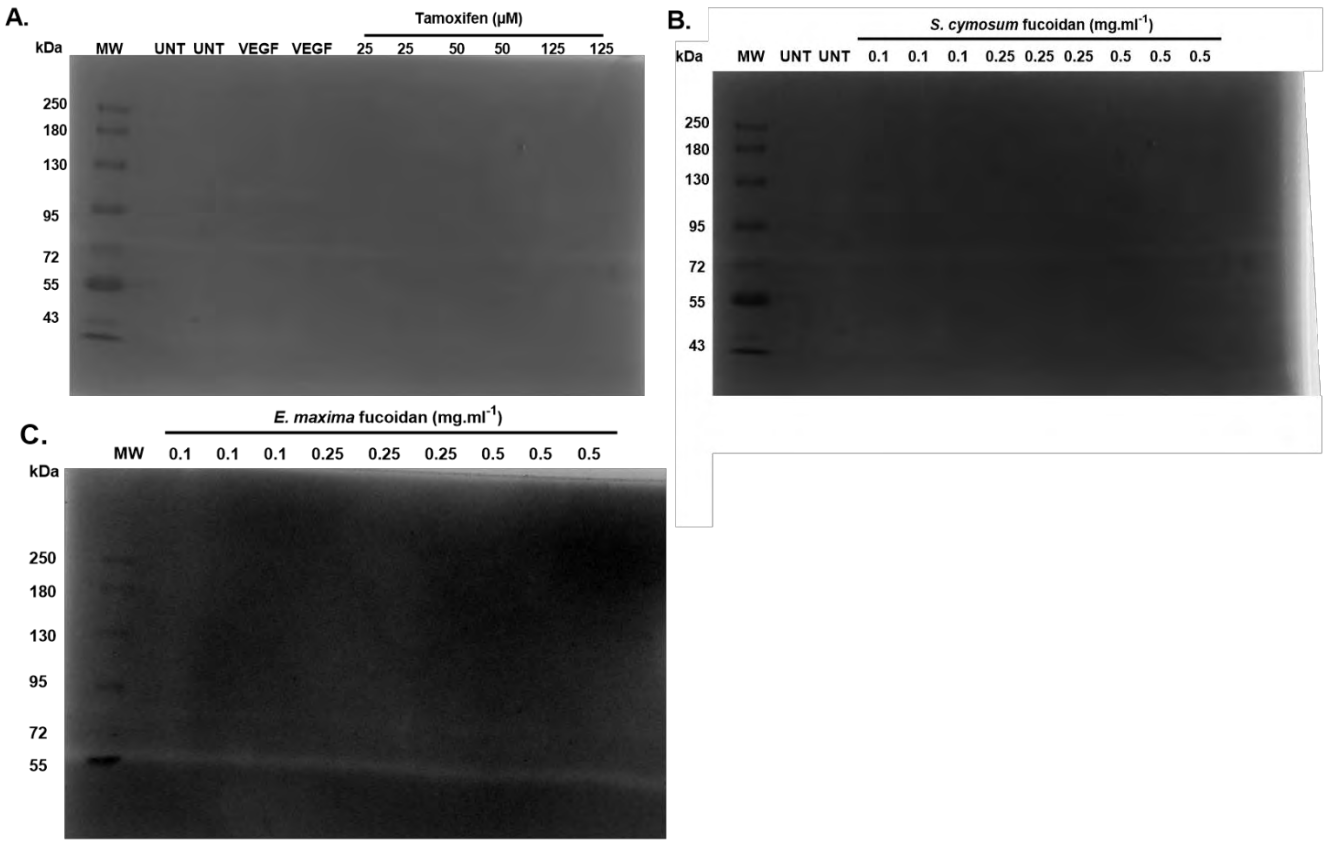

Figure B27: Gelatin zymography analysis of matrix metalloproteinase (MMP) activity. (A) Supernatants collected from HCT116 cells treated for 48 hours with VEGF and Tamoxifen. (B) Supernatants collected from HCT116 cells treated for 48 hours with *S. cymosum* fucoidan. (C) Direct analysis of *E. maxima* fucoidan treatment concentrations.

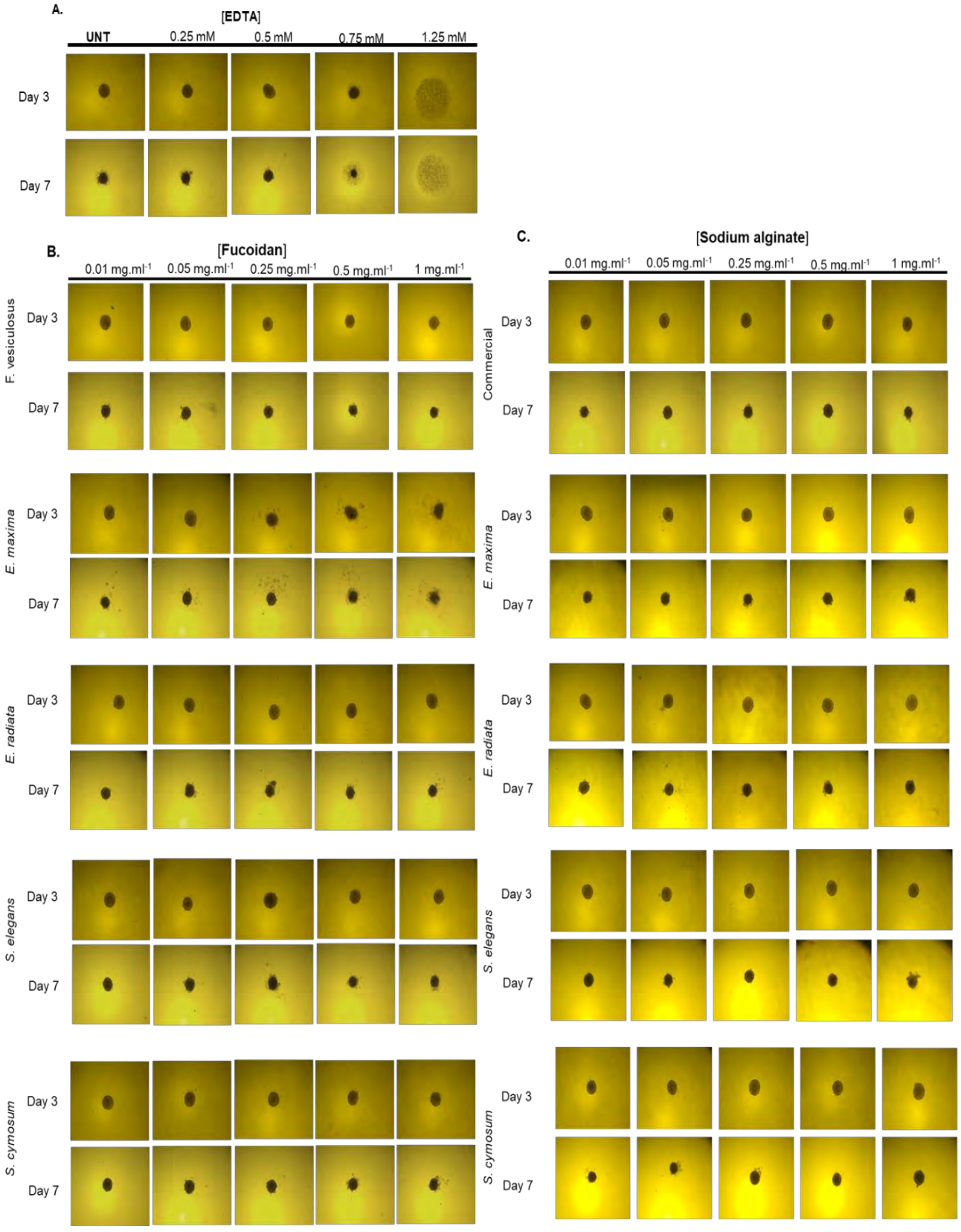

Figure B28: Representative images of the effect EDTA (A) and the various fucoidan (B) and sodium alginate (C) extracts had on HCT116 spheroid formation. Images were taken at 4x magnification.